UNIVERSITY OF CAPE TOWN

MASTERS THESIS

The Effect of Laser Shock Peening and Shot Peening on the Fatigue Performance of Aluminium Alloy 7075

Author:
Alexander BECKER

Supervisors:
Professor R.B. Tait
Dr. S. George

A thesis submitted in fulfilment of the requirements for the degree of Master of Sciences

in the

Centre for Materials Engineering
Department of Mechanical Engineering

June 2017

Declaration of Authorship

I know the meaning of plagiarism and declare that all the work in the document, save for that which is properly acknowledged, is my own. This thesis/dissertation has been submitted to the Turnitin module (or equivalent similarity and originality checking software) and I confirm that my supervisor has seen my report and any concerns revealed by such have been resolved with my supervisor.

Signed by candidate

Signed: Signature removed

Date: 19/06/2017

UNIVERSITY OF CAPE TOWN

Department of Mechanical Engineering

Abstract

The Effect of Laser Shock Peening and Shot Peening on the Fatigue Performance of Aluminium Alloy 7075

It has been well established that most fatigue cracks initiate from stress concentration sites found on the surfaces of components subject to cyclic fatigue loading. The introduction of residual compressive stresses into the surface layers of components, through various means including shot peening and laser shock peening, can result in local residual compressive stresses which provide a resistance to both crack initiation and propagation, thus leading to an increase in the fatigue life of the components.

The effects of both laser shock peening (LSP) and conventional shot peening (SP) on the fatigue properties of both 7075-T6 and 7075-T0 aluminium round bar test specimens were investigated and compared by means of cyclic 3-point bend fatigue testing. This investigation focused on the role that the peening induced microstructure, surface morphology and hardness had on the fatigue life of the test specimens.

It was found that both the laser shock peening and shot peening processes substantially increased the fatigue lives compared to unpeened AA7075-T6. The laser shock peening process more than doubled the fatigue life of the specimens and the shot peening process increased the fatigue life by approximately $1.6\times$. No discernible hardening effects could be determined in the laser shock peened specimens. However, the shot peening process resulted in a distinct hardened region within the surface layers of the AA7075-T6 specimens which was attributed to the longer pressure duration of the shot peening process which results in greater plastic deformation.

It was also shown that polishing the shot peened and laser shock peened specimens after their respective peening procedures resulted in a significant increase in fatigue life. Polishing after peening resulted in a $3.4\times$ fatigue life increase in the shot peened test specimens (T6 condition) and a $5.4\times$ fatigue life increase in the laser shock peened test specimens (T6 condition). This result highlights the role that surface roughness plays in component fatigue life. Furthermore, the increase in the average fatigue life of the polished test specimens shows that the depth of the residual compressive stresses induced by the peening processes were deep enough to allow for surfaces layers to be removed from the test specimens without any detrimental effect to the overall average fatigue life of the components. The result also suggests that the magnitudes of the residual stresses induced by the laser shock peening process being greater than those of the shot peening process.

The main difference between the peening treatments was demonstrated as originating from the surface roughening effects of the two peening procedures. The laser shock peening process only slightly increased the surface roughness of a polished AA7075-T6 test specimens. The shot peening

process severely affected the surface roughness of the test specimens, creating many potential crack initiation sites.

The AA7075-O test specimens (annealed) showed no overall improvement in their fatigue life, regardless of the mechanical treatment received. The increased ductility of the specimens during the 3-point bending fatigue process led to stress relieving of the peening induced compressive stresses. The specimens were however still fatigued to failure. This enabled the analysis of the effect of the peening induced surface roughness to be analysed. It was found that the shot peened and laser shock peened surface roughness values were significantly higher than the roughness values of the T6 specimens owing to the increased ductility and thus workability of the test specimens. These increased surface roughnesses resulted in the shot peened test specimens failing before the laser shock peened specimens. Both sets of peened specimens failed before the "as machined" and polished test specimens highlighting the role that their induced surface roughnesses had on their fatigue lives.

The cross-sectional microstructures of the peened samples in each material condition showed varied changes in the microstructure of the treated aluminium alloy. There was evidence of a large degree of plastic deformation near the surface of shot peened specimens in both material conditions. However, there was limited evidence of changes to the grains structure of the laser shock peened specimens, in both material conditions.

In addition, the ability of the laser shock peening process to recover fatigue life in damaged components was also investigated. This brought into question whether the laser shock peening process can be used on a partially fatigued component at the point of crack initiation, in an attempt to further improve the fatigue life of the component.

It was found that the laser shock peening of the cracks initiated in fatigue life recovery process did little to effectively recover fatigue life in the damaged components. A degree of life extension was present as cracks re-initiated after a few thousand cycles and was attributed to crack tip closure. This closure led to a general reduction in the fatigue crack growth rate when compared to laser shock peened/polished test specimens fatigued at the same stress.

Acknowledgements

This research would not have been possible without the help and assistance from many individuals.

Firstly, I would like to express my gratitude to my supervisors Dr Sarah George and Professor Bob Tait for continuous guidance throughout the research and experimental process. From the project inception to finalisation, their comments, encouragement and support were truly invaluable.

I would like to give special thanks to Daniel Glaser from the CSIR for helping with the laser shock peening process and providing invaluable advice about the process. I would also like to acknowledge the financial support of the South African National research Foundation (NRF) and the Department of Science and Technology for the postgraduate student scholarship awarded to attend the 6th International Conference on Laser Peening and related phenomena held at Skukuza, South Africa (6-11 November 2016).

I would like to thank Ryan Farnham and Eduard Roodt from SAAT for assisting with the shot peening process and doing so free of charge. Thanks must also be given to Dr. Anton du Plessis and Stephan le Roux for conducting the CT scans needed and doing so promptly. In addition, I would like to thank Tshepo Ntsoane and Dr. Andrew Venter from NECSA for performing the initial residual stress measurements needed to start the project.

I would also like to thank the many people involved in facilitating this project at the University of Cape Town. In particular, Penny Louw for her assistance in the the Materials Science Laboratory, Miranda Waldron for her help with regards to the SEM scanning used in the project and Pierre Smith for his efforts in manufacturing the test specimens needed for this project.

Finally, I would like to express sincere gratitude to Annesley Crisp, who provided invaluable moral support throughout the last year of the project and was instrumental in the final stages of project completion.

I would like to dedicate this Masters dissertation to my family. There is no doubt in my mind that without their continued kindness, support and encouragement, I could not have completed this process.

Contents

List of Figures

List of Tables

List of Abbreviations

AA	Aluminium Alloy
AN	Annealed (Material Condition)
AR	As Received (Material Condition)
ASTM	American Society for Testing and Materials
CAD	Computer Aided Drawing
CNC	Computer Numerical Control
CT	Computed Tomography
CSIR	Council for Scientific and Industrial Research
DC	Direct Current
DP	Diamond Polishing
DSP	Display
EDS	Energy Dispersive X-ray Spectroscopy
ESH	Electro-Servo Hydraulic Fatigue Machine
GP	Guinier-Preston
hkl	Three Integers of Miller Indices
HV	Vickers Hardness Number
HRC	Rockwell Hardness Number
ISO	International Organization for Standardization
LEFM	Linear Elastic Fracture Mechanics
LSP	Laser Shock Peening
MD	Magnetic Disk
MTT	Metal and Tool Trade
NLC	National Laser Centre
NECSA	South African Nuclear Energy Corporation SOC Limited
Nd:YAG	Neodymium-doped Yttrium Aluminium Garnet
NDI	Non Destructive Inspection
NDT	Non Destructive Testing
OP	Oxide Polishing
POL	Polished
RC	Rockwell Scale
RPM	Revolutions Per Minute
RRA	Retrogression and Re-ageing
SAE	Society of Automotive Engineers
SAAT	South African Airways Technical
SEM	Scanning Electron Microscope (Microscopy)
S-N	Stress vs. Number of Cycles to Failure
SP	Shot Peening
TEM	Transmission Electron Microscopy
UCT	University of Cape Town
XRD	X-ray Diffraction

List of Symbols

Greek Symbols

α	Homogeneous Solid Solution (Aluminium)	-
α_{ss}	Super Saturated Solid Solution	-
β	Alloying Elements	-
ε_e	Engineering Strain	-
ε_p	Plastic Surface Strain	-
ε_t	True Strain	-
ε_ψ	Strain Along Psi Angle of Inclination	-
$\varepsilon_{\phi\psi}$	Strain in Some Direction	-
ε_x	Strain in the X Direction	-
ε_y	Strain in the Y Direction	-
ε_z	Strain Normal to Component Surface	-
$\Delta\varepsilon_e$	Elastic Strain Amplitude	-
η	$MgZn_2$ Precipitate	-
$\eta^{'}$	Intermediate $MgZn_2$ Precipitate	-
$\triangle K$	Change in Stress Intensity Factor	MPa$\sqrt{m}$
θ	Diffraction Angle	$^\circ$
λ	X-ray Beam Wavelength	m
μ	Pulse Duration	s
μ_{Li}	Linear Absorption Coefficient	cm^{-1}
μ_{Ma}	Mass Absorption Coefficient	cm^2/g
ρ	Mass Density	kg/m^3
ρ_{radius}	Radius	mm
ϕ	Azimuth Angle	Degrees
ψ	Inclination Angle	Degrees
2θ	The Bragg Angle	Degrees
ω	The Between Incident X-ray and Surface	Degrees
$\omega_{specimen}$	Specimen Rotational Speed	degrees/s
χ	Angle of Rotation in Plane Normal to Omega Plane	Degrees
$\Delta\sigma$	Applied Cyclic Stress	MPa
$\bar{\sigma}$	Equivalent Stress	MPa
$\sigma_1, \sigma_2, \sigma_3$	Principal Stresses	MPa
$\sigma_x, \sigma_y, \sigma_z$	Principal Stresses	MPa
σ_a	Stress Amplitude	MPa
σ_e	Engineering Stress	MPa
σ_f	Applied Stress at Failure	MPa
$\sigma_f^{'}$	Fatigue Strength Coefficient	-
σ_m	Mean Stress	MPa
σ_{max}	Maximum Stress	MPa
σ_{min}	Minimum Stress	MPa
σ_N	Endurance Limit	MPa
σ_o	Fatigue Limit	MPa
σ_r	Surface Residual Stress	Pa

σ_s	Surface Stress	MPa
σ_t	True Stress	MPa
σ_{TS}	Tensile Strength of Material	MPa
σ_y	Yield Strength of Material	MPa
σ_y^{dyn}	Dynamic Yield Strengths	MPa
σ_ϕ	Stress Along Component Surface	MPa
σ_{UTS}	Ultimate Tensile Strength	MPa
τ	Shear Stress	Pa
τ_d	Penetration Depth	cm
ν	Poisson's Ratio	Pa
v_e	Elastic Wave Speed	m/s
v_p	Plastic Wave Speed	m/s

Roman Symbols

A	Amplitude Load	N
a	Flaw Size	m
a_{cr}	Critical Flaw Size	m
a_{ls}	Size of Laser Spot Impact	m^2
$\frac{da}{dN}$	Crack Growth Rate	m/cycle
b	Fatigue Strength Exponent	b is negative
C	Material Coefficient	-
$C_{coverage}$	Peening Coverage	spots/cm^2
d	Interplanar Spacing	m
d_n	Interplanar Spacing	m
d_0	Unstrained Interplanar Spacing	m
d_ψ	Inclined Interplanar Spacing	m
$d_{\phi\psi}$	Interplanar Spacing	m
d_c	Diameter of Circle	m
da	Integrand	-
D_p	Plastically Affected Depth	m
E	Young's Modulus	GPa
HEL	Hugoniot Elastic Limit	Pa
I	Second Moment of Area	m^4
K_f	Stress Intensity	MPa$\sqrt{m}$
K	Strength Coefficient	-
K_{IC}	Critical Fracture Toughness	MPa$\sqrt{m}$
L	Span Length	m
M	Applied Bending Moment	(Nm)
m	Material Coefficient	(2 - 4)
mx	Gradient of the Line	-
N	Number of Cycles	Cycles
n	Work Hardening Coefficient	-
$n_1 + . + n_k$	Number of Cycles at a Stress Level	Cycles
$N_1 + . + N_k$	Number of Cycles to Failure at a Stress Level	Cycles
N_f	Number of Cycles to Failure	Cycles
P	Applied Load	N
P_s	Shock Wave Pressure	Pa
P_{max}	Maximum Applied Load	(N)
P_{min}	Minimum Applied Load	(N)
P_{mean}	Mean Applied Load	(N)
R	Stress Ratio	-

R_a	Average Roughness	μm
R_{rate}	Laser Repetition Rate	Hz
R_z	Equivalent Length	μm
S	Applied Stress Range	MPa
S_a	Stress Amplitude	MPa
S_e	Endurance Limit	MPa
T	Time	s
T_m	Melting Point	°C
v_z	Vertical Stage Speed	mm/s
Y	Dimensionless Compliance Function	-
y	Distance from Neutral Axis to Applied Stress	m

Chapter 1

Introduction

Engineered components have numerous and often critical applications in the world around us. Such components are often subject to fatigue through their exposure to repeated cyclic stressing during their everyday operation. In turn, this exposure often results in crack initiation and propagation which may ultimately lead to the overall failure of the component. This failure, if sudden and unexpected, can result in irreversible and often catastrophic consequences, particularly if these components are used in applications where human safety is at stake.

Mitigation against the fatigue failure of engineered components is crucial in order to ensure the overall safety of the component, but also to reduce the cost associated with component manufacture and replacement.

It has been well documented that the surface condition of an engineered component has a major influence on the overall fatigue life of the component. This is because most cracks initiate from stress concentration sites **on the surface**. Through the introduction of residual compressive stresses into the surface layers of an engineered component, resistance to crack initiation and propagation can be achieved, so improving the overall fatigue life of these components.

Residual compressive stresses can be introduced into the surfaces of engineered components through various means, including shot peening (SP) and laser shock peening (LSP). Both treatment processes introduce substantial residual stresses by plastically deforming the surface layers of the treated component, by means of hard spherical bead bombardment in the case of shot peening and laser-induced shock waves in the case of laser shock peening.

In the past, shot peening had been the most effective and widely used means of introducing compressive residual stresses into the surface layers of engineered components. In general, shot peening is relatively inexpensive, uses robust and thus durable process equipment and can be used on different sized areas as required. However, the shot peening process has its limitations. In

determining the degree of the compressive stresses produced, the shot peening process is semi-quantitative. The residual stresses induced by the shot peening process are also limited in depth and do not usually exceed 0.25 mm in soft metals such as aluminium alloys. Arguably, the main limitation of the shot peening process is that the process results in a roughened surface after treatment, especially in softer metals [1]. This induced roughness generally needs to be removed before these components can be put into service. Also, the process used to remove this roughness tends to remove most of the residual compressive stress layer, which has been induced into the component.

With the ever increasing demand for lower operational costs, higher safety measures and better performance characteristics in industry, significant pressure has been placed on manufacturing systems and component surface processing technologies to produce components which are near flawless and require as few processing steps as possible before completion [2]. One of the surface treatment techniques that has been developed in response to these demands is the laser shock peening surface treatment. Laser shock peening utilises high speed and high powered lasers to focus short duration energy pulses onto the surface of the component to peened, creating a shock-wave which propagates into the surface of the component so inducing residual stresses [1].

Laser shock peening allows for residual stress depths of more than 1 mm to be achieved in commercially available aluminium alloys and has been shown to significantly improve fatigue performances of engineered components [1]. The laser shock peening process can also be adjusted and controlled in real time through computer controlled systems, whereby the energy per pulse can be measured and recorded for each location on the component being peened. If the applied laser pulse was below the specified energy, it can be redone at that time rather than after the part has failed. Regions inaccessible to shot peening, such as small fillets and notches, can be treated by laser peening. Laser shock peening also has a minimal effect on the surface quality of the peened component, with hardly any thermal or mechanical (surface roughness) changes occurring at the surface as a result of the treatment process [3]. It has been proposed that laser shock peening can be utilised to restore the strength and durability components partially damaged in service, due to cracking, corrosion or other mechanical causes [4]. By laser shock peening partially fatigue-damaged components, the dislocation “slip band” damage within these components may be able to be effectively "healed", thereby extending the components fatigue life. Engineered components are typically replaced after a pre-specified service time interval or once a fatigue crack has been detected in the component. This procedure can be both labour intensive and expensive. By laser shock peening already fatigued components, some of the costs associated with replacing the components can be mitigated.

The laser shock peening process does however have its problems. Until recently, the high capital cost of laser peening equipment has made the process generally inaccessible to the majority of industry and to those who wish to develop the process further. Recent advances in laser technologies have resulted in the development of a so-called "middle range" of lasers (i.e. the Inlite III from Continuum®). These newly developed lasers provide an affordable off the shelf solution, perfectly suited for the laser shock peening process. Difficulty in controlling the processing variables involved in the peening treatment process has resulted in the laser peening process being confined to high value, low volume parts such as biomedical implants and turbine blades [1]. The operation is generally a slow process as there is a continual need for quality control during the peening operation [3].

The aerospace industry is currently leading the integration of methods in which the laser peening process can be applied to many of its products including turbine blades, rotor components, discs, gear shafts and bearing components [1]. The applications of the laser peening process can be anticipated to expand into various industries as the process becomes more accessible, with laser peening potentially allowing for direct integration into manufacturing production lines with a high degree of automation [1].

1.1 Aims and Objectives

This project aims at helping to develop the theory and understanding towards two of the currently available mechanical means of surface treatment, namely shot peening and laser shock peening. Comparisons between the two surface treatment processes will be made in terms of the modifications each of the processes has on the fatigue strength, surface morphology, microstructure, and hardness on peened test specimens. In addition, the ability of the laser shock peening process to extend fatigue performance in damaged components is investigated. Components fatigued to the point of observable crack initiation were re-laser shock peened in an attempt to extend their fatigue lives. For this “healing process” to occur, the fatigue crack depth must be contained within the penetration depth of the laser shock peened region. By re-laser shock peening fatigued components at the point of observable crack initiation, the limits as to when the fatigue life restoration process can be successfully implemented could be established. The visual observation of fatigue cracks is one of the easiest and most accessible forms of NDT (Non-Destructive Testing). By visually observing fatigue cracks, costs associated with more advanced forms of NDT testing could be mitigated, so helping to further reduce the overall costs associated with laser shock peening. These limits would indicate whether fatigue life could indeed be recovered at the point of observable crack initiation

or whether partially fatigued components needed to be re-laser shock peened at an earlier stage, for fatigue life recovery to occur.

Figure 1.1 below depicts how the fatigue life of a component could potentially be increased with the application of re-laser shock treatment at the onset of crack initiation.

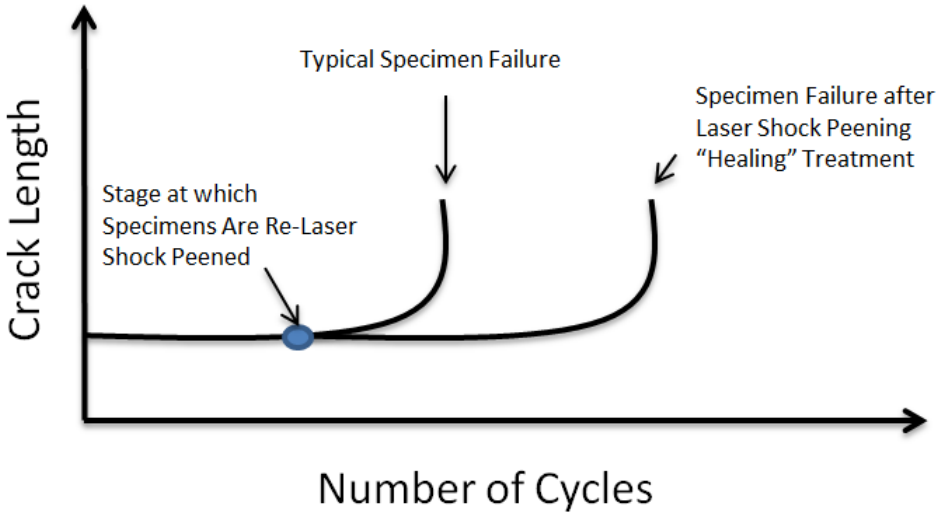

Figure 1.1: Proposed Fatigue Life Extension of laser Shock Peened Components after Multiple Laser Shock Peening's

As this project focuses on the laser shock peening process, all test specimen samples utilised in this study were machined from aluminium alloy 7075. This material is generally utilised in the aerospace industry, where laser shock peening is increasingly being used.

A summarised list of the objectives of this project are presented below:

- To measure the effect both shot peening and laser shock peening have on fatigue life.
- To measure the surface roughness induced by both shot peening and laser shock peening and determine the effect this surface roughness has on fatigue life.
- To measure the microhardness at incremental depths from the surface induced by both shot peening and laser shock peening processes.
- To investigate the effect of the shot peening and laser shock peening process on the microstructure of the AA7075.
- To determine whether laser shock peening can be used to restore and extend fatigue performance in partially fatigued components.

1.2 Methodology

In order to achieve the objectives of this study, varying experimental methodologies were adopted. The effect on fatigue life of the shot peening and laser shock peening processes was studied using round bar 7075 aluminium alloy test specimens, in both the T6 and annealed material conditions, which were subjected to three-point cyclic bend loading.

Test specimens were split into various test groups, each of which underwent a different surface treatment procedure before being subjected to cyclic fatigue loading. These test groups aimed at determining the effect surface morphology (induced by various surface treatment processes) has on fatigue life.

The test groups and the applied processes to the test specimens within each test Group were as follows:

i. Group 1: No surface modification.

ii. Group 2: Test specimens surfaces polished.

iii. Group 3: Test specimens surfaces polished and shot peened.

iv. Group 3: Test specimens surfaces polished, shot peened and re-polished.

v. Group 4: Test specimens surfaces polished and laser shock peened.

vi. Group 4: Test specimens surfaces polished, laser shock peened and re-polished.

vii. Group 5: Fatigue life recover/extension process

Test Group 1 served as a baseline, with no surface modification treatment used. In test Group 2, the test specimens were polished in order to reduce their surface roughnesses. In test Group 3, the test specimens were polished and then shot peened. This allowed for the shot peened induced roughness to be determined. In test Group four, the test specimens were polished and then laser shock peened. This allowed for the laser shock peened induced roughness to be determined. some test specimens in test Groups 3 and 4 were polished after their respective shot peening and laser shock peening procedures. This helped determine whether the peening induced surface roughness could be reduced without compromising the shot peened induced residual stresses.

Once the test specimens had received their surface modification treatments, their surface roughness's were measured and the specimens were then subjected to cyclic three-point bend fatigue testing in order to determine their respective fatigue lives.

Test Group 5 contained test specimens in the T6 condition which were used to investigate the ability of laser shock peening to restore fatigue resistance in already fatigued components. The specimens utilised in this test Group were initially polished and laser shock peened.

After their initial laser shock peening, the test specimens were polished in order to obtain a comparable surface finish to the other polished tests specimens fatigued to failure in this study. The Group 5 test specimens were then sent for computed tomography scanning (CT) to examine, non-destructively, whether there are any defects within the test specimens which may have influenced their fatigue lives. The test specimens were then partially fatigued to the point of observable crack initiation. before being re-laser shock peened. The re-laser shock peened specimens were then re-CT scanned in order to determine whether any crack "healing" could be observed. The test specimens were then re-polished a final time before being fatigued to failure.

The microstructure of the test specimens in each material condition (and in each peened condition) was analysed on etched test samples using an optical light microscope. The fracture surfaces of the fractured test specimens were also analysed using both an optical light microscope and a scanning electron microscope (SEM). Finally, the microhardness-depth distributions of AA7075 (in both the T6 and fully annealed material conditions) before and after the various mechanical surface treatments were determined.

1.3 Thesis Layout

In Chapter two a literature review is presented. The theoretical background of fracture mechanics and classical fatigue life prediction methodologies are presented. The sources of residual stresses in components and the analysis of these stresses are reviewed. A description of both the shot peening and laser shock peening techniques are provided. Finally, a review into current fatigue life "healing" techniques is presented.

Chapter three presents various experimental procedures used in this study. The test material is characterised and the test sample geometries are presented. The methodology used in a preliminary investigation into the test material utilised in this study is then presented. Following on from the preliminary investigation, the techniques used to modify the surfaces of the test specimens are presented, including the shot peening and laser shock peening process used. This if followed by a description of the techniques used to measured and analyse the surface roughness and fatigue performance of the test specimens. The method used to investigate the ability of the laser shock peening process to restore fatigue performance in fatigued test specimens is then given. Finally,

the techniques used to analyse the microstructure, strain and hardness of both the fatigued and healed test specimens are detailed.

The results from all the investigations in this study are given in Chapter four. The first Section of this Chapter deals with the results and observations of the preliminary investigation into the nature of the material used in this study. Following on from the preliminary investigation, the results of the surface analysis and fatigue performance of the test specimens (in the various conditions) is presented. Results from the investigation into the ability of laser shock peening to restore fatigue performance in fatigued test specimens are then given. Finally, the results from the analysis of the microstructure and hardness of both the fatigued and healed test specimens are presented.

The results are then discussed in Chapter five from which an assessment of both the shot peening and laser shock peening process is given along with an assessment of the potential fatigue life "healing" ability of the laser shock peening process. These topics are then concluded in Chapter six, where recommendations for further research are finally presented.

Chapter 2

Literature Review

2.1 Introduction

The purpose of this literature survey is to gain a general knowledge and understanding of the fundamental principles and concepts which are directly applicable towards developing a practical approach for improving the fatigue life of engineered components.

This review has not been limited to any particular sources, rather it aims to introduce the concept of fatigue induced failure, discusses some of the various approaches used in analysing and characterising fatigue and looks at some of the factors that promote fatigue in engineered components. This is followed by an analysis of surface treatment processes, namely shot peening and laser shock peening, which are to be utilised for mitigation against the fatigue-induced failure of test specimens in the experimental section of this study. The literature review will conclude with a brief analysis of the aluminium alloy to be used in the experimental component of this study and relevant stress relieving process applicable to the selected alloy before any surface treatment can take place.

2.2 Fatigue

2.2.1 Introduction to Fatigue

The failure of an engineered component by means of fatigue occurs through the repeated cyclic loading of the component at a stress lower than that required to cause failure during a single application of that stress. Fatigue cracking may be divided into two stages: crack initiation and crack propagation. Both stages require the accumulation of irreversible local plastic deformation due to repeated cyclic stressing. The total fatigue life of an engineered component may thus be the summation of the life spent initiating a crack and subsequently propagating it to some critical

crack length value, which is the crack length needed for fast fracture to occur [5]. This crack life cycle can be seen plotted on a log scale in Figure 2.1.

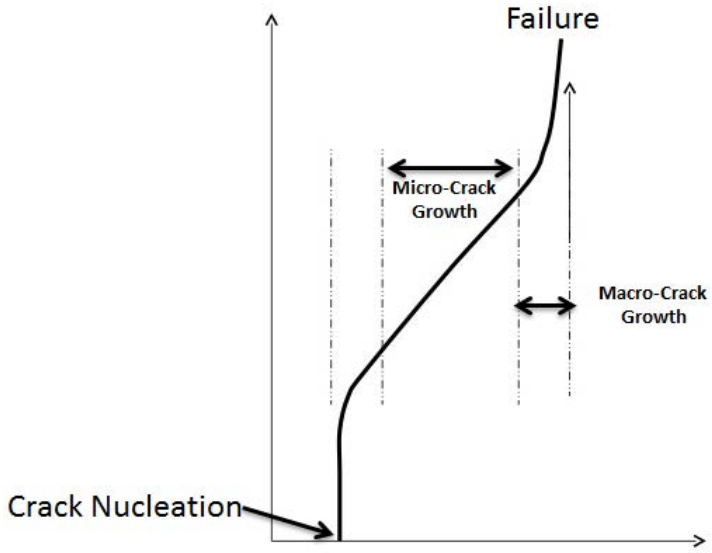

Figure 2.1: A Schematic Graph Showing the Stages of Crack Growth

Typically, cracks tend to initiate on the free surfaces of a component. These free surfaces of the component are where applied stresses on the component are highest. Free surfaces may also be exposed to the environment during the everyday usage of the component, which in turn may affect the overall fatigue life of the component [6]. In idealised defect-free pure metals, cracks initiate as a result of the formation of persistent slip-bands. The various stages of the crack growth cycle will be discussed in detail later in this literature review.

Components can develop these fatigue cracks over a long period of time and under normal cyclic operating conditions, with each repeated application of stress well below that of the material's yield strength. Failure, however, can still prove to be sudden and unexpected as it may occur during the day to day operation of these components, the results of which may prove to be catastrophic, often leading to huge financial losses and even the loss of human life. It is estimated the fatigue contributes to nearly 80% of all mechanical service failures [7].

The cause of fatigue failures can be classified into three groups, namely: poor design (including incorrect material selection), faulty manufacturing techniques and deterioration with time in service [8]. Each of these three factors typically results from the engineered component containing some sort of defect, even if this defect is on a sub-microscopic level (gas porosity, impurities), which acts as a stress concentration site from which crack initiation can occur.

Fatigue can be further classified into two categories: low-cycle fatigue and high-cycle fatigue. Low-cycle fatigue refers to fatigue cycles with large amplitudes and low frequencies where the total number of cycles is typically less than 10^4. High-cycle fatiguing has small amplitudes and high frequencies where the total number of cycles usually exceeds 10^6 cycles. Low-cycle fatigue typically occurs under plastically applied stresses whereas high-cycle fatigue occurs under elastically applied stresses. However, plastic deformation can still occur at crack tips during high-cycle fatigue [7].

2.3 Fatigue Analysis

The need for characterising and predicting the fatigue life of engineered components has led to the development of three main fatigue analysis approaches that can be utilised in the design of engineered components. These approaches are: (i) the S-N approach, which plots stress levels against associated number of cycles (N) to failure, so predicting fatigue life particularly for the high cyclic range; (ii) the fracture mechanics approach, which characterises the critical fatigue crack length at which fast fracture will occur, as well as the number of cycles at which this critical crack length is met; and (iii) the strain-based approach, which helps predict fatigue life in the low cyclic range.

Crack growth laws, which are based on fracture mechanics, are necessary to predict crack propagation rates and hence component lifetimes [6]. In this study, fracture mechanics will be utilised in this study to quantify the fatigue crack growth and fatigue life in both mechanically treated and untreated test specimens. The fracture mechanics approach to fatigue analysis will be discussed in detail later in this literature review. The S-N approach will also be briefly described in this literature review, as it is frequently used in fatigue analysis owing to its ease of implementation, even though it has some severe data limitations which need to be noted. The strain-based approach is uncommon and not necessary for the scope of this project and thus will not be discussed further. The full strain-based approach can be viewed in detail in reference [9].

2.3.1 S-N Approach

The stress-based or S-N curve approach to fatigue is the most frequently used approach in making fatigue life predictions as it utilises existing fatigue test data. The S-N curve approach is typically the easiest of the three fatigue analysis approaches used as it can be implemented for a wide range of design applications [9].

In this approach, a materials performance in high cycle fatiguing situations can be characterised by plotting a graph of the applied stress range ($\Delta\sigma$ or ΔS) or the stress amplitude ($\Delta\sigma_a$) against a logarithmic scale of cycles to failure (N) [9]. Test specimens are subjected to varying degrees of stress and are fatigued until failure at each of these stress amplitudes. This process is repeated for a range of stress amplitudes until sufficient data is obtained from which a complete curve can be constructed. As this is a statistical approach to fatigue analysis, multiple tests are needed at each load level so as to generate curves of statistical confidence. This allows for a useful way to visualise time to failure for specific materials. A basic representation of an S-N curve can be seen in Figure 2.2, where the axes are plotted on a log scale.

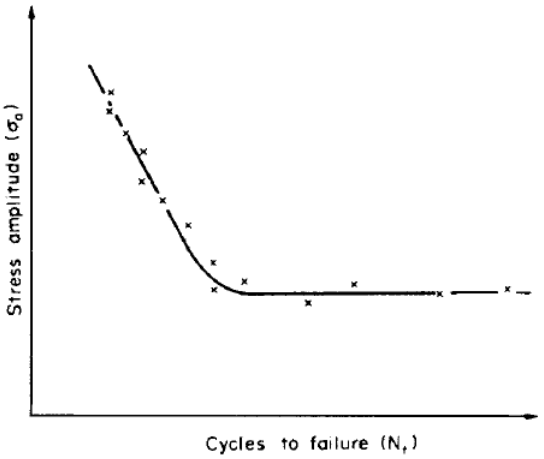

Figure 2.2: S-N Fatigue Life Curve [10]

It must be noted that laboratory-based experiments typically utilise plain, polished test specimens and thus the results generated from these experiments cannot be directly applied to components or structures in the practical world without some sort of modification. The following factors (which will be discussed in detail later on) can affect fatigue life [9]:

- The quality of material processing (size and distribution of inclusions, voids etc.)
- The procedure of material processing (annealed, quenched, tempered etc.)
- The procedure of specimen processing (specimen shape, machining method)
- The quality of specimen manufacture (surface quality, tool marks, scratches etc.)
- Material properties (yield strength, ultimate strength, strain at failure etc.)
- Geometry (length, width, thickness, diameter, transition radius etc.)
- Stress state (uniaxial, multiaxial, stress ratio, mean stress)

- The effect of the environment (temperature, corrosive environment)

When constructing S-N curves through repeated fatigue testing, large amounts of scatter in the data can often be obtained. This scatter can usually be attributed to one or more of the factors mentioned above as most of these factors cannot be accounted for in the modelling of S-N curves. Another limiting factor of the S-N curve approach is that there is no consistent definition of failure. Failure may be the point at which the first small detectable crack is observed, or after a certain percentage decrease in load amplitude or at final fracture [10]. Thus, depending on the approach and experience of a researcher conducting a fatigue experiment, failure for a given material at a set stress may occur at any point along a range of cycles, depending on when he or she deems failure has occurred. This vague definition of fatigue can be overcome through the use of a linear elastic fracture mechanics (LEFM) approach to fatigue.

2.3.2 Fracture Mechanics - Linear Elastic Fracture Mechanics (LEFM) Approach

The study of how materials fracture is known as *fracture mechanics* and it is this branch of engineering which can contribute to the understanding of material failures, be they generic or unique to a specific component, to be investigated and understood [10].

The principles of fracture mechanics allow for a quantitative approach to be used in calculating the critical limit at which fast fracture will occur. This quantitative approach facilitates the relating of flaw size, effective stress and fracture toughness in determining the point at which fracture will occur. This functional relationship between these measurable properties is best represented by the *Triangle of Integrity* depicted in Figure 2.3 [11].

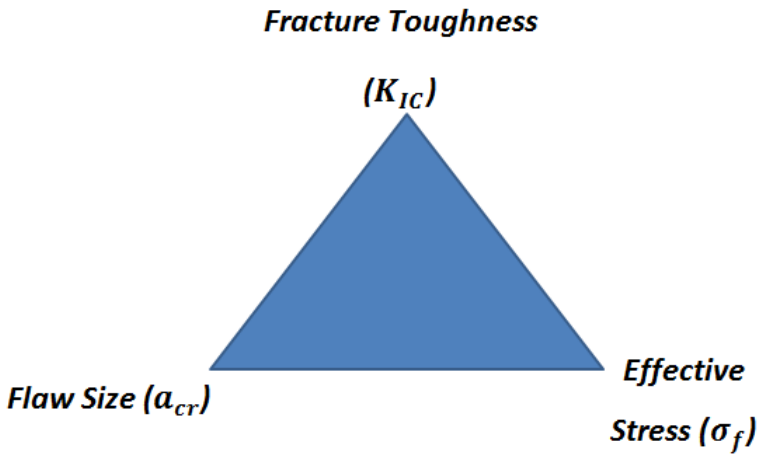

Figure 2.3: Triangle of Integrity

This functional relationship can be characterised by the Equation [12]:

$$K_f = Y\sigma\sqrt{\pi a} \tag{2.1}$$

Where:

K_f: Stress Intensity Factor (MPa$\sqrt{m}$)

σ: Applied Stress (MPa)

a: Flaw Size (m)

Y: Dimensionless Correction Factor/Compliance Function

The parameter K_f is termed the *stress intensity factor* and represents the local stress near the crack tip under elastic loading. Generally, a cracked body can be loaded in one or any combination of the three modes of crack surface displacements for which stress intensity factors can be calculated. These three modes of crack surface displacement can be seen in Figure 2.4. Mode I represents a purely tensile field crack opening whilst modes II and III are in-plane and anti-plane shear modes respectively. In practice, the most commonly found failures are due to cracks propagating is crack opening mode I [6]. This study will focus on crack opening mode I, and hence any stress intensity factors used will be based on this mode of crack opening.

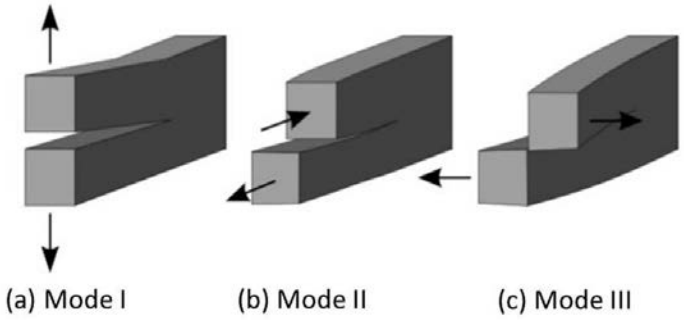

Figure 2.4: Three Modes Associated with Crack Growth: a) Tensile; b) In-plane Shear; c) Anti-plane Shear [13]

When this stress intensity factor K_f, reaches or exceeds some critical fracture toughness value, K_{IC}, which can be determined through experimentation, fast fracture will occur [10]. The LEFM approach defines the point of fast fracture as the point where the stress intensity factor, K, reaches or exceeds the critical toughness value, K_{IC}. This allows us to determine at what length a crack (a) will become critical (a_{cr}) for a given material toughness and applied stress.

As the types of loading and geometries vary for different components, a dimensionless correction factor, Y, is introduced into the equation to account for these differences [14]. For standard loading conditions and component geometries, Y can be obtained from standardised handbooks such as *The Stress Analysis of Cracks Handbook* by Tada, *et al.* [15] and typically ranges between 1 and 3.

Fracture mechanics is based on the assumption that all engineering materials contain flaws or cracks, at which an applied stress will concentrate (so they act as stress raisers) and thus initiate failure. These defects are usually found on the external surfaces of engineered components, where applied stresses are generally higher, but can also be found within the component as voids and cracked second phase particles [16]. After the initiation of a crack, a major part of the fatiguing process is spent in the propagation of the crack through the engineered component under cyclic loading, until some critical length is reached, after which the final fracture of the component occurs. This fatiguing process is classified into three stages, namely: (I) crack initiation; (II) crack propagation; and (III) final fracture.

Crack Initiation - Stage I

Crack initiation usually occurs from a specific initiation site in the material that has a localised stress concentration higher than the stress of the surrounding material. These initiation sites can be attributed to any number of factors including: manufacturing flaws and defects, notches, corrosion causing damage to the surface of the material, component wear, etc. Even in the absence of a surface defect, crack initiation will eventually occur due to the formation of persistent slip bands within the material, caused by irreversible dislocation movement.

A dislocation is a crystallographic flaw or irregularity within the lattice structure of a metal. Upon the application of stress to the metallic component, dislocations can move along favourable crystallographic planes in the lattice of a metallic structure, known as slip planes. As stress values greater than the yield strength are experienced, the number of dislocations locally increase. The dislocations interact with one another as they move along slip planes and have a tenancy to pile up at obstacles, such as grain or phase boundaries, inclusions and particles. Strain localisation then occurs when the dislocation pattern in a few of these pile-ups becomes locally unstable at a critical stress or strain, thus leading to the formation of persistent slip bands. The subsequent deformation is concentrated in these slip bands as they increase in number and fill the volume of the metal lattice. Persistent slip bands get their name from the fact that traces of these bands are always present within the material as they will re-form even when surface damage has been polished away [16]. The back and forth movement of the persistent slip bands (due to cyclic loading) leads to the formation of intrusions and extrusions on the surface of the component, so causing

irreversible plastic damage. Intrusions raise the localised stress on the component surface further, and thus typically act as the site from which fatigue cracks can initiate. Cracks are formed as these slip intrusions deepen by the continual back and forth movement of the material [10]. The intrusions and extrusions formed by the back and forth movement of a material along its slip planes can be seen schematically in Figure 2.5.

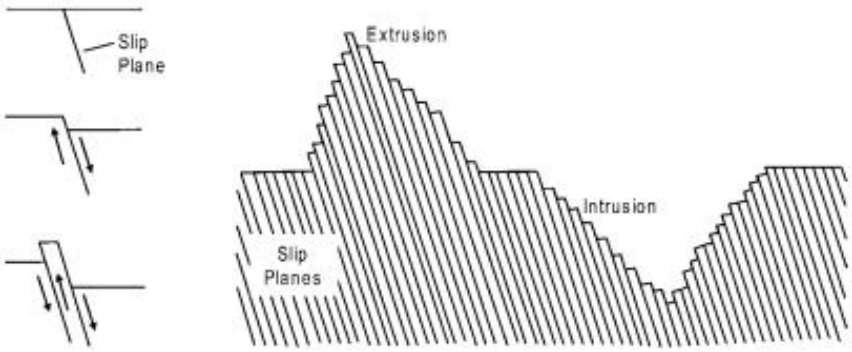

Figure 2.5: Intrusion and Extrusion Development during the Fatiguing Process [16]

Crack growth will occur in a favourably orientated direction in the microstructure of the material, usually parallel to the slip bands. The crack formed will eventually become large enough that the microstructure has a reduced effect on the crack direction as the stress field at the tip of the crack becomes dominant and metallic grain boundaries and other irregularities have a reduced effect on the rate of crack propagation through the material. The crack plane changes and propagates in a direction normal to the maximum principal stress direction [10]. This change in crack growth direction is referred to as stage II growth.

Crack Propagation - Stage II

Stage II growth has attracted the greatest attention in literature as it is the easiest of the three stages of crack growth to quantify, especially with the aid of fracture mechanics. As sophisticated detection techniques are required to identify cracks in the initiation phase (stage II cracks can be identified with the aid of a simple microscope), it is assumed that the lifetime of fatigue cracks is the total number of cycles endured in stage II [17].

Stage II crack growth is relatively stable (growth is unaffected by changes in the microstructure of the material i.e. grain boundaries do not hinder the direction of crack growth) and is governed by a continuum mechanism so allowing it to be characterised by applied mechanics. The transition from micro to macro crack growth is known as stage II growth and occurs when the stage I crack

growth direction changes, causing the crack to propagate in a direction normal to that of the applied stress. Crack propagation during stage II often, but not always, produces striation marks on the material surface along which the crack grows [16]. These striation marks indicate the position of crack fronts on successive load cycles.

Initially, the crack growth rate is slow but increases as the length of the crack grows. The crack growth rate also increases if the applied stress increases. Characterisation of the crack growth rate makes it possible to estimate the life of a component or the required component inspection intervals. Fracture mechanics facilitates the correlation of the crack growth rate with the cyclic stress intensity factor, ΔK [16]. An idealised curve of this relationship showing the typical crack growth behaviour of a material subjected to a constant cyclic load can be seen in Figure 2.6.

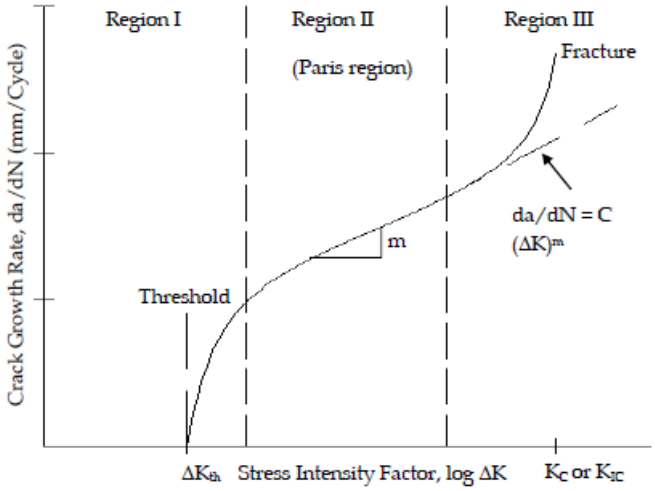

Figure 2.6: Crack Propagation Curve [7]

Region I (stage I) crack growth, as can be seen in Figure 2.6 above, has very low crack growth rates, typically below 10^{-10} m/cycle [17]. Region III (stage III) crack growth rates increase rapidly with increasing $\triangle$K, towards the final fracture of the component [7].

Region II (Stage II) growth is generally stable and almost linear in nature and can be described by the *Paris-Erdogan Law* [16]:

$$\frac{da}{dN} = C\triangle K^m \tag{2.2}$$

Where:

$\frac{da}{dN}$*: Crack Growth Rate (m/cycle)*

C: Material Coefficient

m: Material Coefficient (usually between 2 and 4)

$\triangle K$: Difference between the Maximum and Minimum Stress Intensity Factors (MPa$\sqrt{m}$)

This simple empirical relationship can be used to determine the total life of a component if the stress amplitude remains approximately constant and the maximum crack size is known. If the stress amplitude varies, then the crack growth rate may change drastically from the simple power law as shown by the above Equation 2.2. Occurrences such as crack closure and single overloads can affect the crack growth rate drastically. Elber [18] observed that cracks can physically close behind the crack tip by the contact of the cracked surfaces, even under a nominal tensile load. Crack closure mechanisms effectively reduce $\triangle$K during cyclic fatiguing so reducing crack growth rates. Crack closure is generally caused by four mechanisms including plasticity-induced closure, roughness-induced closure, oxide-induced closure and fluid-induced closure [16].

Plasticity-induced closure resulting from compressive residual stresses developed in the plastic wake of a developing crack, as the fatiguing process forces crack surfaces together. Roughness-induced closure arises due to the rough nature of the fracture surfaces of an advancing crack which comes into contact at some point during crack propagation. Oxide-induced closure results from the continual breaking and reforming of the oxide layer behind the rack tip resulting in debris becoming wedged in the crack interface. Finally, fluid-induced closure results from fluid pressure acting as a wedge as the crack is filled up with fluid from its surroundings. This fluid wedges open the crack during the unloading cycle of the fatiguing process and in all closure cases prevents the crack tip from experiencing the full cyclic load [16].

Environmental effects, such as changes in the concentration of corrosive agents within the environment, can also affect the crack growth rate and will be discussed later on in the Chapter. [16].

The theoretical fatigue life of an engineered component can be calculated by integrating the number of cycles endured by a fatigue crack during stage II. This is done by substituting Equation 2.1 into Equation 2.2 as follows:

$$\frac{da}{dN} = C\left(\Delta\sigma Y\sqrt{\pi a}\right)^m \tag{2.3}$$

Where:

$\frac{da}{dN}$*: Fatigue Crack Growth Rate (m/cycle)*

C: Material Coefficient

m: Material Coefficient (usually between 2 and 4)

$\Delta\sigma$: Applied Cyclic Stress (MPa)

a: Flaw Size (m)

Y: Dimensionless Correction Factor/Compliance Function

Equation 2.3 can be rearranged so as to separate both terms of the fatigue crack growth rate expression, as shown by Equation 2.4, and then integrated from the initial flaw size (a) to the critical flaw size (a_{cr}) so as to obtain the total number of cycles to failure for a component, as shown by Equation 2.5.

$$dN = \frac{da}{C\left(\Delta\sigma Y\sqrt{\pi a}\right)^m} \tag{2.4}$$

$$N = \int_{a_i}^{a_{cr}} \frac{da}{C\left(\Delta\sigma Y\sqrt{\pi a}\right)^m} \tag{2.5}$$

Where:

N: Total Number of Cycles to Failure

a: Flaw Size (m)

a_{cr}: Critical Flaw Size (m)

a_i: Initial Flaw Size (m)

da: Integrand to be Integrated Over

m: Material Coefficient (usually between 2 and 4)

C: Material Coefficient

$\Delta\sigma$: Applied Cyclic Stress (MPa)

Y: Dimensionless Correction Factor/Compliance Function

The number of cycles to failure is dependent on how early the crack within a component can be detected. Crack detection can be undertaken by any number of non-destructive testing (NDT) means. Flaw containing components can remain in service if inspected regularly, so as to ensure that the crack or cracks contained within the component do not exceed the critical crack length.

Final Fracture - Stage III

Growth within the final stage usually makes up a small percentage of the total lifetime of the component and thus is often ignored when calculating the total number of cycles that make up the lifetime of a component [10]. The onset of final fracture is characterised by the stress intensity factor of the component's material equalling and then exceeding the critical fracture toughness value for the material. This is the point at which the crack length becomes critical and the remaining cross section of the component can no longer support the applied load. Crack growth rates increase significantly resulting in fast fracture and subsequent failure of the component.

2.3.3 Factors Affecting Fatigue

a) Surface Quality

Most fatigue failures occur at the surface of a component, which often contain sites of stress concentrations. Crack nucleation is facilitated at micro-crevices and grooves on rough surfaces both of which act as stress concentration sites. Nominal stresses are also typically higher at the surface of a component (i.e. due to bending). These areas of stress concentration on the surface of a component permit local permanent plastic deformation at nominal stress levels. This is because surface grains are not wholly supported by adjoining grains as is the case with grains inside the body of a component [19].

Typical surface factors that act as stress raisers include scratches, pits, fretting fatigue and machining marks. It can be noted that surfaces effects that influence fatigue life include all conditions that can both reduce or enhance fatigue life, by influencing crack initiation mechanisms [19].

For most applications, the surface layer exhibits the highest stress levels in a component. This is aided by the fact that surface layers typically exhibit plane stress conditions (as the stress through the relatively thin surface layer does not vary appreciably) and thus there can be no stress normal to the free surface of a component [20]. This plane stress condition eases the initiation of microplasticity at the surface and is promoted by stress concentration sites.

A major factor in fatigue initiation at the surface is the phenomenon of slip irreversibility. Plastic deformation at the surface, caused by cyclic loading, is only partially reversible. Each loading cycle causes a small amount of fatigue damage, mainly due to the fact that oxygen is absorbed at the fresh metal surface of emerging slip bands (extrusions) so preventing these bands from moving back into their original position during the next phase of the cycle [20].

Three parameters are used to describe a material's surface quality. These parameters are: surface roughness, residual stress and microstructure (the latter two and their influence on a component's surface will be discussed in detail in the following two sections). In designing engineered components, the effects of these parameters are accounted for by introducing empirical reduction factors which modify the endurance limit for the material [19].

As the surface finish of components can often be controlled during the design phase (as opposed to other factors such as environmental influences, which cannot always be controlled), it is frequently considered by designers when trying to increase the fatigue life of a given component.

Surface roughness implies that the free surface of a component is no longer perfectly flat. This non-linearity results in small sized stress concentration sites occurring across the component's free surface. These stress concentration sites can be significant enough to promote cyclic slip and crack nucleation on a components free surface. The effect of surface roughness on a component fatigue life was shown by De Forest [21], who performed rotational bending tests on steel test specimens with two different surface roughness's, namely coarsely machined surfaces and finely machined surfaces. De Forest periodically interrupted his tests to observe possible crack growth, defining the crack initiation period as the time it took for a crack to grow 2.5 mm. The crack growth period lasted from an observable crack length of 2.5 mm until the failure of the component. De Forest's results clearly show that crack initiation life is significantly shorter for the specimens with the rough surface finish. The crack growth period was however hardly affected by the tests specimen's surface finish. De Forest also concluded that if stress amplitude is reduced, fatigue life is increased. At high stress amplitudes, cracks can be initiated early in the fatigue life of a component, regardless of any surface damage. Therefore at low stress amplitudes, the effect of surface damage is more profound on a component's fatigue life [22]. A graph summarising De Forest's results can be seen in Figure 2.7.

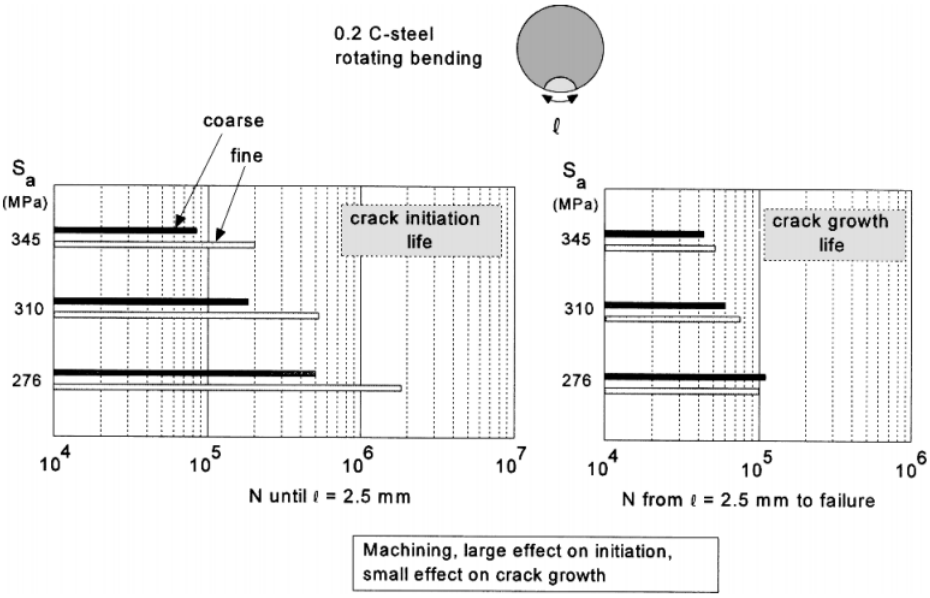

Figure 2.7: Effect of Surface Roughness on Crack Initiation and Growth Period, as found by De Forest [21]

b) Residual Stress

The majority of engineering components contain stresses, of variable magnitude and direction, even before being subjected to service loading conditions [23]. These stresses are termed residual stresses and can significantly affect the fatigue life of a component, by either increasing or decreasing it. Residual stresses can be induced into a component unintentionally, for example during welding, or deliberately through processes such as from shot peening and laser shock peening. Residual stresses can occur through a variety of mechanisms including plastic deformations, temperature gradients or structural changes [24].

Residual stresses generally arise when conditions in the outer layer of the material differ from the inner layer of the material. These residual stresses are locked into the component and act as a datum stress over which service induced stresses are superimposed [23]. This superimposition of stresses can prove to be beneficial to an engineered component. If the residual stresses are opposite in direction to the service stresses then some part of the service load goes towards reducing the residual stresses, so increasing the fatigue life of the component. If however, the residual stresses are in the same direction to the applied stresses (i.e. both stresses are tensile), then a smaller service load is required to produce fatigue crack initiation or failure than would have been the case if there was no residual stress in the component from the start [23]. Residual tensile and compressive stresses must always occur together as they must ultimately balance each other out and the structure be in equilibrium in the absence of an external load. It should be noted that for

this equilibrium to occur, the loads and moments placed on a component must balance; this does not mean that the stresses are the same but rather that the loads (stress multiplied by area) are balanced. Typically surface treatments, such as shot peening, lead to high compressive stresses over a small surface area, which are easily balanced by small internal tensile stresses, which are applied over a much larger area. A typical residual stress profile induced by a mechanical surface treatment can be seen in Figure 2.8.

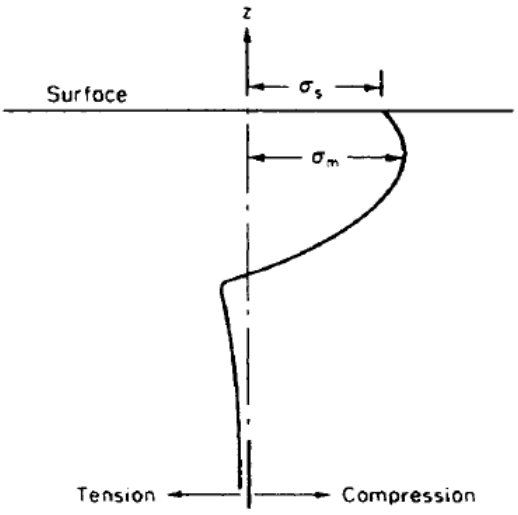

Figure 2.8: Typical Residual Stress Profile after a Mechanical Surface Treatment Profile [23]

In the past, design procedures tended to incorporate large safety factors in the design of components so as to mask the effect of residual stress. However, with drives for economy of manufacture coupled with the strict safety and reliability standards of today, residual stresses are no longer ignored, with many designers looking to incorporate them into the design and subsequent manufacture of components [23].

Compressive residual stresses, typically introduced into a component through mechanical processes, are well known to enhance the fatigue performance and corrosion resistance of components by retarding and even suppressing micro crack growth from the surface into the interior [25]. Processes, such as shot peening, introduce plastic deformation into the surface layer of engineered components, resulting in the formation of residual compressive stresses in a thin layer on the surface of the component. Residual stresses do not however affect the cyclic shear stress imposed on a component and thus cyclic slip may still occur. However, cracks that do arise from cyclic slip tend to grow very slowly. This is because the residual stresses introduced into the component retard the opening of crack tips (i.e. crack tip closure), so lowering the stress concentration at these crack tips [22].

Some of the processes used in introducing residual stresses into an engineered component are further discussed in the next section of the literature review.

With modern analytical and computational techniques, it is often possible to estimate the stress to which a component is subjected to in service component [26]. This however is not sufficient for the reliable prediction for component performance in these service conditions. In many cases, the presence of residual stresses within a component can lead to catastrophic and often unexpected failure of the component. Today, there are a large number of residual stress measurement techniques that can be used to accurately determine the magnitude of the stresses within a component, both before and during it's service life [26]. Some of these techniques are destructive processes whilst other techniques can be used without altering the physical state of the component. Typical methods used in measuring residual stress include: mechanical, magnetic, electrical, chemical, ultrasonic, thermoelastic, thermoplastic and diffraction methods [26]. Of these methods, the most frequently applied are the hole drilling (mechanical) and X-ray diffraction measurement procedures. These two procedures are described further in this literature review.

Residual Stress Measurement Techniques

(i) X-ray Diffraction

X-ray diffraction is a non-destructive technique used for measuring both the residual stress and plastic strain in a component and is generally restricted to specialist measurements in a laboratory. The diffraction method measures the diffraction angle (Θ) of X-ray beams used to bombard the atoms of individual crystals within a polycrystalline metal structure, at certain incidence angles (known as Bragg angles). Using these angles (Θ) and the known wavelength of the X-ray beam, the inter-planar spacing between the atoms can be obtained using *Bragg's Law* [26], which is defined as:

$$\lambda = 2d \times sin\theta \tag{2.6}$$

Where:

λ: X-ray Beam Wavelength (m)

d: Interplanar Spacing (m)

θ: Diffraction Angle (degrees)

A simplified illustration of X-ray beams (at an incident angle of θ and of a wavelength λ) encountering the individual atoms (separated by a distance d from one another) within a crystal lattice

structure and subsequently scattering upon contact can be seen in Figure 2.9. Most of the scattering that occurs interferes with itself resulting in destructive interference. However, diffraction can and does occur when scattered x-ray beams are in phase with rays that have been scattered from other atomic planes [27]. Under this condition, constructive interference occurs resulting in enhanced wave fronts, known as diffraction peaks or Bragg peaks, whose diffraction is governed by *Bragg's Law.*

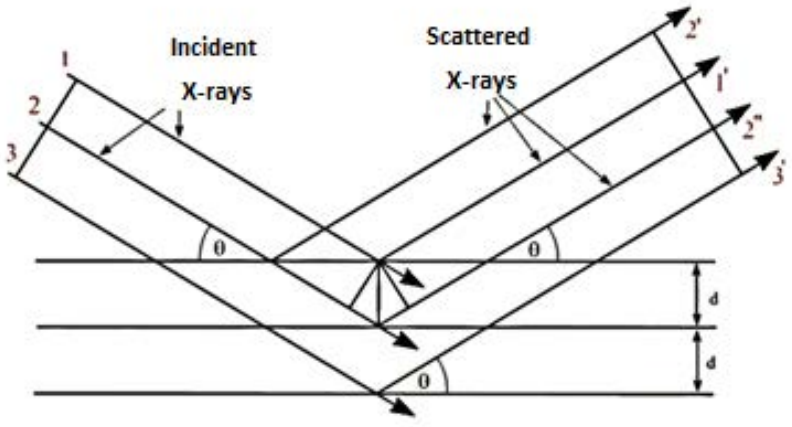

Figure 2.9: Diffraction of Incoming X-ray Beams within a Polycrystalline Metallic Structure [27]

There is a clear relationship between the diffraction pattern, which is observed when X-rays are diffracted through a crystal lattice, and the distance between atomic planes within the material being tested. The inter-planer spacing of a stress free material will produce a characteristic diffraction pattern for that material [28]. When that same material is strained through the application of a stress (residual or applied), elongations and contractions are produced within the crystal lattice structure, changing the spacing of the (*hkl*) lattice planes. The induced change in the distance between the atomic planes will cause a shift in the diffraction pattern. Through measuring this shift from an unstrained lattice structure, the inter-planar spacing can be measured and thus the strain of the material can be calculated.

(ii) Hole Drilling

The hole drilling method of residual stress measurement is typically used when residual stress measurement is required for non-crystalline materials, large grained materials or heavily deformed materials [29]. Hole drilling and other mechanical stress measurement techniques are generally based on the same principle. These methods rely on the monitoring of changes in component distortion, either during the generation of the residual stress or afterwards by deliberately removing material to allow the stresses to relax. [26]. The hole drilling method relies on the stress relaxation

of a material when a hole is drilled into a material through the centre of a rosette strain gauge. When material is removed by the drilling process, the extent of the strain relief is monitored by the strain gauges and the direction and magnitude of the principal stresses can be calculated based on the movement experienced by the gauges. At each depth increment, the stress relief on each of the gauges within the rosette is measured and converted into stress. As subsequent material removal occurs, the stress distribution as a function of depth can be estimated [30]. The hole drilling method is cheap and widely used, with standardised test procedure well established for the process. The process does however also have its disadvantages. It is difficult to obtain stress measurements beyond a depth equal to the diameter of the hole. If three strain gauge rosettes are used it is only possible to measure the two in-plane components of the stress field. Of particular concern is that the method only works for residual stresses equal to or less than 50% of the material's yield strength. If residual stresses exceed this value, localised yielding may occur leading to errors in the data readings obtained [26].

c) Material Effect on Fatigue

Material inhomogeneities such as grain size, pores, and non-metallic inclusions can govern both the fatigue initiation and propagation processes. These micro level defects are not yet fully considered in fatigue crack growth analysis models, as discussed earlier. These defects can lead to non-homogenous stress distribution through the component and are thus one of the main reasons for the wide scatter seen during most fatigue tests [31].

Many of the microstructural effects observed during fatigue crack propagation can be linked to a prominent role in crack closure (cracks may temporarily stop propagating or slow down so leading to a decrease in the overall crack growth rate), particularly at near threshold levels. The principle microstructural variables affecting closure and low growth rates are grain size, precipitate type and distribution, slip characteristics and, in duplex structures, the proportion and morphology of the two phases. Many of the microstructural variables effectively act as barriers to crack propagation, slowing down the crack growth driving force by deviating the path of crack propagation through a component and causing roughness induced closure, where there is a mismatch between the upper and lower faces of the crack resulting in contact. In many cases, optimising these variables in an attempt to maximise fatigue life for both engineered components and structures, can have the opposite effect on other mechanical properties such as toughness, ductility, and resistance to crack initiation [32].

During the fabrication of many components, the development of natural defects such as pores and non-metallic inclusions are almost unavoidable. Some defects, including pores (voids/cavities)

and non-metallic precipitates, act as stress raisers, which in turn can facilitate crack initiation. Both pores and precipitates can also allow for rapid crack propagation through a material as they allow different micro-cracks to link up rapidly within the component. Pores are typically the result of non-uniform solidification during a casting process, caused by either gas encapsulation or shrinkage. Other types of non-metallic inclusions may have different elastic properties or different coefficients of expansion when compared to the parent material, which can act to raise the mechanical stress in the vicinity of the interface during loading, eventually leading to crack initiation [20].

d) Specimen Geometry

In most engineered components that develop fatigue cracks, cracking usually initiates at stress concentration sites, as mentioned previously. Engineering components often contain discontinuities, which arise as part of their design, in the form of holes, notches, joints, grooves, fillets, threads, keyways etc. The stress at each of these discontinuities is likely to be greater than assumed or calculated value and as such act as stress raisers. The fundamental mechanisms of crack initiation and growth are similar to those presented earlier in this Chapter. It is important that designers understand the role that geometric features can have on the life of their design by introducing stress concentration factors to the nominal stresses, which act on the components they are designing.

Notches and holes within engineered components are often unavoidable as they are required for component functionality. The presence of a notch introduces an increase in the stress concentration at the root of the notch. Stresses around the edges of a hole are significantly greater than those found elsewhere in the component. The effect that a notch or hole has on the stress concentration within a component can be accounted for by using a stress concentration factor, which can be multiplied with the stress applied to a component, resulting in a stress value that accounts for holes/notches and can be used in subsequent fatigue analysis [23].

Stress concentration factors vary for differing component geometries and loading conditions. Graphs relating stress concentration factors to different geometrical feature sizes and loading conditions can be found in published data and used to determine stress concentration factors relatively accurately without the need for experimentation. Fatigue strength is also influenced by the specimen size/volume. This is because the larger the volume of material (for the same stress), the higher the number of possible stress concentration sites, and thus when subjected to an alternating stress, the higher the probability of crack initiation occurring at one of the stress concentration sites.

2.4 Fatigue Alleviation Techniques

Fatigue life improvement for engineered components can be achieved through various post-manufacture surface treatments. It is well known that fatigue failures most often develop from the surfaces of engineered components and thus treatment of these surfaces can help prolong the fatigue life of such components. Some of the more basic treatment processes include flame hardening [33, 34] and induction hardening [34], which are commonly referred to as surface heat treatments, carburizing [35, 36] and nitriding [37, 38] which are both forms of case hardening, and roller burnishing [39], which is a cold working mechanical surface treatment. This section will focus on and analyse the mechanical surface treatment processes of shot peening and laser shock peening as a means of fatigue life enhancement, as these treatment techniques will form the basis of this project. Each treatment process employs at least one of the following [31]:

- Reduction of local stress concentrations
- Removal or neutralisation of existing defects
- Reduction of tensile residual stress through the introduction of compressive residual stress

2.4.1 Shot Peening

a) General Process and Methodology

Shot peening is a cold working process in which the surface of an engineered metal component is bombarded with small spherical media, called shot, by means of an air blast or rotating wheel. Each piece of shot acts as a small peening hammer and imparts a small indentation (dimple) on the surface of the component being treated. In order for the dimple to be created, the surface of the metal component must yield in tension, so creating a region of plastic compression deformation surrounded by a region of elastic deformation [40]. This shot peening process changes the state of the surface in terms of residual stress, microstructure, hardness, surface roughness, cracks, crystallographic texture and dislocation density [26]. The principles of the process can be seen in Figure 2.10.

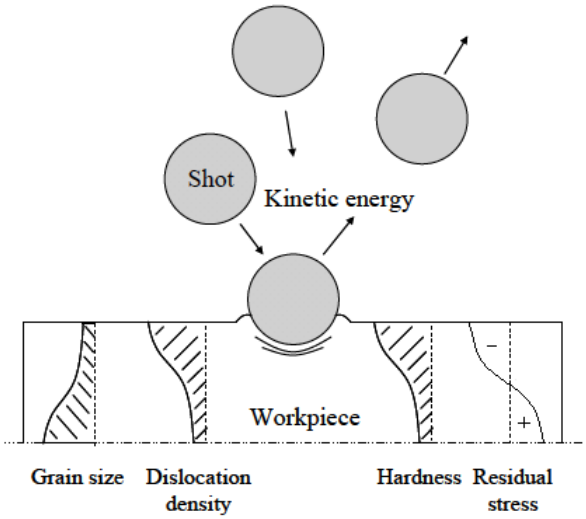

Figure 2.10: Impact of Shot on Metal Surface resulting in Localised Yielding [25]

Below the surface of the component, the compressed metal grains produce a hemisphere of work hardened metal which is highly stressed in compression. This can be seen schematically in Figure 2.11. Multiple shot impacts on the surface of a metal result in the formation of overlapping dimples so producing a uniform layer of compressive stress [40].

Figure 2.11: Residual Stress Formation during Localised Surface Compression [40]

Shot peening is one of the most economical and practical means of extending the fatigue life of an engineered component. The compressive stresses induced in the surface layer of a component delay crack initiation and reduce crack propagation rates, by effectively pushing the grains of the surface layer together. The magnitudes of the residual stresses produced by a shot peening process are at least as great the tensile strength of the material being peened [40]. Shot peening can be used on any shaped component and geometrical feature, where line of sight to the surface area of the component to be peened is possible.

b) Equipment Used in the Process

Generally, and in the case of the South African shot peening industry, there are two main types of shot peening processes used, both of which utilise two different machine types. One process utilises air blast machines to propel shot towards a component is to be peened, whilst the second process utilises a centrifugal wheel to impart a rotational force on the shot so propelling it towards the component being peened.

The main difference between centrifugal and air blast machines is that the air blast machines tend to propel each shot particle at a higher velocity and thus higher intensity than the centrifugal wheel machines do. However, the centrifugal method of shot peening produces a blast pattern that contains a greater number of shot particles, meaning that the centrifugal method of peening can produce a greater throughput than the air blast method. If the centrifugal method is required to impart the same peening intensity as the air blast method, larger shot size can be used. The blast pattern of the centrifugal method is however not uniform as shot velocities vary from the centres to the edge of the blast stream. This can be overcome by peening components to saturation [41].

Air blast systems require tight regulation and control on a number of adjustable processes that are part of the systems so as to ensure the reproducibility of required peening intensities. Air pressure regulation ensures that any peening intensity can be reached when combined with an appropriate shot size. The feeding rate of the shot is also important and needs to be controlled and steady. The orifice, through which the shot passes, needs to be able to adjust for different sized shot whilst still maintaining an appropriate flow rate [40].

Centrifugal systems are the more common shot peening technique as well as the most economical. This process has evolved from using flat turbine blades on the centrifugal wheel to using tubular impeller blades. These impeller blades offset the slowing down caused by air drag when a shot is propelled from the wheel. The peening intensity at the centre of the blast pattern is much greater than the blast pattern created by a flat turbine bladed wheel. The distribution of the blast pattern also has a larger area of high intensity shot when compared to the bladed wheel and this is especially noticeable with finer shot [40]. Centrifugal machines are generally used for heavy peening applications, where large components need to be processed. Examples include coil springs, torsion bars and leaf springs. For delicate and small components such as valves, push rods and rocker arms, air blasting systems are generally preferred [40].

c) Factors Affecting Process Quality Control

In order to understand the controlled shot peening process, the various factors governing the consistency of the process need to be understood. This process is summarised in Figure 2.12. The dashed line represents a division between process inputs and process outputs.

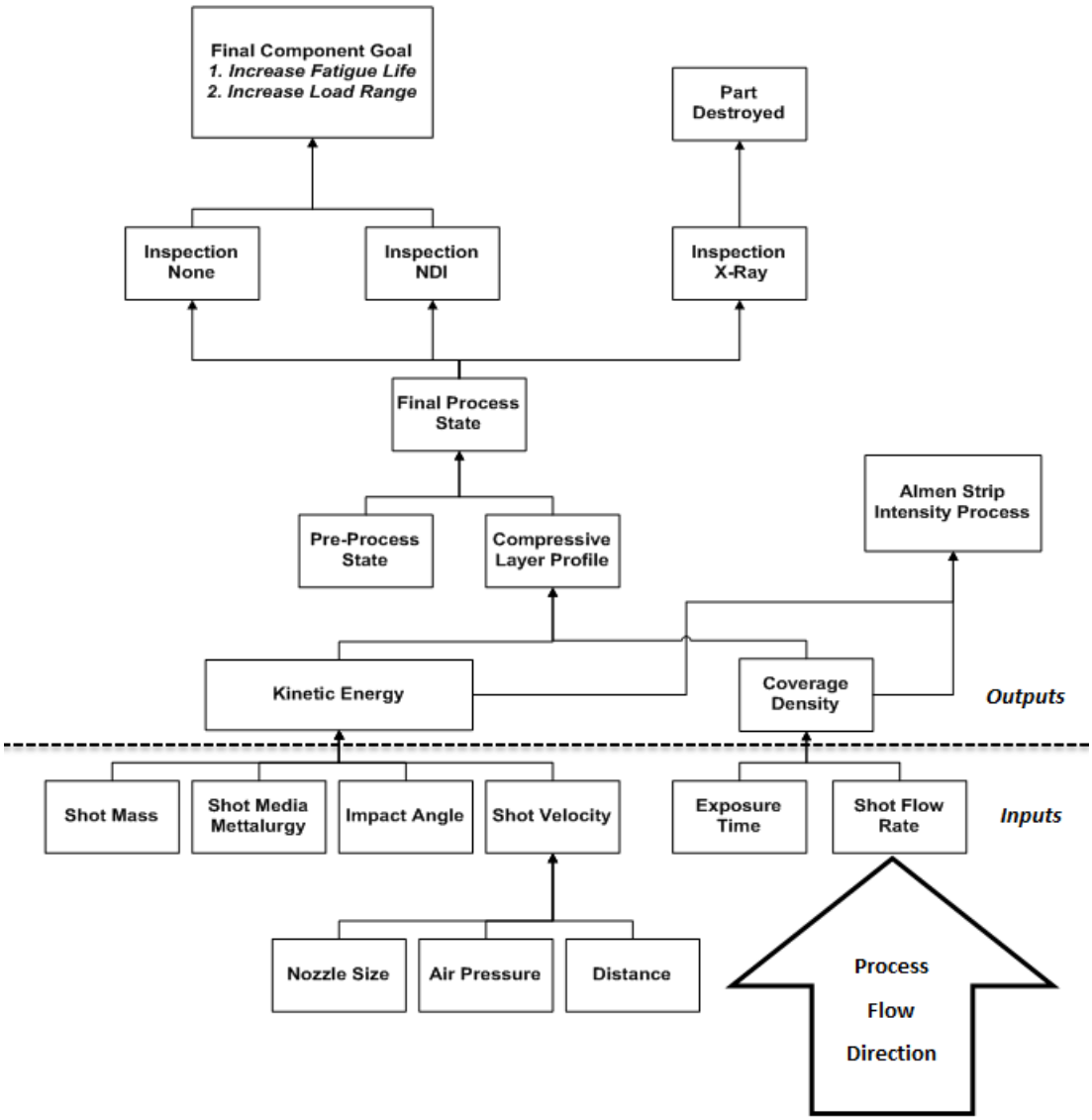

Figure 2.12: Controlled Shot Peening Process [42]

i) Media Material

In a typical shot peening process, small spheres of either cast steel, carbon steel conditioned cut wire, stainless steel conditioned cut wire, ceramic or glass beads are used to bombard engineered components. Cast or carbon steel is the most often used type of media. However, if iron contamination of the surface is a factor (ferrous contamination of a non-ferrous surface) of concern,

stainless steel, ceramic or glass beads media can be used instead [40].

Carbon steel cut wire, which is conditioned into near round shapes (cut steel wire is blasted against plates in order to blunt sharp edges), is being increasingly used on an industrial scale as it has a uniform and wrought consistency coupled with great durability. It is also available in various grades of hardness and its manufacturing process results in a tighter size control than typical cast steel shot [40].

Glass beads are typically used when iron contamination is of a concern (for non-ferrous materials). The glass shot is generally lighter and smaller than other forms of shot and can be used to peen the sharp radii of threads and delicate areas of components, where low intensities are required. Both glass and ceramic beads help preserve surface integrity and allow for relatively smooth surface finishes when compared to other metallic types of shot media [40].

The hardness of the shot media influences the magnitude of the residual compressive stress imparted on an engineered component during the shot peening process. The peening media must be at least as hard as or harder than the component it is peening in order to impart a satisfactory residual stress on a peened component [40]. That is unless the surface finish of the component is critical.

ii) Media Shape and Size

Peening media is primarily spherical in shape, as edged media can potentially inflict surface damage upon impact. Figure 2.13. shows both desirable and undesirable shot media shapes.

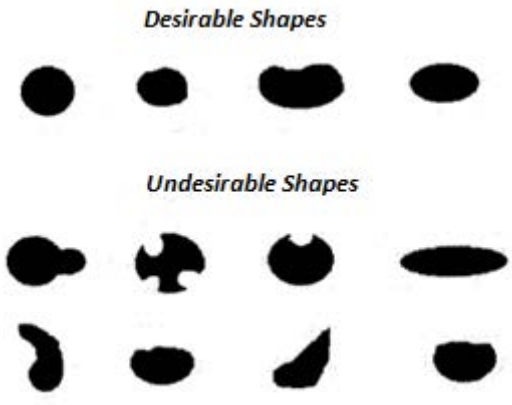

Figure 2.13: Desirable and Undesirable Shot Media Shapes [43]

Broken or damaged media must thus be removed from usage before damage to the peened component can occur through the re-use of this media in the peening process. This sorting process is

done automatically, using a stacked sieving process, where media is poured through sieves with different sized holes and sorted accordingly. A spiral separator can also be used, where shot media rolls down a cone with an inner and outer flight. Spherical media will gain velocity more quickly than non-uniform media and move to the outer flight from where it can be reused. Broken shot media will remain on the inner flight from where it can be discarded [41]. In Figure 2.14, surface damage from broken media can be seen and compared to Figure 2.15 (below), which shows a peened surface using unbroken media.

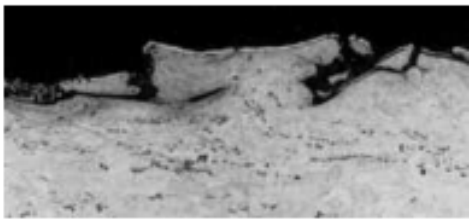

Figure 2.14: Surface Damage due to Broken Shot Media (100x magnification) [44]

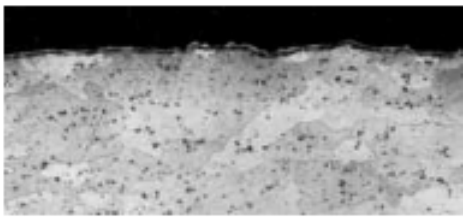

Figure 2.15: Surface Uniformity due to Unbroken Shot Media (100x magnification) [44]

Shot peening media must have a uniform diameter. The impact energy imparted by the media upon a surface is a function of the media's mass and velocity. As the shot size increases, so does its mass leading to an increase in impact energy, provided the velocity of the shot media remains constant. If a mixed batch of shot media is used for peening, larger media will form compressive residual stresses deeper in the component being peened. This in turn will lead to a non-uniform compressive residual stress layer leading to inconsistent fatigue behaviour [44]. A rule of thumb is that the shot size should be small enough to fit inside the smallest inside radius or fillet of the component being peened and should in fact have a diameter less than one-third that of the fillet radius [41].

iii) Intensity

Shot peening intensity is a measure of the kinetic energy of a shot stream. Through controlling the intensity of a shot stream, and thus peening parameters, which influence intensity, process

repeatability, can be achieved allowing component fatigue behaviour to be relatively accurately modelled and thus predicted. The energy of the shot stream is directly related to the compressive stress imparted into a component [45].

Intensity control involves controlling the media size, hardness, shape, impingement angle, flow rate, exposure time, shot velocity and other factors, which can be found in Figure 2.12 above. Using larger media or increasing the velocity of the shot stream will increase the intensity of the shot peening process. It is impractical to count, weigh and measure the velocity and angle of the individual shot media used during the peening process.

A simple comparative technique has thus been designed to measure peening intensity by J.O Almen. Intensity is measured using Almen strips (typically made from flat strips of SAE1070 spring steel). One side of the Almen strip is peened, so causing the strip to deform into an arc towards the peened side due to the induced compressive stress from the peening process. By measuring the height of the arc, the intensity of the peening process can be calculated [45].

Three thickness's of Almen strips are typically used and denoted by the letters "N", "A" and "C". An *N* strip is 0.79 mm thick, an *A* strip is 1.29 mm thick and a *C* strip is 2.39 mm thick. The more aggressive the shot peening processes the thicker the size of the Almen strip used [45].

When peening intensity is measured it is important to subject the Almen strip to exactly the same peening conditions as will be experienced by the component to be peened. Almen strips are therefore typically clamped to blocks of tool steel, known as Almen blocks, which are passed through the blast stream in the same manner and relative position (Almen blocks can be clamped onto the desired locations of a component where peening intensity needs to be determined) as the component that is to be peened. After peening, strip heights are measured using a gauge. It is this value that is known as the Almen number and is a measure of the peening intensity [41]. A simplified version of the Almen strip process can be seen in Figure 2.16.

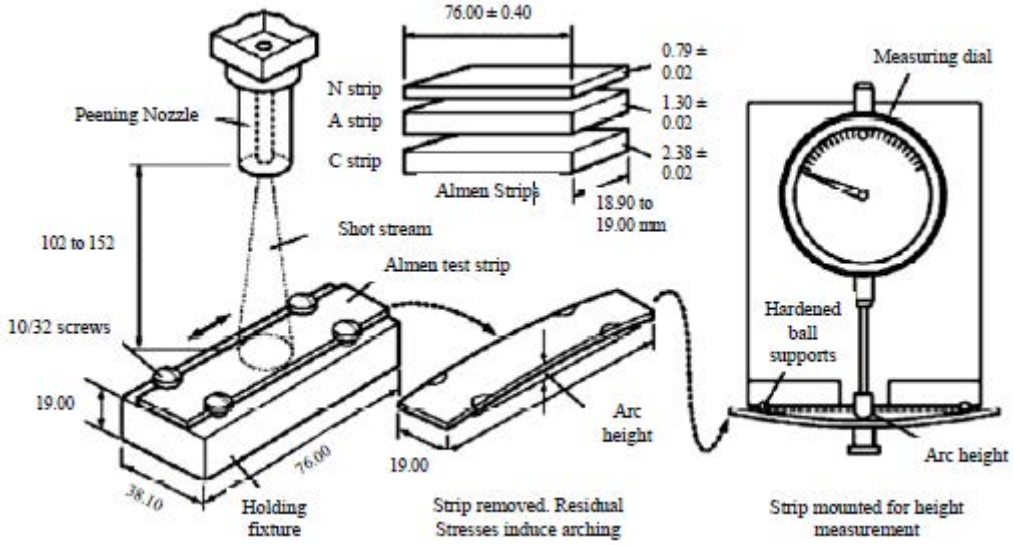

Figure 2.16: Almen Strip Intensity Process (dimensions in mm) [25]

Although peening intensity is dependent on a number of interrelated factors, the time a component is exposed to a shot blast stream is one of the more critical factors when it comes to peening intensity. In order to determine the time a component should be exposed to the shot peening process a saturation curve is developed. Saturation is defined as the earliest point on the curve where doubling the exposure time produces no more than a 10% increase in arc height. Saturation establishes the actual intensity of a shot stream at a given location on a component at fixed machine settings. The saturation curve is developed through shot peening a number of Almen strips at fixed machine settings in order to establish when the doubling occurs [44]. Figure 2.17. shows a typical saturation curve which shows that the doubling of time (2T) from the initial exposure time (T) results in less than a 10% increase in arc height. Thus intensity is reached at the initial exposure time of T [44].

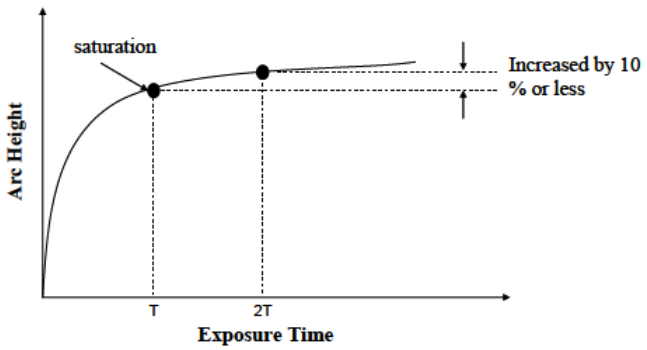

Figure 2.17: Typical Saturation Curve [21]

iv) Coverage

In order for a uniform residual compressive stress surface layer to be produced in an engineered component, uniform and total shot peening coverage of the engineered is essential. A peening process should state the percentage of coverage required for the given engineered component being peened. This coverage is typically estimated through inspection with the aid of a microscope or magnifying glass, where the number of peening impacts (in the form of dimples) can be calculated per unit of area. Most applications require 100% coverage as fatigue cracks can develop in the unpeened areas not encased in residual stresses [41]. A non-uniform layer of residual stress may also develop from uneven peening coverage, resulting in varying fatigue lives for similar components.

If coverage is specified as greater than 100% it means that the processing time to achieve the 100% has been increased by a certain factor i.e. percentage coverage of 200% means that a component has been shot peened twice at the same exposure time taken to reach a coverage of 100% [44].

d) Properties of Shot Peened Materials

The following properties discussed below are introduced of affected by the shot peening process. These properties will be analysed later on in this report for the various surface treatments to be utilised in this study.

i) Residual Stresses

The residual stress generated by the shot peening process is of a compressive nature. Deformation of the surface layers during the shot peening process involves the plastic flow of metal near the surface which in turn stretches the subsurface core. This results in the core of the material to try and force the deformed metal back into its original shape. This results in the surface of the material going into compression, leaving the core of the material in tension [46].

The compressive stress created by the peening process tends to offset or lower applied tensile stresses to the peened component. Simply put, less tensile stress equates to a longer fatigue life [40]. A typical shot peening stress profile can be seen in Figure 2.18.

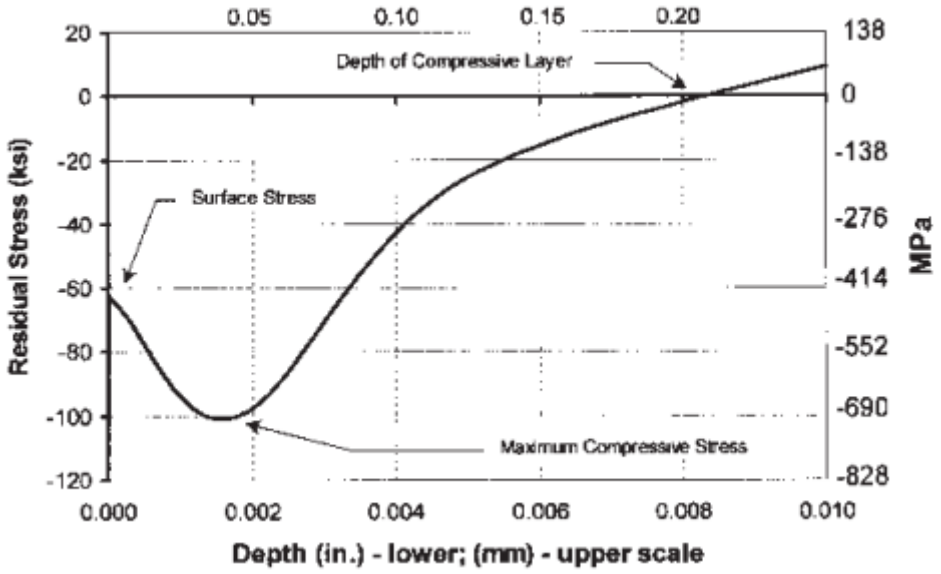

Figure 2.18: Residual Stress Profile Induced into a Material by a Typical Shot Peening Process [40]

The maximum compressive stress level is generated just below the surface of the peened material. As the magnitude of the maximum residual stress increases, so does the resistance to fatigue cracking of a peened component. The magnitude of the residual stress decreases as the depth of the compression layer increases. The depth of the compressed surface layer depends on the size of the shot used during the peening process and the degree of shot peening. For any hardness and given size of shot, the compression residual stress layer gets deeper as the peening process progresses. However, over peening a component should be avoided because this process will exhaust the ductility of the component material [47]. Figure 2.19. shows how the depth of compressive stress induced into a component increases with an increase in the hardness of the shot used to peen a component. Steel shot of a regular hardness lies in the range of 45 to 52 HRC (*Rockwell Hardness Number*) whilst high strength steel shot lies in the range of 55 to 62 HRC.

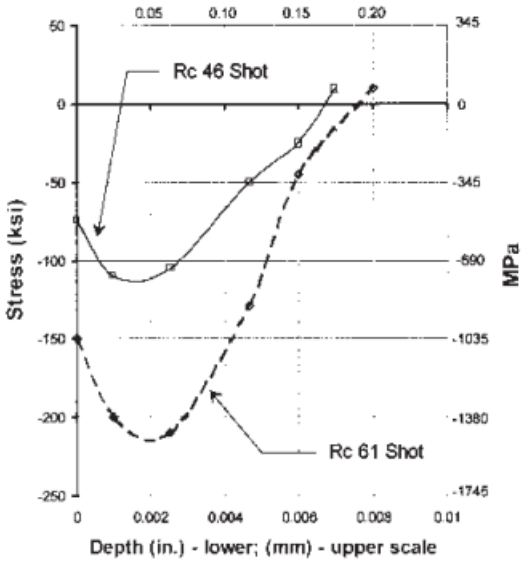

Figure 2.19: Depth of Compressive Stress in Relation to Hardness of Shot Media [40]

When a component is shot peened and subjected to an applied load at the same time, the surface of the component experiences the net stress resulting from the summation of the applied load and the residual stresses induced by the peening process. This interaction between the applied load and the residual compressive stress can be seen in Figure 2.20. The diagonal dashed line in the Figure is indicative of the tensile stress created from the bending process. The dashed curve line represents the residual compressive stress created from the peening process. The summation of the two dashed lines produces the solid curved line which shows a significant reduction in the tensile stress at the surface [40].

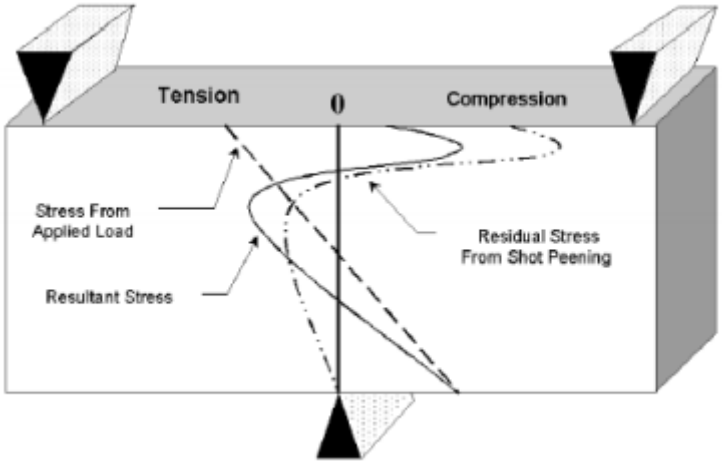

Figure 2.20: Resultant Stress in a Shot Peened Component under an Applied Load [40]

In practice, stress relaxation can occur. That is to say, residual stresses may be alleviated during loading. There are two main causes for stress relaxation, namely cyclic stressing and temperature. Cyclic stressing at levels above one-third the value of the material's yield strength leads to a reduction in the residual stresses imposed on a component during the peening process [48]. The relaxation of residual stresses with an increase in temperature can be a limitation on the application of the process. It was shown by J. Hoffman *et al.* that annealing a shot peened 0.45C normalised steel part at $400\,^{\circ}\mathrm{C}$ for half an hour reduced the stress at the surface of the material from 400 MPa to 200 MPa, but had little effect on stress levels below a depth of 20 μm [49].

Numerous studies into how the shot peening process affects the residual stress have been conducted. Peyre *et al.* [50] conducted studies on AA7075-T7531 to determine the through thickness residual stress imparted on shot peened test specimens, peened to a coverage of between 100 and 200%. Selected results of the study can be seen in the graph shown in Figure 2.21.

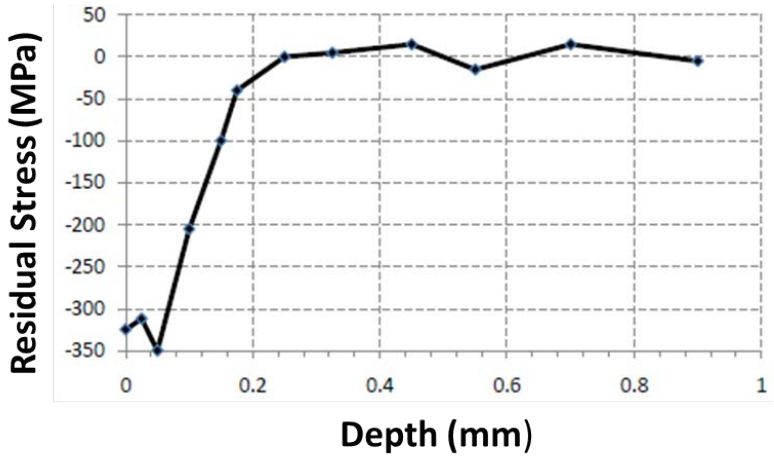

Figure 2.21: Induced Residual Stresses in Shot Peened Al7076-T7531 Test Specimens by Peyre *et al.* [50]

From the above Figure, it can be seen that the surface residual compressive stress imparted into the test specimen is 325 MPa which is roughly equivalent to 75% of the material's yield strength. The maximum compressive residual stress imparted into the component occurs just below the surface layers of the component and is equal to 350 MPa at a depth of 75 μm, which equates to around 80% of the material's yield strength. The maximum depth the shot peening process was able to impart a residual stress into the test specimens was 200 μm. The graph in Figure 2.21 above also depicts the classic hook shape which is associated with the residual stress profile in a shot peened specimen.

Hammond *et al.* [51] conducted similar studies on AA7075-T7531, where test specimens were peened to 100% coverage. The surface residual compressive stress of the test specimens was found to be 129 MPa, which is approximately 28% of the yield strength of the material whilst the maximum compressive residual stress was found to be 208 MPa or 47% of the maximum yield strength of the material at a depth of 100 μm. These results can be seen in Figure 2.22.

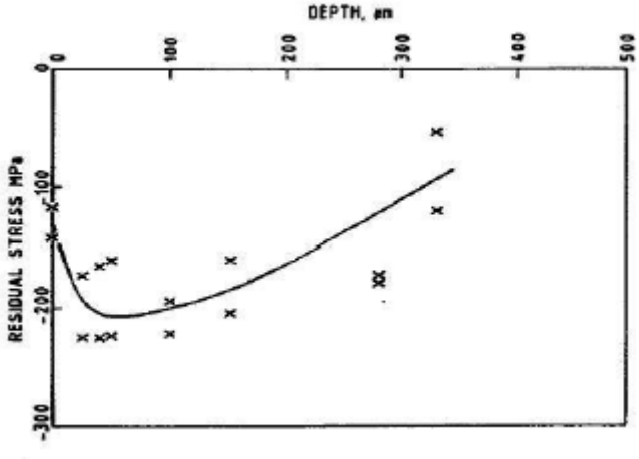

Figure 2.22: Induced Residual Stresses in Shot Peened AA7076-T7531 Test Specimens by Hammond *et al.* [51]

ii) Surface Roughness

Surface roughness typically increases after the shot peening process. Each dent produced by a shot may be considered a source of geometrical stress concentration and hence a site for possible crack initiation.

Surface induced roughness from the peening process is highly dependent on peening intensity, which in turn can be attributed to both the size and type of material of the shot media used. Softer shot material has relatively little effect on surface roughness whereas harder materials can have a large influence. In contrast, the material of the component being peened can also play a part in how the shot media will affect it. Softer component materials will have a greater surface roughness after the peening process when compared to harder material. Broken shot must also be avoided as sharp indentations may occur during the peening process. It is thus crucial that shot be sorted both during (on a continual basis) and after the peening process [41].

Shot peening coverage can also have a critical role on the degree of surface roughness present after the peening process. Complete peening coverage of a component i.e. 100%, produces a uniform layer of residual stress in a component, where the stress concentrations formed by the overlapping edges of the shot peening dimples are somewhat negated by the induced layer of residual

compressive stress in the component. Incomplete shot peening coverage i.e. less than 100%, results in areas of non-uniform stress distribution within the surface layer of the component. This uneven stress distribution can result in areas of stress concentration from which crack initiation can take place. Sites of existing stress concentrations i.e. scratches, tool marks, sharp corners etc. may also not be treated in an incomplete peening process so resulting in areas containing stress concentrations with no surface layer of residual stress [41].

If surfaces roughness is undesired after the peening process (components with small tolerances may be affected by surface roughness) various surface polishing techniques can be employed so as to reduce surface roughness levels without greatly affecting the residual compressive stress layer introduced into the component by the peening process (an electro-polishing process is typically used).

Peyre *et al.* [51] found that the surface roughness of shot peened AA7075 and A356 specimens increased significantly from the peening surface treatment. Large increases in both the mean (R_a) and peak (R_z) roughness were found. The results of this study can be seen in Table 2.1.

Table 2.1: Comparative Roughness Effects of the Shot Peening Process [50]

Material and Processing	R_a (μm)	R_z (μm)
A356 as milled	0.7	6.2
A356 shot peened (100%, 0.3 mm beads)	5.8	33
AA7075 as milled	0.6	5.2
AA7075 shot peened (125%, 0.6 mm beads)	5.7	42

iii) Microstructure

The shot peening process causes changes in structure beneath the surface of a treated component in terms of hardness, grain morphology and even phase transformation (which is highly dependent on the type of material being shot peened).

In general, the dislocation structure of a metal tends to re-distribute itself uniformly near the surface of a peened component causing the dislocation density to increase both at and near the surface. This grain distortion caused by the shot peening process leads to an increase in the microstructural barriers within a metallic component that can impede slip movement, causing cracks to propagate at slower rates [52].

2.4.2 Laser Shock Peening (Mechanical Treatment)

a) General Process and Methodology

Laser shock peening (LSP) is a cold working, mechanical surface treatment used to increase the resistance of metals and alloys to both fatigue and fretting fatigue. This is achieved by a high pulse laser that introduces compressive residual stresses and strain hardening into the surface of a metallic component without having a thermal effect on the laser peened area.

The laser shock peening process requires that the area of a component to be laser shock peened is locally covered with two types of overlays. Firstly, an opaque layer is placed directly onto the surface of the component and can be any material that is opaque to the laser beam. This is generally a black painted coating although tape and metal foil can also be used. A transparent layer (transparent to the laser beam), typically water between 1 and 3 mm deep, is then placed over the opaque layer [53]. This set up can be seen schematically in Figure 2.23.

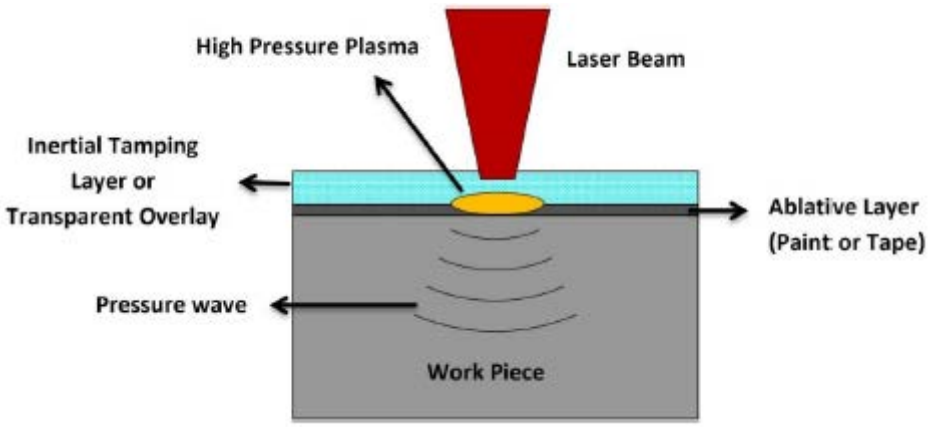

Figure 2.23: Laser Shock Peening Process [54]

A laser beam is then directed onto the surface of the component being treated and passes through the transparent overlay before striking the opaque overlay. The laser beam heats up and vaporises a thin surface layer of the opaque overlay on contact. This vaporisation of the "sacrificial" opaque overlay forms a high temperature plasma which rapidly expands against the surfaces of both the component and the transparent overlay. The expanding plasma is trapped against the surfaces of the transparent overlay and the workpiece resulting in the plasma gas pressure increasing to an extremely high value. This high pressure gas acts against the surface of the component, causing a shock wave to propagate into the material. If the peak stress of this shock wave is above the yield strength of the material, plastic deformation in the material occurs. Deformation in the material continues as the shock wave travels deeper into it until the peak stress of the shock wave

falls below the yield strength of the material. This localised plastic deformation produces both strain hardening and residual compressive stress both at and below the surface of the laser peened component [53].

It may be necessary to make repeated passes (2 - 4) with the laser over the same area and replace the opaque layer in that particular area. This is done because after the initial laser peening treatment, the surface is denser and more receptive to transmitting the compressive residual stresses to greater depths. This repetition however does not increase the levels of residual stress in the component [45].

The intensity of the laser used in the laser shock peening process can be controlled and monitored, so allowing the process to be tailored to specific service, manufacturing and geometrical requirements. Some of the controllable aspects of the laser shock peening process will be discussed later on in the Chapter. The process can be used on both internal and external surfaces. Laser shock peening surfaces with line of sight access are straightforward and progress is being made for application of the process to internal surfaces where line of sight access to the surface is not possible. The laser shock peening process can also be used in conjunction with other surface treatment processes so as to achieve the most advantageous material properties given the application of the component and also save on overall costs [53].

The applications of LSP include improvement of fatigue life, stress corrosion cracking/corrosion resistance and wear resistance [55]. Several materials have been peened successfully proving the effectiveness of LSP and the associated residual stresses induced. The materials laser peened include titanium alloys, aluminium alloys, different steel grades, copper alloys, zinc, nickel based alloys, super alloys, brass, magnesium alloys, bulk metallic glass and other materials [55].

b) Equipment Used in the Process

The laser shock peening process is relatively new to South Africa, with the CSIR (Council for Scientific and Industrial Research) the only current facility capable of applying this process as a means of fatigue life enhancement to various engineered components. A schematic of the current laser shock peening setup at the CSIR is depicted in Figure 2.24.

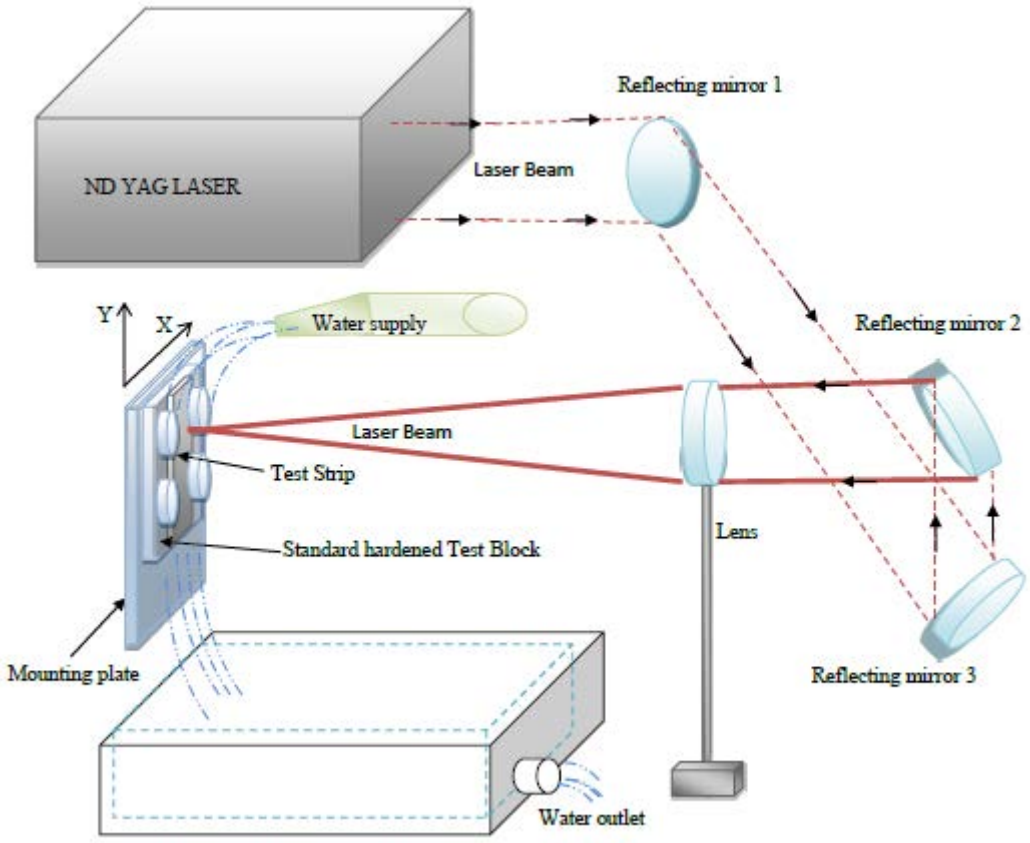

Figure 2.24: Schematic Diagram of CSIR Laser Shock Peening System [54]

Typically a pulsed Nd:YAG laser (neodymium-doped yttrium aluminium garnet) or Nd:glass laser (both of which are generated from a Q-switched laser) are used in the shock peening process, which provides energy in the range of 1 to 100 J per pulse. Pulse durations typically last from between 5 to 50 nanoseconds. The output from the laser system is directed via an optical chain of mirrors, a power meter (to measure laser energy) and a focusing lens onto the surface of the workpiece, which is clamped in position on a movable positioning table. The workpiece can be repositioned using a XY axis positioning system and can be moved into desired positions or until the designated amount of laser peening coverage has been achieved [56].

Water is used as an inertial tamp and, in the case of the CSIR's machine, is sprayed onto the surface of the work piece via a nozzle. A continual stream of water is used as opposed to placing the work piece in a vessel of stationary water, as flowing water allows for any debris generated during the peening process to be carried away from the work piece. The flowing water also facilitates efficient work piece cooling, so that any potential laser heating effect is negated. Water is continuously cycled by means of a water pump. The air valve ensures that water and other debris does not splash in the direction of the focusing lens and laser. A splash barrier is also utilised to minimise the effects of water splashing off the work piece [57].

c) Factors Affecting Process Quality Control

In order to understand the laser shock peening process, various factors governing the consistency of the process need to be understood. The goal of laser shock peening is to impart a compressive residual stress into a component. The two primary factors that determine this are: the amount and quality of the energy emitted from the laser and the amount of energy received by the component being treated [45]. The parameters that govern these two requirements are discussed below.

i) Transparent Overlay and Absorbent Coating

The transparent overlay used in the laser shock peening process can be any material transparent to the laser beam, such as water, glass, fused quartz or acrylic, all of which are used as an inertial barrier. This confining overlay traps rapidly expanding plasma over the surface of the metal component, causing the plasma pressure to rise much higher than would be the case if the layer were not present. The choice of confining medium solely depends on the substrate material, density and acoustic velocity, which gives the so-called "impedance effect" [55]. This results in more of the laser energy being delivered into the material as a shock wave The transparent overlay is placed over the thermal protective layer (opaque coating) given to the component and is typically water, either flowing or stationary, as it is relatively cheap and removes any heat generated by the laser peening process [58].

When laser shock peening without a transparent overlay, the laser induced plasma, created from the laser vaporising the opaque coating, expands freely from the solid surface of the component. This incident laser energy cannot be efficiently converted into a pressure shock wave that induces compressive stress in the component being treated [58]. For example when a Hadfield steel specimen was laser peened with no transparent overlay, the resulting surface of the specimen was only slightly compressive [58]. This occurred even when a high powered laser density of 2.4 TW/cm^2 was used in the peening process as compared with power densities of 1 TW/cm^2 commonly used elsewhere [1].

The mechanical effects of laser induced shock waves in a metallic component are also dependent on the type of absorbent sacrificial coating used on the component being treated. If no coating is used, the heated zone caused by the thermal effect of the laser is compressively plasticised by the surrounding material during the dilatation. Thus tensile stresses and strains may occur after cooling. This also induces excess surface roughening [58]. However, the residual stress induced into a component without the use of an absorbent coating, although tensile, are comparable to those induced with an absorbent coating at similar depths. The CSIR currently does not make use of an absorbent layer whilst laser shock peening, and thermal effects, such as local melting, are controlled by the intensity of the laser energy used. This can be seen in Figure 2.25, which is based on tests undertaken by Peyre *et al.* [59] in which different coatings were used on 55Cl steel test samples. Peyre *et al.* [59] stated that specimens coated had the highest compressive stresses whereas the absence of protective coating led to tensile stresses as shown in Figure 2.25. The tensile stresses could be attributed to the effect of laser ablation from the LSP process.

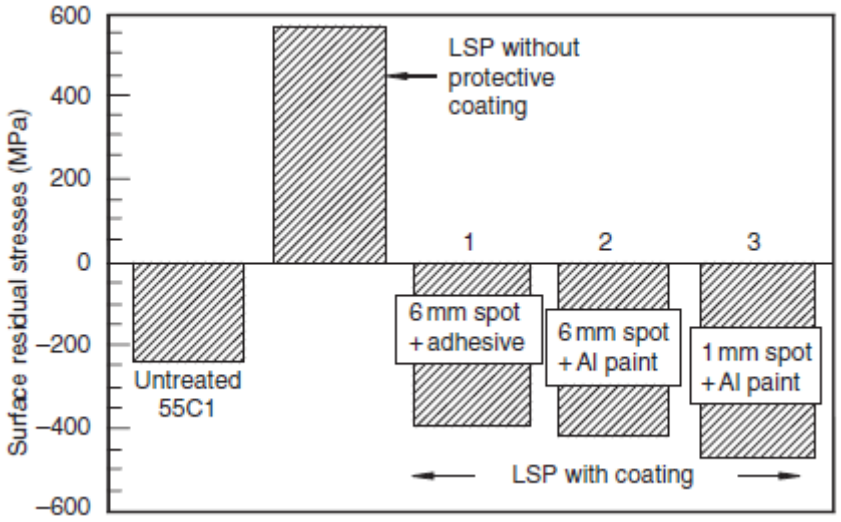

Figure 2.25: Surface Residual Stresses Induced in 55Cl Steel Test Specimens with Different Surface Coatings [59]

If the metal surface is coated with a protective material (i.e. black paint) the thermal effect occurs only in the coating layer. Thermal protective coatings may be metallic foils (aluminium foil), organic paints (black paint) or adhesives (black tape). The use of laser absorbent sacrificial coatings have also been found to increase the shock wave intensity in addition to the protection of the metal's surface from laser ablation and melting. When a laser pulse with sufficient intensity irradiates a metal target with an absorbent coating, the absorbent coating vaporises and forms a plasma. The hydrodynamic expansion of the heated plasma in the confined region between the metal target and the transparent overlay creates a high amplitude, short duration pressure pulse.

A portion of this energy propagates as a shock wave into the treated metal. When the pressure of the shock wave exceeds the dynamic yield strength of the metal, plastic deformation occurs which modifies the near-surface microstructure and properties of the treated metal [1].

ii) Laser Spot Size and Duration

The laser spot diameter can be varied and is only limited by the power density (GW/cm^2) and overall laser power (GW) available. The shape of laser spots generally used are circular, while studies have shown the possibility of using square shaped laser beam with improved features [55]. When using circular laser spots, the residual stresses at the centre of the spot can be unstable owing to the complicated interactions between shock waves in this region [60]. This phenomenon can be minimised by changing the geometry of the laser spot to a shape that provides the most efficient and effective processing conditions [58]. In practice, the diameter of the laser spot typically ranges from 6 to 10 mm, although the size of the laser spot can be varied as it is only confined by the selected power and power density of the laser [55]. Larger spot sizes produce residual stresses much deeper below the surface of a treated specimen than a smaller one. However, the magnitude of the compressive residual stress does not increase, as was discovered by Peyre *et al.* [59] in a study comparing fifty 1 mm diameter laser spots with a 25% overlap with four 6 mm diameter laser spots with a 50% overlap on 55Cl steel test samples. Selected results of this study can be seen in Figure 2.26. It was found that the 1 mm diameter laser spots displayed a fatigue strength improvement of 490 MPa at 2×10^6 cycles with the 6 mm diameter laser spots only displaying a fatigue strength improvement of 470 MPa for the same number of cycles. These improvements were compared over the untreated material fatigue strength of 380 MPa at the same number of cycles. This indicates that laser shock peening with small diameter impacts can be considered as a more effective means of improving the fatigue life of components when compared to larger diameter impacts over the same surface area.

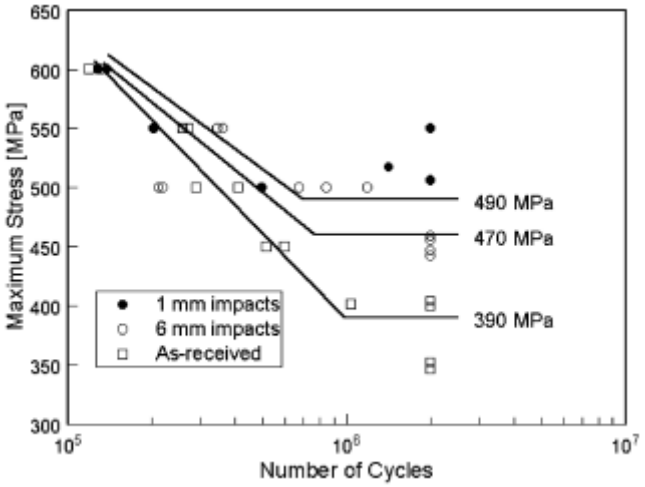

Figure 2.26: S-N Curve for 55Cl Test Specimens Treated by Laser Peening [59]

Laser shock peening is limited to the area covered by the laser spot per peening pass and thus the overlapping of the laser spots is used to treat large areas in practice. The coverage ratio is an important factor for optimising the residual stress field in a material. The coverage ratio is defined as the ratio between the overlapping area and the impact spot size for two successive laser shock peening processes. Peyre *et al.* [50] showed that an increase in the coverage ratio increases the plastically affected depth. Thus optimisation of the coverage ratio may lead to improved treatment results. Coverage ratios of between 50% and 70% are typically used for circular laser spots in practice [58]. The coverage ratio also affects the surface roughness induced by the laser peening process, with larger coverage ratios tending to have a lower surface roughness when compared to coverage ratios with low overlap percentages. Laser pulses are generally overlapped and scanned in a zig-zag type pattern which allows for complete coverage of the area to be treated [61]. This pattern can be seen in Figure 2.27.

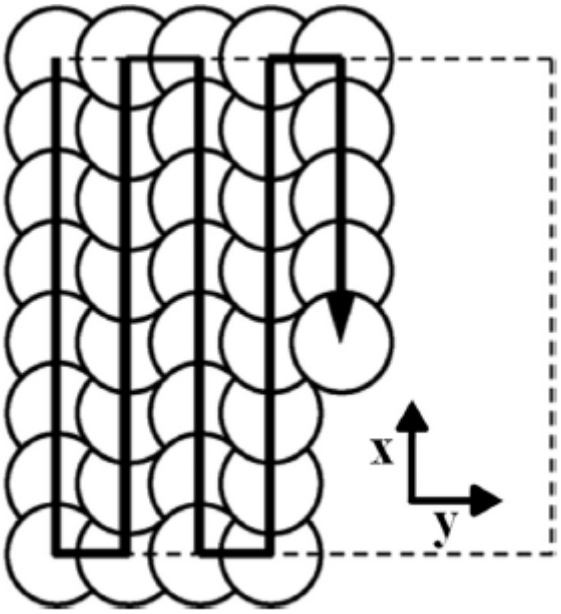

Figure 2.27: Zig-Zag Scanning Pattern [61]

A laser system can deliver a wide range of pulse durations, from anywhere between 0.1 and 50 ns. For laser shock peening, the laser pulse duration directly controls the pressure pulse duration. Laser pulses need to be long enough for sufficient shock pressures to be generated, which can produce residual compressive stresses, but not too long, as melting and surface damage may occur. Pulse durations are typically determined through a trial and error process.

iii) Laser Power Density and Wavelength

The magnitude of surface residual stresses increases with the magnitude of the plasma pressure, which in turn is related to the incident laser power density. When the laser power density exceeds a certain threshold, residual stresses increase with depth but decrease at the surface because of surface release waves (pressure waves which are reflected in the metallic component being treated). This indicates that there are optimal laser shock peening conditions. Peyre *et al.* [50] found that surface residual compressive stresses in an A356-T6 alloy specimen increased to 145 MPa for an increase in laser induced pressure from 1.3 to 1.5 GPa when the laser pulse density was changed from 1.5 to 2 GW/cm^2. However, as the power density was increased further to 3 GW/cm^2, a reduction in the surface compressive stress level to 100 MPa was seen, with in-depth compressive residual stresses continuing to increase. It was concluded that all materials have an optimum shock condition.

A laser system normally delivers two kinds of temporal shapes of laser pulse, a Gaussian pulse shape and a short rise time pulse shape. Peyre *et al.* [50] found that the laser induced pressure is

a function of the laser power density of the laser pulse with two different temporal shapes. The Gaussian pulse saturation pressure was found to be 4 GW/cm^2, whilst the saturation pressure increased to 10 GW/cm^2, for a short rise time laser pulse [58].

Berthe *et al.* [62] characterised laser shockwaves with respect to changes in laser wavelengths from the inferred to ultraviolet spectrum. It was found that the pressure pulse produced by ultraviolet wavelengths of 0.355 μm were similar in profile to those generated by an inferred wavelength of 1.06 μm. It was also found that whilst keeping the laser power density constant, decreasing the wavelength of the lasers used during experimentation from 1.06 μm to 0.355 μm increased the photon-metal interaction so enhancing shock wave generation. However, the maximum peak pressure that could be generated decreased with the shortening laser wavelength as the critical power density threshold for dielectric breakdown also decreases as a result of the shortening laser wavelength. This results in the generation of a plasma which is not on the target metal's surface and which absorbs the incoming energy laser pulse so limiting the energy available to generate a shock wave [1].

iv) Multiple Laser Shock Peening

Compressive residual stresses can be driven deeper below the surface of a treated component by using successive shocks. Clauer [53] conducted multiple laser peening shock tests on 0.55% carbon steel and found that the plastically affected depth with residual stress increased almost linearly with the number of impacts (until a saturation point is reached) on the same spot, although no increase in the magnitude of the residual surface stresses were observed. This increase in residual compressive stress depth per increase in the number of impacts can be seen in Figure 2.28.

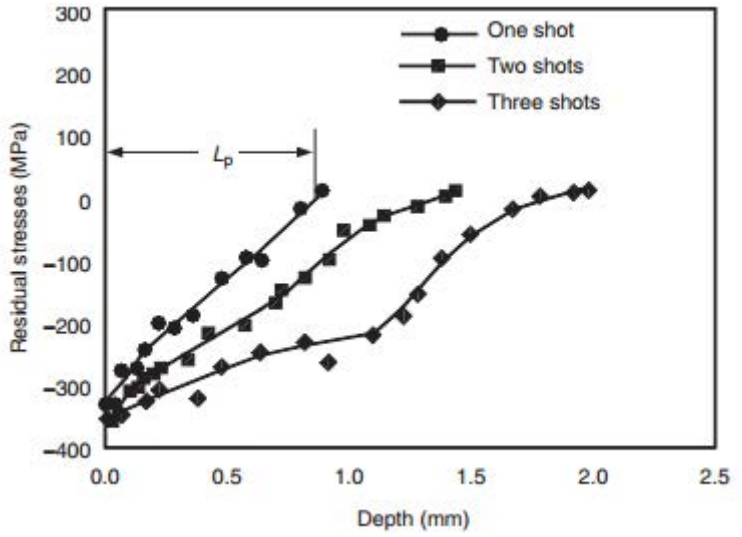

Figure 2.28: Residual Stress Profiles Induced By Multiple Impacts [53]

d) Properties of Laser Shock Peened Materials

i) Residual Stress

During the laser shock peening process, the pressure pulse generated from the plasma (generated from the vaporisation of the opaque layer, which absorbs energy as it vaporises) and subsequent confinement of this plasma expansion against both the transparent layer and the surface material, results in the formation of a high pressure shock wave that propagates through the material of the treated component. The impact of this shock wave on the surface of the work piece creates pure uniaxial compression in the direction of the shock wave propagation and tensile extension in the plane parallel to the surface. After the reaction in the zones surrounding the shock peening impact, a resultant compressive stress field is generated in the affected volume, while the underlying layers are in a lower magnitude tensile state [63]. This effect can be seen in Figure 2.29, which illustrates experimental results from tests conducted by Clauer [53] in which Al2024-T351 test specimens were laser shock peened. The graph in the Figure also illustrates the definite introduction of residual stresses into treated components.

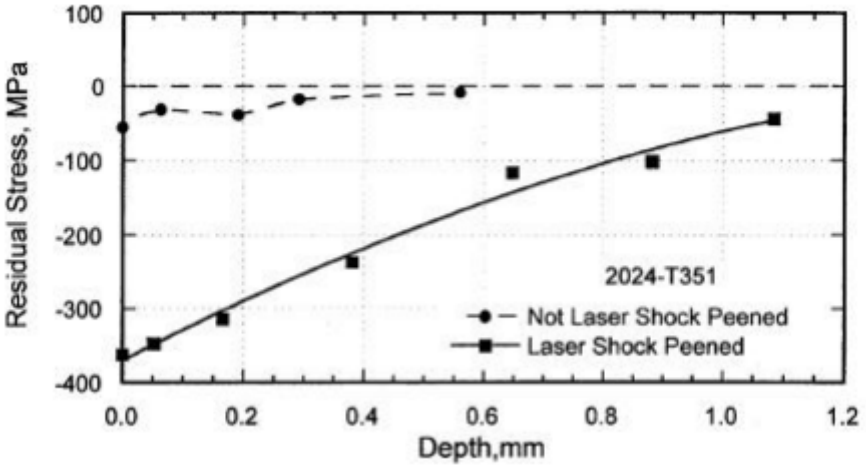

Figure 2.29: Residual Stress Profiles before and after Laser Shock Peening [53]

As the shock wave propagates through the material, plastic deformation occurs to a depth at which the peak stress no longer exceeds the Hugoniot elastic limit of the material. The Hugoniot elastic limit is related to the dynamic yield strength and is defined by the Equation [64]:

$$HEL = \frac{(1-\nu)\,\sigma_y^{dyn}}{(1-2\nu)} \tag{2.7}$$

Where:

HEL: Hugoniot Elastic Limit (Pa)

ν: Poisson's Ratio (Pa)

σ_y^{dyn}: Dynamic Yield Strength at High Strain Rates

The plastic deformation induced by shock wave propagation through the work piece results in strain hardening and residual compressive stresses in the surface of the material [1]. As discussed previously, residual stress distributions are strongly dependent on both laser intensity and pulse repetition. Repeated laser shocks increase the magnitude of the surface and subsurface residual stresses within a component until a saturation point is reached. This is due to strain hardening. Each shock wave which travels through a material activates a certain number of plastic mechanisms (i.e. cause a certain amount of plasticity) in the material until all the plastic mechanisms have been activated whereby repeated shocking will only cause elastic deformation [65].

The pressure generated from the laser shock peening process results in the formation of two stress waves, elastic and plastic, within the material. The speed of the elastic wave is faster than the

plastic wave. When the applied pressure is removed, a release (unloading) wave travels in the same direction as the unloading. If the unloading is compressive in nature, then the release wave is always tensile. The laser induced elastic wave travels until it reaches the boundary of the material through which it is propagating and then reflects back. The speed of the release wave is greater than the speed of the plastic wave and it is thus possible for the waves to meet and interact. This results in a complex distribution of elastic and plastic strains and stresses in the laser peened material [64].

The complicated interaction between the different waves propagating through a shock peened component results in the formation of both compressive and tensile regions [65]. The physics of this formation of different stress states within a laser peened component can be seen in Figure 2.30.

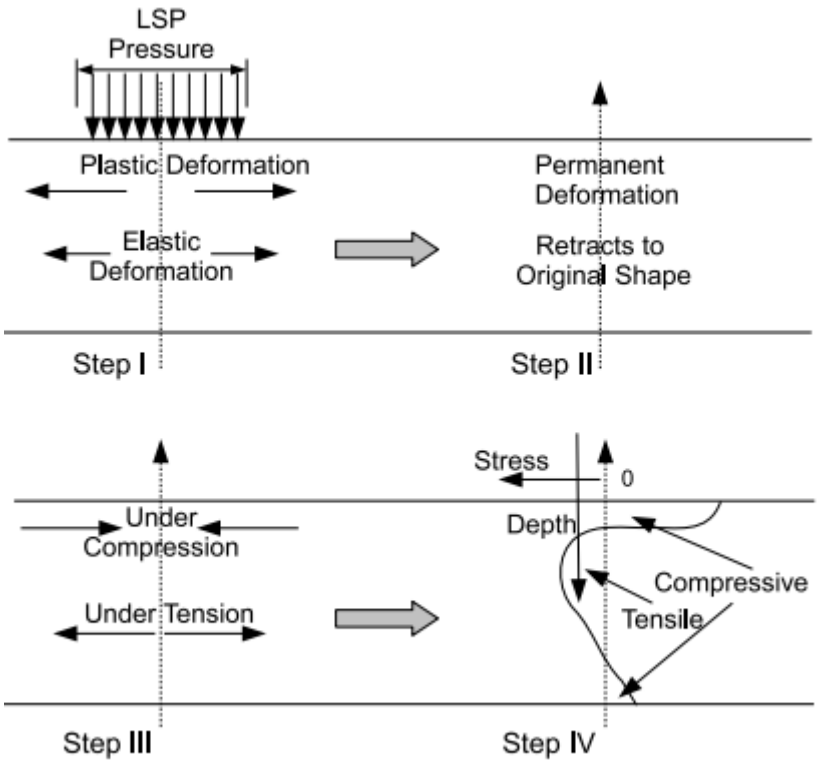

Figure 2.30: Residual Stress Generation in a Laser Peened Material [64]

The depth of compressive stress is directly related to the depth of the plastically affected zone. It is recommended that compressive residual stresses on any material top surface should be confined to 10 percent of the specimen thickness in order to avoid distortion [55].

The overall effect that the residual stresses induced into a workpiece by the laser shock peening

process can be seen in Figure 2.31, which illustrates the results of some experimental testing performed by A. Clauer [53] on welded Al5456 test specimens, which were fatigued until failure for both an untreated and laser shock peened case. The graph in Figure 2.31. clearly illustrates to improvement in fatigue life that accompanies the laser shock peening process.

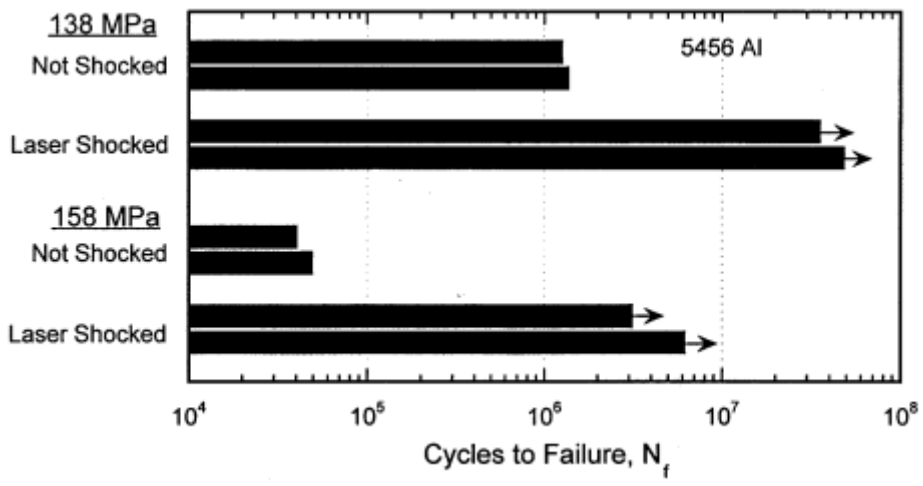

Figure 2.31: Fatigue Life Increase in Welded AA5456 Test Specimens after Laser Shock Treatment [53]

ii) Surface Roughness

The surfaces roughness values typically generated during the laser peening process are substantially lower than those generated by conventional shot peening processes. This difference in generated surface roughness between conventional shot peening and laser shock peening was illustrated by Peyre *et al.* [50] in a study on aluminium alloys. In this study, the surface roughness's of A356 and AA7075 test specimens were determined before and after treatment. The effect of both surface treatments on the surface roughness of the two materials can be seen in Table 2.2. These results illustrate the drastic difference between the surface roughness's of both shot peened and laser shock peened components.

Table 2.2: Comparative Roughness Effects of the Laser Shock Process [50]

Material and Processing	R_a (μm)	R_z (μm)
Shot Peening		
A356 as milled	0.7	6.2
A356 shot peened (100%, 0.3 mm beads)	5.8	33
AA7075 as milled	0.6	5.2
AA7075 shot peened (125%, 0.6 mm beads)	5.7	42
Laser Shock Peening		
A356 as milled	0.7	6.2
A356 laser shock peened (2 GW/cm^2, 2 impacts)	1.1	7.5
AA7075 as milled	0.6	5.2
AA7075 laser shock peened (4 GW/cm^2, 3 impacts)	1.3	11

Laser textured surfaces also have the ability to improve the performance of wear, friction and lubrication. Micro dents generated on a component's surface layer by the laser shock peening process can serve as fluid reservoirs and effectively retain lubricant, which in turn acts as micro bearings, sustaining load and reducing surface wear. Under flooded and boundary lubricated conditions, micro-dents will also function as traps for wear debris, eliminating a potential ploughing effect caused by entrapped particles [66]. The study of this lubrication effect is however beyond the scope of this project.

iii) Microstructure

LSP treated material undergoes high strain rates due to plastic deformation thereby resulting in microstructural changes near the metal surface. This results in refinement of the grains and has been linked to the enhanced material properties such as hardness, which translates to higher fatigue strength, tensile strength and wear resistance [55]. In the past these changes have been tracked and studied by means of transmission electron microscopy (TEM), scanning electron microscopy (SEM) and x-ray diffraction analysis. The induced microstructural changes in laser shock peened treated components have been related to the laser parameters and heat treatment conditions of the component alloys [49].

In studies of laser peened alloys, including welded AA5086-H32 and AA6061-T6 by Clauer *et al.* [67], it was found that the dislocation density increased significantly after the laser treatment process. High dislocation densities were also prominent microstructural features in studies by both

Peyre *et al.* [50] for low carbon steels and for Z. Hong *et al.* [68] for AA2024-T62 test specimens after laser treatment. Electron micrographs of the pre and post treatment tests specimens for Z. Hong *et al.* [68] can be seen in Figure 2.32. The laser shock peening process typically results in an increase in dislocation density within a treated component, which results in both higher surface harnesses and strength, whilst the plastic deformation caused by the process results in reduced porosity. This increased dislocation density is due to the formation of fine grain structures in the surface layer of the treated component through phase transformation.

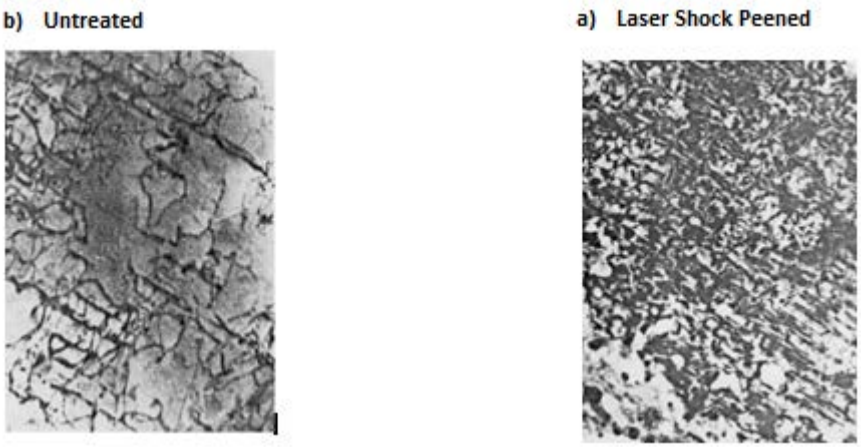

Figure 2.32: AA2024-T62 Test Specimens before and after Laser Shock Peening (Scale Unknown) [68]

Investigations into the effect of laser shock peening on weld zones in 18NI(250) maraging steel showed that after the laser treatment process, the austenite weld phase reverted to martensite and the dislocation density qualitatively increased in the martensite matrix [67].

Minimal changes in the hardness of the bulk material outside the heat affected zone have been observed at laser peen pulse pressures around 3.5 GPa. Laser shock peening has been reported to improve the hardness of underaged materials such as AA2024-T352 but not peak aged material such as AA2024-T851, AA7075-T651 or AA7075-T73. For alloys such as AA6061-T6 however, it was reported by Fairand *et al.* [69], that no changes in hardness or strength could be observed. It was subsequently hypothesised that the precipitation hardening in the T6 condition was large enough to mask shock wave induced strain hardening. It was also hypothesised that by exceeding a shock wave pressure of 7.5 GPa, the properties in peak aged aluminium alloy could be changed and that a shock wave pressure of 6 GPa was significant enough to increase the bulk hardness in AA6061-T6 aluminium [58].

It can be noted from some of the above observations that both the microstructural and phase changes which may occur in a component during the laser shock peening treatment process are

highly dependent on the type of material being treated, with few observations on the effects of laser shock peening on the microstructure of materials available in literature.

e) Comparison Between laser Shock Peening and Conventional Shot peening

The properties of both shot peened and laser shock peened materials have been detailed in the preceding sections of this literature review. The surface roughness, residual stress and microstructure of the material are affected by both treatment processes and can thus be compared.

Shot peened surfaces are typically rougher than the surfaces generated by laser shock peening. This can be advantageous for paint cohesion but detrimental to wear and fatigue properties as it is well known that rough surfaces contain stress concentration sites from which crack initiation can occur. For wear applications, the rough surface of a shot peened component can be removed through various polishing techniques. However, care must be taken as the conventional shot peening process results in components having a relatively thin surface compressive layer. Removal of the rough surface can result in a reduction of this already thin compressive surface layer [58]. Smaller surface stress gradients are also found in laser treated components. This is beneficial as smaller gradients help reduce the effects of cyclic relaxation of the induced residual stresses in components [66].

The stress induced depth in laser shock peened components is dependent on a number of conditions but usually ranges from between 0.5 mm to over 1.0 mm [58]. Laser shock peened components can have residual stress depths of over 1 mm, as multiple peening shots is possible, each of which drives residual compressive stresses deeper into the treated component. A comparison between the depths of the residual stress induced by the two surface treatments can be seen in Figure 2.33.

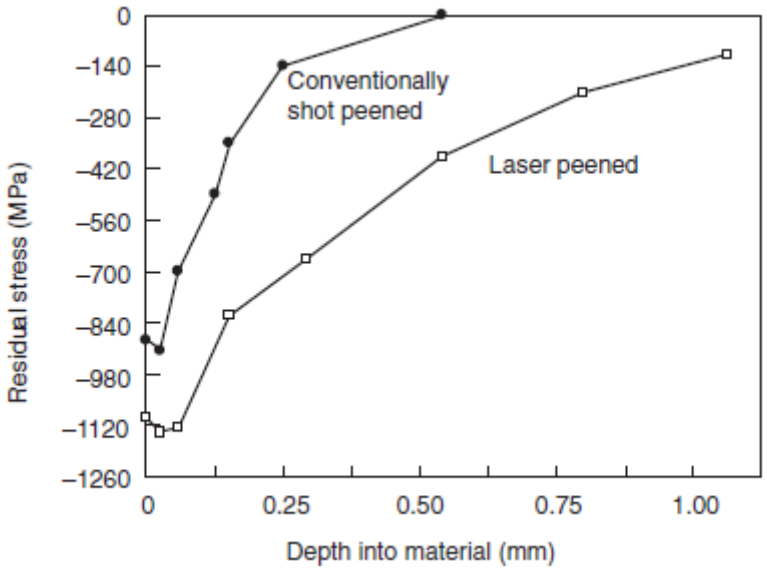

Figure 2.33: Residual Stress Depth of Inconel 718 Induced by Laser Shock Peening and Conventional Shock Peening [70]

A quantitative comparison between the loading conditions induced by laser shock peening with a water overlay and conventional shot peening can be seen in Table 2.3. The most significant difference is that the induced peak pressure in conventional shot peening is significantly greater than that of laser shock peening. Shot peened surfaces are subjected to more multiaxial, intense loadings than laser peened surfaces [58].

Table 2.3: Comparative Loading Conditions Induced by Laser Shock Peening and Conventional Shot Peening [50]

	Process	
	Laser Shock Peening	**Shot Peening**
Peak Pressure (GPa)	0 - 6	3 - 10
Diameter of Impacts (mm)	1 - 15	0.2 - 1
Pressure Duration (μs)	0.05	0.5 - 1
Mechanical Impulse ($GPa.\mu s$)	0 - 0.3	1 - 10
Induced Strain Rate (s^{-1})	10^6	10^4

For both laser shock peening and shot peening, the shock hardening effect below the surface decreases with increasing depth [50]. Conventional shot peening, however, has almost twice the surface hardness when compared to laser shock peening and this can be attributed to the longer

application of surface pressure caused by the peening media, which results in greater dislocation density generated at the surface of a treated component [58].

A. Clauer [53] compared the effects of bending fatigue on AA7075-T7351 notched test specimens which were either shot peened, laser shock peened (3.8 GW/cm^2) or left untreated. The fatigue results, which can be seen in Figure 2.34, indicate that shot peening provides an 11% increase in the run out stress at 10^7 cycles, whilst laser shock peening provides a 22% increase. Figure 2.35, shows the total number of cycles experienced by each sample until failure. The surface roughness induced by the shot peening process was determined to be the main detrimental contributor to the fatigue behaviour of the shot peened samples.

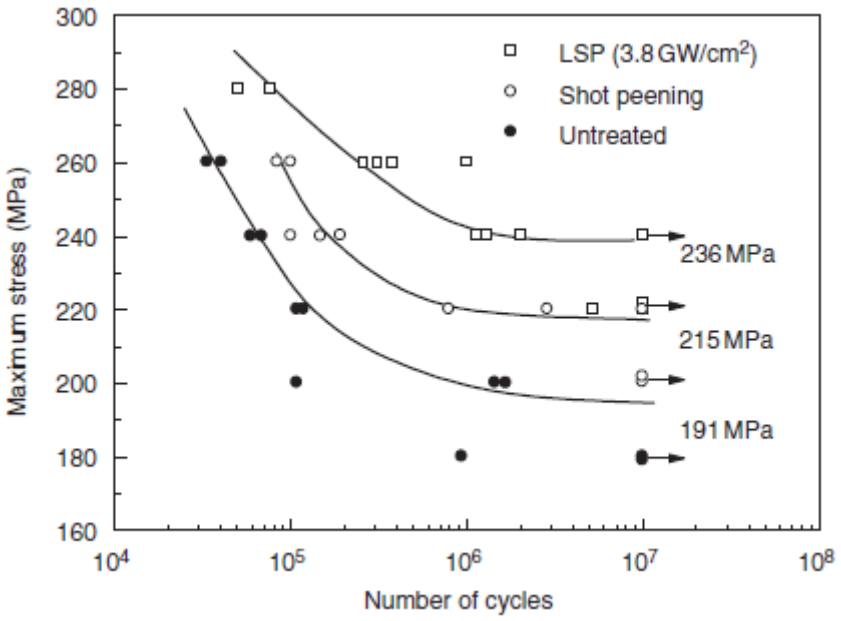

Figure 2.34: Comparison of Notched bending Fatigue of Untreated, Shot Peened and Laser Shock Peened AA7075-T7351 Test Specimens [50]

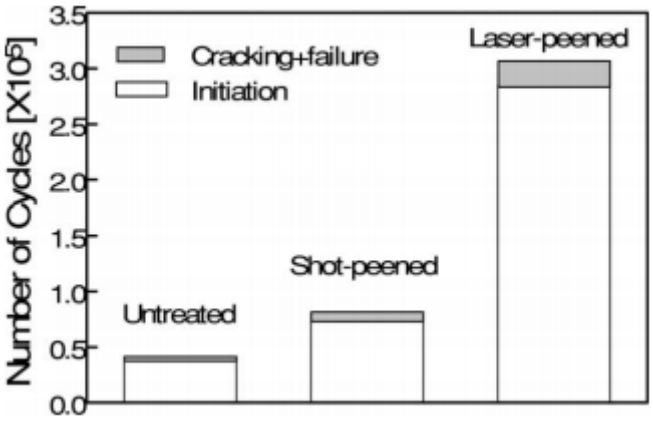

Figure 2.35: Comparison of AA7075-T7351 Test Specimen Fatigue Lives [53]

Peyre *et al.* [50] showed through experimentation on A356 cast alloy tests specimens that surface stresses of -210 MPa were achievable with shot peening against only -150 MPa for laser shock peening. This suggests that the plastic deformation induced by laser shock peening is lower than that introduced into test samples by shot peening. However, further testing, as seen in Figure 2.36, showed that the residual stresses developed over the first 100 μm in AA7075-T351 test samples were approximately equal if multiple laser peening impacts were used. A second comparative study into the surface hardening effect of each treatment process was also conducted. It was found that shot peening induces double the surface hardening of laser shock peening. This was attributed to the fact that shot peening has a higher pressure duration (from media shot contact) resulting in higher dislocation generation and motion. These results can be seen in Figure 2.37. It can be concluded that laser shock peening generates residual stresses much deeper into a component and produces a smoother surface finish than shot peening, whereas shot peening generates higher residual stresses and surface hardening.

For every new technical concept, the cost of conducting research and applying it in industry is a major challenge and laser shock peening is no exception. Laser shock peening is a high-cost technology as compared to shot peening. For this reason, when considering high scale production, companies find it difficult to laser peen fabricated components. However, the integration of laser shock peening technology at a strategic point during the production line could help minimise the cost. More so, investigations using modelling might further minimise the experimental cost by reducing the need to do all the parametric combinations [55].

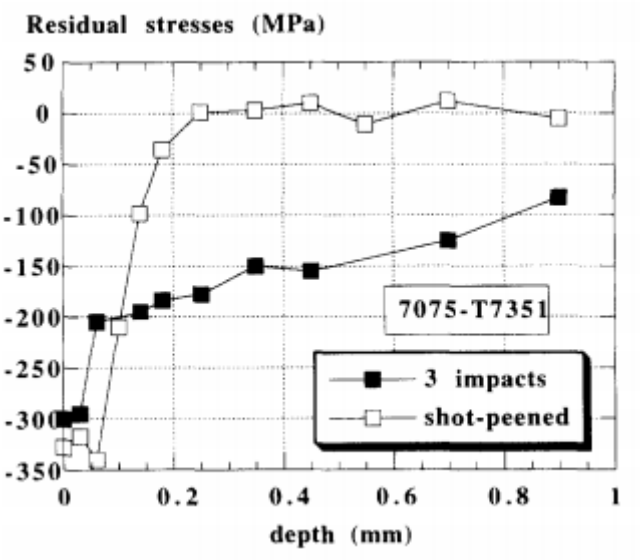

Figure 2.36: Comparison of Residual Stress Fields Induced by Shot Peening and Laser Shock Peening [50]

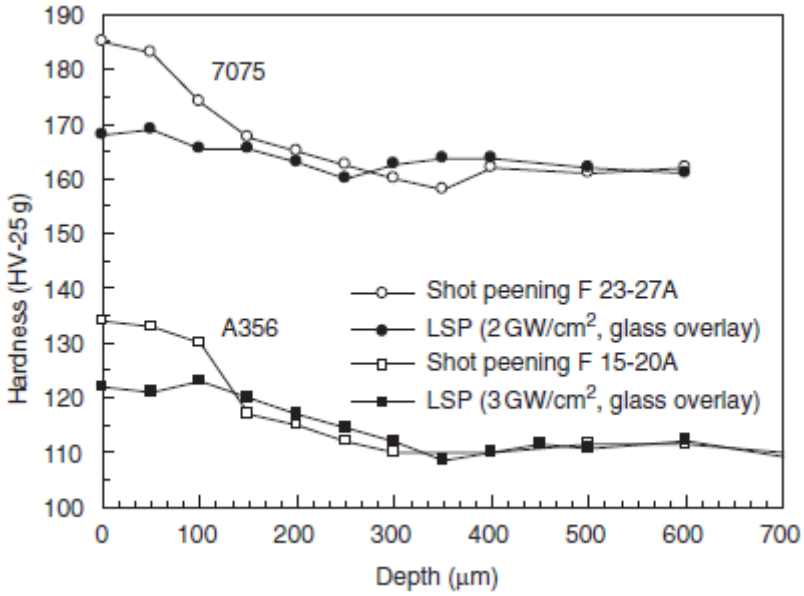

Figure 2.37: Comparison of Surface Harness Values Induced by Shock Peening and Laser Shock Peening [50]

2.5 Fatigue Life Recovery

It has been well established that fatigue life extension in components prior to their usage can be achieved by extending the crack initiation period, as this accounts for roughly 90% of the service life of the component, or through retarding crack propagation through the component [71]. This is typically done with the introduction of compressive residual stresses into the surface layers of the component, which counter-acts any stresses applied to the component.

There is however economic pressure to further extend the service life of partially fatigue damaged in-service components. By re-introducing compressive residual stresses into the surface layers of partially fatigue damaged components, some of the fatigue damage in the components can be undone, thus extend their fatigue lives [71].

Various treatment methods have been tested to try and bring about localised healing in the surface layers of partially fatigued components. A localised heating method is a popular technique for extending fatigue life in welded structures. These welded structures are heated locally so as to produce localised yielding, which in turn results in a localised compressive thermal stress in the structure. As the locally heated metal cools, it shrinks, thus causing residual stresses. This was demonstrated on a through thickness fatigue crack by Jang *et al.* [72]. It has been reported by Branco *et al.* [73] that localised healing of welds was achieved through a hammer peening process. Compressive stresses close to the yield stress of the material were obtained through the hammer peening process and it is thought that these stresses resulted in the increase in fatigue life. The cold expansion of holes is another technique that has been effectively used to delay the initiation and propagation of fatigue cracks and has been used to repair in-service aircraft for a number of years [74]. The cold expansion technique requires the insertion of an oversized tapered mandrel into a hole. This induces a compressive residual stress field around the hole, which reduces the stress concentration stress. Boni *et al.* [74] found that the double application of this method, performed on opposing sides of a hole, induced compressive residual stress fields around the hole. The magnitude of these induced stress fields remained constant after the fatigue loading of the holes and the subsequent initiation of small fatigue cracks within the holes.

Mid-life reworking of a component has also been investigated using a shot peening process by Sharp *et al.* [4]. In this study, a two-step process was applied to re-work fatigued areas of aluminium alloy 7075 test specimens. The first step required that a surface layer of material be removed as the surface layer would contain any micro cracks which may have initiated during the

fatiguing process. Generally, surface removal in any highly stressed fatigue component is considered undesirable, as the amount of material removed must be carefully controlled so as to avoid weakening the component, and yet there must be a high level of confidence that the damaged material has in fact been removed. Recognising that the controlled removal of surface material is a critical aspect of the specimen repair process, the study developed a surface removal method, with the aim of removing any developing fatigue cracks, which were as yet undetectable and any damaged surface layer. The method involves polishing off the damaged surface layer in order to reveal any developing fatigue cracks. An indent was then made into the now polished surface to a depth equal to the desired amount of surface to be removed (i.e. to the level at which the surface crack has propagated). The surface was then re-polished, until the indentation was no longer visible, so ensuring that the correct amount of material was removed [4]. This undamaged surface could then be re-peened to further extend the fatigue life of the component. This process can be seen in Figure 2.38.

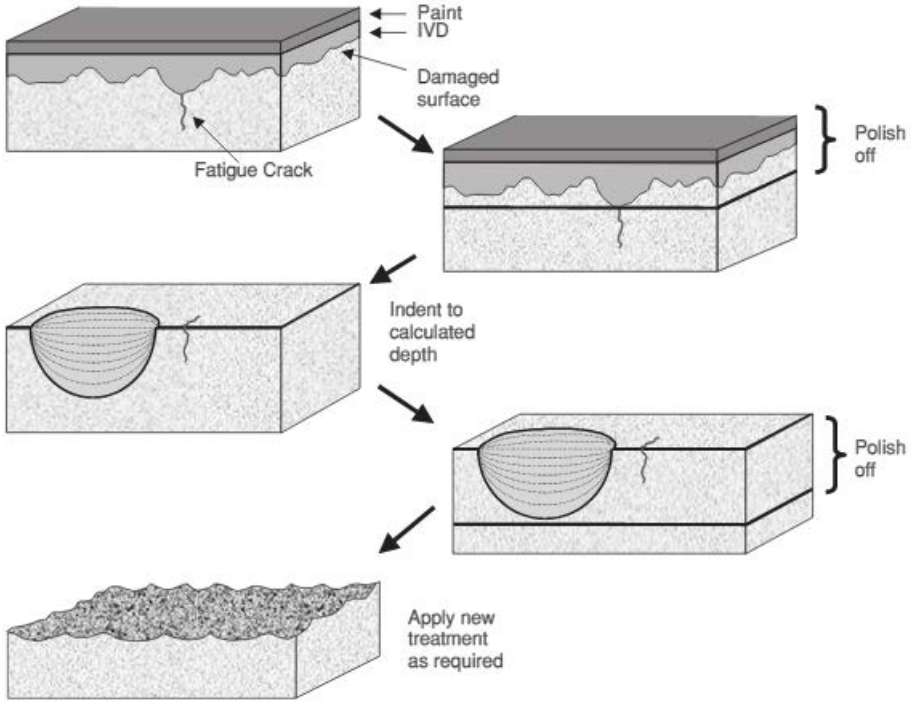

Figure 2.38: A Schematic Representation of the Complete Repair Process [4]

This layer removal process was developed as there was concern that peening over a surface which already contained growing fatigue cracks might not result in any component life extension. This concern is illustrated in Figure 2.39, which shows that peening a specimen which has seen less than 50% of its fatigue life (fatigue life is defined as the total life of the test specimen in the unpeened condition as generated by an S-N curve) can be beneficial. However, re-peening specimens that

have seen more that 50% of their fatigue lives proved to be ineffective as the residual stress is imparted into the surface layers of a component during the peening process can no longer contain the growing crack once it is sufficiently large [4].

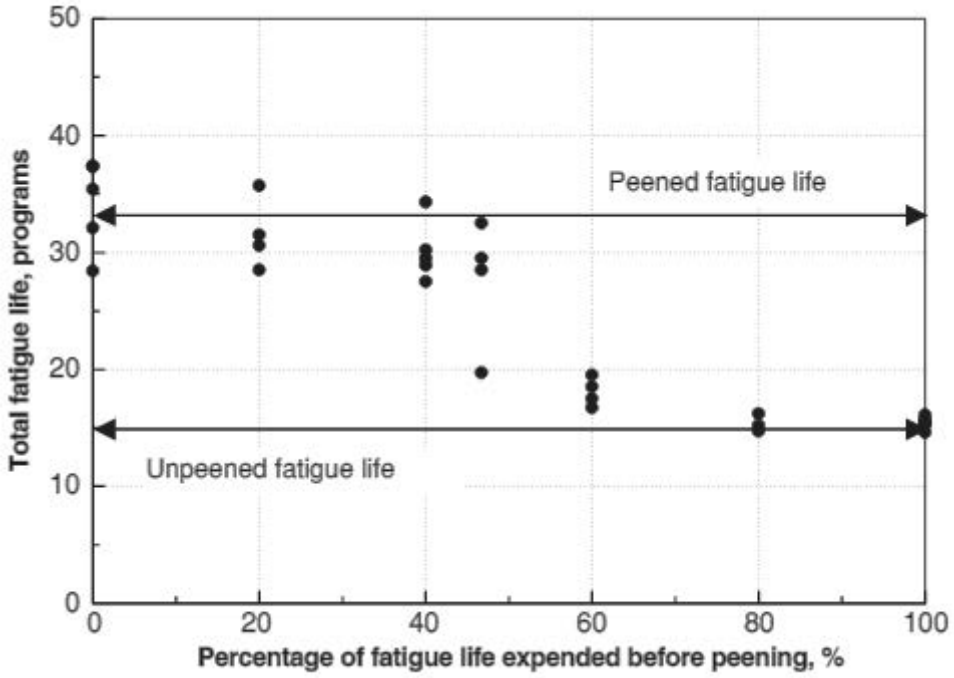

Figure 2.39: Fatigue Life Of Specimens Peened After Various Periods of Service [4]

Liu *et al.* [75] also used shot peening to recover the fatigue resistance of aluminium alloy 7050 that had experienced prior fatigue damage. The results from this study showed that shot peening could be used to heal damaged material, but the effectiveness strongly depended on the amount of prior damage to the material. The study concluded that if the surface cracks initiated during the fatiguing process had extended past the depth of the compressive residual stresses provided by the peening process, then beneficial effect of compressive residual stress was significantly reduced [75]. These results are illustrated graphically in the Figures below, where fatigue life recovery is defined as follows:

$$Fatigue\ Live\ Recovery\ (\%) = \frac{total\ life - unpeened\ life}{fully\ peened\ life - unpeened\ life} \times 100\% \tag{2.8}$$

Where:

Total Life - Number of Prior Fatigue Cycles in Unpeened Condition Plus the Total Number of Cycles to Failure in the Peened Condition

Unpeened Life - Total Number of Cycles to Failure in the Unpeened Condition

Fully Peened Life - Total Number of Cycles to Failure in the Peened Condition

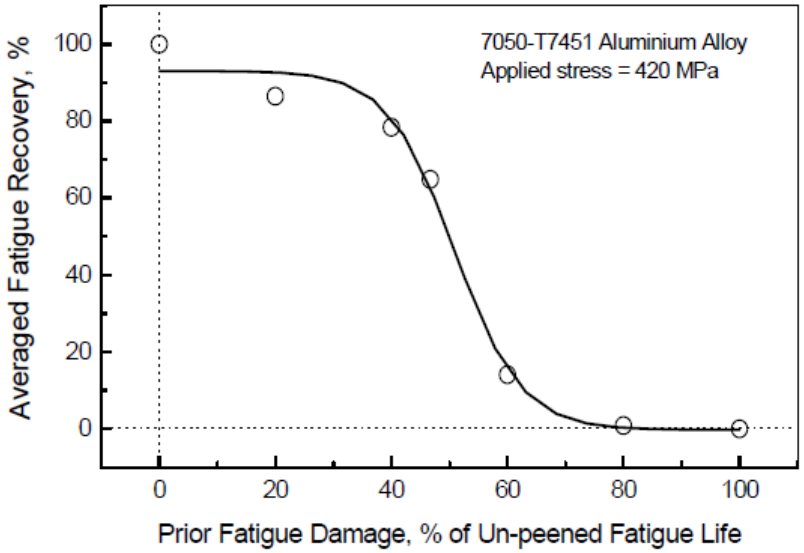

Figure 2.40: Average Fatigue Recovery as a Function of Prior Fatigue Damage [75]

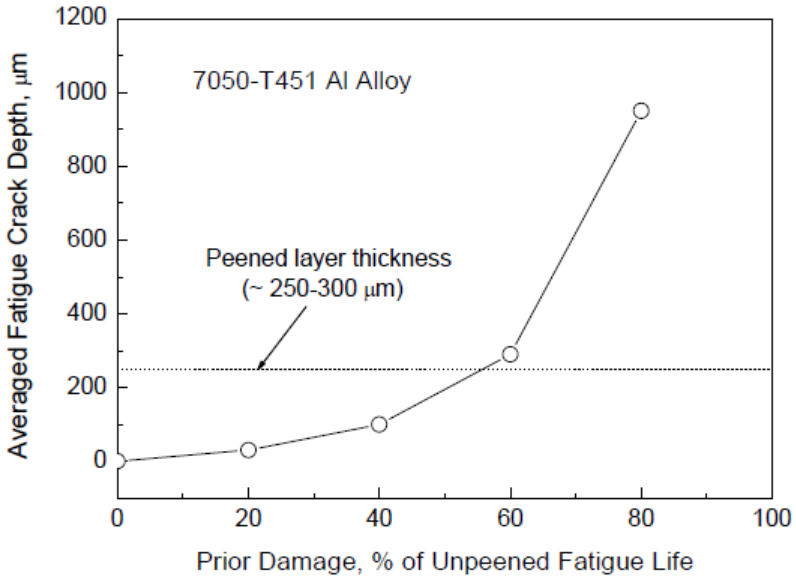

Figure 2.41: Relationship Between Average Fatigue Crack Length and Prior Damage [75]

From the Figures above, it can be seen that when the prior fatigue damage is less than about 50% of the un-peened fatigue life, shot peening can produce fatigue life recovery. However, when the prior fatigue damage is greater than 50%, the fatigue life improvement or recovery is significantly

reduced. At around 80% prior fatigue damage, there is no life improvement as compared to an unpeened specimen [75].

In recent years, laser shock peening has emerged as a potential candidate for the fatigue life extension process. Solid-state lasers have already been used to heal initial fatigue damage. Altus *et al.* [76] used a solid-state laser to heal fatigue damage in Ti-6Al-4V alloy. This healing process was attributed to two main mechanisms: (i) a healing mechanism where dislocations piled up at stress concentration sites i.e. crack tips, were eradicated by the laser heating process thus erasing prior fatigue damage (ii) a microstructural mechanism, which saw a significant increase in the near surface dislocation density, induced by the laser transient temperature-space field. The evidence for this microstructural mechanism and its effect on fatigue life was however not sufficiently clear. Both mechanisms were however only effective up to a critical point in fatigue life, after which fatigue damage reaches singular macro-crack growth. It was also concluded that this process could be repeated a number of times to repair fatigue damage up to the appearance of a macro crack. Yee *et al.* [77] used a solid-state CO_2 laser to retard fatigue crack growth in 2024-T3 aluminium alloy. Yee attributed the fatigue crack retardation to the introduction of a sufficiently high tensile stress, acting in the direction that is 90° to the line of the fatigue load stress, to the region in front of the crack path. This in turn reduced the magnitude of the crack tip shear stress associated with crack tip opening.

Ganesh *et al.* [71] conducted a study on the fatigue life enhancement of pre-fatigued spring steel (SAE 920) specimens using laser shock peening. The approach adopted by the study involved the laser shock peening of partially fatigue bend test specimens (about 50% of their expected fatigue life as determined through an S-N curve), which then had their fatigue lives compared with untreated specimens. The study was performed in two parts:(i) characterization of fatigue life of the specimens, (ii) fatigue testing of specimens up to 50% of their expected life, followed by laser shock peening of these partly fatigue-tested specimens and their subsequent fatigue testing [71]. In the study, results clearly established that the compressive residual stress field introduced by laser shock peening effectively extended the fatigue crack initiation period in partly fatigue-damaged spring steel specimens when compared to untreated test specimens. This was also done without adversely affecting the original surface finish of the test specimens. Selected results of this study can be seen in Figure 2.42.

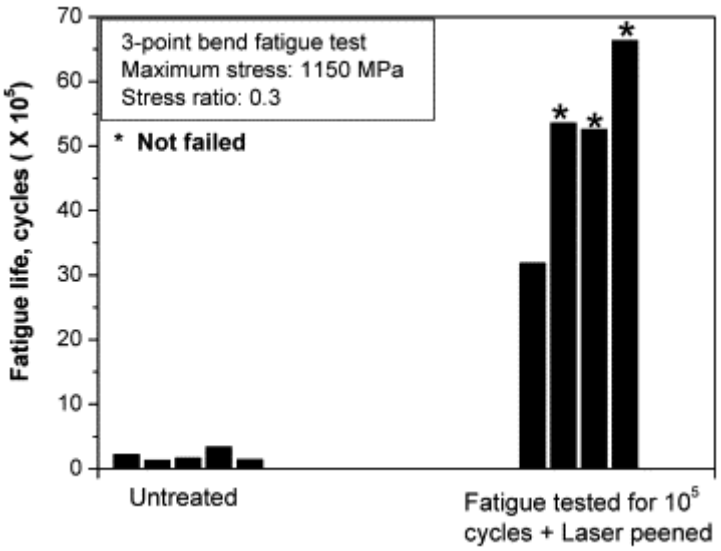

Figure 2.42: Comparison of fatigue Lives [71]

It has been theorised that the re-treatment of component's surface, using a laser shock peening process, shortly after the onset of crack initiation can result in possible fatigue life healing. This process will only work if the fatigue crack depth is confined to the layer of plastic deformation induced by the shock peening process into the treated component. Within this plastically deformed layer, the induced residual compressive stress will slow down the crack growth rate in the specimen. There is also a potential for any cracks in the surface layer to be "welded" over (if these cracks are sufficiently small enough) during the plastic deformation process brought about by shock waves generated during the laser peening process.

2.6 Conclusion

The sections discussed in this literature review have highlighted the important aspects of fatigue and some of the methods used to mitigate it.

The literature review started off by introducing fatigue and fatigue induced failure. Some of the approaches used in analysing fatigue, as well as some of the factors which contribute towards fatigue failures, were also presented.

This was followed by a discussion of some of the surface treatment techniques used to increase the fatigue life of engineered components, including shot peening and laser shock peening. These techniques introduce compressive residual stresses into the surface layers of components through a process of plastic deformation.

The literature review concluded with an analysis of some of the current approaches to fatigue life recovery in partially fatigued components. These techniques centre around the removal of damaged surface layers from components before they are subjected to an appropriate surface treatment process.

The next Chapter outlines the experimental techniques used in this study to assess the effect of laser shock peening and shot peening on the fatigue performance of aluminium alloy.

Chapter 3

Experimental Materials and Test Methods

3.1 Introduction

This Chapter introduces the experimental details and techniques used to assess the effects of laser shock peening and shot peening on the fatigue performance of AA7075. In addition, the post processing methodology used to assess the results of the analysis is also discussed. The material used in this study is characterised in Section 3.2 and the geometry of the test specimens used is defined in Section 3.3.

The study began with a preliminary investigation into the high bending stress required for crack initiation to occur in a reasonable number of fatigue cycles (i.e. less than 30000 cycles). This required that the material composition, heat treatment condition and tensile strength be analysed. The methodology for this analysis is presented in Section 3.4. Results of this preliminary investigation are given in Chapter 4, and were used to inform subsequent experimental methodology.

Following on from the preliminary investigation, analysis of the effect of shot peening and laser shock peening on the fatigue performance of aluminium alloy was conducted as described in Section 3.5. A polishing procedure was used on test specimen surfaces to make these surfaces comparable to one another before further surface treatments. This polishing procedure is described in Section 3.5.1. The surface roughness measurement procedure used to compare the effects of various surface treatments is described in Section 3.5.2. The shot peening and laser shock peening processes used to induce residual compressive stresses into the test specimens are described in Sections 3.5.3 and 3.5.4 respectively. The 3-point bending fatigue test used to compare the effects of the surface treatments procedures is described in Section 3.5.5.

The process used to investigate the ability of laser shock peening to restore fatigue performance in fatigued components is described in Section 3.6.

Finally, the techniques used to analyse the microstructure and hardness of both the fatigued and healed test specimens are detailed in Section 3.7.

3.2 Material Selection

The material selected for the test specimens in this research project was AA7075-T6 supplied by MTT (Metal and Tool Trade) Pty Ltd. South Africa. AA7075-T6 is a high strength alloy with good fatigue resistance and is typically used for component manufacture in the aerospace industry. The strength of AA7075 in the T6 condition is mainly derived from finely dispersed $MgZn_2$ precipitates, which interfere with the motion of dislocations within the material. These precipitates are formed during the ageing heat treatment of the material and are typically found within grains and along grain boundaries. The material properties for AA7075 can be seen in Table 3.1 [78]. A copy of the supplied data sheet can be found in Appendix A.

Table 3.1: AA7075 Material Properties

	AA7075-T6	**AA7075-O**	
Material Property	**Value**	**Value**	**Unit**
Mass Density	2800	2800	kg/m^3
Hardness (Brinell)	150	60	HB
Ultimate Tensile Strength	540	228	MPa
0.2 % Proof Stress	480	102	MPa
Modulus of Elasticity	72	72	GPa
Melting Range	475 to 630	475 to 630	°C
Shear Strength	331	152	MPa

3.3 Test Specimen Geometry

3.3.1 Fatigue Test Specimens

The material allocated for this project came in the form of an extruded cylindrical bar, 6 m long and 25 mm in diameter. From this extruded bar, 71 test specimens were machined with each specimen having a diameter of 17 mm and a length of 78 mm. The decrease in diameter meant surface material loss which had the added advantage of reducing possible residual stresses in the outer layers of the test specimens, which may have arisen as a result of the ageing heat treatment process used to derive the T6 condition.

Cylindrical specimens were chosen as they are relatively easy and quick to manufacture. These specimens are also representative of various components used in the aerospace industry including

shafts, bolts and other cylindrical parts. As the cylindrical bar was extruded during its manufacture, the grains within the cylindrical test specimens were parallel to the bar's cylindrical axis.

The length of each test specimen ensured that each specimen's span was equivalent to 4 times the specimen diameter (i.e. S = 4D), with 10 mm of extra material length being added to each test specimen so as to allow for easy specimen positioning during the fatigue testing process. The span to diameter ratio used in choosing the dimensions for the test specimens corresponds to dimensions suggested in both the ASTM E1290-02 [79] and E399-90 Standards [80] for fracture toughness testing, although no Standard specifically makes use of cylindrical bend test specimens for fatigue testing.

A typical 3-point cyclic bending fatigue test produces a tensile stress in the convex side of the specimen and a compressive stress in the concave side. This creates an area of shear stress along the mid-line of the test specimen To ensure that primary failure, as a result of the testing, comes from tensile or compressive stress, the shear stress must be minimised. This is achieved by ensuring that the span length of the test specimen is sufficiently wide [81].

A CAD image of the fatigue test specimens can be seen in Figure 3.1, with a full test specimen drawing available in Appendix B.

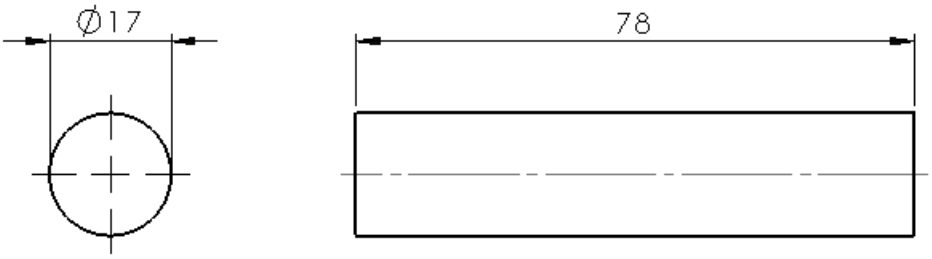

Figure 3.1: Fatigue Test Specimen CAD Drawing (Dimensions in mm)

The fatigue test specimens used in this study were tested in two material conditions, the T6 material condition and the fully annealed material conditions. Test specimens in each of these material conditions were exposed to a series of experimental processes. These processes aimed at determining the effects of shot peening and laser shock peening on the fatigue life, surface morphology, microstructure and hardness of the peened specimens. Furthermore, the ability of the laser shock peening process to restore fatigue performance in partially fatigued specimens was also investigated.

8 test specimens were used to determine an appropriate heat treatment procedure in this study, 17 test specimens were used to determine the appropriate fatigue loading conditions needed in this study and 46 test specimens were used for the various treatment and fatiguing procedures followed in this study. The 46 test specimens were split into five tests groups. Each group received a different mechanical surface treatment aimed at modifying the test specimen's fatigue lives.

The various test specimen groups and the surface treatments used in each group are given in Table 3.2. It must be noted that test specimens in the annealed material condition were fully annealed prior to the testing procedure.

Experimental Test Groups

Table 3.2: Experimental Processes

Group Number	Material Condition	Number of Specimens	Experimental Process Steps
1	T6	4	Record Surface Roughness/Diameters → Fatigue to Failure
	Annealed	4	Record Surface Roughness/Diameters → Fatigue to Failure
2	T6	4	Polish Specimens → Record Surface Roughness/Diameters → Fatigue to Failure
	Annealed	4	Polish Specimens → Record Surface Roughness/Diameters → Fatigue to Failure
3	T6	3	Polish Specimens → Record Diameters → SP → Record Surface Roughness/Diameters → Fatigue to Failure
	Annealed	3	Polish Specimens → Record Diameters → SP → Record Surface Roughness/Diameters → Fatigue to Failure
	T6	3	Polish Specimens → SP Specimens → Record Surface Roughness/Diameters → Polish Specimens
	Annealed	3	Polish Specimens → SP Specimens → Record Surface Roughness/Diameters → Polish Specimens
4	T6	3	Polish Specimens → Record Diameters → LSP Specimens → Record Surface Roughness/Diameters → Fatigue to Failure
	Annealed	3	Polish Specimens → Record Diameters → LSP Specimens → Record Surface Roughness/Diameters → Fatigue to Failure
	T6	3	Polish Specimens → LSP Specimens → Record Surface Roughness/Diameters → Polish Specimens
	Annealed	3	Polish Specimens → LSP Specimens → Record Surface Roughness/Diameters → Polish Specimens
5	T6	6	LSP → Record Surface Roughness/Diameters → Polish → Record Surface Roughness/Diameters → CT Scan → Fatigue to Crack initiation → CT Scan → Re-LSP → CT Scan → Record Surface Roughness/Diameters → Polish → Fatigue to Failure

** Note: SP - Shot Peen; LSP - Laser Shock Peen*

3.3.2 Tensile Test Specimens

Round double shouldered Hounsfield tensile testing specimens were used in order to determine the tensile strength of the aluminium alloy in both the T6 material condition and the fully annealed material condition. This configuration was chosen due to size constraints of the specimens available for testing as the tensile test specimens were machined from the cylindrical round bar fatigue test specimens. The dimensions of the test specimens were in accordance with Standard ASTM E8M [82].

A CAD image of the tensile specimens can be seen in Figure 3.2, with a full test specimen drawing available in Appendix B.

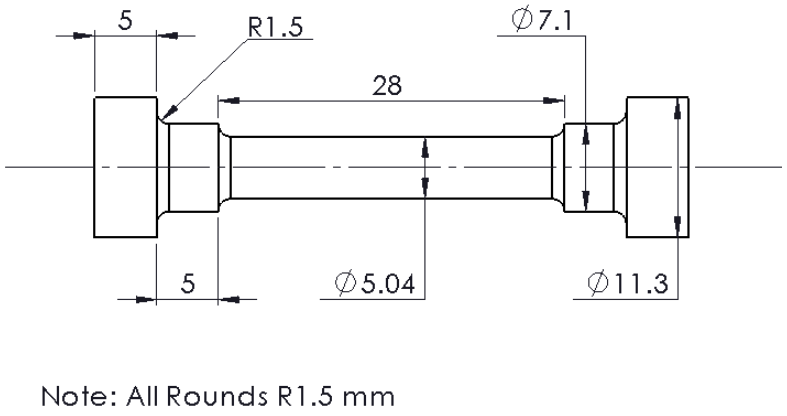

Figure 3.2: Tensile Test Specimen CAD Drawing (Dimensions in mm)

3.4 Preliminary Investigation

During initial fatigue bend testing, it was found that a bending load greater that the yield stress of the material quoted in literature [83], was required for crack initiation to occur in a reasonable number of fatigue cycles (i.e. less than 30000 cycles). Results similar to this had also previously been determined in the author's laboratory, in a study by P.M. Rammego [84]. However, a satisfactory reason for the large bending stress needed for crack initiation was not identified in the study by P.M. Rammego.

Three reasons were subsequently identified for the large bending stress. These reasons include: Incorrect heat treatment of the AA7075 resulting in large residual stresses within the material which counteracted the applied bending load; a chemical composition differing to that typically found in AA7075-T6; the fact that the bending strength of a material is in fact greater than the tensile strength of the material. These factors were further investigated in a preliminary study so as to further understand the fatigue characteristics of the aluminium alloy used in this project.

3.4.1 Material Characterisation

A full material compositional analysis was performed on the AA7075 in the T6 condition using energy dispersive spectroscopy (EDS). This was done in order to verify the grade of the aluminium alloy supplied by comparing it to the chemical composition guidelines given by The Aluminium Association [78] for AA7075.

The nominal chemical composition (as a weight percentage) of AA7075, according to The Aluminium Association [78], can be seen in Table 3.3. Element limits in the Table are expressed as a maximum unless shown as a range.

Table 3.3: Chemical Composition Limits for Aluminium Alloy 7075-T6

Mg	Al	Si	Ti	Cr	Mn	Fe	Cu	Zn	Other
2.10 - 2.90	87.10 - 91.40	0.40	0.20	0.18 - 0.28	0.30	0.50	1.20 - 2.00	5.10 - 6.10	0.15

The material compositional analysis was performed using a ZEISS/LEO 1450 scanning electron microscope (SEM) equipped with a spectrometer. The analysis was conducted at the University of Cape Town Centre for Imaging and Analysis with assistance from Miranda Waldron. Five point scans were performed at different sites on a flat, sectioned surface taken from an aluminium test specimen. The mean average weight percentage of the different elements contained with the sample was then calculated.

A scanning electron microscope generates a beam of electrons in an electron column above the sample to be analysed. The electrons are focused into a small beam via a series of electromagnetic lenses in a SEM column. Scanning coils near the end of the column direct and position the focused beam onto the sample surface where the electron beam is scanned in a specific pattern over the specimen surface for imaging. The beam can be focused at a single point or scanned along a line for x-ray analysis [85].

As the electrons strike the sample, a variety of signals are generated from the emission of secondary electrons, backscattered electrons or X-rays. In order to measure the elemental composition of a specimen, a scanning electron microscope is equipped with a spectrometer which is able to detect X-rays emitted by the sample during electron beam excitation. These X-rays hold a typical energy and wavelength, which when measured will divulge the elemental composition of an area. A common type of X-ray analysis used in combination with SEM'S is an Energy Dispersive X-ray Spectroscopy (EDS) [86].

For this study, the SEM was operated at a beam energy of 20 keV, spot size of 5 and a working distance of 5.5 mm.

3.4.2 Heat Treatments

In order to determine whether the correct heat treatment procedure was followed by the AA7075 manufacture's, six test specimens were heat treated with varying heat treatment processes aimed at establishing the T6 material condition. The main aim of this procedure was to identify whether the

correct heat treatment process had initially been used on the aluminium alloy during its manufacturing and if not, whether this incorrect heat treatment process could be corrected. An incorrectly applied heat treatment process may have resulted in large compressive residual stresses within the aluminium alloy which may have counteracted the applied bending stress

A secondary aim of the heat treatment procedure was to identify a suitable heat treatment process that would maintain the high strength typically associated with AA7075-T6 whilst at the same time reducing any of the residual stresses present within the test samples as a result of their production. Stress-free test specimens would provide a suitable base onto which various surface treatments (most of which look to introduce residual stresses as a means of fatigue life enhancement) could be imposed.

It was suggested by Dr. Sarah George, from the University of Cape Town Centre for Materials Engineering, that the T6 heat treatment process be re-done. This required that the cylindrical test specimens be solution heat treated from an annealed state, before being artificially aged resulting in a T62 temper. The solution treatment temperatures and times of the heat treatment process to be conducted was varied in order to determine an appropriate heat treatment procedure applicable to this study. Literature has shown that the solution treatment step has potential for large variability in terms of both time and temperature [87]. The solution treatment step is the stage where possible residual stress relief can occur through the dissolution of precipitates and equilibration of stresses and it was therefore decided to vary the times and temperatures of this step in order to limit the possible number of potential heat treatments that could be applied to the test specimens. Solution heat treatment times and temperature were sourced from various literature sources, which are referenced in Table 3.4. The annealing time and temperature were sourced from G.E. Totten and D.S. MacKenzie[88] and the precipitation time and temperature were sourced from J. Davies[89].

Six AA7075-T6 samples were annealed, then solution heat treated at various temperatures and heating times followed by a water quench and re-ageing treatment, the time and temperature of which were kept constant. After these heat treatment processes, their hardness and surface residual stresses were measured so as to determine the change in strength which resulted from the process (hardness can be related to material strength as will be shown later). All heat treatment procedures were carried out in accordance with ASTM Standard B918-01 [90], with the exact process followed in this study described below. Figure 3.3 shows each stage of the precipitation hardening process followed.

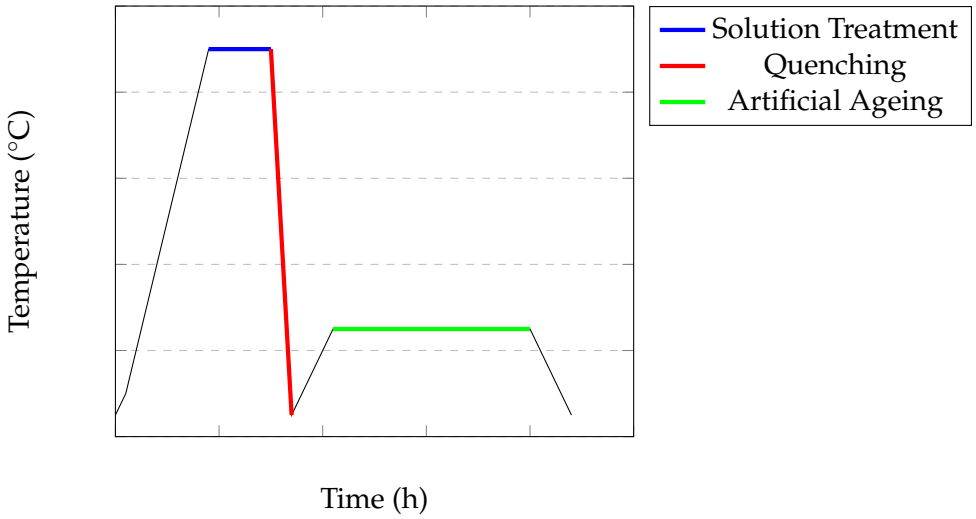

Figure 3.3: Heat Treatment Procedure

The applied heat treatment to each test specimen presented in Table 3.4.

Table 3.4: Initial Heat Treatment Trial And Error Process

Specimen Number	Initial Anneal (Two Stage Process)	Solution Heat Treatment Time and Temperature (°C)	Water Quench (Quench at 20°C)	Artificial Ageing at 120°C for 24 h	Reference
1	Yes	420°C for 1 h	Yes	Yes	[87]
2	Yes	450°C for 1 h	Yes	Yes	[87]
3	Yes	480°C for 1 h	Yes	Yes	[87]
4	Yes	440°C for 2 h	Yes	Yes	Temperature selected to cover 2h range
5	Yes	465°C for 2 h	Yes	Yes	[89]
6	Yes	490°C for 2 h	Yes	Yes	[89]

3.4.3 X-Ray Diffraction of Heat Treated Specimens

The six test specimens used in the initial heat treatment trial and error process, together with a specimen in the T6 material condition and a specimen in the fully annealed material condition, were sent to NECSA (South African Nuclear Energy Corporation SOC Limited) for residual stress analysis of their surface layers by means of X-ray diffraction. The X-ray diffraction tests were performed by Mr. Tshepo Ntsoane, under the supervision of Dr. Andrew Venter. A fully annealed, stress-free specimen was needed as a baseline with which to compare peak shifts in stress containing specimens.

Residual stress/strain measurements were carried out by XRD techniques employing the BRUKER D8 Discover X-ray theta-2theta goniometer diffractometer in side-inclination mode (ψ goniometer mode) fitted with a Vantec 500 detector. Measurements were done using the $Sin^2\psi$ technique based on a linear dependence existing between the strain and $Sin^2\psi$, with ψ being the tilt angle of the scanned sample from the surface normal. A The BRUKER D8 Discover diffractometer used for the residual stress analysis can be seen in Figure 3.4.

Figure 3.4: Laboratory Diffractometer [91]

The Vantec 500 detector used in this experiment was a 2D detector, which facilitated the collection of large portions of diffraction rings, known as Debye diffraction rings. Debye rings are typically associated with conventional powder diffraction but can be used for grain size and texture analysis. X-rays, which have been diffracted from polycrystalline test samples, form a series of diffraction cones, where each diffraction cone corresponds to the diffraction of X-rays from the same family of crystalline planes in all the participating grains. When a 2D detector is used for stress measurement, the distortion of the diffraction cone produced at each orientation of the sample, is used for the stress calculations. The diagram shown in Figure 3.5, depicts how stress affects conic sections formed from diffracted X-rays.

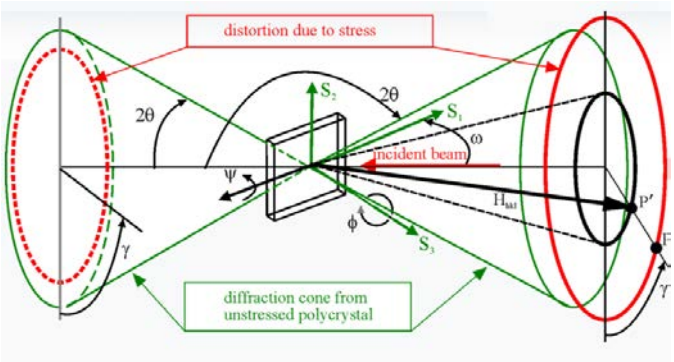

Figure 3.5: Conic Section Formed from Diffracted X-rays [92]

As a result of the Debye patterns generated (large grain sizes and texture were present in the X-Ray diffracted samples), the test specimens were oscillated during their respective diffraction procedures. Oscillation increases the number of grains being measured without increasing the collimator size or reducing resolution

The following Table summarises the parameters used during the residual stress measurements:

Table 3.5: X-ray Diffraction Measurement Parameters

Measurement Parameter	**Value**
Goniometer	$\Theta - 2\Theta$
Target Tube	Cu
X-Ray Radiation	Cu-Kα1
X-ray Wavelength	1.54055 A°
X-Ray Radiation Energy	8 keV A°
Anode Settings	40 kV & 40 mA
$\kappa - \beta$ filter	Nickle
$2 - \theta$	137.5°
(*hkl*)	422
Beam Diameter	8 mm
Azimuthal Orientation (ϕ)	0°, 45°, 90°
Psi Tilt (ψ)	0.10° to 60.10° in steps of 10°, giving 7 sample tilt angles
Counting Time/Frame	200 s
Reflection Utilised	Al(4 2 2) investigated at a scattering angle of 137.462°
Diffractometer	D 8 Discover equipped with Vantec 500 area detector

Measurements of the test samples were taken at three different azimuth angles (ϕ) including: 0°, 45° and 90° so as to determine the full stress tensor using the $Sin^2\psi$ method. The azimuth angle

is defined as the rotation around the surface normal of the test specimen. At each azimuth angle, the test specimens were rotated through a series of seven psi, ψ, tilt angles in 10° steps from 0.10 to 60.10°. Negative ψ tilt angles were achieved by rotating the samples by 180°, so as to investigate any possible psi-splitting, which indicates the presence of shear stresses within the samples. These measurements were performed at three equally spaced points around the circumference of each test specimen (i.e. 120° points along the circumference). The lattice strain was obtained from the shift of the (*hkl*) *Bragg* peak positions of the various test specimens when compared to that of an unstrained specimen (fully annealed specimen 7). Data was analysed for residual stress determination using Bruker LEPTOS, version 6 software.

3.4.4 Macrohardness Testing of Heat Treated Specimens

The surface hardnesses of the eight X-ray diffracted test specimens were taken as surface hardness can be related to the yield strength of a material. Therefore the surface hardness of the heat treated test specimens could provide an indication as to the decrease in strength of the various test specimens (from the T6 case) as a result of their specific heat treatments. Surface hardness measurements were made using a Zwick Vickers Hardness testing machine, seen in Figure 3.6. The Vickers Hardness of a given material is determined by measuring the diagonal lengths of an indent left on the test material, using a diamond indenter with a given load.

Figure 3.6: Zwick Vickers Hardness Testing Machine

The hardness testing was performed in accordance with ASTM Standard E92-82 [93]. Eight hardness tests were performed for each of the test specimens, in 45° increments (the increments were measured and marked off around the centre of each specimen using a marker pen). Figure 3.7, shows where the hardness measurements were taken on each specimen.

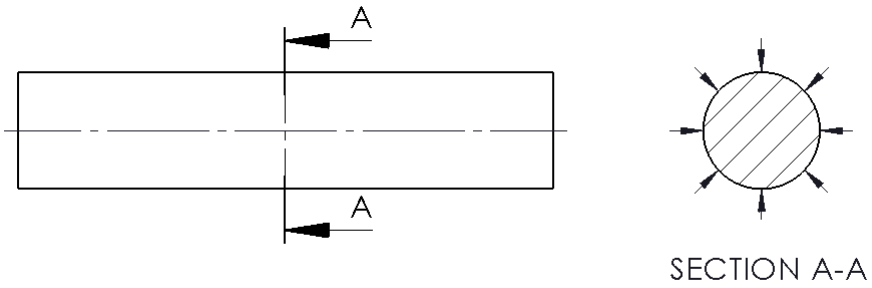

Figure 3.7: Vickers Hardness Measurement Spacings

The surfaces of all eight specimens were lightly polished using 1200 grit sandpaper (see Section 3.5.1 for the polishing procedure) and subsequently cleaned using an ethanol solvent prior to the hardness testing. An anvil (v-block) was used to rigidly support the cylindrical test specimens on the machine testing surface.

As the surfaces of the test specimens were cylindrical, a correction factor was applied to each hardness value obtained from the Vickers Hardness testing. The correction factors were obtained from the ASTM Standard E92-82 [93], and are presented graphically.

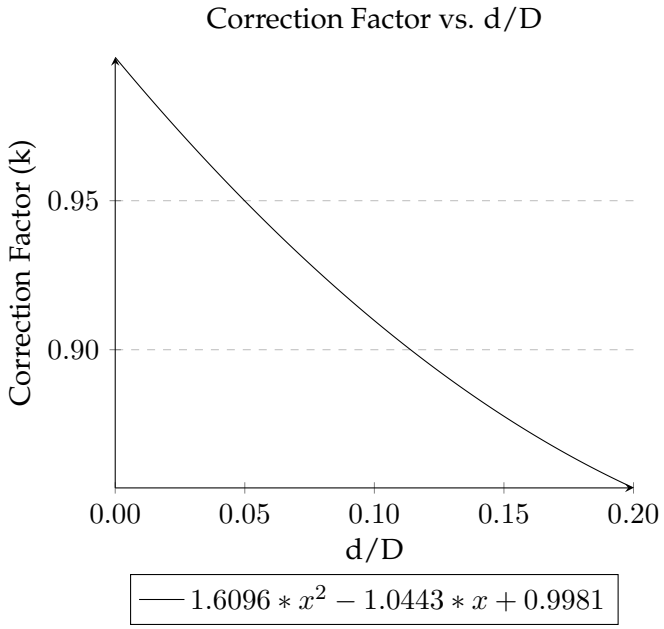

Figure 3.8: Vickers Hardness Correction Factor for Curved Surfaces

Using the measured Vickers Hardness values for each of the heat treated test specimens, an estimated ultimate tensile strength for each test specimens was established based on the relationship

[94]:

$$HV \approx 0.3 * \sigma_{UTS} \tag{3.1}$$

Where:

HV: Vickers Hardness (HV)

σ_{UTS}: Ultimate Tensile Strength (MPa)

Although this relationship can be used as an approximate relationship, it is not always strictly correct. For this study, it was a good indication into the percentage reduction in ultimate tensile strength each heat treatment had on the various test specimens.

3.4.5 Tensile Testing

Uniaxial tensile tests were performed as the final part of the preliminary investigation. At this stage of the study, it had been decided that heat treating the AA7075 was unnecessary. Residual tresses (as measured at NECSA) induced into the AA7075 were significantly larger than the residual stresses within the "as received" AA7075. It was thus decided to use test specimens in the "as received" T6 condition as well as in the annealed condition for comparative purposes.

Tensile tests were performed to determine the ultimate tensile strength and work hardening coefficient of the aluminium alloy using in this study. This tensile stress could then be compared to the bending stress needed for crack initiation in the cyclic fatiguing Section of this project. Tensile tests were carried out on round Hounsfield test specimens in both the AA7075-T6 and AA7075-O (annealed) conditions, using the Zwick tensile tester shown in Figure 3.9. Tests were performed in accordance with Standard ASTM E8M [82].

Figure 3.9: Zwick Tensile Testing Machine

All specimens were tested in displacement control mode at a strain rate of 0.001 s^{-1}. Three test specimens in both the AA7075-T6 and AA7075-O conditions were tested.

Further material properties determined from the tensile test data include: 0.2 % tensile yield strength, ultimate tensile strength, the elongation (%) at fracture/failure and the work hardening exponent.

The 0.2 % tensile yield strength and ultimate tensile strength were simply read off the engineering stress-strain curves generated for each test specimen. The elongation (%) at failure was read off from both the engineering stress-strain curves generated and manually measured from the fractured tensile specimens. This manual measurement would help determine if specimen slippage and specimen settling (i.e. settling into the grips) occurred during testing. The work hardening exponent for each material condition required that the engineering stress and strain data be converted into true stress and true strain data respectively. After this conversion, a logarithmic plot of the true stress-true strain data (after the yield point for each tensile test) was created.This enabled the relationship between true stress and work hardening to be determined (a logarithmic plot of true stress-true strain data can be seen in Figure 3.10). The slope of a straight line-of-best fit through the logarithmic plot is equal to the work hardening exponent of the material, with the

equation for the straight line-of-best being:

$$log(\sigma_t) = nlog(\varepsilon_t) + log(K) \tag{3.2}$$

Where:

σ_t*: True Stress (MPa)*

n*: Work Hardening Coefficient*

ε_t*: True Strain (%)*

K*: Strength Coefficient*

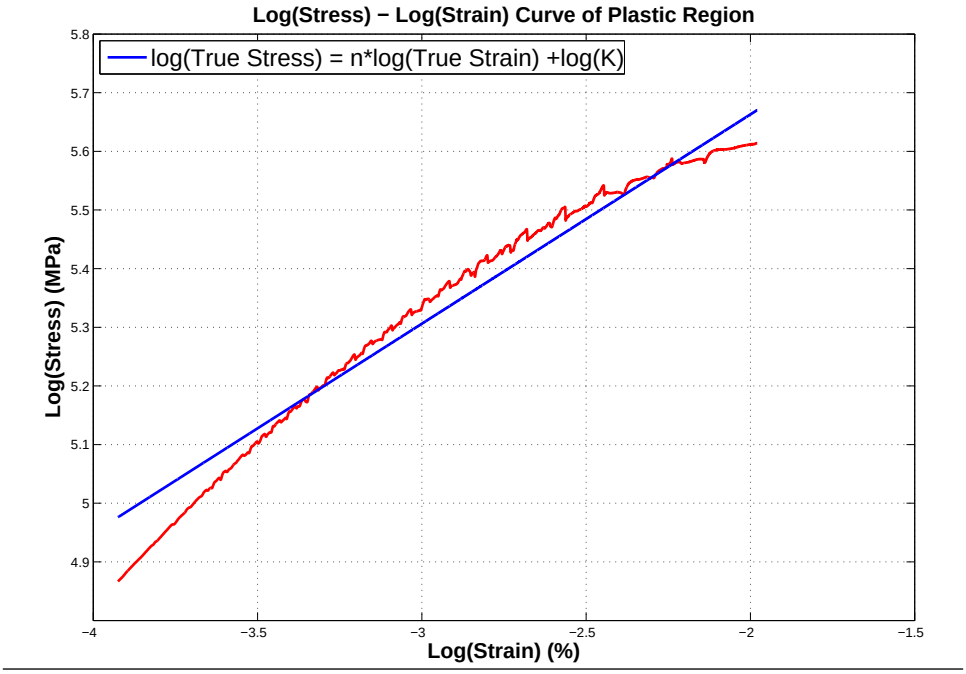

Figure 3.10: Logarithmic Plot of the True Stress-True Strain Curve

3.4.6 Preliminary Investigation Conclusion

The preliminary investigation into AA7075 found that the properties of the aluminium alloy were comparable to the properties as defined by The Aluminium Association [78].

A chemical compositional analysis found that the alloying elements present within the AA7075 were within the acceptable tolerance limits. However, the zinc content was 0.44 weight % over the maximum recommended level for zinc as defined by The Aluminium Association [78]. Subsequent testing (macrohardness and tensile tests) showed that this increased zinc content had no detrimental effect on the AA7075-T6 hardness and strength.

Six test specimens were subjected to various heat treatments in order to identify whether the correct heat treatment process had been used on the aluminium alloy during its manufacturing. A secondary aim of the heat treatments was to determine if the high strength typically associated with AA7075-T6 could be maintained whilst eliminating any residual stresses present within the alloy. X-ray diffraction of the various heat treated test specimens found that residual stresses within the AA7075 test specimens "as received" from the supplier were substantially lower than the stresses within the "re-heat" treated specimens.

It is suspected that an error with the quenching process used during the heat treatments tested in this project may have resulted in a large increase in residual stresses within the test specimens. During specimen production the machining down of the surface layers of the test specimens (i.e. reducing the diameter of the test specimens from 25 mm to 17 mm) facilitated in the reduction of residual stresses which are induced into the aluminium as a result of its manufacturing. Macrohardness testing of the specimens used during the preliminary investigation allowed for the ultimate tensile strengths of the specimens to be estimated. This proved to be a useful technique to estimate the material strength relatively quickly and were comparable to subsequent tensile testing generated values.

The tensile tests confirmed that the AA7075-T6 had a relatively high tensile strength, which in turn required high bending stresses to fatigue the samples. During bending the maximum stresses occur on a small area (usually only on the edge) of the tensile bending section. Conversely, during a tensile test the entire cross section of the sample is under maximum stress. Therefore, it is more likely that during tensile testing a "weak point" is found within the material microstructure from where rupturing of the sample can initiate. As bending stresses are confined to the outer surface of the material, the probability of a "weak spot" from which rupturing can occur is less. This means that materials under bending can often withstand higher stresses than materials under tension [95].

3.5 The Effect of Shot Peening and Laser Shock Peening on Fatigue Performance

Following on from the preliminary investigation, analysis of the effects of polishing, shot peening and laser shock peening on the fatigue performance of aluminium alloy was conducted. This investigation was conducted on test specimens in the "as received"/T6 and annealed material conditions based on the results of the preliminary investigation discussed in Chapter 5. The experimental process steps used on these test specimens are outlined in Table 3.2 above and discussed in detail in the following Sections.

3.5.1 Test Specimen Polishing

One of the major factors which influences the fatigue life of an engineered component is the component's surface roughness. Crack nucleation is often facilitated at micro-crevices and grooves on rough surfaces, both of which act as stress concentration sites.

In order to facilitate data acquisition and to determine the influence of surface roughness on fatigue life, the surface roughness of some of the test specimens was reduced. This reduction in surface roughness enabled the surface roughness's induced by the mechanical surface treatment processes to be accurately gauged and thus allowed for surface roughness as a variable to be reduced.

Surface roughness values of around 0.20 $\pm 0.05 \mu$m or less were desirable for the polished test specimens as this is the feasible range of R_a values for manual polishing as a means of material removal as described in literature [96]. Test specimens in both material conditions were polished as part of the experimental processes for test Groups 2, 3, 4 and 5. The test specimens which required annealing were polished after their annealing process. The diameters of the polished test specimens were measured before and after the polishing procedure in order to determine how much material was removed as a result of the polishing procedure. Care was taken not to over-polish the specimens and thus substantially reduce their diameters. Specimens from Group 5 undergoing the fatigue life restoration procedure, were also polished during their experimental procedure. The diameters of the specimens were measured before and after the polishing procedures used during this process. The diameter measuring procedure is further described in Section 3.5.2.

In order to polish the test specimens uniformly and thus their curved surfaces, the specimens were held in a chuck adaptor for a Bosch drill press and rotated against the varying grades of sand paper, which were manually held, at 500 revolutions per minute. The drill press, seen in Figure 3.11, allowed the test specimens to be rotated in a balanced manner and at a controlled speed. Each test

specimen was rotated for 10 seconds against the 1200 grit sandpaper. After 10 seconds of polishing, the specimen surface roughnesses were check using the Taylor Hobson Talysurf testing machine. If these surface roughness values were not within the desired range, the polishing procedure was repeated. Water was used as a polishing lubricant and aided in reducing friction and thus heat generated during the process. Once the polishing process was completed the test specimens were cleaned in a vibrating bath.

Figure 3.11: Drill Press

3.5.2 Surface Roughness Testing and Specimen Diameter Measurements

The surface roughness values of the test specimens used in this study were measured using a Taylor Hobson Talysurf testing machine, seen in Figure 3.12.

Figure 3.12: Taylor Hobson Talysurf

The Hobson Talysurf testing machine works by traversing a stylus across the surface of the material for a specified distance and with a specified contact force. The vertical movement of the stylus is

then converted into an electrical signal by a transducer (or gauge) and is sent to a processor which converts this signal into a number. For accurate readings, the stylus must be moved in a straight line [97]. In Figure 3.13, a stylus is shown moving over a surface whilst creating a profile chart of the testing surface at the same time.

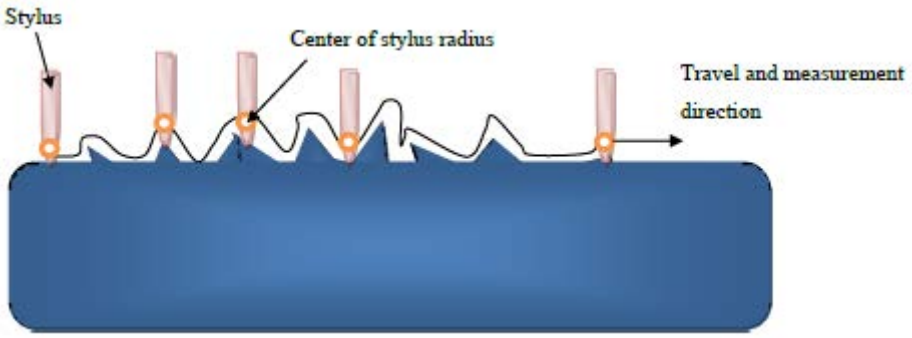

Figure 3.13: Stylus Dragged Across the Surface of Component [54]

The Taylor Hobson Talysurf testing machine displays the arithmetic mean surface roughness (R_a) of the measured surface. The arithmetic mean surface roughness is the most common parameter used to measure surface roughness and is calculated across a sampling length which measures the average length between peaks and valleys on the material surface as well as the deviation from the mean line within this sampling length. An example of a typical sample length and the deviations which occur along it can be seen in Figure 3.14.

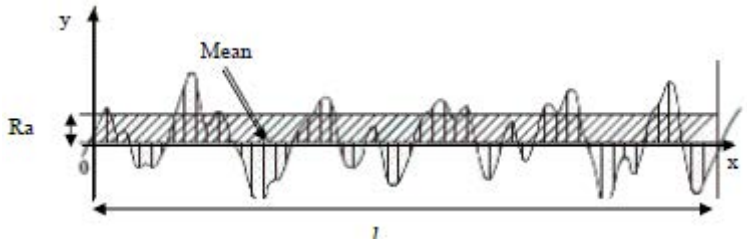

Figure 3.14: Sample Length for Arithmetic Mean Surface Roughness [54]

All surface roughness measurements were performed in accordance with the British Standard BS 1134: 1988 [98]. In this study, the circumference of each test specimen was divided into five equally spaced segments (72° sections) from which the mean average of the five surface roughness was calculated. The surface roughness measurements of each test specimen were then measured axially along each of these five segments, starting 12.5 mm away from the middle of each test specimens. The total sample measuring length was 25 mm, which meant that the surface roughness 12.5 mm

on either side of the mid-section of the test specimen was measured. Figure 3.15, shows where the surface roughness measurements were taken on each specimen. From the surface roughness measurements, surface roughness profiles were generated for each test specimen. These profiles enabled a visual representation of the arithmetic mean surface roughness (R_a).

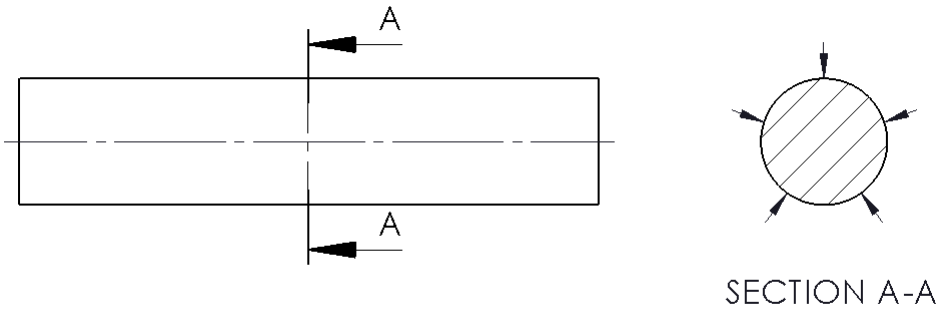

Figure 3.15: Surface Roughness Measurement Spacings

The test specimens were placed in a v-block (anvil) to hold them securely, with their cylindrical axes (longitudinal axes) parallel to the direction in which the stylus would be dragged. This allowed the stylus to move in a straight line across the specimen surface, without slipping to either side of the curved surface. The stylus moved across the sample surface at a speed of 1 mm/s. A schematic of the set-up used for the surface roughness testing can be seen in Figure 3.16, where the major components have been labelled.

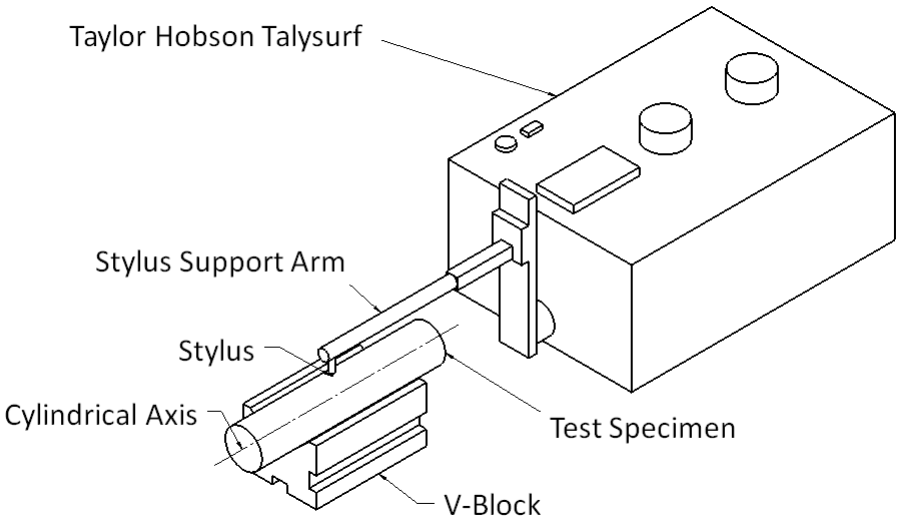

Figure 3.16: Surface Roughness Testing Set-Up

The diameters of the test specimens were also measured during each experimental process. Specimen diameters were measured prior to the fatiguing process in order to calculate the applied bending stress needed during the fatiguing process. Diameter measurements were also taken on the test specimens before and after the polishing, shot peening and laser shock peening treatments. This enabled the amount of material removed from the polishing procedures to be determined as well as for the degree of compression which resulted from the peening procedures to be determined.

3.5.3 Shot Peening Treatment

In this study test specimens from test Group 3 were shot peened at South African Airways Technical (SAAT) by Ryan Farnham and Eduard Roodt. Six test specimens in the T6 condition were shot peened and six test specimens in the annealed condition were shot peened. The shot peening process was conducted using a robotically operated air blast shot peening machine installed by Straaltechniek Int. Ltd. A photograph of the machine can be seen in Figure 3.17.

The shot peening machine utilised compressed air as the moving force behind the shot delivery system. The compressed air shoots the peening material through two nozzles attached to the end of a robotic arm prior to the shot material striking the target surface. This robotic arm facilitated the shot blast stream to be controlled and manipulated with a high degree of precision and repeatability. The robotic arm facilitated a constant shot intensity to be delivered at any required angle and was manually operated through a control remote. The shot peening process was confined to a specially designed blast chamber with rubber lined walls. Shot was stored in a pressurised vessel and was metered into a compressed air stream through a shot flow valve for delivery. To overcome the problem of stopping the shot peening process to refill the pressurised vessel with shot, a dual vessel system was used. In this system, another pressure vessel was mounted above the blast pressure vessel, with a valve in between the two vessels. When blasting starts the lower blast vessel pressurises and blasts as normal. The upper pressure vessel stays de-pressurised with an open dump valve. This allows it to receive recovered shot from the shot peening chamber. The bottom of the shot blast chamber was covered in a steel grid which facilitated used shot to pass through and get sucked up and collected automatically by the de-pressurised vessel. Before reaching the de-pressurised vessel, the shot travels through a series of grates which separated damaged shot from re-usable shot.

Figure 3.17: Robotically Operated Shot Peening Machine

In order to achieve the optimum shot peening treatment possible for the test specimens, determination of the correct process control parameters was essential. The effect of these various parameters on the shot peening process can be found in Section 2.4.1 of the Literature review. The initial parameters selected were based on the parameters used by SAAT to shot peen aluminium aircraft wheel hubs and landing gear struts. Slight modifications were made to the peening intensity and cycle time parameters used by SAAT so as to accommodate the specimens of this study. These modifications were made with the aid of Almen strips, which facilitated the measurement of the shot peening intensity. The shot peening parameters used in this study can be seen in Table 3.6.

Table 3.6: Controlled Shot Peening Parameters

Parameter	Value	Unit
Media Size	S230	Cut Wire (Steel)
Media Hardness	45 - 50	HRC
Number of Nozzles	2	
Table Speed	30	RPM
Pressure	2000	kPa
Flow Rate (per nozzle)	3.5	kg/min
Shot Peening Time	1.49	min
Cycles	6	
Intensity	12A	
Coverage	100	%
Robot Control Speed	40	mm/s

Almen strip measurement is a standardised process used to measure the kinetic energy transferred

by a shot stream. In this study, "A" type Almen strips (1.30 mm thick, 76 mm long and 19 mm wide) of SAE 1070 steel were used to quantify the exposure time and coverage of a shot peening process with the aid of a saturation curve. Once the desired coverage of 100 % had been achieved (same coverage used by SAAT), AA7075-T6 Almen strips (3.98 mm thick, 76 mm long and 19 mm wide) were shot peened at the same intensity as determined by the "A" type Almen strips for the varying cycle times. This helped verify that the parameters determined by the "A" type Almen Strips were transferable to AA7075.

Both sets of Almen strips were orientated at 90° to the shot stream, with the lengths of the Almen strips perpendicular to the ground. The tool used to hold the Almen strips was fixed in the Y, X and Z directions. The standoff distance between the strips and shot peening nozzles was set to a distance of 177.8 mm (7 inches). This set-up can be seen in Figure 3.18.

Figure 3.18: Tool Used to Mount Almen Strips

The shot peening nozzels, which were connected to the end of a robotic arm, moved vertically along the length of the Almen strips (Y direction) during the peening process in order to ensure full strip coverage. The time length of the shot peening process was determined in terms of cycles, where one cycle comprised of the shot peening nozzles moving from the top of the Almen strip to the bottom of the strip and then back up to the top again. Seven Almen strips (7 x SAE 1070 steel) were peened for 1, 2, 3, 4, 8, 8 and 16 cycles respectively at 18 PSI. After each peening process the midspan deflection (residual compressive stresses from the peening process causes the Almen strip to arc convexly towards the peened side) of each Almen strip was measured using an Almen gauge, seen in Figure 3.19. The Almen strip arc height is a function of the energy of the shot stream and is very repeatable. Each deflection was then plotted against its respective cycle time, using a programme called Saturation Curve Solver SC1 [99]. This programme enabled the point of peening

saturation to be determined (first point on the line of best fit through the data points, when the exposure time is doubled, there is a 10 % increase in arc height). This point of saturation correspond to a surface coverage of 100 %, and enabled the required peening cycle time and intensity to be determined accordingly.

Figure 3.19: Almen Gauge

It was determined that saturation occurred at 6 cycles, with a peening intensity of 12A. The saturation curve produced can be seen in Figure 3.20. In order to verify that a peening intensity of 12A for 6 cycles would result in 100 % coverage on the AA7075-T6 specimens, Almen strips made from AA7075-T6 were peened for 1, 2, 3, 4, 8, 8 and 16 cycles at an intensity of 12A. Coverage of 100 % was verified after 6 cycles on the AA7075-T6 Almen strip by visual inspection, which corresponded to the cycle time determined through peening the "A" type Almen strips. The SAE 1070 steel type "A" Almen strips and the AA7075-T6 Almen strips can be seen in Figure 3.21 after their respective peening procedures.

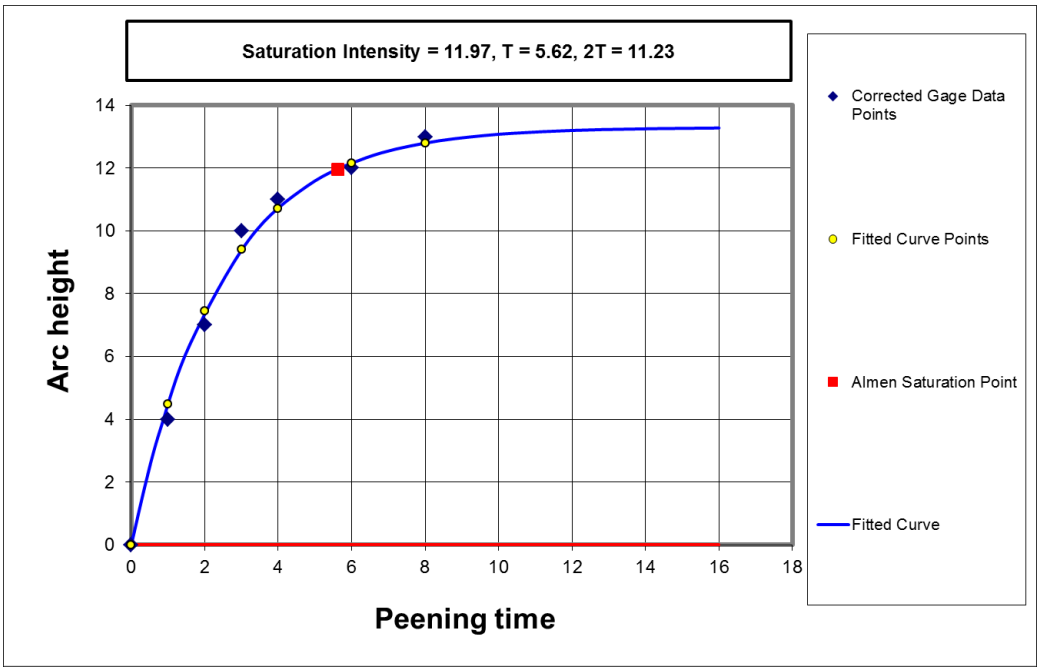

Figure 3.20: Almen Strip Saturation Curve

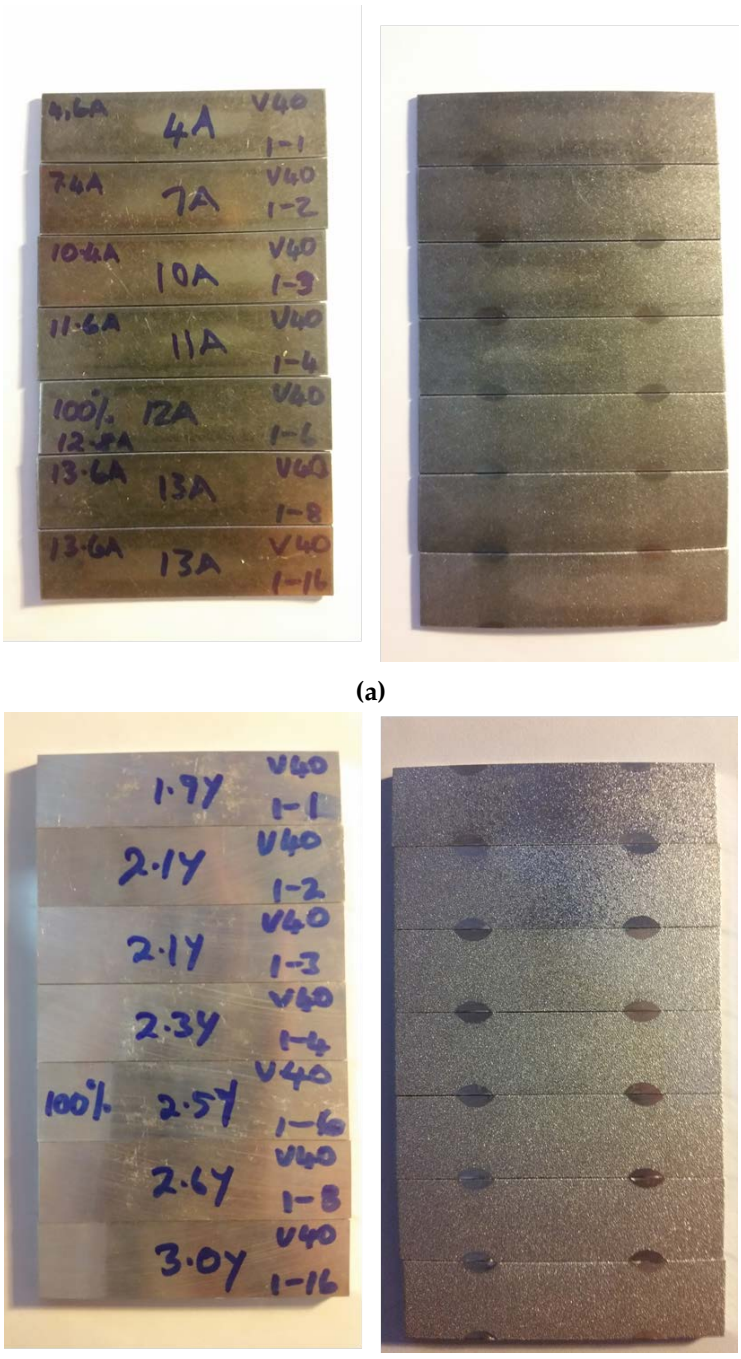

(a)

(b)

Figure 3.21: Almen Test Strips After Shot Peening
(a) "A" Type SAE 1070 Steel Almen Strip; (b) Aluminium 7075-T6 Almen Strip

After the shot peening process parameters were determined, the round bar test specimens used in this study were shot peened. Six specimens in the T6 material condition and six specimens in the annealed condition were subjected to the same peening procedure. During each peening procedure, a test specimen was clamped at one end in a chuck and held vertically. The chuck was centred on a rotating table within the shot peening machine chamber. The table was set to rotate at 30 rpm, which would enable the entire cylindrical surface of the test specimen to be evenly peened.

The blast nozzles were set perpendicular to the test specimen surface at a distance of 177.8 mm. After the test specimen was set up, the doors to the shot peening chamber were closed and the peening process was initiated. The robotic arm moved the blast nozzles up and down along the length of the specimen at a speed of 40 mm/s for a total of six cycles. This process was repeated for all test specimens in both the T6 and annealed material conditions. Figure 3.22, shows how the test specimens were held vertically in the clamp.

Figure 3.22: Test Specimens Clamped for Shot Peening

3.5.4 Laser Shock Peening Treatment

In this study, test specimens undergoing laser shock peening treatment process were tested at the National Laser Centre (NLC) located at the Council for Scientific and Industrial Research (CSIR), by Daniel Glaser. The laser used was part of the 'CSIR NLC Rental Pool Programme' by the National Laser Centre and was used under the grant held by Professor Claudia Polese from the University of the Witwatersrand. Twelve test specimens in the T6 condition were laser shock peened (six of these test specimens were to be used for the fatigue life restoration process of this study) and six test specimens in the annealed condition were laser shock peened.

The process utilised was as follows; a laser beam pulse, generated by a Q-Switched Pulse ND: YAG (Neodymium-doped Yttrium Aluminium Garnet) Laser was sent from the laser through a beam splitter. The laser used can be seen in Figure 3.23.

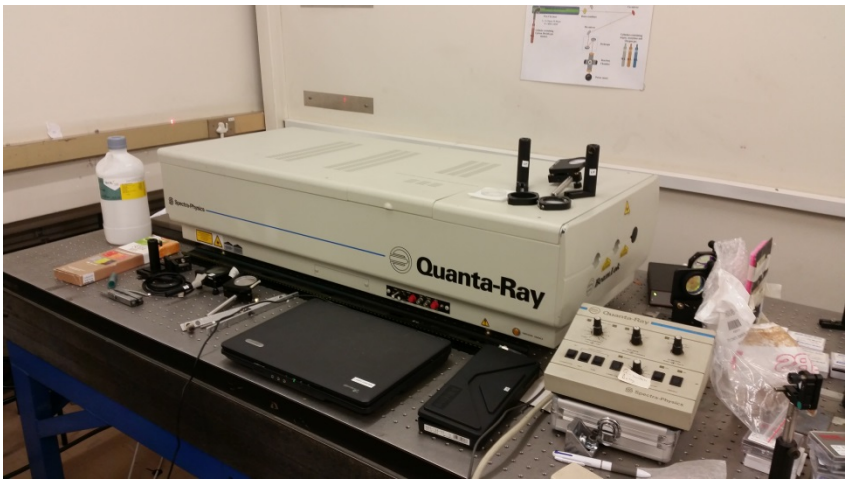

Figure 3.23: Q-Switched Pulse ND: YAG Laser

The beam splitter enabled a portion of energy (2 %) from the laser to be diverted and measured using an energy meter, seen in Figure 3.24. The bulk of the laser beam exited the beam splitter and moved through a chain of mirrors before being focused through a lens and concentrated onto the surface of the test specimen, where it vaporised a small section of the specimen surface. Before impacting on the surface of the test specimen, the laser beam moved through a moving water overlay, which ran across the surface of the specimen. This water overlay confined the plasma created through the vaporisation of the specimen surface, resulting in a shockwave which was able to propagate into the test specimen, so causing plastic deformation of the specimen's surface layers. The specimens laser shock peened in this study were not coated with an ablative layer prior to their shock peening. Ablative coatings are generally used to enhance laser absorption and prevent the treated surface from melting or being damaged [100]. Through controlling the laser pulse energy, surface melting can be mitigated so negating the need for an ablative coating. This in turn facilitated a quicker and less complicated peening process. Laser shock peening without an ablative coating was initially studied and developed by the Toshiba Company [100]. The Laser parameters used in this study were based on previous experience gained from the University of the Witwatersrand and the CSIR with aluminium alloys, including AA6056-T4, AA6082, AA2024, AA7075-T6, AA1050 [54, 101]. The parameters used can be seen in Table 3.7.

Figure 3.24: Laser Energy Meter

In order to laser shock peen the cylindrical test specimens used in this study with an 'overlapping-peening' pattern, a specially designed mounting platform was required. The platform enabled the specimens to be rotated and moved vertically (i.e. in the Z direction, see Figure 3.25) at the same time. Specimens were mounted vertically in a chuck which was attached to a motor and enabled chuck rotation. The chuck used can be seen in Figure 3.25.

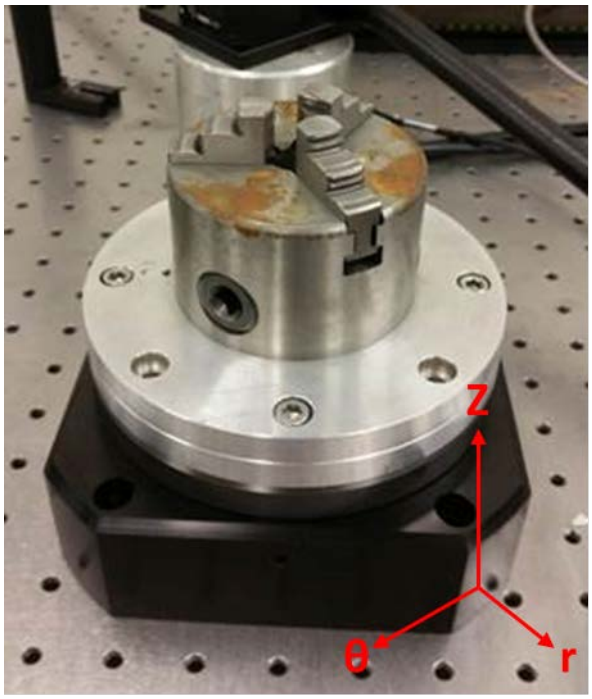

Figure 3.25: Laser Shock Peening Rotational Chuck

The chuck was then attached upside down (i.e. the free end of the specimen faced downwards) to a platform which was able to move in a vertical direction. This arrangement can be seen in Figure 3.26. This vertical movement, when coupled with the rotation of the test specimen ensured that an overlapping helical peening pattern could be achieved along the length of each test specimen. The rotation of the chuck and vertical movement of the stage to which the chuck was connected was controlled using a computer software based on a CNC control programme. The test specimens were rotated clockwise at a speed of 60 degrees/s and the chuck was moved upwards at a rate of 0.075 mm/s. This movement allowed for a spot coverage of 500 spots/cm^2.

The two equations used to determine the specimens rotational velocity and vertical stage velocity are defined as follows:

Vertical Stage Speed:

$$v_z = \frac{R_{rate}}{(C_{coverage})^{0.5}(2\pi \times \rho_{radius})} \tag{3.3}$$

Where:

v_z*: Vertical Stage Speed (mm/s)*

R_{rate}*: Laser Repetition Rate (Hz)*

$C_{coverage}$*: Coverage (spots/mm^2)*

ρ_{radius}*: Specimen Radius (mm)*

Specimen Rotational Speed:

$$\omega_{specimen} = \frac{R_{rate} \times 180}{(C_{coverage})^{0.5}(\pi \times \rho_{radius})} \tag{3.4}$$

Where:

$\omega_{specimen}$*: Specimen Rotational Speed (degrees/s)*

R_{rate}*: Laser Repetition Rate (Hz)*

$C_{coverage}$*: Coverage (spots/cm^2)*

ρ_{radius}*: Specimen Radius (cm)*

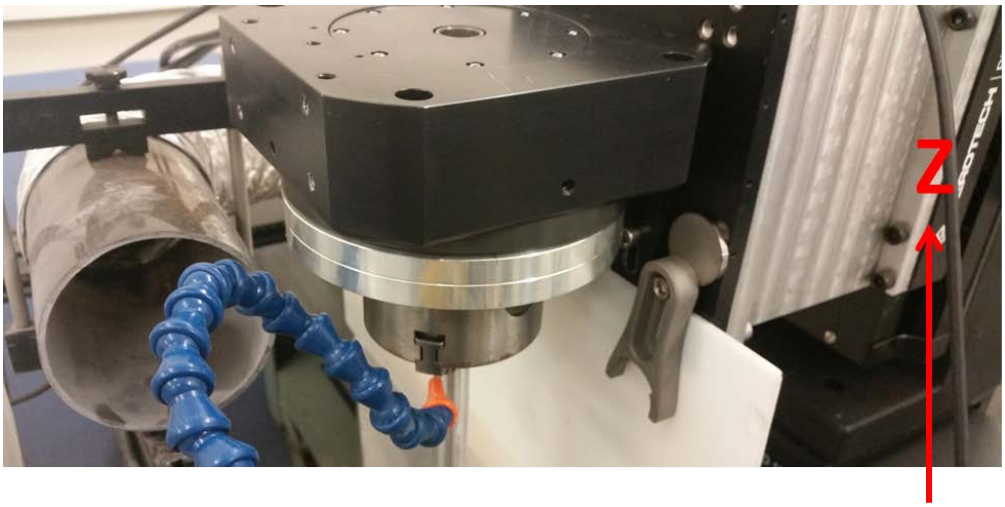

Figure 3.26: Laser Shock Peening Rotational Stage

Two laser shock peening runs were required per test specimen. This ensured complete peening across the entire length of each specimen and thus, a uniform compressive layer was imposed into the surface of each specimen. Due to the test specimens being clamped in the chuck (10 mm of each specimen length was clamped), a proportion of their lengths remained "un-peened" after the first peening run. In order to ensure the entire length of each specimen was peened, the specimens were flipped in the chuck, this enabled the un-peened length to be treated. A two-millimetre overlap of the 'already-peened' region occurred during the second peening run and can be seen in Figure 3.27. This ensured that there was no un-peened region between the two peening runs. A schematic flow diagram of this process can be seen in the Figure 3.28.

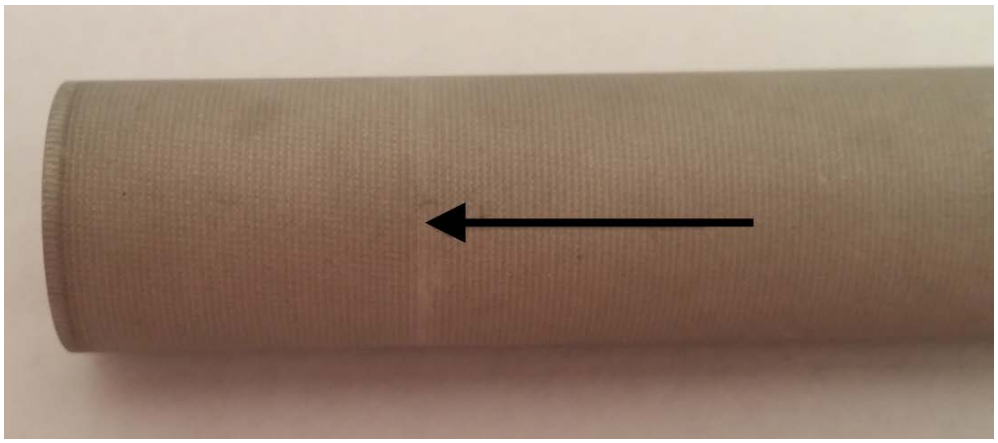

Figure 3.27: Laser Shock Peening Overlap Line

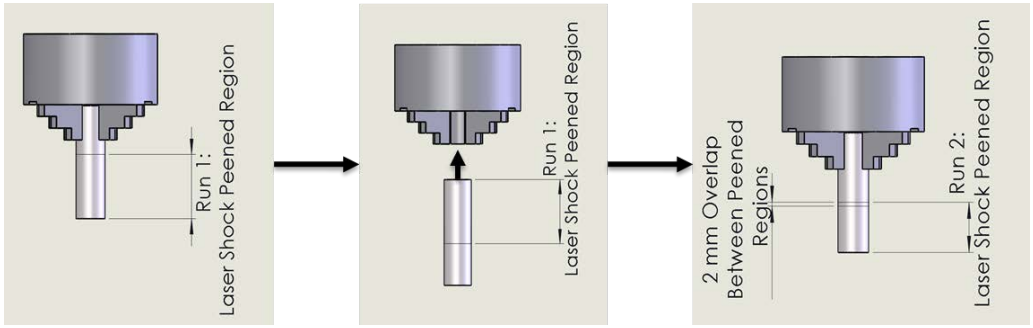

Figure 3.28: Laser Shock Peening Specimen Rotation

The laser shock parameters used by the for the specimens in this study can be seen in Table 3.7.

Table 3.7: Laser Shock Peening Peening Parameters

Parameter	Value	Unit
Laser Type	Q-switch Pulse ND: YAG (Yttrium Aluminum Garnet)	-
Laser Model	Spectra-Physics Quanta-Ray Pro 270	-
Laser Dimensions	117.25 x 50.81 x 30.58	cm
Spot Size Diameter	1.5	mm
Laser Power intensity	3	GW/cm^2
Repetition Rate	20	Hz
Coverage	500	$spots/cm^2$
Wavelength	1064	nm
Chuck Rotational Speed	59.94	degrees/s
Vertical Stage Speed	8 to 10	mm/s

3.5.5 Fatigue Testing

Cyclic Loading

The fatigue performance of the various test specimens was evaluated under cyclic loading using a 100 kN electro-servo hydraulic fatigue machine (ESH), seen in Figure 3.29.

Figure 3.29: Electro-Servo Hydraulic Fatigue Machine

The ESH machine consists of two main units, namely the servo controller and the servo-valve amplifier. The machine operates using a closed-loop continuous feedback system. The servo controller measures the performance of the actuator which is operated by a servo-valve which delivers hydraulic power to the actuator allowing it to move axially. This measured performance is compared to the initial input parameter requirements. Any difference in performance between the compared values is displayed as a so called "error" signal which is amplified by the servo-valve amplifier and sent back to the relevant servo-valve in a negative feedback loop. The relevant servo-valve is then able to make an adjustment in order to meet the initially calculated requirement [102].

The designation of test specimens, in both the T6 and annealed material conditions, to be fatigued during this study can be seen in Table 3.8.

Fatiguing Parameters

All bending fatigue tests were performed using a 3-point bending system using a constant amplitude bending stress at room temperature. Test specimens in two different material conditions, namely T6 and fully annealed, and with varying surface treatment procedures were fatigued through the 3-point bending system. All the dimensions of the testing fixtures used were in accordance with ASTM E399-90 [80]. No standard specifically refers to the fatigue bend testing of

Table 3.8: Fatigue Test Specimen Designation

Test Group	Material Condition	Surface Condition	Number of Specimens
Practise Group	T6	"As Machined"	8
Practise Group	Annealed	"As Machined"	9
Group 1	T6	"As Machined"	4
Group 1	Annealed	"As Machined"	4
Group 2	T6	Polished	4
Group 2	Annealed	Polished	4
Group 3	T6	Polished/Shot Peened	3
Group 3	T6	Polished/Shot Peened/Polished	3
Group 3	Annealed	Polished/Shot Peened	3
Group 3	Annealed	Polished/Shot Peened/Polished	3
Group 4	T6	Polished/Laser Shock Peened	3
Group 4	T6	Polished/Laser Shock/Polished	3
Group 4	Annealed	Polished/Laser Shock	3
Group 4	Annealed	Polished/Laser Shock/Polished	3
Group 5	T6	LSP/Polished/Partially Fatigue/LSP/Polish	5

metallic materials and thus the ASTM E399-90 Standard, with reference to fracture toughness testing, was followed up to the point of the fatiguing process.

In order to ensure that the cyclic stress applied to each specimen remained constant throughout the experimental procedure, the diameter of each specimen was accounted for and was enable by the operation of the ESH fatigue in load-control. The diameters of the test specimens varied as a result of their initial machining, individual polishing requirements and the various surface treatments procedures used on their surfaces. To account for any variance in diameter between the specimens, the loads used in the fatigue testing procedure were varied on a specimen by specimen basis, taking account of each specimen's cross-sectional area. The load-controlled mode used to perform the tests also ensured that the applied cyclic bending stress remained constant through the course of the fatigue test with any changes to the diameters of the test specimens as a result of compliance changes or contact damage (between the 3-point bending fixtures and the test specimens) sustained during the fatiguing process.

The load was determined using simple bending theory according to the elastic bending Equation 3.5 [103]:

$$\frac{M}{I} = \frac{\sigma}{y} \tag{3.5}$$

Where:

M: Applied Bending Moment (Nm)

I: Second Moment of Area (m^4)

σ: Applied Stress (N)

y: Distance from Neutral Axis to applied Stress (m)

The CAD drawing in Figure 3.30 depicts how this Equation is applied to a cylindrical section.

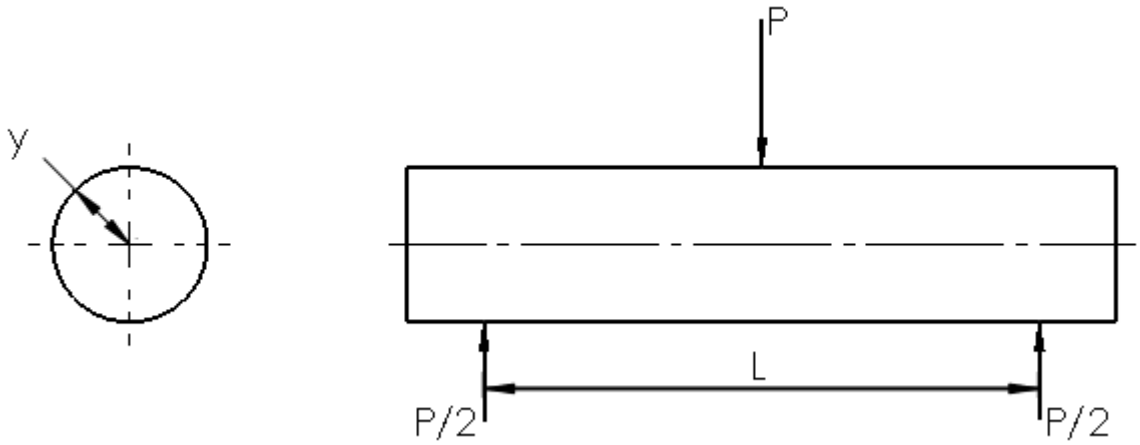

Figure 3.30: Applied Forces During 3-Point Bending on Cylindrical Specimen

The following Equations, based on the specimens loading conditions, were substituted into Equation 3.5 above:

$$M = \frac{PL}{4} \tag{3.6}$$

$$I = \frac{\pi d_c^4}{64} \tag{3.7}$$

$$y = \frac{d_c}{2} \tag{3.8}$$

This substitution simplified into an Equation of the form:

$$\frac{16PL}{\pi d_c^4} = \frac{2\sigma}{d_c} \tag{3.9}$$

Where:

d_c*: Diameter (m)*

P*: Applied Load (N)*

σ*: Applied Stress (N)*

L: Span Length (L)

By rearranging Equation 3.8, the applied load term could be isolated and used for determining the specific load needed for each specimen. The resulting Equation used to determine the load was:

$$P = \frac{\sigma \pi d^3}{8L} \tag{3.10}$$

The span length was kept constant at 68 mm, as adjusting the bend test supports on a fractional scale to match the span of each test specimens proved to be almost impossible using the 3-point bend testing rig. The testing frequency was set at 10 Hz using a sinusoidal wave at a stress ratio (*R*) of 0.1. Using this stress ratio, the loads used in the fatiguing process (the loads were based on initial stress estimates as determined later on in this Section) were calculated using the following Equations, which are based on the sinusoidal nature of the fatiguing process:

$$P_{max} = \frac{P}{1 - 0.1} \tag{3.11}$$

$$P_{min} = P_{max}(0.1) \tag{3.12}$$

$$P_{mean} = \frac{P_{max} + P_{min}}{2} \tag{3.13}$$

$$A = P_{max} - P_{min} \tag{3.14}$$

Where:

P_{max}: Maximum Applied Load (N)

P: Applied Load (N)

P_{min}: Minimum Applied Load (N)

P_{max}: Mean Applied Load (N)

A: Amplitude Load (N)

The initial stress estimate used to calculate the required load for the fatiguing of the test specimens in the T6 material condition was determined by looking at stresses used to generate S-N curves

for AA7075-T6 found in literature [104]. A trial and error bending fatigue approach was then implemented to incrementally adjust the stress level to a level at which crack initiation occurred at a desirable cycle count. As the S-N curve used initial stress estimate was not generated under the same fatiguing conditions used in this study, it could only be used as a rough estimate. A fatigue life of 30 000 cycles was chosen as the desirable fatigue life of the test specimens in the T6 case. This fatigue life would enable the testing of specimens later on in the project which received treatments aimed at increasing their fatigue lives to be conducted in a manageable time period

The S-N curve used to provide the initial stress estimate can be seen in Figure 3.31. The S-N curves on the Figure were generated using 0.2 inch (5.08 mm) diameter, unnotched, round bar AA7075-T6 test specimens at various stress ratios and at a frequency of 30 Hz. At this frequency, the surface condition of the test specimens has a large impact on the fatigue life of the specimens as the effect of any surface defects (i.e. notches, manufacturing flaws, defects, wear, corrosion damage) become more pronounced, leading to larger stress concentrations forming as compared to fatiguing these same samples at a lower frequency. It can therefore be reasonably assumed that the fatigue life of the test specimens tested in order to create the S-N curves would increase slightly if the fatiguing tests were conducted at a lower frequency. The S-N curves in Figure 3.31 were also generated by fatiguing the round bar test specimens in the longitudinal direction i.e. along the direction of their grains, assuming that the test specimens have been extruded along their cylindrical axes. In the 3-point bend testing of round bar test specimens, the specimens are fatigued perpendicularly to the direction of their grains. This difference in grain direction between the tensile and bend test specimens may result in differing stresses needed by the two fatiguing approaches for the same fatigue life of a given test specimen, as depicted on an S-N curve, to be achieved.

A curve (red curve seen in Figure 3.31 below) was superimposed on the S-N curve, in order to estimate the projected stress level of the fatigue test specimens at a stress ratio of 0.1 and desired fatigue life of 30 000 cycles.

Based on the superimposed curve, a fatigue life of 30 000 cycles could be achieved somewhere in the applied stress range of 70 ksi (482.64 MPa) to 80 ksi (551.58 MPa). Therefore an initial estimated stress level of 480 MPa was used for testing. This initial stress level did however not achieve the desired fatigue life cycle count as the fatiguing process ran to 100 000 cycles without an observable crack forming on the surface of the test specimen. A trial and error approach was then adopted with incremental increases in the fatigue testing stress level. With each incremental increase in stress, a new test specimen was used to determine the resulting fatigue life of the changed stress level. A final stress of 585 MPa was found to result in specimens failing at around

30 000 cycles. This stress was then applied to all the test specimens in the T6 condition, including those which received surface modifying treatments (see Chapter 5, Section 5.3 for justification of bending stresses).

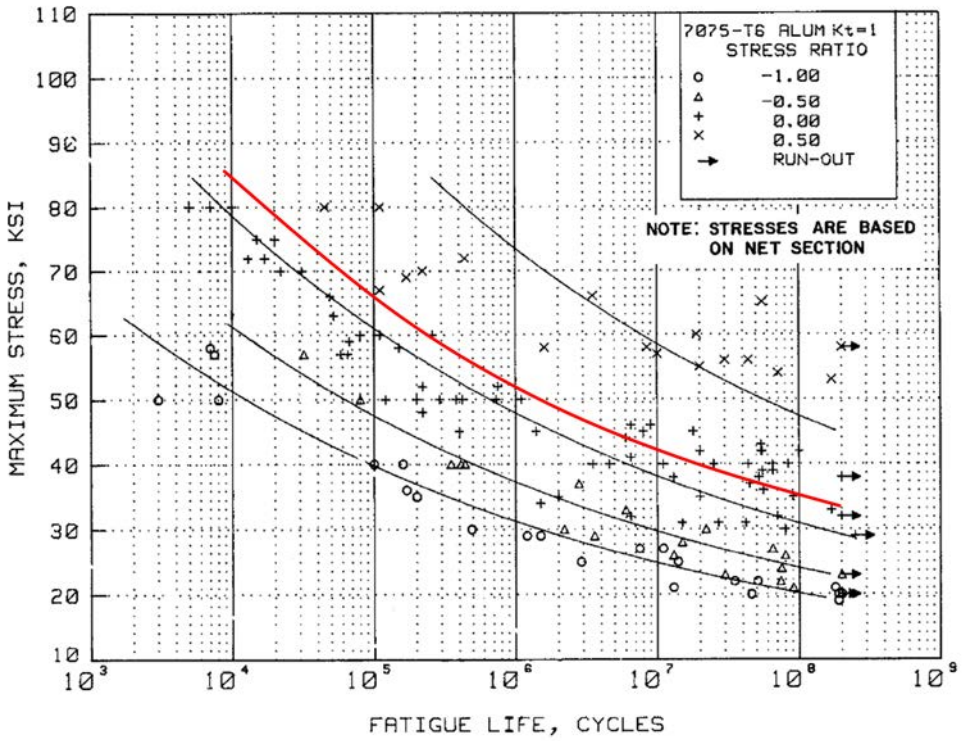

Figure 3.31: Best Fit S-N Curves for Unnotched 7075-T6 Aluminium Alloy, Various Product Forms, Longitudinal Direction

For test specimens in the fully annealed condition, A fatigue life of 30 000 cycles was chosen as the desired life of the test specimens as this was comparable to the test specimens in the T6 condition.

No S-N curves could be found for annealed AA7075 in order to provide an initial estimate as to what stress the fatiguing process should be started. A trial and error approach was again adopted, with incremental increases in the fatigue testing stress level from an initial estimate (225 MPa which corresponded to the tensile strength of AA7074-O), with a new test specimen was used for each new stress level. At 450 Mpa the practice specimen was found to fail at around 30 000 cycles.

3.6 Fatigue Life Restoration Process

The fatigue life restoration process of partially fatigued test specimens combined various elements of the experimental procedure described thus far. A flow diagram illustrating the steps used in the fatigue life restoration process can be seen in Figure 3.32.

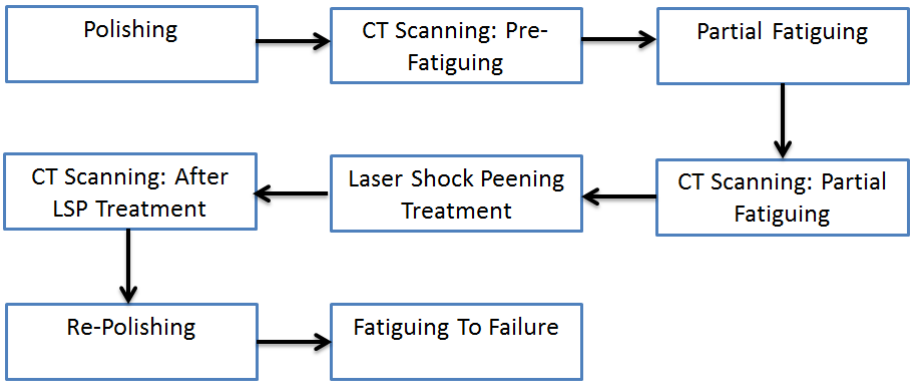

Figure 3.32: Fatigue Life Restoration Process Flow Diagram

The T6 material condition was chosen as the only material condition to undergo the fatigue life restoration process as it showed an overall improvement in fatigue life as a result of laser shock peening surface treatment which was not evident in the annealed test specimens which received the same surface treatment. All the specimens were initially subjected to laser shock peening before the start of the restoration process. The test specimens were initially laser shock peened before the fatigue life restoration process (using the process and parameters outlined in Section 3.5.4) as this would allow for the specimens to be laser shock peened twice during their entire testing procedure. Laser shock peened components can have residual stress depths over 1 mm with multiple peening shots, each of which drives residual compressive stresses deeper into the treated component.

3.6.1 Test Specimen Polishing and Surface Roughness Profiling

Test specimens (in the T6 condition) used in the fatigue life restoration process were polished after their initial laser shock peening treatments. This polishing was done in order to assess the impact of the laser shock peening induced surface roughness on the fatigue performance of the specimens. The polished fatigue life restoration specimens could then be compared to previously polished and fatigued specimens. The polishing also made it easier to view crack initiation during the partial fatiguing stage of the fatigue life restoration process.

Test specimen diameters were measured both before and after the polishing process. This enabled the amount of surface material removed during the polishing process to be determined. The test specimens were manually polished using the same procedure described in Section 3.5.1 of this Chapter. Surface roughness profiles were generated for the surface roughness measurements of the test specimens both before and after the polishing procedure in order to illustrate the reduction in surface roughness.

3.6.2 CT Scanning: Pre-Fatiguing

The test specimens used in the fatigue life recovery process were sent for micro-computed tomography (CT) scanning at various stages throughout the fatigue life restoration process. These scans aimed to provide information relating to the internal structure of the test specimens prior to the partial fatiguing process, after the partial fatiguing and after the re-laser shock peening process. The micro-CT scans also allowed for stress cracks initiated during the partial fatiguing process to be mapped before and after the re-laser shock peening process.

Initial scans were made to ensure that there were no detectable flaws within the specimens which may have influenced the fatigue life of the test samples. The micro-CT scans were performed at the Stellenbosch University CT Scanner Facility and were conducted by Dr. Anton du Plessis and Mr. Stefan le Roux.

X-ray computed tomography is a non-destructive testing technique for generating a 3-dimensional representation of the density of an object [105]. A CT machine consists of a number of X-ray emitters and detectors. The object for which the 3-dimensional representation is being constructed is placed between the emitter and the detectors. The detectors measure how much the object attenuates the stream of X-rays projected by the X-Ray emitter and uses this information to generate a 3-dimensional representation of the scanned object [105].

Images, in the form of cross sectional slices, are acquired for hundreds of angular views of the scanned object, captured while the object rotates. A computer synthesises a stack of these virtual cross section slices using various algorithms, to produce a 3D image of the scanned object [106]. The algorithms used are able to determine small differences in the relative density and atomic number within each scanned projection. These differences account for defects contained within the scanned object and can be mapped accordingly within the scanned object. A schematic of the measuring principle can be seen in Figure 3.33.

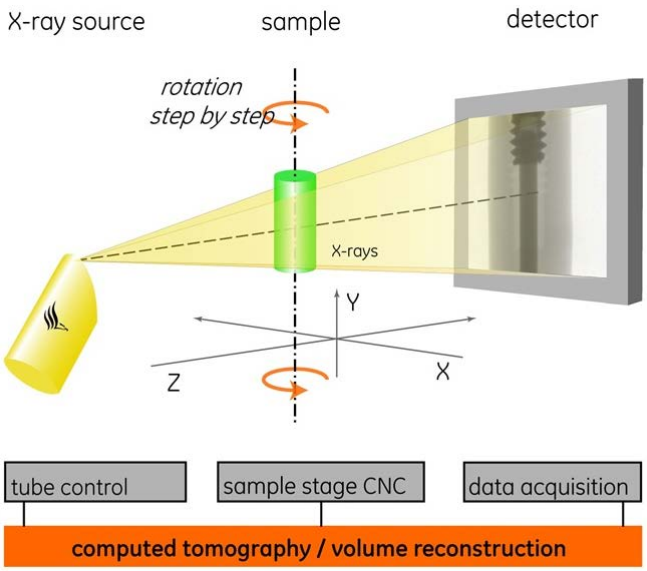

Figure 3.33: CT Scanning Principle [107]

X-ray CT scans were done using a General Electric Phoenix V|Tome|X L240, using scan settings of 160 kV and 110 μa for X-ray generation. Copper beam filters of 1 mm were used to reduce beam hardening artefacts X-ray projection images were recorded at 500 ms per image, with 1600 images recorded in one slow stepwise rotation of the sample, with no averaging and no skipping of images. Detector shift was activated to minimise ring artefacts. Background calibration was performed and the scan time was approximately 27 minutes per scan reconstruction of the 3D volume data was done with system-supplied Datos 2.2, using a beam hardening correction module incorporated into the software to reduce beam hardening artefacts. A beam hardening correction factor of 8 was used (values from 0–10 are possible). Analysis of the images was performed with Volume Graphics VGStudioMax 2.2. The parameters used during the CT scanning process are summarised in Table 3.9.

Table 3.9: Initial CT Scanning Parameters

Parameter	Value	Unit
Voltage	160	kV
Current	110	μa
Filter Type	Copper	
Filter Thickness	1	mm
Exposure Time	500	ms
Number of Images Collected	1600	
Detector Pixel Size	0.2	mm
Beam Hardness Correction Factor	8	
Total Scan Time	27	min

The CT machine used at the Stellenbosch University CT Scanner Facility can be seen in Figure 3.34 below, where its major components are labelled.

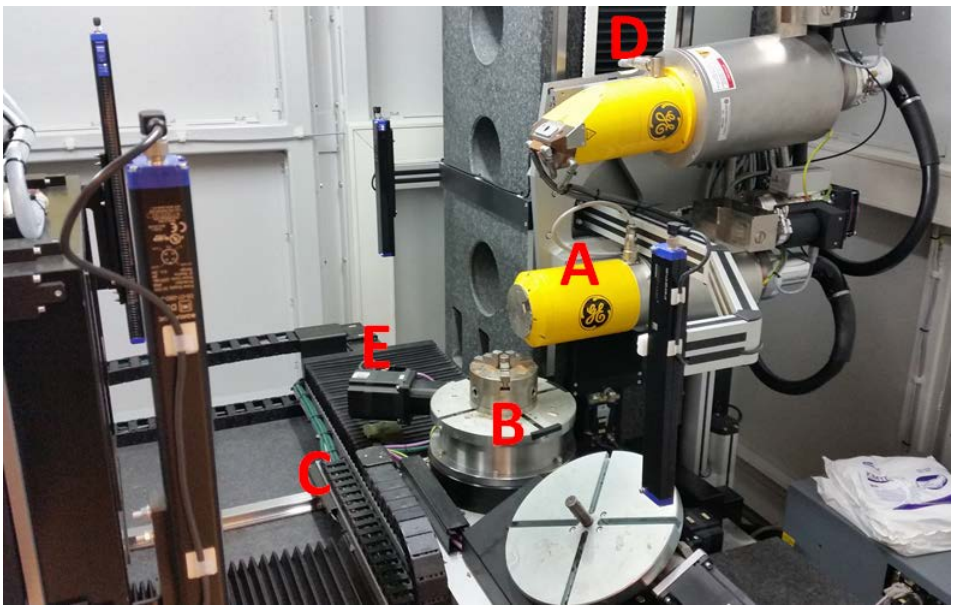

Figure 3.34: Micro-CT Scanner
A - X-ray Source
B - Rotational Stage
C - X and Y Axis Translation Stages
D - Z Axis Translation Stage
E - X-Ray Detector

The resolution of the CT scanning process is dependent upon the size of the area scanned. The relationship between image resolution and sample size is illustrated in Figure 3.35 below, where the achievable resolution ranges between the two lines on the graph. In this study, the central region of each test specimen was scanned. A detector pixel size (resolution) of 0.2 mm was achieved by limiting the area of the scan to the midsection of each bend test specimen.

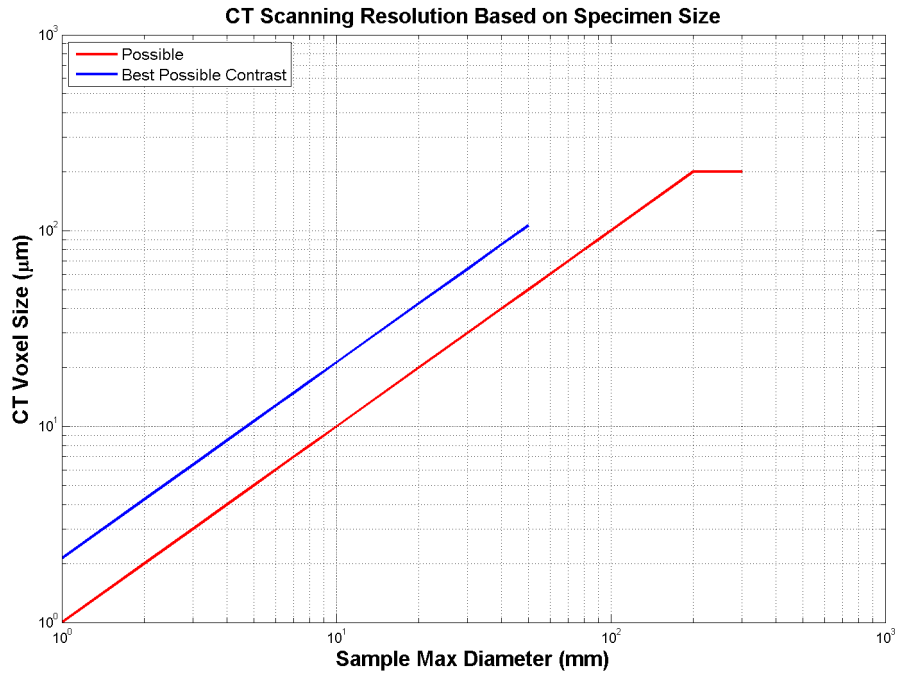

Figure 3.35: CT Scanning Resolution

3.6.3 Partial Fatiguing

Following the CT mapping of the test specimens used in the fatigue life restoration process, the test specimens were partially fatigued using the 100 kN electro-servo hydraulic fatigue machine (ESH). This fatiguing process was again undertaken using the 3-point bend system described earlier in Section 3.5.5. A testing frequency of 10 Hz, stress ratio of 0.1 and applied stress of 585 MPa were employed during the fatigue testing procedure.

Once placed on the 3-point bend stand, the bottom (tension side) of each test specimen was continually monitored during the fatiguing process. The orientation at which each test specimen was placed on the bend test stand was also marked off on the sides of each test specimen. This would allow for the test specimens to be correctly orientated during the final fatiguing stage of the experimental process.

Figure 3.36: ESH Microscope Set-Up

Each test specimen was fatigued to the point where an observable crack formed on the surface (cracks of between 1.0 and 2.0 mm were observed). Once a crack was observed the fatigue test was stopped. The crack lengths - 2C (seen in Figure 3.37 below) were then measured using the built-in scale bar on the microscope lens.

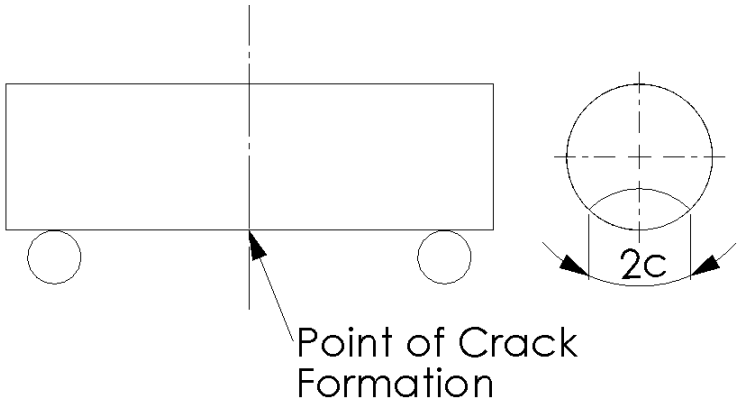

Figure 3.37: Observable Crack Location

3.6.4 CT Scanning: After Partial Fatiguing

After the test specimens had been partially fatigued, they were once again sent for micro-computed tomography (CT) scanning. This next set of CT scans was aimed at mapping the exact geometry

(size and depth) of the visible cracks which had formed in each test specimen during the partial fatiguing process.

In order to ensure that the cracks were visible on the generated CT scan images, each test specimen was placed into a slight 3-point bend during their respective scanning procedures. This was done using a bending jig, designed to replicate the 3-point bend test. The test specimens were placed into the jig. A bolt, used in place of the fatiguing bend fixture, was tightened on the side opposite to the crack. Both the bending jig and the bolt were made from aluminium alloy 6082-T6 (ρ - 2700 kg/m^3), which is less dense than AA7075-T6 (ρ - 2810 kg/m^3) [108]. This difference in densities would not create interference artefacts between the jig and the test specimens during the CT scanning process and thus allow a clear image of the test specimens to be created.

Artefacts typically occur when scanning materials of differing densities. When the X-ray beam passes through denser of the two materials, the lower energy photons are absorbed rapidly, leaving the higher energy photons to pass through to the detectors. This results in the beam becoming "harder", which leads to dark streaks forming on the CT scanned images. It is then difficult to differentiate these dark streaks from actual features within the scanned object. The bending jig can be seen in Figure 3.38.

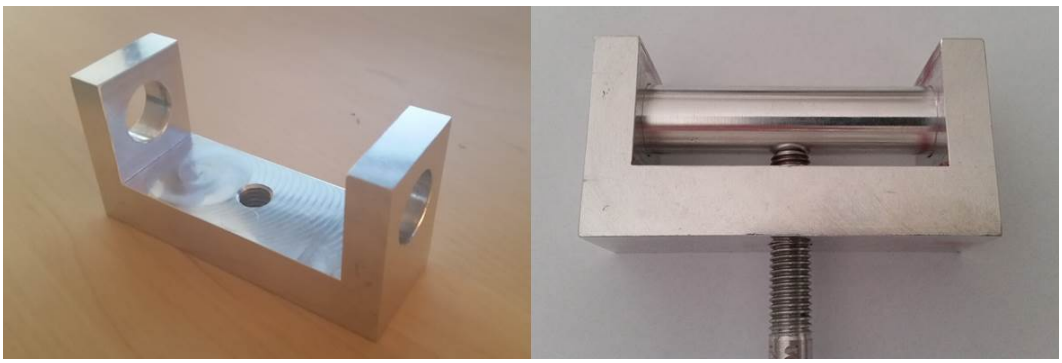

Figure 3.38: Bending Jig

By reducing the scan area on the specimens, the scan resolution was increased and defects with a size of $\approx$ 0.127 mm or larger could be detected. The parameters used during this CT scanning process are summarised in Table 3.10.

Table 3.10: Partially Fatigued CT Scanning Parameters

Parameter	Value	Unit
Voltage	200	kV
Current	200	μa
Filter Type	Copper	
Filter Thickness	1.5	mm
Exposure Time	500	ms
Number of Images Collected	4000	
Detector Pixel Size	0.127	mm
Beam Hardness Correction Factor	0	
Total Scan Time	67	min

3.6.5 Re-Laser Shock Peening Treatment

Once the test specimens were CT scanned and had their fatigue cracks mapped, they were sent again to the CSIR to be re-laser shock peened. The laser shock peening process initially used on test specimens in this study was repeated (the process is described in Section 3.5.4 of this Chapter). This process aimed to determine whether the observed fatigue cracks could be "healed" by laser peening over them, resulting in a proportion of the test specimens fatigue life being restored.

The laser shock parameters used for the laser shock peening "healing" treatment can be seen in Table 3.11.

Table 3.11: Laser Shock Peening Peening Parameters Used on Partially fatigued Test Specimens

Parameter	Value	Unit
Laser Type	Q-switch Pulse ND: YAG (Yttrium Aluminum Garnet)	-
Laser Model	Spectra-Physics Quanta-Ray Pro 270	-
Laser Dimensions	117.25 x 50.81 x 30.58	cm
Spot Size Diameter	1.5	mm
Laser Power intensity	3	GW/cm^2
Repetition Rate	20	Hz
Coverage	500	$spots/cm^2$
Wavelength	1064	nm
Chuck Rotational Speed	59.94	degrees/s
Vertical Stage Speed	8 to 10	mm/s

3.6.6 CT Scanning: After Laser Shock Peening Treatment

After the test specimens were re-laser shock peened, three test specimens were selected for CT scanning. The three test specimens selected for the CT scanning had previously shown visible cracks which were easily mapped when CT scanned before the re-laser shock peening process (CT scans of test specimens 3 and 4 displayed no visible cracks. The crack depths/widths with the specimens fell outside of the scanning resolution). The effect of the laser peening process on these mapped cracks could thus be gauged.

In order for fatigue life restoration to occur, it is theorised that fatigue crack depths must be contained to within the penetration depth of the laser shock peened region so as to be influenced by the laser induced plastic deformation. The test specimens selected for re-CT scanning can be seen in Table 3.12.

Table 3.12: Test Specimen's Selected for Re-CT Scanning after Laser Shock Peening

Specimen Number	Cycles to Crack Initiation	Circumferential Length (mm)	Crack Depth (mm)
1	794591	1.80	2.06
2	185826	1.60	0.40
5	161113	1.40	0.49

The CT scanning process, described in Section 3.6.4 above, was again used to scan the re-laser shock peened specimens. The specimens were again placed in the bending jig in order to ensure that any cracks present within the test specimens were visible during the CT scanning process. This also ensured scanning continuity with the previous CT scans. The scanning resolution of this set of CT scans increased from 0.127 mm to 0.2 mm as scanning time was minimised due to time constraints at the CT scanning facility.

The parameters used during this CT scanning process are summarised in Table 3.13.

Table 3.13: Re-Laser Shock Peened CT Scanning Parameters

Parameter	Value	Unit
Voltage	160	kV
Current	200	μa
Filter Type	Copper	
Filter Thickness	1.5	mm
Exposure Time	500	ms
Number of Images Collected	3200	
Detector Pixel Size	0.2	mm
Beam Hardness Correction Factor	0	
Total Scan Time	53	min

3.6.7 Final Polishing and Surface Roughness Profiling

The fatigue life restoration specimens were polished prior to undergoing their final fatiguing procedure.

Test specimen diameters were measured both before and after the polishing process. Surface roughness values of around 0.2 $\pm 0.05\mu$m were again desirable. Surface roughness profiles were

also generated for the surface roughness measurements of the test specimens both before and after the polishing procedure.

3.6.8 Fatiguing to Failure

The last stage of the fatigue life restoration process required that the test specimens be fatigued to failure. The time taken (i.e. number of cycles) for each specimen to fail would serve as an indication as to the degree of fatigue life restoration each specimen experienced.

The test specimens were fatigued using the 100 kN electro-servo hydraulic fatigue machine (ESH). This fatiguing process was again done using the 3-point bend system described earlier in Section 3.5.5. A testing frequency of 10 Hz, stress ratio of 0.1 and applied stress of 585 MPa were during the fatigue testing procedure. Care was taken to position each test specimens on the bending stand in the same orientation used during the partial fatiguing process. This required that the side of the specimen at which crack initiation occurred was positioned facing downwards between the bending stand support rollers. i.e. the side opposite to where the bending fixture applied force was placed facing downwards. Damage to the test specimen surfaces made during the partial fatiguing process by the 3-point bend test support rollers as well as the fatiguing piston, was clearly visible on the test specimens, even after the re-laser shock peening process. These damage marks enabled the test specimens to be orientated in the same manner as was done during the partial fatiguing process.

3.7 Metallographic Examination

The effects of the surface treatments used in this study on the AA7075-T6 and AA7075-O test specimens were analysed using various metallographic techniques. This analysis would in turn help explain the implications of the various surface treatments on the fatigue life of treated components.

Metallographic examinations of the fracture surfaces, internal microstructures and hardness of the various test specimens was undertaken. These examinations utilised varying techniques including optical microscopy, scanning electron microscopy and incremental micro-hardness measurements.

The test specimens selected for the metallographic examination process are shown in Table 3.14. It can be noted that only samples in the T6 condition (polished, shot peened, laser shock peened and fatigue life healed) were selected for SEM fractography. This was because these samples exhibited a significant difference in their fatigue lives as a result of the surface modifying treatment they received.

The preparation of all the metallographic samples for the various analysis techniques was done in accordance with ASTM Standard E3-01 [109].

Table 3.14: Test Specimen's Selected for Metallographic Examination

Test Group	Specimen Number	Material Condition	Analysis Techniques
Group 1	3	T6/As Machined	Optical Fractography
Group 1	1	Annealed/As Machined	Optical Fractography
Group 2	1	T6/Polished	Optical Fractography; SEM Fractography Light Microscopy; Micro-Hardness
Group 2	4	Annealed/Polished	Optical Fractography; Light Microscopy Micro-Hardness
Group 3	1	T6/SP	Optical Fractography; SEM Fractography Light Microscopy; Micro-Hardness
Group 3	4	T6/SP/Polished	Optical Fractography
Group 3	7	Annealed/SP	Optical Fractography; Light Microscopy Micro-Hardness
Group 3	10	Annealed/SP/Polished	Optical Fractography
Group 4	1	T6/LSP	Fractography; SEM Fractography
Group 4	3	T6/LSP/Polished	Optical Fractography Light Microscopy; Micro-Hardness
Group 4	7	Annealed/LSP	Optical Fractography; Light Microscopy Micro-Hardness
Group 4	10	Annealed/LSP/Polished	Optical Fractography
Group 5	5	T6/Fully Healed	Optical Fractography; SEM Fractography Light Microscopy; Micro-Hardness

** Note: SP - Shot Peen; LSP - Laser Shock Peen*

3.7.1 Fractography

i) Optical Light Microscope Fractography

Optical Light Microscope Fractography was performed on the fracture surfaces of all the aluminium test specimens after fatigue failure had occurred. This was done in order to identify various characteristic features on the fractured surfaces.

A stereo optical microscope fitted with a Leica DCF 320 camera was used for the optical microscopy. This camera was in turn connected to a computer that ran the Leica acquisition software. This software captured images of the fracture surfaces. A magnification level of 0.64 x was used for image acquisition. This set-up can be seen in Figure 3.39.

Figure 3.39: Leica Stereo Microscope

ii) SEM Fractography

Fractography using a scanning electron microscope was performed in order to view the crack propogation and initiation regions on the T6 specimens fracture surfaces. This enabled a magnification level not accessible to optical light microscopes. The fracture surface of the test specimens from test Groups 2, 3 (unpolished), 4 (unpolished) and 5 in the T6 material conditions were subjected to SEM fractography as these specimens showed a variance in their fatigue lives as a result of the differing surface treatments they received. Fractographs were taken at crack initiation sites and at the end of the crack propagation sites on all the test specimens examined in order to determine what effects the different surface treatments had on the crack propagation path.

The SEM fractography was performed using a ZEISS/LEO 1450 scanning electron microscope (SEM). The analysis was conducted at the University of Cape Town Centre for Imaging and Analysis with the assistance of Miranda Waldron.

For this study, the scanning electron microscope was operated at a beam energy of 10 keV and a working distance of between 15 to 20 mm, depending on the size of the specimen. This SEM used seen in Figure 3.40.

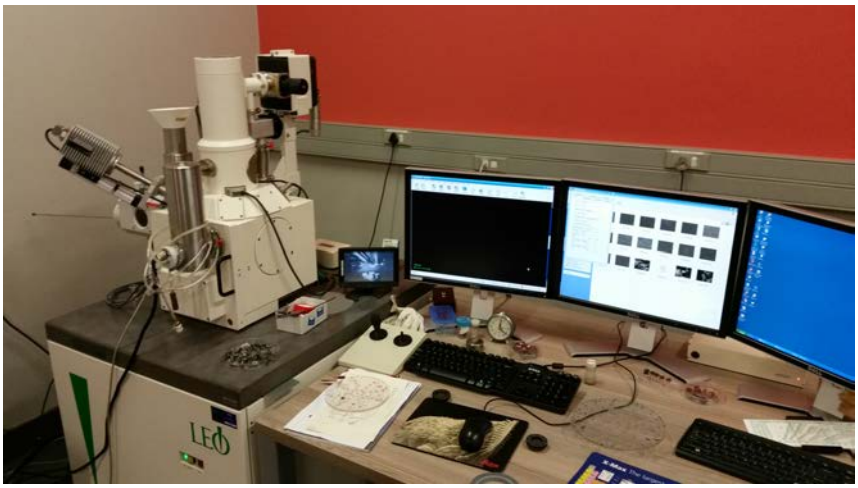

Figure 3.40: ZEISS/LEO 1450 Scanning Electron Microscope

3.7.2 Sample Preparation for Light Microscopy

Samples prepare for light microscopy required various preparation steps before analysis could occur. These steps are listed below.

i) Sample Sectioning

Test Specimens that were to undergo light microscopy required sectioning in order to expose the surfaces to be analysed Sectioning was done using a low-speed micro-slicer with diamond tipped blade (Bueler Isomet Low Speed Saw), seen in Figure 3.41.

Figure 3.41: Bueler Isomet Low Speed Saw

The quality of any sectioning cut is dependent on a number of factors including type of cut-off blade used, cutting lubricant, cutting speed, blade pressure and material hardness. The Bueler Isomet micro-slicer makes use of a counterbalance load in order to avoid excessive pressure on the sample, thus ensuring a relatively straight cut, with minimal surface damage to the test specimen. Simultaneous lubrication of the cutting wheel with cutting oil ensures that the structure of the material being sectioned is not altered through heat generation caused by the cutting process.

ii) Sample Mounting

The test specimen sections for light microscopy were mounted before analysis. Mounted test samples are easier to handle, which minimises the potential for damage to occur to the test sample surface during subsequent polishing procedures.

The samples were cold mounted in resin to avoid thermal effects on the aluminium microstructure, which may be caused by hot mounting. A resin ratio of 7:1 (weight ratio) for Specifix Resin to Specifix-20 Curing Agent was mixed. The specimen sections were placed in individual Vaseline greased rubber pots. The surfaces to be analysed were placed face downwards in the pots. The resin mixture was then poured over the samples and left to cure for 24 hours. The apparatus used for the cold mounting process can be seen in Figure 3.42.

Figure 3.42: Cold Mounting Apparatus

iii) Sample Grinding and Polishing

The mounted test specimen sections were ground and polished before further analysis. The rough ends (i.e. the tops of the mounted samples, opposite the sample surfaces) of the cold mounted samples were manually ground flat and level before polishing was undertaken.

Figure 3.43: Exposed Stub Tip

Grinding was done using 800 grit grinding paper on a the Struers Dol-25 grinding wheel. Water was used as a lubricant during the grinding process and was used to remove debris and heat from the mounted sample. These ends were ground flat so as to ensure that the force applied by the automatic polishing machine during subsequent polishing steps was evenly distributed across the surface of the sample being polished. This ensured a smooth and level polished sample surface. The Struers Dol-25 grinding wheel can be seen in Figure 3.44.

Figure 3.44: Struers Dol-25 Manual Grinding Machine

The surfaces of the mounted samples were then automatically ground and polished using the using the Struers TegraPol-11 automatic polisher, seen in Figure 3.45.

Figure 3.45: Struers TegraPol-11 Automatic Polisher

Initially, the mounted test specimen surfaces were ground flat using 1200 grit paper glued to a RAC pad. This process was repeated using old 1200 grit paper to ensure a uniformly smooth surface.

Next, the surfaces were polished in order to obtain a mirror-like finish using an aluminium procedure derived by the University of Cape Town Centre for Materials Engineering. The aluminium polishing procedure followed can be seen in Table 3.15.

The mounted samples were placed into sample holders on the machine and the aluminium polishing process was started. Between each step in the process, the samples were washed using warm, soapy water in an effort to remove contaminants left over from the previous grinding/polishing step. Each polishing step utilised a different MD (magnetic disk) polishing pad and a different lubricant, including a diamond suspension lubricant and a colloidal silica lubricant. A final water polish was necessary as the colloidal silica often stains the test specimen surface. Once the steps were completed, the samples were washed using soapy warm water, then ethanol and then dried using a hair dryer. The samples were then inspected for large, non-uniform scratches. If such scratches were present, the OP-AA and water polishing steps were repeated.

Table 3.15: Polishing Procedure for AA7075-T6 Samples

Step	Process	Lubricant	Cloth	Time (min)	Force (N)	Speed (RPM)
1	Grinding	Water	1200 Grit	1	20	150
2	Grinding	Water	1200 Grit (old paper)	0.67	20	300
3	Diamond Polishing (DP)	DiaDuo 3 μm	MD-Mol	6	20	150
4	Oxide Polishing (OP)	OP-AA	MD-Nap	4	20	150
5	Oxide Polishing (OP)	Water	MD-Nap	2	10	150

iv) Sample Etching

The polished test samples were subjected to an etching procedure. Etching was the final step before light microscopy. Etching is a controlled corrosion process resulting from electrolytic action between surface areas of different potential. With two-phase or multiphase alloys, potential differences are present between phases of different composition [110]. These potential differences are used to produce controlled dissolution of the sample surface layer which helps reveal the samples grain structure.

The test sample surfaces were immersed in Keller's reagent with tongs and gently agitated for 20 s. The specimens were then removed and rinsed with warm water followed by ethanol. The samples were then dried using a hair dryer before the analysis of their grain structure. The composition of Keller's reagent can be in Table 3.16.

Table 3.16: Keller's Reagent Composition

Constituent	Amount (ml)
Hydrofluoric Acid	1.0
Hydrochloric Acid	1.5
Nitric Acid	2.5
Distilled Water	95

3.7.3 Nomarski Lens Light Microscopy

The etched samples were viewed through a Nomarski lens in order to view their microstructure. A Nikon Eclipse MA200 Inverted Metallurgical Microscope was used to conduct the light microscopy and can be seen in Figure 3.46.

Figure 3.46: Nikon Eclipse MA200 Inverted Metallurgical Microscope

3.7.4 Microhardness Testing

A MATSUSAWA MXT-CX7 Optical Microhardness Tester was used to conduct incremental hardness measurements on specimens in both material conditions. These hardness tests were aimed at determining the shot peening and laser shock peening penetration depths. The MATSUSAWA MXT-CX7 Optical Microhardness Tester can be seen in Figure 3.47. The microhardness testing was performed in accordance with ASTM Standard B384-99 [111]. It is important to note that the hardness testing machine was calibrated before the start of the testing procedure using a standardised calibration block of a known hardness. One test specimen in each of the T6 and annealed material conditions were analysed from test Groups 2 (polished), 3 (shot peened/Un-polished), 4 (laser shock peened/Un-polished) and 5 (polished/laser shock peened/polished/partially fatigued/re-laser shock peened/polished).

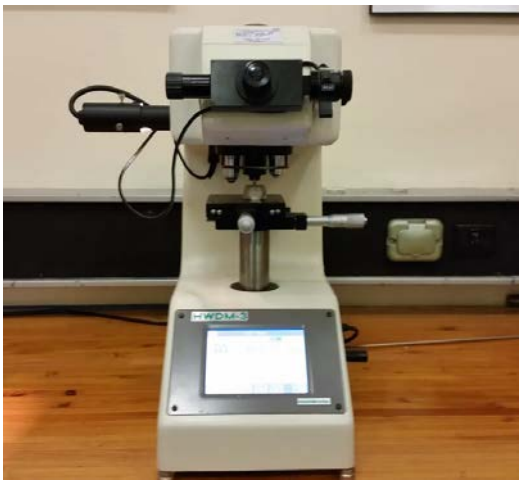

Figure 3.47: MATSUSAWA MXT-CX7 Optical Microhardness Tester

A test specimen section, 20 mm in length, was used for each hardness testing procedure. The diameter of the specimen was measured and recorded before hardness testing using a micrometer. The specimen was then cold mounted (as described in Section 3.7.2(ii)) in order to keep it level during the hardness testing procedure. The diameter of the specimen set in the resin was measured at the exposed section. This enabled the thickness of the resin to be determined when compared to the initial measurement of the specimen's diameter. An example of the specimen set in resin with the exposed strip can be seen in Figure 3.48.

Figure 3.48: Microhardness Specimen Set in Resin

Hardness measurements were made along the visible strip on the top, curved surface of the test specimen (i.e. perpendicularly to the specimen's cylindrical axis). This strip was initially polished using a two-step process involving the "old" 1200 grit step and the DiaDua 3 μm step from the aluminium polishing procedure described in Section 3.7.4. The diameter of the specimen was then

measured in order to determine how much material had been removed during the polishing step. Three hardness measurements were then taken along the exposed strip. These hardness values were then averaged to determine the mean average hardness to be calculated. This process was repeated a number of times, with the diameter of the specimen measured after each polishing procedure. This enabled the hardness at incremental depths to be measured. For the shot peened and laser shock peened specimens, incremental hardness values were measured until the hardness measurements remained constant over five consecutive incremental depths. This indicated the end of the plastically affected depth in the specimens. The polished test samples incremental hardness values were measured to a depth comparable to that measured in the laser shock peened samples (it was expected that the laser shock peened samples would exhibit the deepest plastically affected depth). The experimental parameters used for the microhardness testing are shown in Table 3.17.

Table 3.17: Microhardness Testing Parameters

Parameter	Value
Indenter Shape	Pyramid
Static Load for T6 Specimens	500 N
Static Load for Annealed Specimens	300 N
Average Material Removed During Polishing	6 μm
Distance between Indentations	> 200 μm

3.8 Summary

This Chapter described the experimental details and techniques used to assess the effects of laser shock peening and shot peening on the fatigue performance of aluminium alloy.

The study began with a preliminary investigation into the high bending stress required for crack initiation to occur in a reasonable number of fatigue cycles. The results of this preliminary investigation, which were presented above, were used to inform subsequent experimental methodology.

Following on from the preliminary investigation, the techniques used to analyse the effects of shot peening and laser shock peening were described.

Furthermore, a laser shock peening based fatigue life extension technique was outlined.

Finally, the techniques used to analyse the microstructure and hardness of both the fatigued and healed test specimens were presented. The next Chapter presents the results obtained from the experimental methods outlined above.

Chapter 4

Experimental Results and Observations

4.1 Introduction

This Chapter presents the results and observations of the experimental processes undertaken during the course of this project.

The first Section of this Chapter, Section 4.1, presents the results and observations of the preliminary investigation. The preliminary investigation looked at the material characteristics of the aluminium test specimens used in this project. Results from this were used to inform subsequent experimental methodology.

Following on from the preliminary investigation, analysis of the effect of shot peening and laser shock peening on the fatigue performance of aluminium alloy was conducted. The surface roughness measurements taken before the fatiguing process are given in Section 4.2. The fatigue performance results of various surface treatment procedures are presented in Section 4.3.

Results from the investigation into the ability of laser shock peening to restore fatigue performance in damaged components are presented in Section 4.4.

Finally, the results from the analysis of the fracture surfaces, microstructure and hardness of both the fatigued and fatigue life recovered test specimens are presented in Section 4.5.

4.2 Preliminary Investigation

4.2.1 Material Characterisation

The measured chemical composition of the AA7075 used in this study is presented in Table 4.1. Five point scans were performed at random sites on the surface of an aluminium sample. The mean average weight percentage of each element detected during the point scans was calculated to provide an overall chemical composition for the AA7075.

Table 4.1: Measured Chemical Composition of AA7075-T6 (as weight percentages)

	Mg	Al	Si	Ti	Cr	Mn	Fe	Cu	Zn	Other
Mean	**2.26**	**89.00**	**0.28**	**0.00**	**0.20**	**0.00**	**0.07**	**1.65**	**6.54**	**0.00**

The mean averaged weight percentages of the all the elements contained within the AA7075, with the exception of zinc, fall within the guidelines given by The Aluminium Association [78]. These guidelines can be seen in Table 3.3, in Chapter 3, Section 3.4.1. The mean average zinc contained within the aluminium is 0.44 weight % greater than the maximum limit (6.10 weight %) given by The Aluminium Association [78].

4.2.2 Residual Stress Evaluation of Heat Treated Specimens using X-Ray Diffraction

The residual stresses within the eight test specimens sent for X-ray diffraction were determined using the $Sin^2\psi$ method. Diffracted peak positions generated from Debye images were used to calculate the inter-planar spacing between the atoms of the aluminium alloy test specimens. These inter-planer spacings were then used to determine the associated strains within each of the test specimens, by comparing them to the inter-planar spacings in an unstrained (annealed) reference sample.

The initial 2D diffraction data generated in the form of Debye rings for test specimens 1, 7 (annealed) and 8 (T6) can be seen in Figure 4.1.

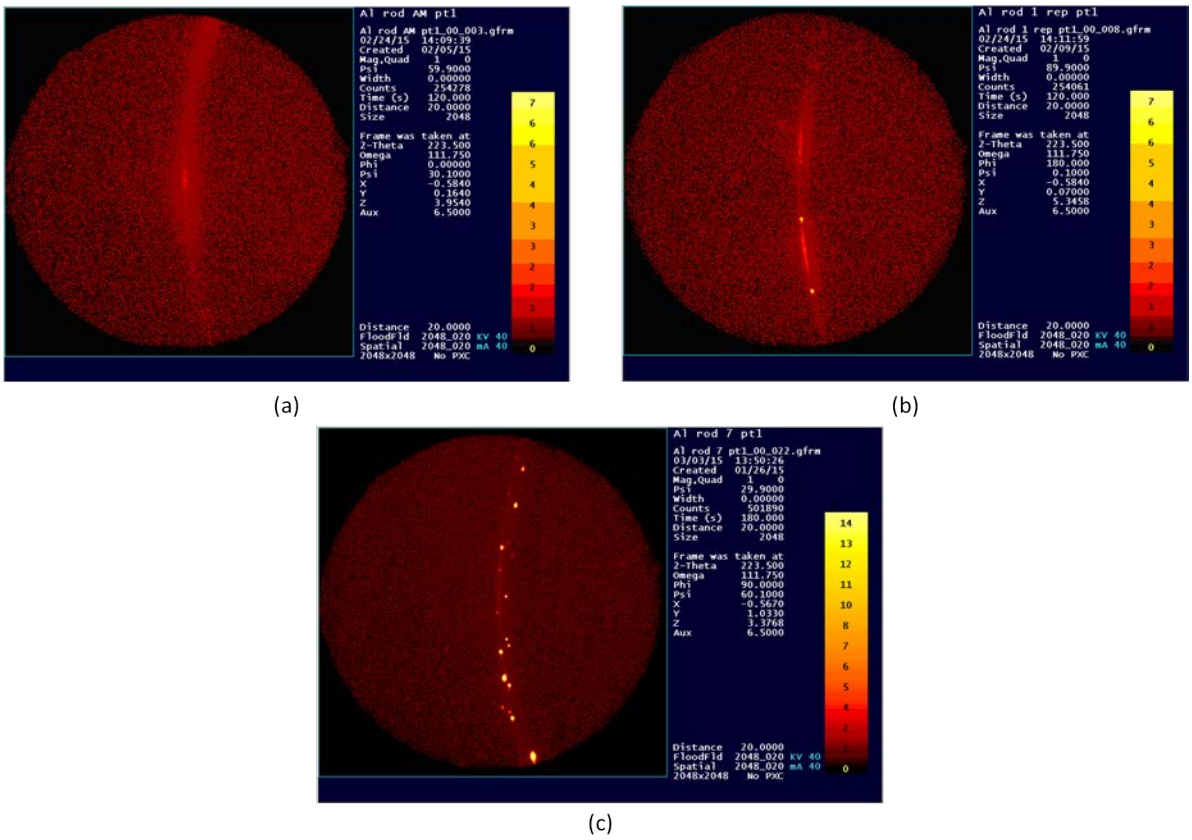

Figure 4.1: 2D Diffraction Data Indicating Different Features of the Samples
(a) T6 Test Specimen; (b) Test Specimen 1; (c) Test Specimen 7

$Sin^2\psi$ curves generated from the X-ray diffraction procedure can be seen in Appendix C in Figures C.1 to C.24. These Graphs were generated by the LEPTOS software and received from NECSA in this form. Three computer plots were generated per specimen, corresponding to the three points around the circumference of each specimen at which measurements were taken. Using a conventional least-squares method, the LEPTOS software fitted a linear plot to the data points in the $Sin^2\psi$ curves, which allowed a gradient to be calculated.

For conversion of strain to stress from the generated $Sin^2\psi$ curves, the elastic constants used were: ν = 0.35 (Poisson's ratio) and E = 69.3 GPa (Young's modulus). The elastic constants used were determined by the X-Ray diffraction operator, Mr T. Ntsoane (NECSA), who used idealised elastic constant values for AA7075-T6 from literature.

Using the computer generated stress tensors, the normal stresses within each tensor were used to calculate both an axial stress(σ_{11}) and a radial stress (σ_{22}) respectively (with reference to the geometry of the test samples). For each of the three measured circumferential points, the σ_{11} values of the respective stress tensors were averaged generating an overall axial stress for the specimen.

This process was repeated for the σ_{22} values in the tensors, thus generating an overall radial stress for the test specimens. This averaging process can be seen in Tables 4.2 and 4.3 respectively.

Table 4.2: Axial Residual Stress Values for Three Equally Spaced Measured Points

Specimen Number	1	2	3	4	5	6	7	8
σ_{11}: Point 1	-120.00	-95.80	-135.30	-142.90	-112.00	-139.20	7.40	-52.00
σ_{11}: Point 2	-94.50	-142.10	-158.60	-138.30	-135.40	-114.70	-17.10	-45.20
σ_{11}: Point 3	-111.30	-138.10	-150.70	-139.30	-137.50	-128.10	0.50	-37.70
σ_{11}: Average	-108.60	-125.33	-148.20	-140.17	-128.30	-127.33	-3.07	-44.97

Table 4.3: Radial Residual Stress Values for Three Equally Spaced Measured Points

Specimen Number	1	2	3	4	5	6	7	8
σ_{22}: Point 1	-193.00	-133.80	-127.40	-185.50	-126.10	-119.80	0.60	-59.90
σ_{22}: Point 2	-97.10	-121.50	-163.40	-172.30	-152.00	-116.10	-38.60	-50.30
σ_{22}: Point 3	-128.00	-128.40	-172.40	-163.60	-195.50	-85.50	23.10	-38.10
σ_{22}: Average	-139.37	-127.90	-154.37	-173.80	-157.87	-107.13	-4.97	-49.43

Using the averaged stress tensor values, two Graphs, seen in Figures 4.2 and 4.3, were generated so as to display the overall findings of the X-ray diffraction procedure for each of the eight test specimens tested. The results show that the T6 test specimen residual stresses were the lowest residual stresses within any of the test specimens (apart from the fully annealed test specimen). The stresses measured at the three circumferential points are compressive in nature and do not exceed -52 and -60 MPa, irrespective of the point on the specimen circumference at which these stresses were measured. The annealed test specimen had the lowest axial and radial residual stresses which were generally tensile in nature (as indicated by the generally positive trends of the fitted lines in Figures C.19 and C.21). The heat treatment and ageing processes attempted in this study, all significantly increased the residual compressive stresses within the respective test specimens as compared to the residual stresses within the T6 test specimen. The highest average radial stress was found to be -148.20 MPa in test specimen 2 and the highest average axial stress was found to be -173.80 MPa in test specimen 3.

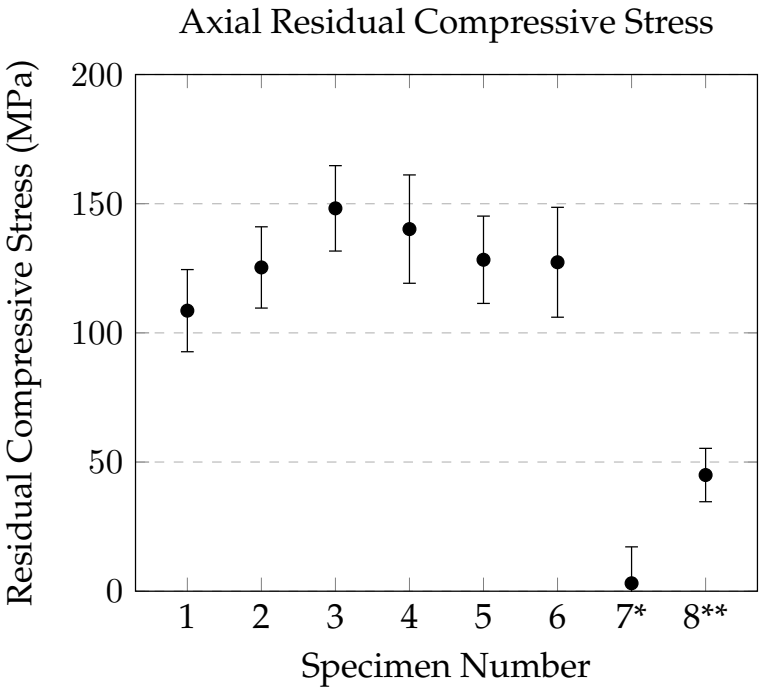

*Note: * - Annealed; ** - T6 (As received)*

Figure 4.2: Axial Residual Stresses in Various Test Specimens

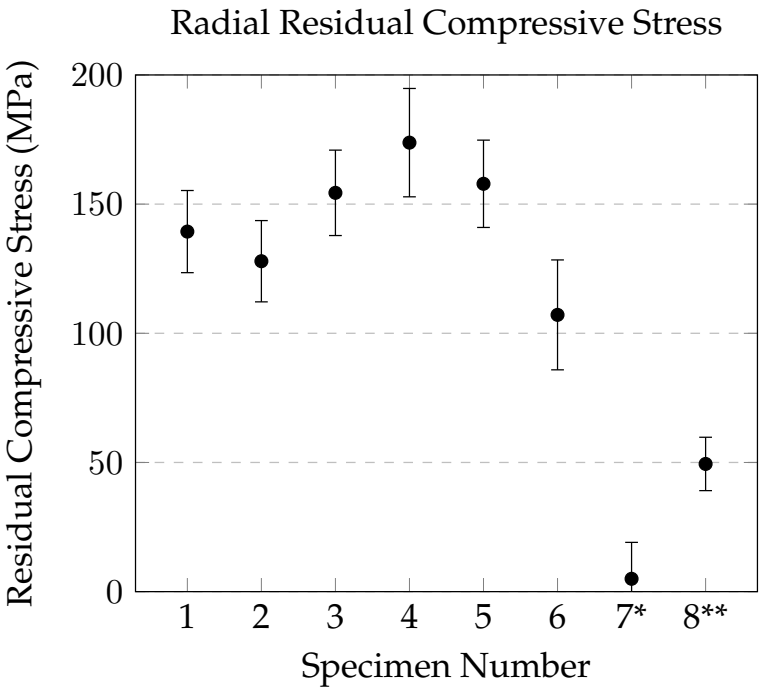

*Note: * - Annealed; ** - T6 (As received)*

Figure 4.3: Radial Residual Stresses in Various Test Specimens

4.2.3 Macrohardness Testing of Heat Treated Specimens

The Vickers hardness values measured from the X-ray diffracted test specimens can bee seen in Tables4.4.

Table 4.4: Heat Treated Specimen Material Properties

Test Specimen Number	1	2	3	4	5	6	7	8
Average Hardness Value (HV)	181	183	182	182	181	177	65	169
Estimated Ultimate Tensile Strength (MPa)	603	610	607	607	603	590	217	557

The Vickers Hardness value of the T6 test specimen (test specimen 8) was found to be 169 HV. This value is slightly higher than the typical Vickers Hardness value of 160 HV associated with AA7075-T6, as found in literature [112]. The subsequent heat treatments resulted in a general increase in the hardness values of the heat treated specimens when compared to the T6 material condition. Test specimen 7, which was fully annealed, had a hardness value of 64 HV which compared relatively well to the hardness value of 54 HV for AA7075-O found in literature [112].

The estimated ultimate tensile strengths of each test specimen, based on Equation 3.1, were found to be relatively high when compared to the typical ultimate tensile strengths of AA7075-T6 and AA7075-O, as found in literature [112]. The T6 test specimen had an estimated ultimate tensile strength of 557 MPa and the fully annealed test specimen had an estimated ultimate tensile strength of 217 MPa. This compared to ultimate tensile strengths of 570 MPa and 225 MP for AA7075-T6 and AA7075-O respectively, as found in literature [112].

4.2.4 Tensile Testing

Mechanical tensile testing was performed on test specimens in both the T6 and fully annealed material conditions. The average ultimate tensile strength of the material in the T6 condition was found to be nominally 632 MPa and the average ultimate tensile strength in the annealed material condition was found to be nominally 243 MPa. These values are higher than the estimated ultimate tensile strengths using the materials Vickers hardness values (557 MPa and 217 MPa for the T6 and annealed material conditions respectively) and are higher than the ultimate tensile strength values found in literature [78].

Material properties determined from the tensile test data include: 0.2 % tensile yield strength, ultimate tensile strength, the elongation (%) at break and the work hardening exponent. These

properties can be seen in Tables 4.5 and 4.6, with the curves used to generate the values found in Appendix D.

From the engineering stress-strain curves found in Appendix D, it can be observed that the annealed test specimens are more ductile than the T6 test specimens (i.e. the fully annealed curves are shorter and longer that the T6 curves). This increased ductility results in differing material properties between the two material conditions.

Tensile Testing Results

Table 4.5: Tensile Test Results of T6 Material Condition

Tensile Specimen Number	0.2 % Yield Stress (MPa)	Ultimate Tensile Strength (MPa)	Elongation - Cross Head (%)	Elongation - Manual (%)	Work Hardening Exponent (n)
1	574.63	634.71	15.19	6.56	0.20
2	561.15	633.35	13.79	7.74	0.20
3	561.40	627.94	14.92	6.60	0.19
Standard Deviation	6.30	2.93	0.61	0.55	0.00
Average	**565.73**	**632.00**	**14.63**	**6.97**	**0.20**

Table 4.6: Tensile Test Results of Annealed Material Condition

Tensile Specimen Number	0.2 % Yield Stress (MPa)	Ultimate Tensile Strength (MPa)	Elongation - Cross Head (%)	Elongation - Manual (%)	Work Hardening Exponent (n)
1	128.99	242.62	18.28	12.24	0.36
2	124.76	244.58	18.61	12.82	0.39
3	126.43	241.61	17.93	13.16	0.36
Standard Deviation	1.74	1.24	0.28	0.38	0.02
Average	**126.73**	**242.94**	**18.27**	**12.74**	**0.37**

4.3 The Effect of Shot Peening and Laser Shock Peening on Fatigue Performance

The effects of both laser shock peening and conventional shot peening on the fatigue properties of AA7075-T6 and AA7075-O aluminium round bar test specimens were investigated and compared by means of cyclic 3-point bend fatigue testing. The results of this investigation are presented in Appendices E and F respectively, with the averaged results presented in Figures 4.4 and 4.5.

An overview of the test groups and the surface treatments used in each group is given in Table 4.7, for use as a reference in this Chapter.

Experimental Test Groups

Table 4.7: Experimental Processes

Group Number	Material Condition	Number of Specimens	Specimen Surface Condition
1	T6	4	As Machined
	Annealed	4	As Machined
2	T6	4	Polished
	Annealed	4	Polished
3	T6	3	Polished/Shot Peened
	Annealed	3	Polished/Shot Peened
	T6	3	Polished/Shot Peened/Polished
	Annealed	3	Polished/Shot Peened/Polished
4	T6	3	Polished/Laser Shock Peened
	Annealed	3	Polished/Laser Shock Peened
	T6	3	Polished/Laser Shock Peened/Polished
	Annealed	3	Polished/Laser Shock Peened/Polished
5	T6	6	Polished/Laser Shock Peened/Partially Fatigued/Laser Shock Peened/Polished

4.3.1 Surface Morphology

The surface roughness R_a values were measured for all test specimens prior and after to their respective fatiguing procedures. These measurements enabled a mean average surface roughness R_a to be determined for each surface condition. A mean average surface roughness profile was also generated for each test specimen.

The surface roughness profiles seen in Appendix F, show consistent surface roughness profiles between test specimens in the same material condition, having received the same surface treatments. The surface roughness profile graphs initially start from a surface roughness value slightly higher than the mean average surface roughness value before adjusting to oscillate around the respective

mean average surface roughness value for the surface being measured. This is because the stylus of the testing machine initially starts from rest before traversing across the surface of the test specimens and thus has to overcome friction before it can start moving.

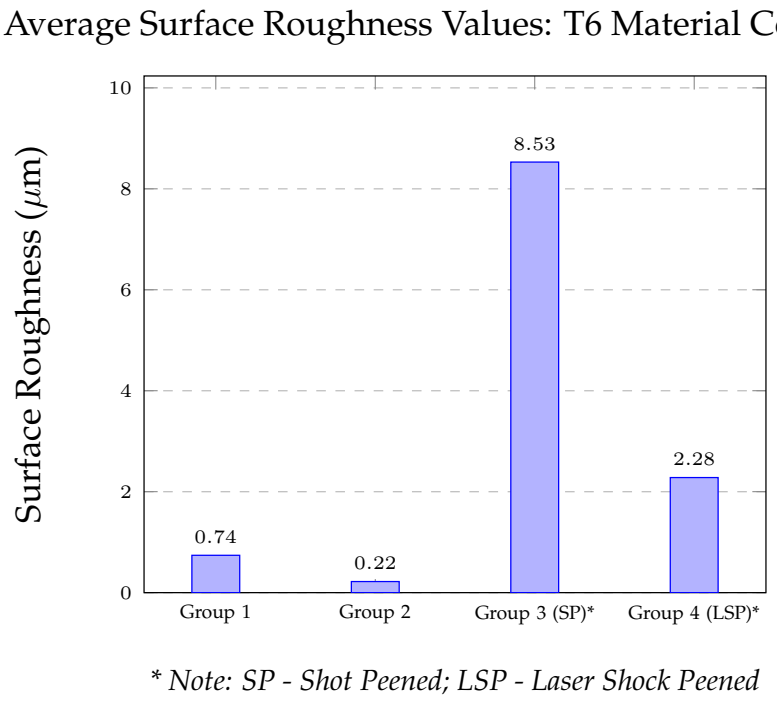

Figure 4.4: Average Surface Roughness Values: T6 Material Condition

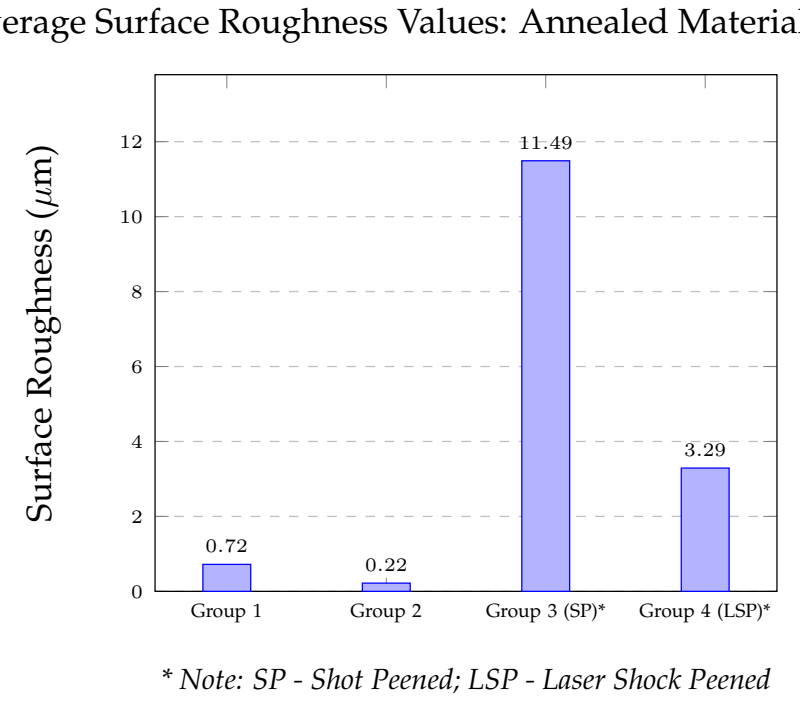

Figure 4.5: Average Surface Roughness Values: Annealed Condition

The surface roughness values of both the shot peened and laser shock peened samples are significantly higher than the reference surface roughness values (Group 1 in both material conditions). There is a significant reduction in the surface roughness values of all the test specimens after their respective polishing procedures (Group 2). The average surface roughness values for the test specimens (in both material conditions) before any processes are applied to them is 0.73 μm. The average polished surface roughness for the test specimens, in both material conditions, is 0.20 μm.

The shot peened samples (Group 3) have the roughest surface of all the samples. The shot peened samples in the T6 condition have a surface roughness of 8.15 μm and the shot peened samples in the annealed condition have an average surface roughness of 11.12 μm. The annealed test specimens are softer than the "as received" test specimens and thus yield to a larger extent when struck by the same shot and the same intensity.

The laser shock peened sample (Group 4) in both the T6 and annealed conditions, have a relatively uniform surface roughness for test samples in the same material condition. The average surface roughness for the annealed laser shock peened test specimens, 3.29 μm, is larger than the average surface roughness for the "as received" laser shock peened test specimens, 2.28 μm, as the material is softer and thus yields to a larger extent when shock peened by a laser at the same intensity.

4.3.2 Fatigue Performance

Test specimens were cyclically fatigued in a 3-point bend test to failure after their respective surface treatments. This allowed for the effects of the shot peening and laser shock peening surface treatments on the specimens fatigue lives to be compared and contrasted. The fatigue life data of the test specimens for each experimental process and in each material condition is presented in the form of a bar graph (one bar per test specimen) in Appendix G, with the averaged results presented in Table 4.8 and Figures 4.6 and 4.7.

Table 4.8: Experimental Process Fatigue Data Averages

Group	Material Condition	Average Diameter	Applied Stress	Average Observable Crack Length	Cycles to	Cycles to
	(mm)	(μm)	(kN)	(mm)	Crack Initiation	Failure
1	T6	16.94	585.00	2.95	28137	32167
	AN	16.95	450.00	2.48	26335	29190
2	T6	16.92	585.00	2.01	35722	39307
	AN	16.92	450.00	1.83	30102	33307
3	T6	17.05	585.00	3.70	59723	61971
SP	AN	17.06	450.00	3.47	14550	16276
3	T6	16.94	585.00	2.06	125693	131653
SP/Polished	AN	16.91	450.00	2.00	22236	25774
4	T6	16.99	585.00	3.37	91462	95806
LSP	AN	17.00	450.00	3.20	25471	27531
4	T6	16.99	585.00	1.60	207661	211271
LSP/Polished	AN	16.98	450.00	1.77	28317	32425

** Note: SP - Shot Peened; LSP - Laser Shock Peened; AN - Annealed*

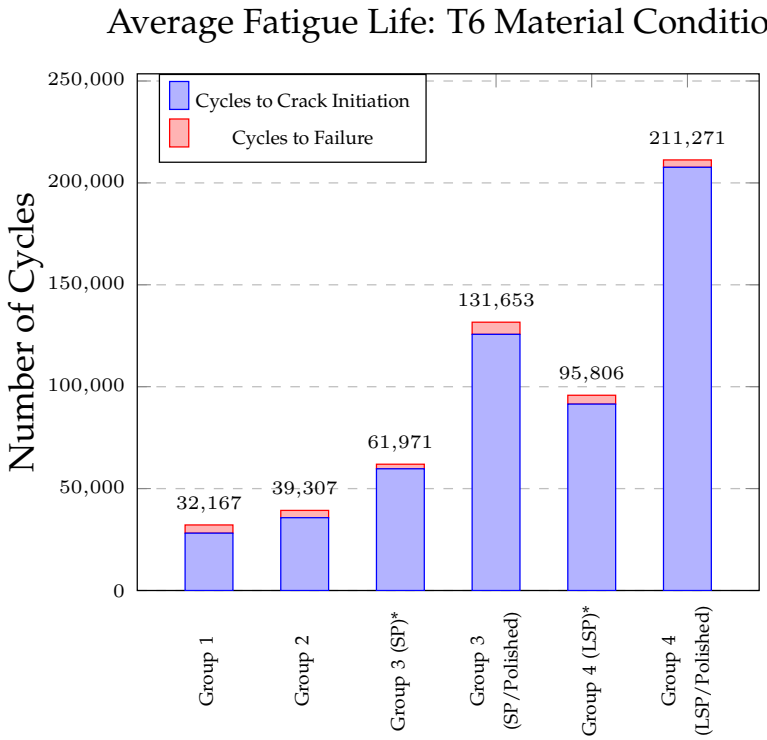

** Note: SP - Shot Peened; LSP - Laser Shock Peened*

Figure 4.6: Average Fatigue Life: T6 Material Condition

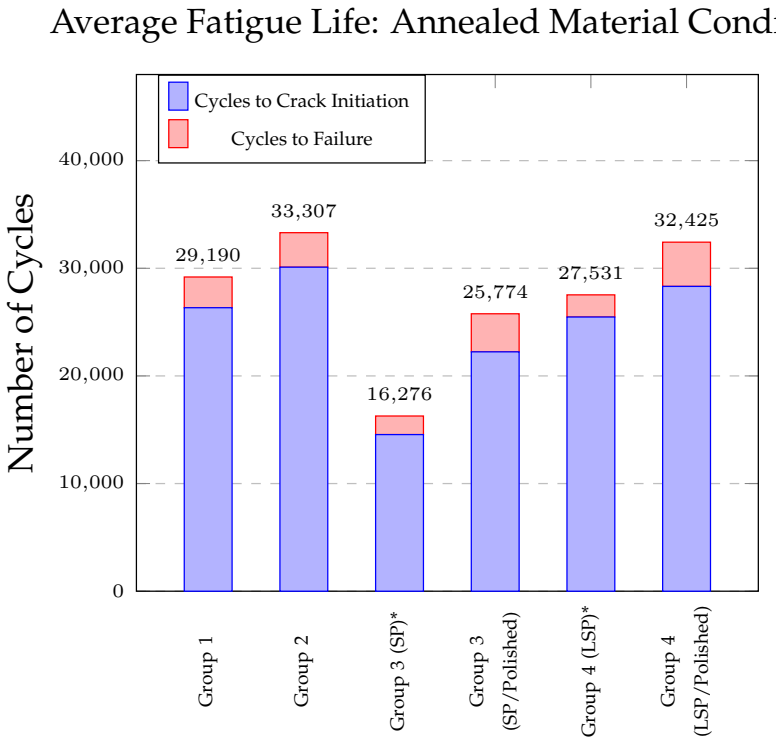

** Note: SP - Shot Peened; LSP - Laser Shock Peened*

Figure 4.7: Average Fatigue Life: Annealed Material Condition

From Figure 4.6 it can be seen that the average fatigue lives of the test specimens in the T6 material condition vary based on their respective surface treatments. With each surface treatment, an increase in fatigue life is observed from the "as machined" test specimens in Group 1. A significant increase in fatigue life occurs in the test specimens which were polished after their respective shot peening and laser shock peening treatments. In both instances, the fatigue life more than doubles (131653 and 211271 for shot peening and laser shock peening respectively), once the induced roughnesses of each peening procedure is polished away.

The average fatigue lives of the test specimens in the annealed material condition, Figure 4.7, vary little irrespective of their respective surface treatments. There is however a reduction in the fatigue lives of the shot peened specimens (Group 3) when compared to the other test specimens, presumably because of the induced surface roughness.

The observable crack lengths at crack initiation also differ depending on the surface roughness of the test specimen. Unpolished test specimens from test Group 1 in both material conditions had an observable crack length average of nominally 2.72 mm. This average observable crack length was reduced through the polishing of the test specimens surfaces. Polished test specimens (from Groups 2, 3 and 4 in both material conditions) had an observable crack length average of nominally

1.88 mm. Samples from test Groups 3 and 4 (shot peening and laser shock peening respectively) had relatively rough surfaces which made it difficult to observe crack initiation.

4.4 Fatigue Life Recovery Process

The ability of the laser shock peening process to recover fatigue life in *partially fatigued* components was investigated. This investigation looked at whether the laser shock peening process could be used on partially fatigued components at the point of crack initiation in an attempt to further improve the fatigue life of the component. The results of this investigation (performed on test specimens from Group 5) are presented.

4.4.1 Surface Roughness Profiling: Pre-Partial Fatiguing

The surface roughness R_a values were measured for the fatigue life recovery procedure prior to their testing process. The average material removed during the polishing procedure was 0.05 mm which was equivalent to 0.025 mm from opposing sides of the specimen diameter. The surface roughness profiles generated during the surface roughness measurements for the specimens can be seen in Appendix E. The surface roughness achieved after polishing was 0.18 μm which was within the desired surface roughness range of 0.20 $\pm 0.05 \mu$m.

- Material Condition: T6/Polished/Laser Shock Peened/Polished

Average Surface Roughness (R_a) Values

Table 4.9: Average Surface Roughness Values

Process	Material Condition	$\mathbf{Ra_{average}}$ (μm)
Fatigue Life Healing	T6 Before Polish	2.28
Fatigue Life Healing	T6 After Polish	0.18

4.4.2 CT Scanning: Pre-Fatiguing

Computed tomography (CT) scanning was initially used in the fatigue life recovery process to examine whether there were any defects within the test specimens prior to the partial fatiguing process. All the CT scan images generated during the fatigue life recovery process can be found in Appendix H.

Due to the resolution of the instrument (based on the size of the scanned area), defects with a size $\approx$ 0.20 mm or larger could be detected. Results revealed that no defects were observed with a size greater than 0.20 mm in the test specimens. An example of one of the CT scans generated, prior

to the partial fatiguing process is presented in Figure 4.8. The dark shadows seen in some of the images near the specimen circumferences are artefacts from the scanning procedure.

Test Specimen 1

- Material Condition: T6/Polished/Laser Shock Peened/Polished

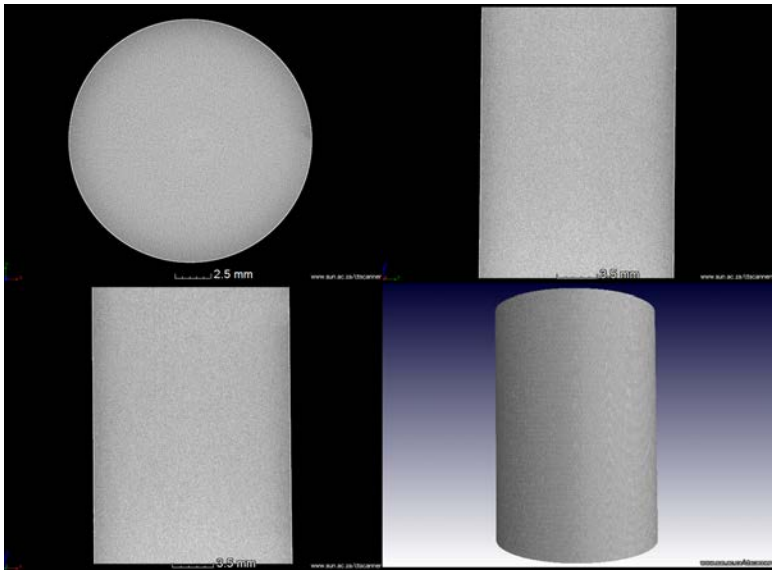

Figure 4.8: CT Scan of Test Specimen 1

4.4.3 Partial Fatiguing Process

Test specimens were fatigued in 3-point bending to the point of crack initiation as part of the fatigue life recovery process. The fatigue life data of the test specimens for the fatigue life recovery process is presented in the form of a bar graph seen. The fatigue data for each test is presented in Table 4.10.

Table 4.10: Fatigue Life Healing Process: Partial Fatiguing

Specimen Number	Diameter (mm)	Applied Stress (MPa)	Applied Force (kN)	P_{max} (kN)	P_{min} (kN)	P_{mean} (kN)	Amplitude (kN)	Circumferential Crack Length (mm)	Cycles to Crack Initiation
1	16.97	585.00	16.51	18.34	1.83	-10.09	8.18	1.80	794591
2	17.05	585.00	16.74	18.61	1.86	-10.23	8.37	1.60	185826
3	17.00	585.00	16.60	18.44	1.84	-10.14	8.30	1.00	256061
4	17.04	585.00	16.72	18.57	1.86	-10.21	8.36	2.00	216316
5	17.00	585.00	16.60	18.44	1.84	-10.14	8.30	1.40	191113
Average	**17.01**	**585.00**	**16.42**	**18.24**	**1.82**	**-10.03**	**8.21**	**1.56**	**328772**

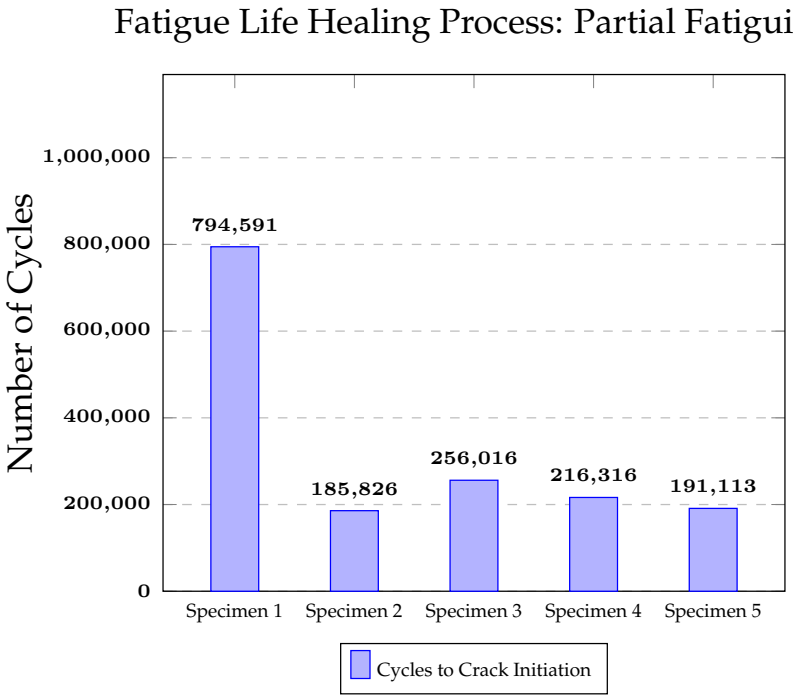

Figure 4.9: Fatigue Life Healing Process: Partial Fatiguing

From Figure 4.9 above, it can be seen that test specimens 2 to 5 failed between 185 000 and 270 000 cycles. Test specimen 1 was an outlier to this trend and failed just short of 800 000 cycles.

4.4.4 CT Scanning: Post Partial Fatiguing

Computed tomography (CT) scanning was used to map the observed cracks generated in the test samples during the partial fatiguing process.

By limiting the area of the scan to the midsection of each bend test specimen, defects with a size ≈ 0.127 mm or larger could be detected. The CT scanned images of the five partially fatigued test specimens are shown in Appendix H.

The observed circumferential crack lengths (observed during the partial fatiguing process with the aid of a microscope) and the measured crack depths are presented in Table 4.11. As no cracks could be found in test specimens 3 and 4, it was assumed that the crack lengths were < 0.127 mm.

Table 4.11: Partial Fatiguing Crack Lengths and Depths

Specimen	Circumferential Length (mm)	Crack Depth (mm)
1	1.80	2.06
2	1.60	0.40
3	1.00	< 0.127
4	2.00	< 0.127
5	1.40	0.49

4.4.5 CT Scanning: After Laser Shock Peening Treatment

After the test specimens were re-laser shock peened, test specimens 1, 2 and 5 were selected for the post laser shock peening treatment CT scanning process as these samples had previously had their crack depths successfully measured and mapped as seen in Section 4.4.4. Due to the resolution of the scan (based on the size of the scanned area), defects with a size $\approx$ 0.20 mm or larger could be detected.

The CT scanned images of the three partially fatigued/laser shock peened test specimens are shown in Appendix H.

The measured crack depths are presented in Table 4.12. As no cracks could be found in test specimens 2 and 5, it was assumed that the crack lengths were < 0.20 mm.

Table 4.12: Partial Fatiguing Crack Lengths and Depths

Specimen	**Crack Depth Before Laser Shock Peening Treatment (mm)**	**Crack Depth After Laser Shock Peening Treatment (mm)**
1	2.06	1.82
2	0.40	< 0.20
5	0.49	< 0.20

4.4.6 Surface Roughness Profiling: Pre-Final Fatiguing

The surface roughness $\boldsymbol{R_a}$ values were measured for the fatigue life recovery procedure after both their re-laser shock peening treatment and final polishing. A mean average surface roughness profile was also generated for each test specimen, before and after their respective polishing procedures. The surface roughness profiles can be seen in Appendix F. The surface roughness achieved after polishing was 0.20 $\boldsymbol{\mu m}$ which was again within the desired surface roughness range of 0.20 $\pm \mathbf{0.05} \mu$m.

- Material Condition: T6/Polished/Laser Shock Peened/Polished/Partially Fatigued/Re-Laser Shock Peened/Polished

Average Surface Roughness (R_a) Values

Table 4.13: Average Surface Roughness Values

Process	Material Condition	$Ra_{average}$ (μm)
Fatigue Life Healing	T6 Before Polish	2.22
Fatigue Life Healing	T6 After Polish	0.20

4.4.7 Fatiguing to Failure

Test specimens were fatigued in 3-point bending to the point of failure so as to determine the degree of fatigue life recovery achieved through the laser shock peening process. The fatigue life data is presented in the form of a bar graph seen. The fatigue data for each test is presented in Table 4.14.

Table 4.14: Fatigue Life Healing Process: Partial Fatiguing

Specimen Number	Diameter (mm)	Applied Stress (MPa)	Applied Force (kN)	P_{max} (kN)	P_{min} (kN)	P_{mean} (kN)	Amplitude (kN)	Cycles to Crack Initiation	Cycles to Failure
1	16.90	585.00	16.31	18.12	1.81	-9.97	8.15	100	3186
2	16.97	585.00	16.51	18.34	1.83	-10.09	8.26	6945	13196
3	16.92	585.00	16.36	18.18	1.82	-10.00	8.18	7983	14134
4	16.98	585.00	16.54	18.38	1.84	-10.11	8.27	9559	15559
5	16.92	585.00	16.36	18.18	1.82	-10.00	8.18	14800	20086
Average	**16.94**	**585.00**	**16.42**	**18.24**	**1.82**	**-10.03**	**8.29**	**7877**	**13232**

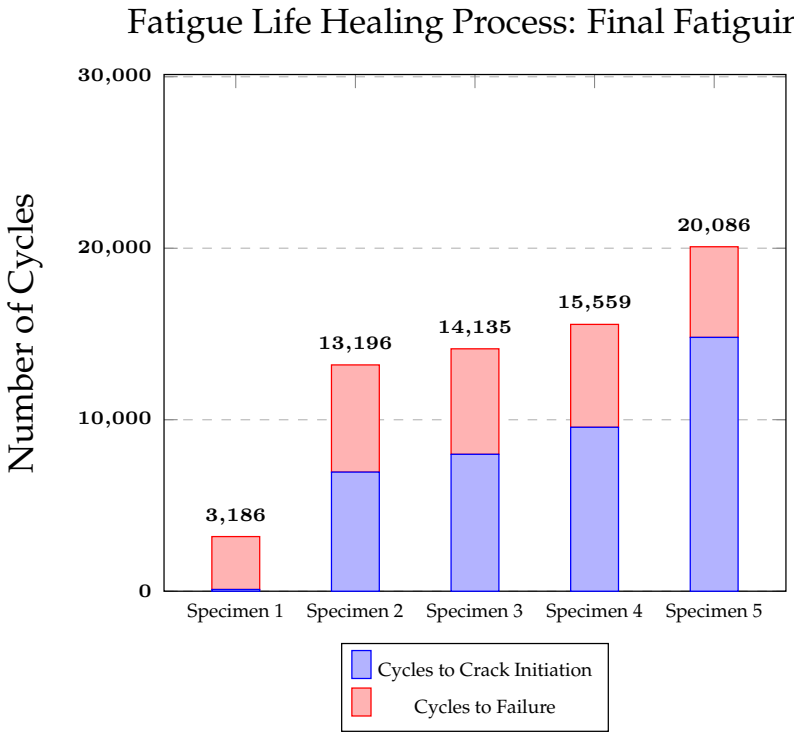

Figure 4.10: Fatigue Life Healing Process: Fatigue Fatiguing

From Figure 4.10 above, it can be seen that test specimens 2 to 5 failed between 13000 and 20100 cycles. Test specimen 1 was an outlier to this trend and failed just short of 3200 cycles. The period from observable crack initiation to final fracture of the test specimens was greater than the periods observed for the Laser shock peened and polished test samples from Group 4.

4.5 Metallographic Examination

4.5.1 Fractography

i) Optical Fractography

Optical fractography was performed on the fracture surfaces of the AA7075 test specimens. Two distinct types of fracture surfaces were observed, based on the material condition i.e. T6 or annealed. These distinct types of fracture surfaces were relatively consistent for each material condition regardless of the mechanical surface treatments (or lack thereof) used on the specimens.

An example of the opposing fracture surfaces in each material condition can be seen in Figures 4.11 and 4.12. Observations from these fracture surfaces are given and key features of the fracture surfaces are labelled. Labelled fractographs of each test specimen per test group can be found in Appendix I.

- **Material Condition: T6**

The T6 material fracture surfaces seen below, contain three regions which can be associated with crack initiation, crack growth and final overload. Inspection of these fracture surfaces reveals some distinctive macroscopic features, which are indicative of a mixed mode of fracture (i.e. both brittle and ductile features are present) and of uni-axial cyclic bending fatigue.

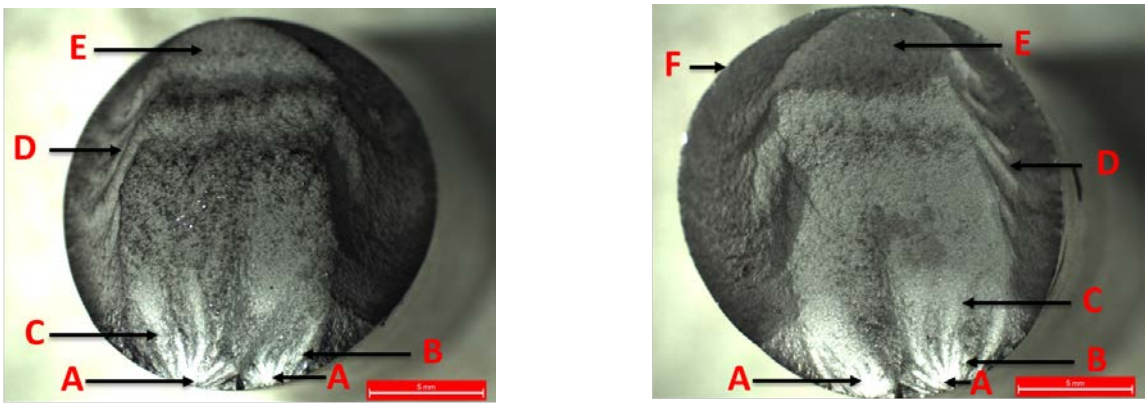

(a) **(b)**

Figure 4.11: Fractograph of T6 Test Specimen

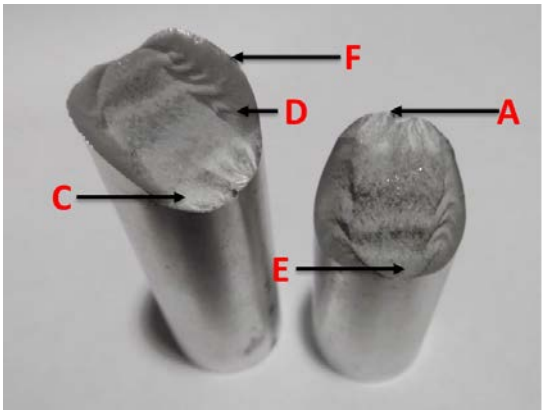

(c)

(d)

Figure 4.11: Side View of Fractured T6 Test Specimen

Table 4.15: T6 Fracture Surface Labelling Key

Label	Surface Feature
A	Crack Initiation Site
B	Ratchet Marks
C	Crack Growth Region
D	Chevron Marks
E	Final Fracture Zone
F	Shear Lips
G	Compression Curl (Cantilever Curl)

- **Material Condition: Annealed**

The annealed material fracture surfaces seen in Appendix I contain three regions that can be associated with crack initiation, crack growth and final overload. Inspection of these fracture surfaces reveals some distinctive macroscopic features, which are indicative of a typically ductile mode of fracture.

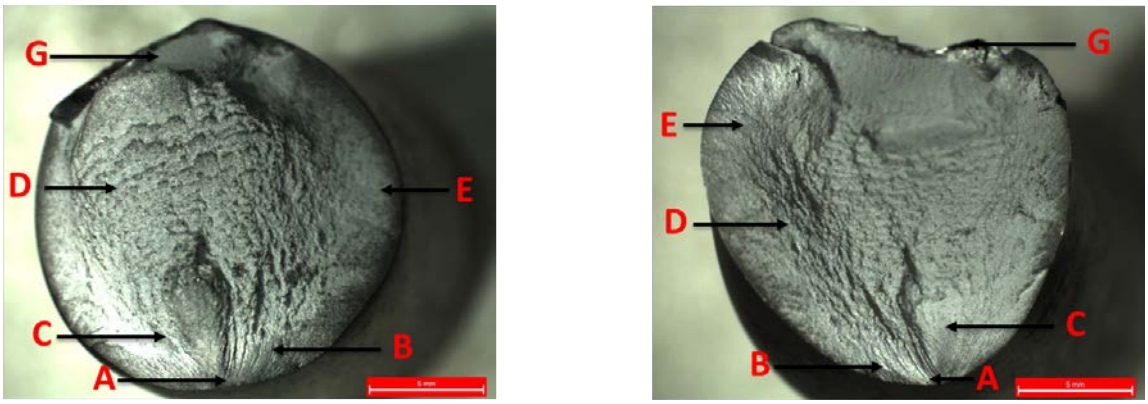

(a) (b)

Figure 4.12: Fractograph of Annealed Test Specimen

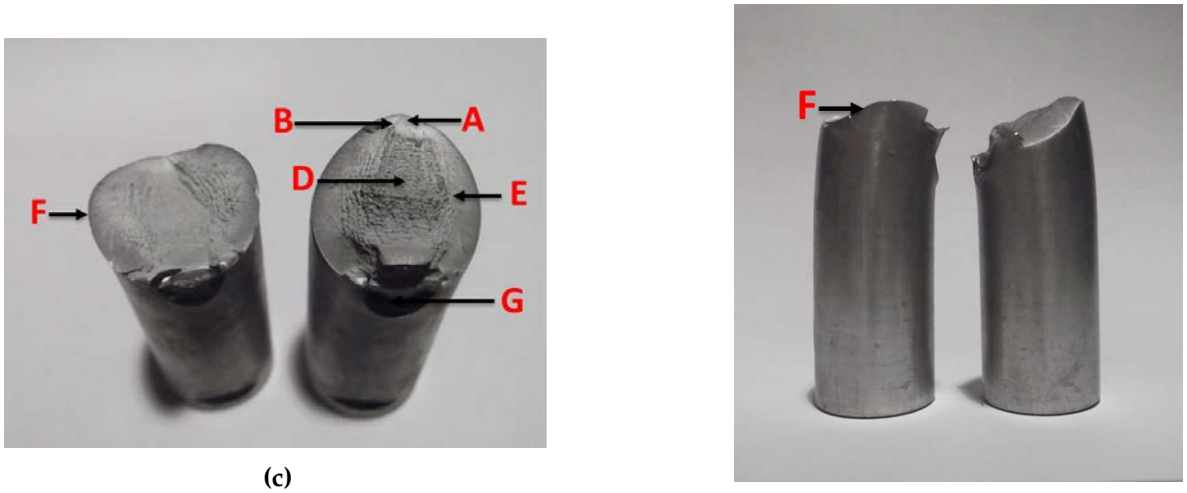

(c) (d)

Figure 4.12: Side View of Fractured Annealed Test Specimen

Table 4.16: Annealed Fracture Surface Labelling Key

Label	Surface Feature
A	Crack Initiation Site
B	Ratchet Marks
C	Crack Growth Region
D	Rough/Dimpled Surface
E	Smooth Radial Zone
F	Shear Lips
G	Post Fracture Damage

ii) SEM Fractography

SEM images of the various fracture surfaces of test specimens in the T6 condition from test Groups 1 to 5 were captured. The images were taken at the site of crack initiation, with the white arrows on the images indicating crack initiation points.

Crack initiation (A) was observed to occur on the surface of the test specimens from Groups 1 to 4 and was observed to occur subsurface on the specimens from Group 5, as seen in Figure 4.17.

Test Group 2

- Material Condition: T6/Polished

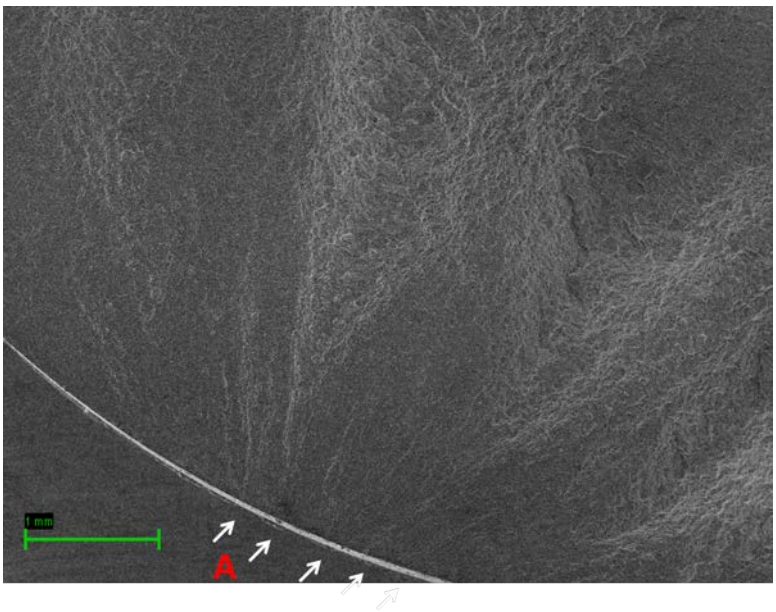

Figure 4.13: Fractograph of T6/Polished Test Specimen

Test Group 3

- Material Condition: T6/Polished/Shot Peened

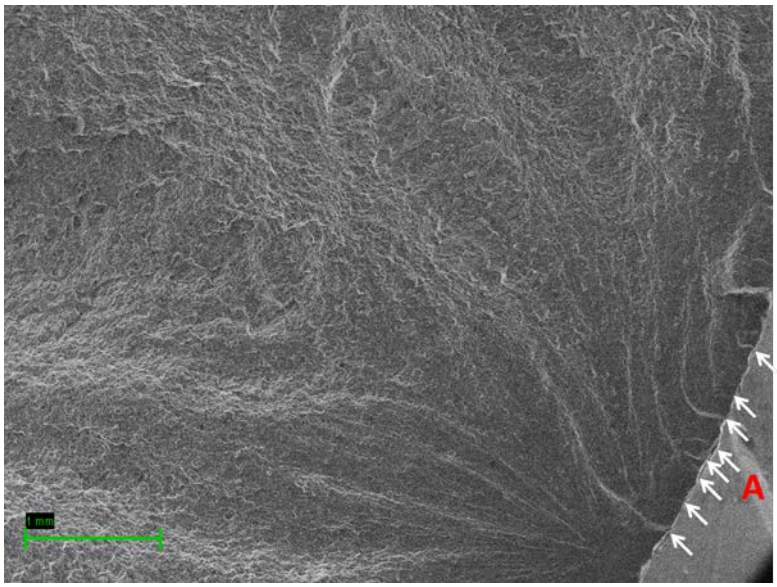

Figure 4.14

Figure 4.15: Fractograph of T6/Polished/Shot Peened Test Specimen

Test Group 4

- Material Condition: T6/Polished/Laser Shock Peened

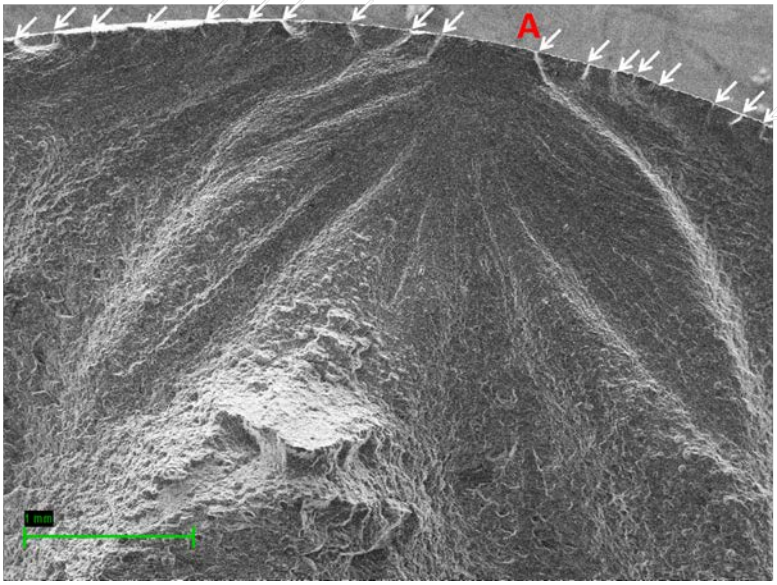

Figure 4.16: Fractograph of T6/Polished/Laser Shock Peened Test Specimen

Test Group 5

- Material Condition: T6/Polished/Laser Shock Peened/Partially Fatigued/Laser Shock Peened/Polished/

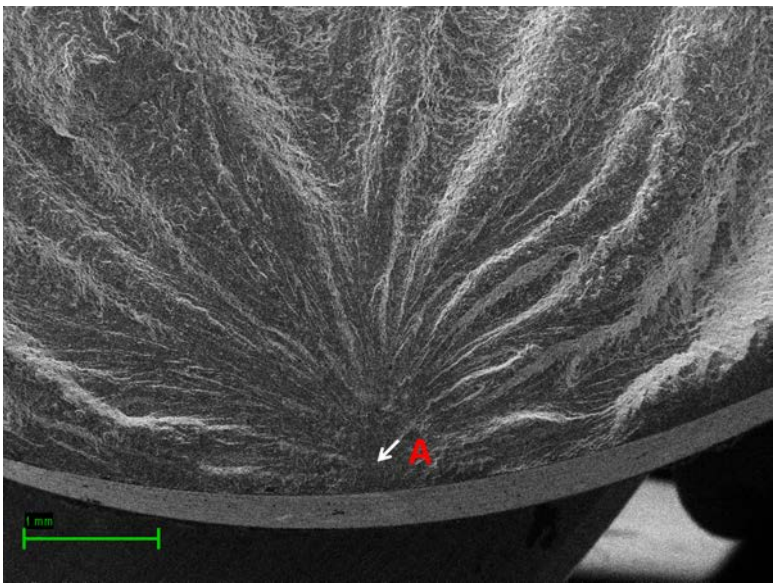

Figure 4.17: Fractograph of Fatigue Life Healed Test Specimen

4.5.2 Nomarski Lens Light Microscopy

Micrographs of etched sample sections in each material condition utilised in this study (polishing, shot peening and laser shock peening) are presented below. The surface of the test specimens (tops of the micrographs), parallel to the extrusion direction, are shown in the micrographs, facilitating the observation of the effects of the various mechanical surface treatments on the specimen surfaces at a magnified level.

The surfaces of the test specimens in the T6 material condition, Figures 4.18 and 4.19, show surface deformation and roughening as a result of the shot peening and laser shock peening processes. The shot peening and laser shock peening processes have no significant observable effect on the near-surface grain structure within each respective specimen, with slight deformation to the grains near the surface of the shot peened specimens.

The surfaces of the test specimens in the annealed material condition, Figure 4.18, show severe surface deformation and roughening as a result of the shot peening and laser shock peening processes. Some deformation to the grains near the surface of the shot peened specimen and laser shock peened specimens was observed.

- **Material Condition: T6**

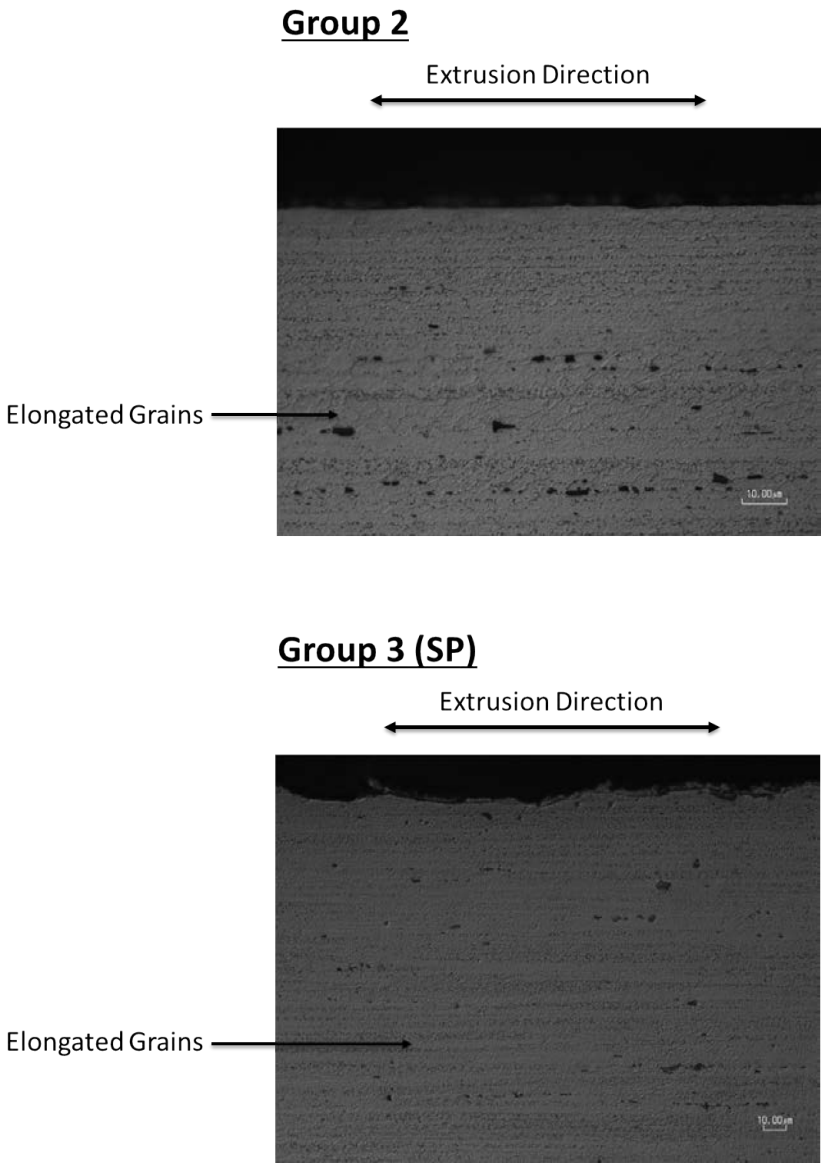

Figure 4.18: T6 Test Specimen Micrographs

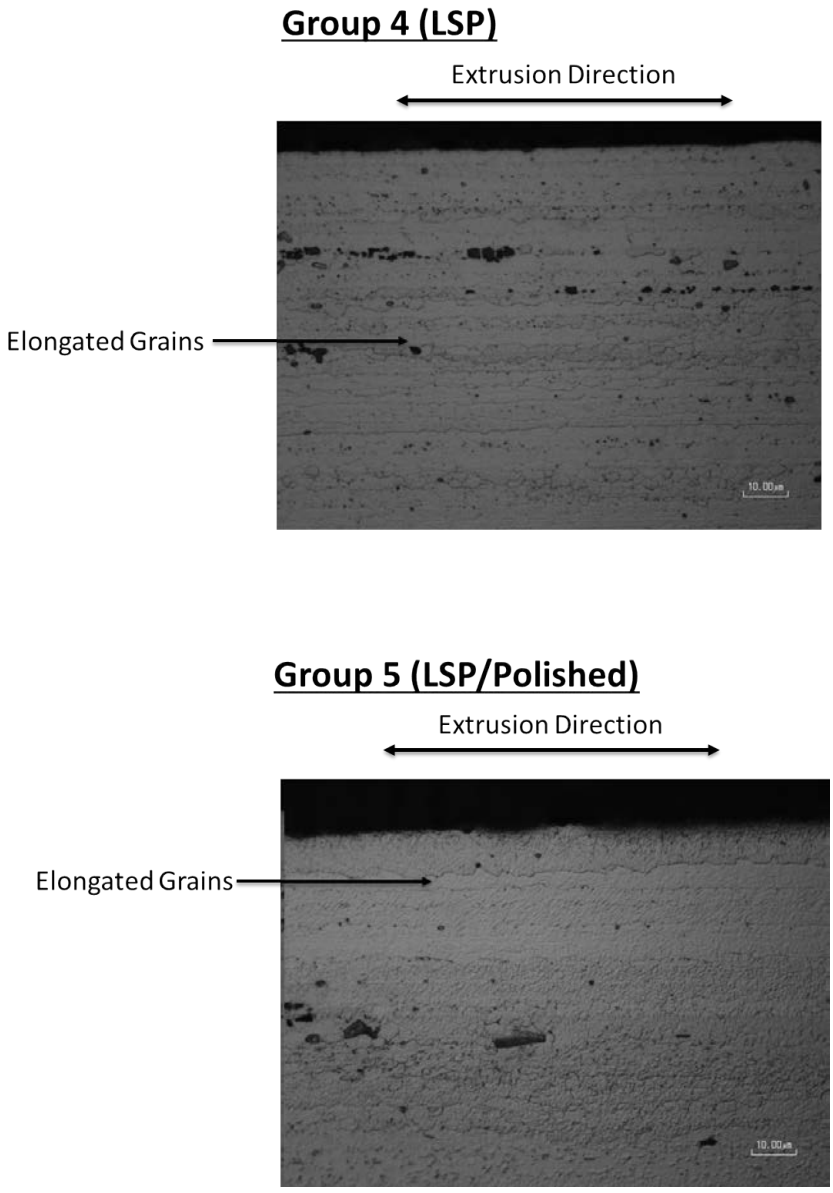

Figure 4.19: T6 Test Specimen Micrographs

- **Material Condition: Annealed**

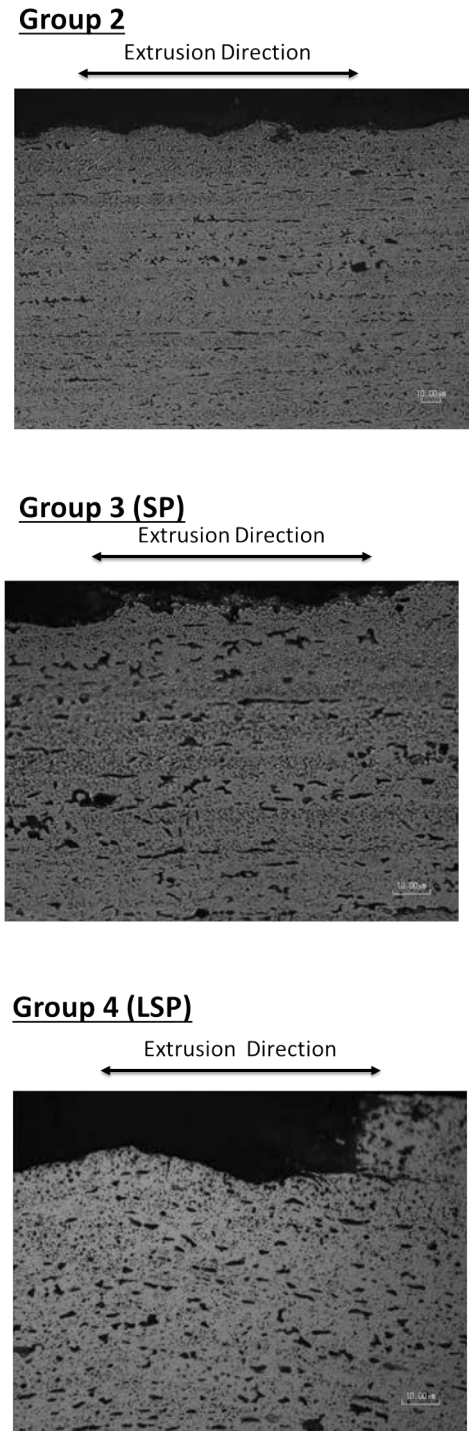

Figure 4.20: Annealed Test Specimen Micrographs

4.5.3 Microhardness Testing

The microhardness (as a function of depth from the surface) distributions of AA7075 (in both the T6 and fully annealed material conditions) before and after various mechanical surface treatments are shown in Figures 4.21 and 4.22. A summary of the test data obtain during the microhardness testing can also be seen in Table 4.17.

The mean average bulk hardness in the aluminium in the T6 condition, without any of the mechanical surface treatments applied to the material, was 168 HV. The mean average bulk hardness in the aluminium in the annealed condition, without any of the mechanical surface treatments applied to the material, was 64.4 HV. The depth of plastic deformation in the laser shock peened specimens in the T6 material condition (Group 4) could not be established with any confidence.

Hardening of the surface layers of the test specimens in the T6 material condition was observed for the shot peened and fatigue life recovery test specimens, to depths of 0.34 and 0.76 mm respectively.

Hardening of the surface layers of the test specimens in the annealed material condition was observed for the shot peened and laser shock peened test specimens, to depths of 0.42 and 1.14 mm respectively.

Table 4.17: Incremental Depth Microhardness Testing Results

Group	Material Condition	Measurement Depth (mm)	Number of Measurements	Estimated Depth of Plastic Deformation (mm)
1	T6	1.03	21	Baseline
1	AN	1.27	29	Baseline
3	T6	0.34	33	0.34
3	AN	0.47	33	0.42
4	T6	1.04	17	-
4	AN	1.28	26	1.14
5	T6	0.78	39	0.78

** Note: AN - Annealed*

Material Condition: T6

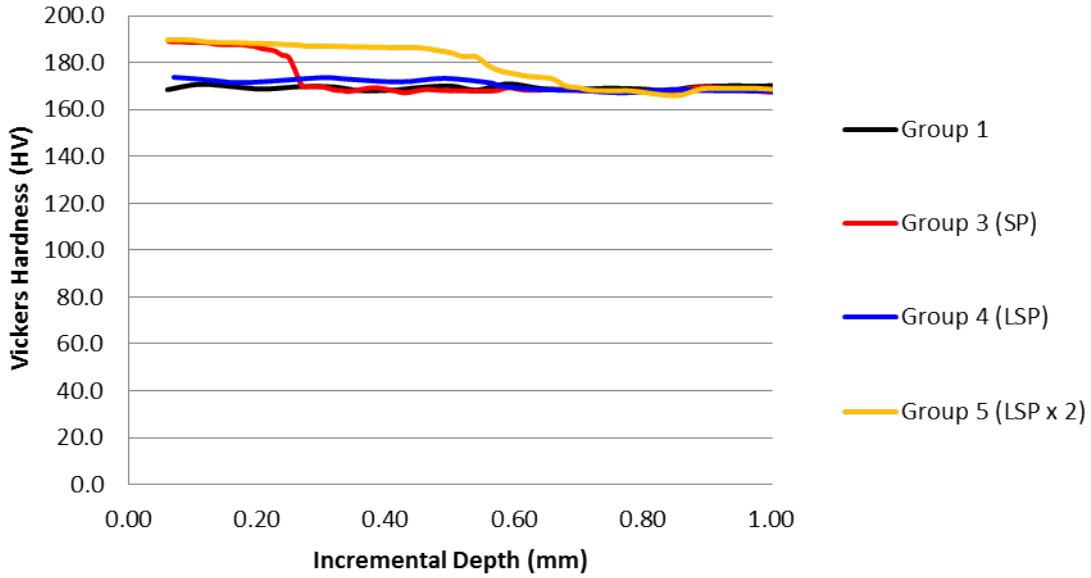

Figure 4.21: Vickers Hardness of T6 Specimens

Material Condition: Annealed

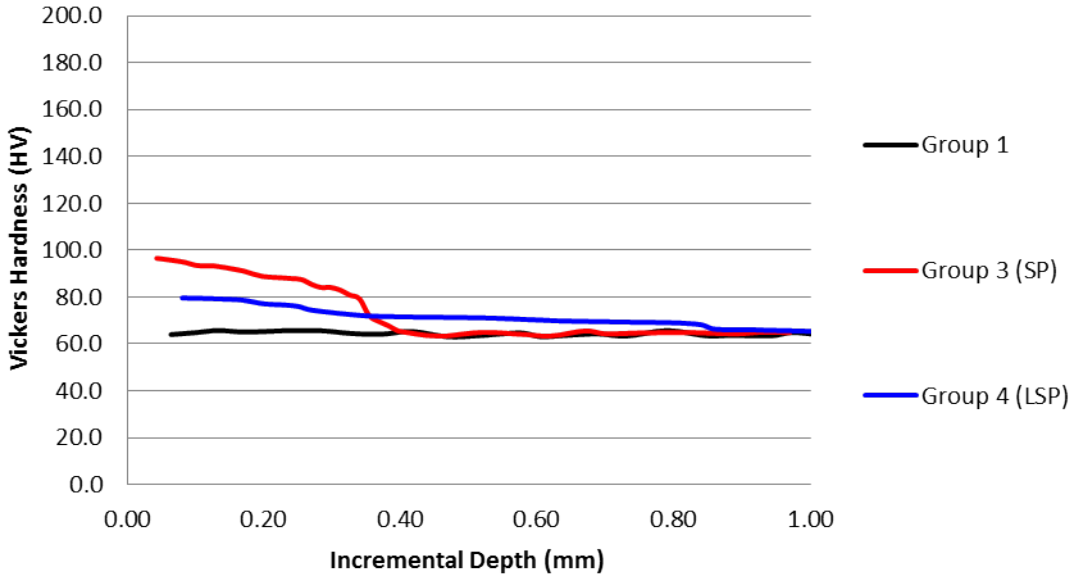

Figure 4.22: Vickers Hardness of Annealed Specimens

4.6 Summary

This Chapter presented the results obtained from the preliminary study and resulting investigation into the fatigue performance of AA7075 subjected to various surface treatments.

The preliminary investigation revealed high residual stresses within the heat treated test specimens. The test specimen "as received" in the T6 material condition revealed a moderate residual stress and subsequent tensile testing revealed that the T6 condition had material properties which were greater than those found in literature [78].

Following on from the preliminary investigation, analysis of the effect of shot peening and laser shock peening on the fatigue performance of aluminium alloy was conducted. It was found that laser shock peening resulted in increasing the fatigue life of the AA7075-T6 test specimens by the largest degree. Both the shot peening and laser shock peening processes significantly increased the surface roughness of the test specimens.

Results from the investigation into the ability of laser shock peening to restore fatigue life in damaged components were then presented. From these results, it was seen that cracks can be accurately mapped using the CT scanning process. There was also a small degree of fatigue life recovery for the partially fatigued test specimens.

Finally, the results from the analysis of the fracture surfaces, microstructure, strain and hardness of both the fatigued and fatigue life recovered test specimens were presented.

The Chapter which follows discusses the results obtained in detail and the implications of these results and draws conclusions based on the evidence presented.

Chapter 5

Discussion

5.1 Introduction

This Chapter discusses the results obtained and observations and interpretations made during the experimental processes undertaken in this project. The main objective of this project was to investigate the effects of both shot peening and laser shock peening of the fatigue properties of high strength aluminium alloy as well as to investigate the ability of the laser shock peening process to recover fatigue life in damaged components.

5.2 Surface Morphology

Changes to the surface morphology of the aluminium alloy 7075 test specimens brought about by the shot peening and laser shock peening procedures were investigated.

Increased surface roughness facilitates the development of stress concentration sites from which fatigue cracks can initiate and therefore have a significant negative effect on the fatigue life of a component.

Table 5.1, compares surface roughness values for baseline, shot peened and laser shock peened materials as obtained in this study.

Table 5.1: Average Surface Roughness (R_a) Values

		Material Condition	
Group	**Surface Treatment**	**T6**	**Annealed**
Group 1	As Machined	0.74	0.72
Group 2	Polished	0.22	0.22
Group 3	Polished/Shot Peened	8.53	11.49
Group 4	Polished/Laser Shock Peened Peened	2.28	3.29

From Table 5.1 above, it can be seen that a higher surface roughness was observed after the shot peening process for test specimens in each material condition. The extreme multi-axial loading nature of the shot peening process results in numerous and random overlapping dimples. This inhomogeneous dimpling, together with any sharp indentations caused by broken shot media, give rise to the relatively high surface roughness generated during the shot peening process. By contrast, laser shock peening is uni-axial in nature, creating homogeneous, shallow indentations during the peening process, which only slightly increases the surface roughness from the polished condition when compared to the shot peened test specimens.

The annealed AA7075-O showed the highest increase in surface roughness for each respective surface treatment procedure. This is because the material is highly ductile and therefore relatively soft in its annealed state. This ductility leads to increased plastic flow during the peening processes, facilitating increased surface roughness. A visual comparison of the different surface roughnesses can be seen in Figures 5.1 and 5.2. The measured surface roughness of each surface treatment process (for both material conditions) are superimposed on one another in the Figures, showing the significant differences in the measured surface roughnesses.

Material Condition: T6

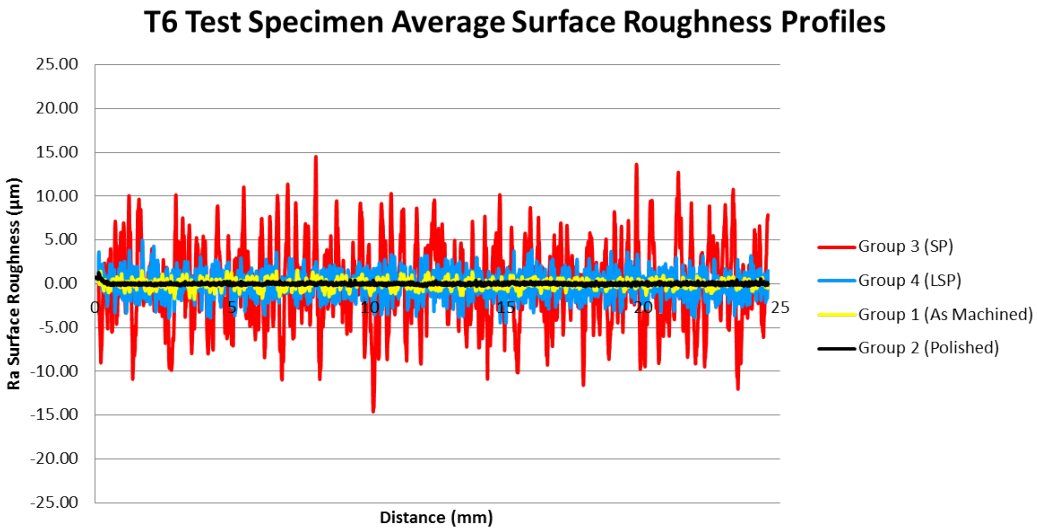

Figure 5.1: Surface Roughness Profiles of T6 Test Specimens

Material Condition: Annealed

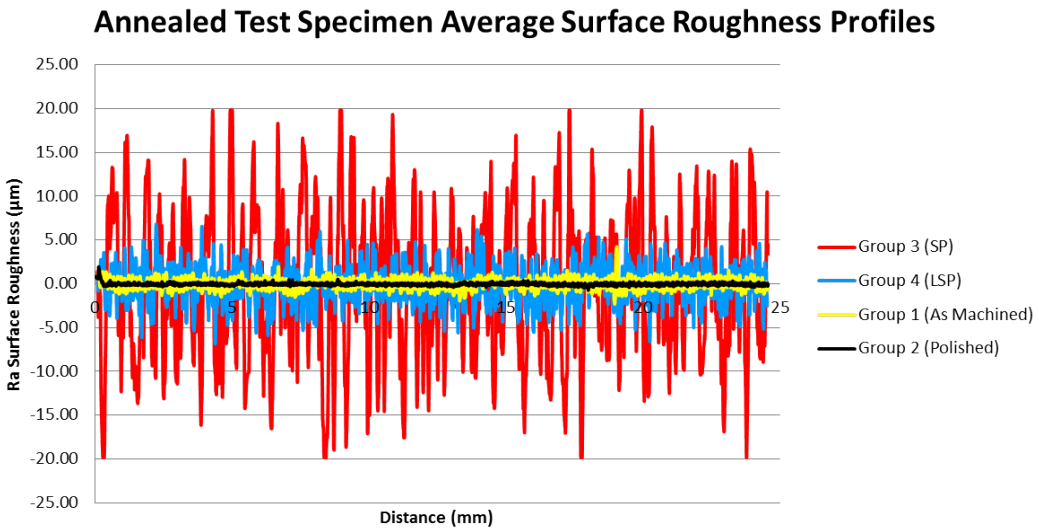

Figure 5.2: Surface Roughness Profiles of Annealed Test Specimens

Furthermore, it was found that the surface roughness induced by both the shot peened and the laser shock peened AA7075-T6 could be reduced through a polishing procedure, enabling comparison with the un-peened/polished specimens (Group 3). This reduction in surface roughness led to an increase in the mean fatigue life of the shot peened AA7075-T6 specimens from 95806 cycles to 141656 cycles. There was an increase in the mean fatigue life for laser shock peened AA7075-T6 specimens from 61971 cycles to 211171 cycles. Furthermore, the polishing procedure also allowed for the shot peened and laser shock peened samples to be compared to one another in terms of their fatigue lives separate from the effect of their respective surfaces roughnesses. The significant increase in the laser shock peened test specimens fatigue life after polishing, when compared to the shot peened/polished test specimens, is consistent with the magnitude of the residual stresses within the laser shock peened specimens being of a greater magnitude than the shot peened specimens.

The annealed test specimens showed no consistent increase in fatigue life as a result of the various surface treatments they received. Rather, the fatigue lives of the shot peened and laser shock peened specimens decreased when compared to the baseline polished test specimens (Group 3). This decrease in fatigue life can be attributed to the peening induced surface roughnesses of the specimens. The shot peened and annealed specimens average fatigue life was 16276 cycles and the laser shock peened and annealed specimens average fatigue life was 27531 cycles. These values

are less than the average polished and annealed test specimen fatigue life of 33307 cycles, with the shot peened specimen average fatigue life significantly lower due to the extremely rough surface.

For the specimens polishing after their respective peening treatments, the amount of material needed to be removed also varied between the samples. The T6 shot peened test specimen's required an average diameter reduction of 0.09 mm the annealed test specimen's required an average diameter reduction of 0.15 mm in order to obtain a polished surface finish. The T6 laser shock test specimen's required an average diameter reduction of 0.05 mm the annealed test specimen's required an average diameter reduction of 0.05 mm in order to obtain a polished surface finish. The shot peened surfaces were highly damaged, with a large reduction in specimens diameter needed in order to remove the peening induced roughness.

In service, polishing to this extent may not always be possible as a reduction in component size would typically lead to an increase in the stress experienced by the component (if the component is under load in service), leading to potential increased failure rates or even the possibility of component yielding.

5.3 Fatigue Performance

Shot peening and laser shock peening surface treatment processes were applied to the test specimens in both the T6 and fully annealed condition with the aim of improving the fatigue lives of the test specimens. These processes aim to both delay crack initiation as well as retard crack propagation. The results of the fatigue testing can be seen in Figures 5.3 and 5.4.

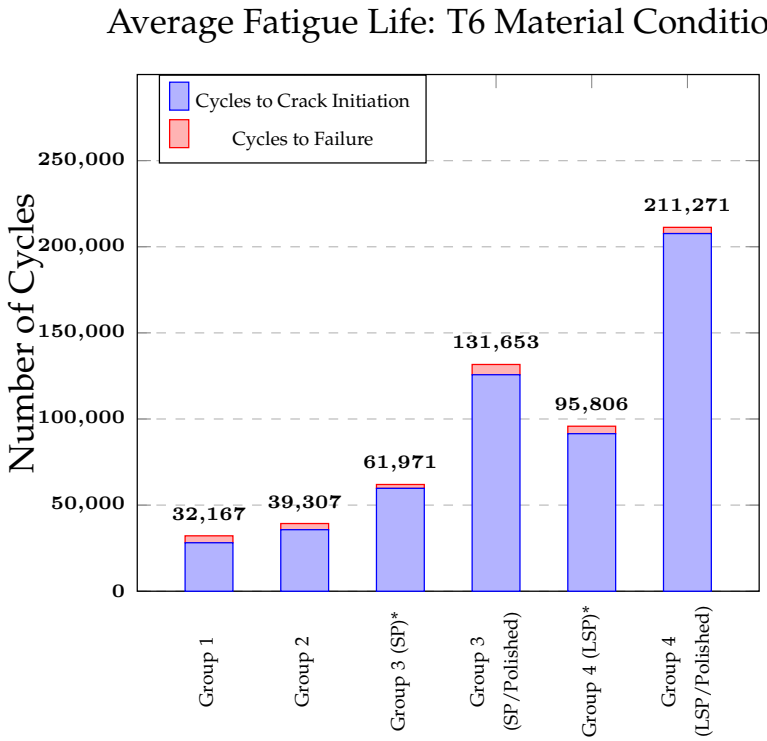

** Note: SP - Shot Peened; LSP - Laser Shock Peened*

Figure 5.3: Average Fatigue Life: T6 Material Condition

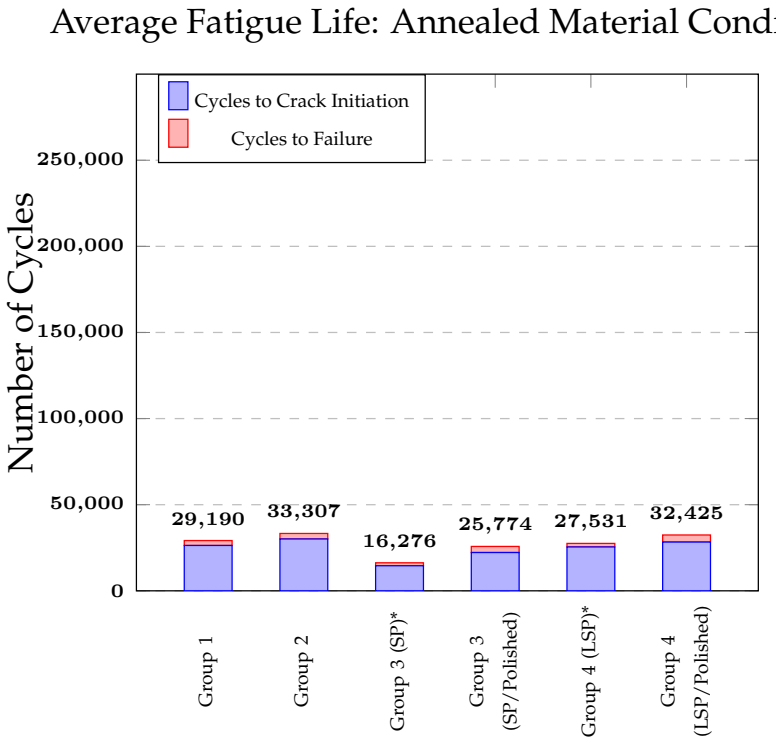

** Note: SP - Shot Peened; LSP - Laser Shock Peened*

Figure 5.4: Average Fatigue Life: Annealed Material Condition

The bending stresses used to fatigue the AA7075-T6 and AA7075-O specimens, as determined through a trial and error process, were marginally higher than the yield stresses of the respective materials found during the preliminary investigation (AA7075-T6: 566 MPa and AA7075-O: 127 Mpa). Typically, it is thought that the yield strength of a material in bending is slightly larger than the tensile yield strength of the same material[113]. The mechanical properties of an extruded material (i.e. round aluminium bars) depend on the orientation of the tested specimens in relation to the flow patterns (i.e. grain orientation) developed during specimen extrusion. Materials are generally more ductile in a direction parallel to their grain orientation as stresses can generally 'flow' through the grains structure without obstruction. Bending stresses are applied perpendicular to the grain direction and thus can experience resistance when trying to 'flow' between grains. Additional factors which may have contributed to the relatively high bending stress needed to fatigue the specimens include; load cell calibration errors (i.e. the load output of the ESH machine was lower than the displayed value) and pre-existing residual stresses (nominally 50 MPa in both the axial and radial directions) in the case of the AA7075-T6 test specimens which may have counteracted the applied bending load.

There is a risk that the use of cyclic stresses above the yield strength of a material will cause plasticisation, inducing a redistribution of any induced compressive residual stresses (as was the case with the annealed test specimens). However, the fatigue results of the AA7075-T6 specimens suggests that this did not occur, as there were significant differences in the fatigue life of test specimens having received different surface treatments with none of the specimens tests having undergone visible plastic deformation (i.e. tests specimens which were laser shock peened and polished had a far greater fatigue life that test specimens which were simply polished. This suggests that peening induced residual stresses counteracted the applied bending load within the laser shock peened specimens and were not removed by the high bending loads).

The AA7075-T6 shot peened test specimens used in this study (Group three) had a $\times\mathbf{1.6}$ increase in their mean fatigue life when compared to the baseline polished test specimens in the same material condition (Group two). The shot peened samples which were polished after their peening procedures, had a $\times\mathbf{3.4}$ increase in their mean fatigue life when compared to the baseline polished test specimens in the same material condition. This result highlights the role that surface roughness plays in component fatigue life.

Furthermore, the increase in the average fatigue life of the polished test specimens shows that the depth of the residual compressive stresses induced by the shot peening process was also deep enough to allow for surfaces layers to be removed without any detrimental effect to the overall

average fatigue life of the components.

The AA7075-T6 laser shock peened test specimens used in this study (Group four) had a $\times\mathbf{2.4}$ increase in their mean fatigue life when compared to polished test specimens in the same material condition. Laser shock peened samples which were polished in order to reduce their surface roughness (Group four), had a $\times\mathbf{5.4}$ increase in their mean fatigue life when compared to polished test specimens in the same material condition.

This again shows the significant increase in fatigue life of the polished/laser shock peened test specimens when compared to the polished/shot peened test specimens, is consistent with the magnitudes of the residual stresses induced by the laser shock peening process being greater than those of the shot peening process. These higher compressive residual stresses, when combined with the applied tensile bending stress, result in an applied stress which is smaller in magnitude in the laser shock peened specimens, leading to an increase in fatigue life.

The AA7075-O specimens used in this study had a relatively uniform fatigue life, regardless of their surface condition (i.e. polished, shot peened or laser shock peened). This uniformity in mean fatigue life between the peened and un-peened test specimens is attributed to the relaxation of the peening induced compressive residual stresses. The increased ductility of these annealed specimens led to a significant degree of specimen bending during their cyclic fatigue testing. Upon the application of the bending stress to the annealed test specimens, the specimens yielded and deformed into "U" shaped specimens, seen in Figure 5.5, leading to a redistribution of the stresses and strains within the test sample, effectively removing the peening induced compressive residual stresses and allowing for the fatigue lives of the test specimens to be determined by their surface roughnesses.

Figure 5.5: "U-Bend" Annealed Test Specimen

5.4 Fatigue Life Recovery Process

The ability of the laser shock peening process to recover fatigue life in damaged components was investigated. This investigation looked at whether the laser shock peening process could be used on partially fatigued components at the point of crack initiation in an attempt to further improve the fatigue life of the component.

It was decided to use test specimens in the T6 material condition only as both the shot peened and laser shock peened test specimens in this condition showed a significant increase in fatigue life when compared to the un-peened and polished test specimens. The annealed test specimens proved to be too ductile during the fatiguing process leading to the stress relaxation of the beneficial residual stresses induced into the test specimens by the two peening processes.

The test specimens undergoing the fatigue life recovery procedure were initially polished in order to reduce their surface roughness. This removed any surface irregularities, which in turn may have acted as stress concentration sites and also made the surfaces of the specimens comparable to other polished test specimens in this study. The polishing procedure also made it easier to identify the point of crack initiation on the surface of the test specimens.

The initial CT scans performed on the test specimens indicated that there were no significant defects (defects with a size of 0.20 mm or larger could be detected) within the test samples which may have affected their fatigue lives.

In order to track the effect of the laser shock peening process on the partially fatigued test specimens, it was decided to fatigue the specimens to the point of a visible crack. This allowed for cracks generated within the samples to be mapped using a CT scanning process. It was theorised that as long as the crack could be contained within the depth of the compressive residual stresses provided by the peening process, then the effect of the compressive residual stress induced into the specimen would have an effect on the crack [75]. This method relied on continually observing the surface of the test specimens during their cyclic bend testing and stopping the test once a crack could be observed.

Once the test specimens had been fatigued to the point of observable crack initiation, they were sent to be re-CT scanned. In order to give the CT scanning the best possible chance of mapping cracks, the size of the scanned area was reduced. As the initiation of cracks on the test specimen surfaces were viewed, it was known where the cracks had developed within the test specimens. These crack sites were marked off using a pen when the 3-point bend fatiguing process was stopped. This allowed for the CT scanning to be concentrated around the cracked areas of the test

specimens. By doing so the scanning resolution was reduced from 0.20 mm (pre-fatigue CT scans) to 0.127 mm. This reduction in scanning resolution did however increase the overall average scan time from 27 min to 67 min.

The crack specimens were also scanned in a bending rig which aimed to replicate the 3-point bend test, as a much lower bending force, in an attempt to open up the crack front. There was a possibility that even though cracks had formed within the test specimens, the width between opposing crack faces would be smaller than the detectable resolution of the CT scanning process. A schematic image of this crack width is shown in Figure 5.6.

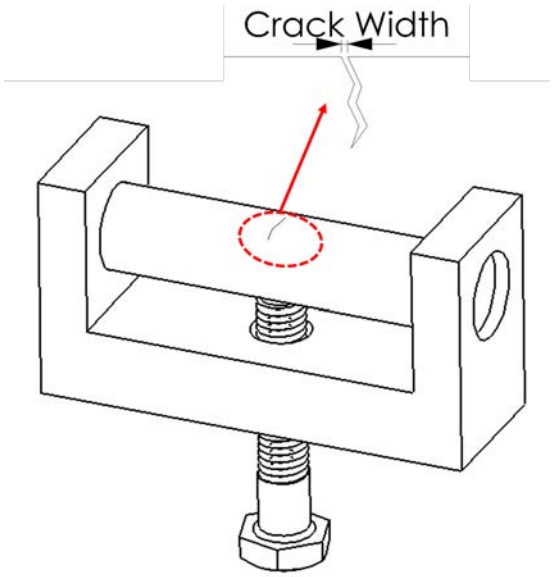

Figure 5.6: Crack Width

The crack depths which were mapped were less than 0.5 mm in length, apart from the crack depth of test specimen 1 which was 2.06 mm in length. However, there is the possibility that the cracks that were mapped extended further into the test specimens then was observable. If the crack width at the crack tip narrowed to a size smaller than 0.127 mm then it would not be detected by the CT scanning process. An example of one of the mapped cracks is shown in Figure 5.7, where the depth of the fatigue crack could be measured with a high degree of accuracy.

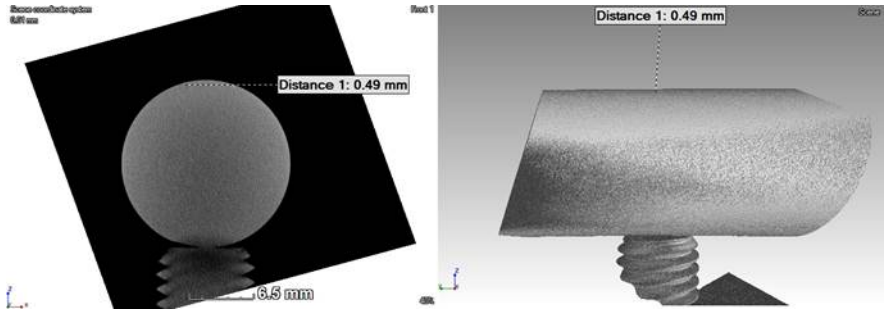

Figure 5.7: Apparent Crack Closure Within the Re-Laser Shock Peened Specimens

The average test specimens fatigue lives to the point of crack initiation compare well to the results obtained during the general fatigue testing of the laser shock peened/polished test specimens from test Group 4. However, test specimen 1 was an anomaly, taking 794591 cycles for crack initiation to be observed when compared to a mean of 212329 for the remaining test specimens (i.e.excluding test specimen 1). Fatigue, by its nature, generally produces varying results for tests performed under the same conditions. That is why analysis of the data is best done using a statistical approach. If the fatigue lives of the test specimens were analysed and plotted using a S-N log graph, the logarithmic values of the varying cycles counts would differ fractionally from one another. The logarithmic nature of S-N curves allows for outliers in data trends to be "normalised" and made statistically relevant.

After the re-laser shock peening of the fatigue life recovery test specimens, test specimens one, two and five were re-CT scanned. In order to determine the effect of the re-laser shock peening process on fatigued specimens. From the generated CT images, a crack could only be found in test specimen 1. However, the length of this crack was reduced from its original length of 2.03 mm before the laser shock peening process to 1.82 mm. Crack closure was attributed to the plastic flow of the material in a thin layer adjacent to the crack surfaces. This flow of material of plastic deformation smeared over the crack sections (i.e. filled up the crack sections), giving them the appearance of having closed up on the CT scan images.

Prior to their final fatiguing, the test specimens were re-polished. This polishing procedure once again removed the laser shock peened induced surface roughness of the test specimens and made the specimens comparable to the other polished test specimens used in the study.

After the final fatiguing process it was found that a limited amount of pristine fatigue life had been recovered in the test specimens. This was shown by comparing the cycle count to failure of the Group 5 specimens to the observed cycle count to failure after crack initiation of the specimens from Group 4.

The laser shock peening process did little to recover the fatigue life in the partially fatigued test specimens. The laser peening process of the partially fatigued test specimens added an average of 13232 cycles to the test specimens after the crack initiation was first detected during the partial fatiguing process. This compares to the T6/polished/laser shock peened/polished test specimens from Group 4, which averaged 3610 cycles after crack initiation. Test specimen 1 which contained the largest crack prior to the re-laser shock peening treatment failed significantly earlier than the other test specimens in Group 5, failing after 3186 cycles. This is comparable to the test specimens from Group 4, which averaged 3610 cycles after crack initiation and indicates that in order for the laser shock peening treatment to have an effect, crack length must be minimised. The laser shock peening of open defects (i.e. holes) can interfere with shock wave propagation into a material, with a resulting backlash effect inducing residual tensile stresses at the crack tip It is possible that a tensile residual stress was introduced to the crack tip of Test specimen 1 from Group 5, resulting in its comparatively early failure to other specimens from the same group.

The mechanism attributed to the slight life extension seen in test specimens 2 to 5 was plasticity-induced crack closure. If crack tip is directly laser shock peened, a residual compressive stress field can be induced in the material surrounding crack tip. Compressive stresses of varying magnitudes (dependant of shockwave interaction at the crack tip) were induced at the crack tip caused the crack faces to close up. These faces did not separate until the applied load was sufficiently large to overcome the compressive residual stresses at the crack tip (i.e. during cyclic fatigue testing, residual plastic deformation is built up in the wake of an advancing fatigue crack. This plastic deformation induces a compressive stress, the magnitude of which can be increased by the laser shock peening processes, causing the crack faces to close prior to the minimum load being reached. Upon reapplication of the applied external load the crack faces do not separate at the minimum load but at a greater load termed the opening stress level).

The results from this study suggest that partially fatigued components need to be re-peened before the onset of crack initiation. In order to do this, a series of crack propagation curves should be created which would allow for the potential cycle count range in which crack initiation occurs to be determined with confidence, as shown in Figure 5.8. By laser shock peening a partially fatigued component before the region of potential crack initiation, dislocation slip band damage within the components could be eradicated, potentially extending the life of the component.

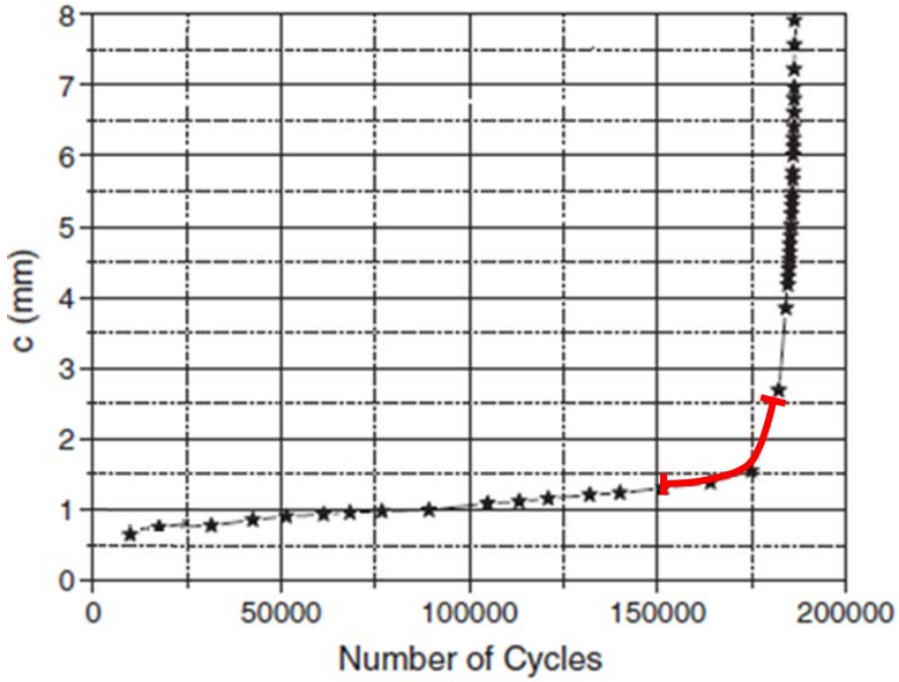

Figure 5.8: Crack Propagation Curve Illustrating Region of Potential Crack Initiation

5.5 Metallographic Examination

5.5.1 Fractography

Optical Fractography

i) Test Specimens in the T6 Material Condition

The T6 material fracture surfaces seen in Figure 5.9, contains three regions that can be associated with crack initiation, crack growth and final overload. Inspection of these fracture surfaces revealed some distinctive macroscopic features are indicative of a mixed mode of fracture (i.e. both brittle and ductile features are present) and of uni-axial cyclic bending fatigue.

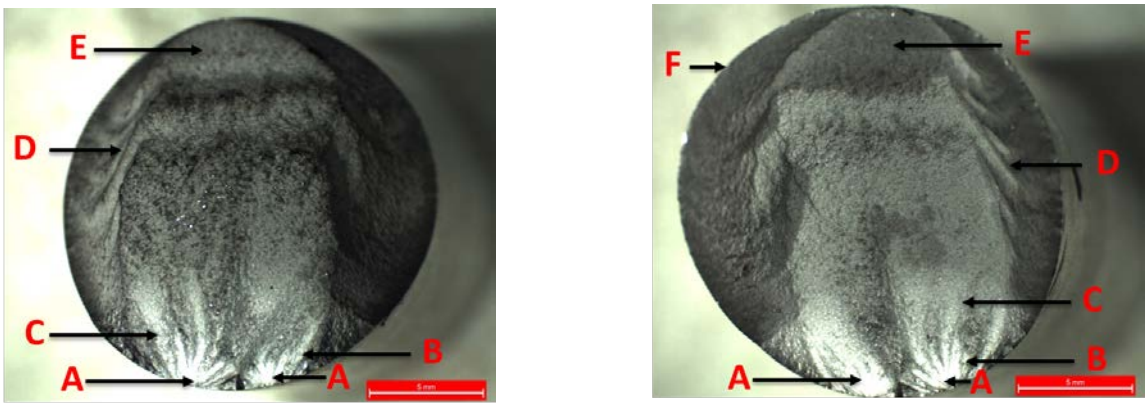

(a) (b)

Figure 5.9: Fractograph of T6 Test Specimen

Table 5.2: T6 Fracture Surface Labelling Key

Label	Surface Feature
A	Crack Initiation Site
B	Ratchet Marks
C	Crack Growth Region
D	Chevron Marks
E	Final Fracture Zone
F	Shear Lips
G	Compression Curl (Cantilever Curl)

An initial inspection of the various fracture surfaces revealed multiple crack initiation sites [A]. Multiple crack initiation sites show that a relatively high bending stress was used for crack initiation. Further inspection of the fracture surfaces reveals ratchet markings [B], radial to the circumferences of the test specimens. Ratchet markings represent the intersection and joining of multiple fatigue cracks into a common crack front in each test specimen and are indicative of multiple cracks joining up to form a uniform crack front under cyclic loading.

The shiny regions [C], which are clearly visible, indicate crack growth regions, extending outwards in a convex manner from the point of crack initiation. These thumbnail-shaped regions indicate the length to which the fatigue cracks grew during their respective crack propagation periods before the onset of fast fracture.

Chevron like marks [D] appear as semi-elliptical concentric rings (almost "V" shaped) along the outer perimeter of the test specimen fracture surfaces and point towards crack initiation sites on the respective surfaces.

The relatively large final fracture regions [E], which can be differentiated from the crack initiation and propagation regions by an increase in the fracture surface roughness, suggest the application of a high nominal stress to the test specimens (i.e. the final fracture region excludes the thumbnail-shaped crack propagation region and the crack initiation site).

Crack propagation through the test specimens results in a decrease in the cross-sectional area of each test specimen, leading to an increase in the applied stress experienced by each specimen. This increase in applied stress deflects the crack path, from the perpendicular plane (where crack propagation is under a plane strain condition), to a plane inclined to the load direction (where crack propagation is under a plane stress condition), forming a compression/cantilever curl [G] type feature. This type of curved fracture path is typical for materials of a high toughness and illustrated in Figure 5.10.

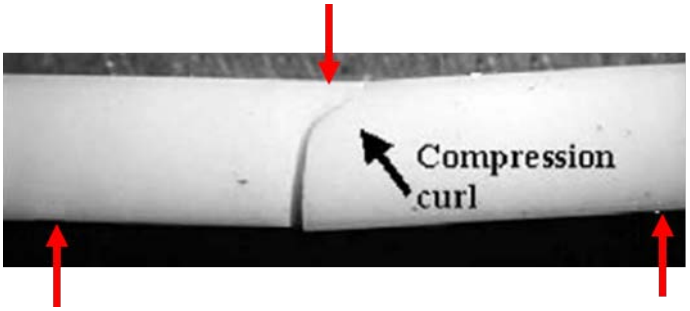

Figure 5.10: Compression Curl [114]

Shear lips [F] are formed during the final stage of specimen failure and extend after the crack propagation regions (i.e. the edge where the two curved sides of the thumbnail-like region meet), as a result of the specimen overloading. Shear lips are indicative of a shear-dominated final overload, as well as a level of ductility within the test specimens.

Signs of fretting fatigue [H] were observed around the crack initiation and propagation regions on the fracture surfaces of the test specimens from Group 5. Fretting is indicated by the black powder found on opposing fracture surfaces and is indicative of damage induced under load in the presence of repeated relative, but small amplitude, surface motion. The crack generated in the test specimens during the partial fatiguing process were "filled/smeared" with a thin layer of material, which was plastically deformed during the laser shock peening process, which increases the friction between the opposing crack surfaces, so leading to the fretting fatigue. Fretting is further evidence that the cracks did not "heal" and only close up upon application of the laser shock peening process.

ii) Test Specimens in the Annealed Material Condition

Inspection of the annealed fracture surfaces reveals some distinctive macroscopic features which are indicative of a typically ductile mode of fracture, as seen in Figure I.6

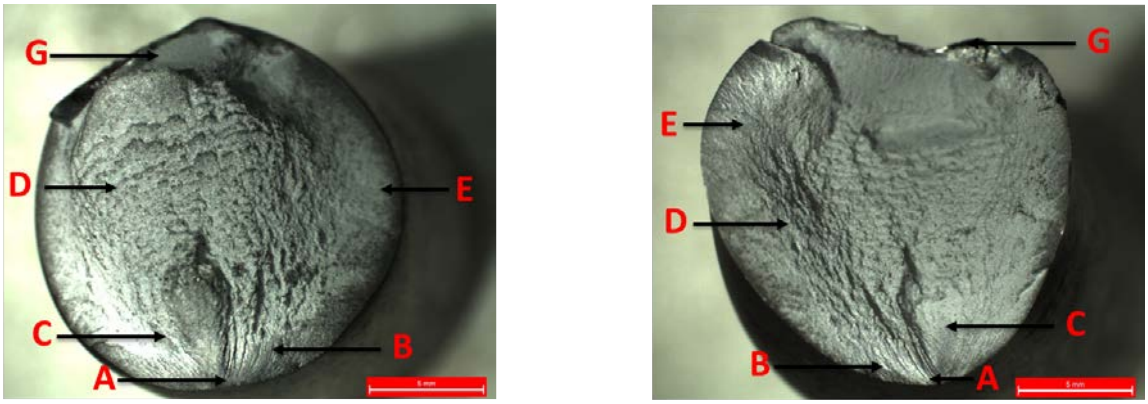

(a) **(b)**

Figure 5.11: Fractograph of Annealed Test Specimen

Table 5.3: Annealed Fracture Surface Labelling Key

Label	Surface Feature
A	Crack Initiation Site
B	Ratchet Marks
C	Crack Growth Region
D	Rough/Dimpled Surface
E	Smooth Radial Zone
F	Shear Lips
G	Post Fracture Damage

An initial visual analysis of the various fracture surfaces reveals multiple crack initiation sites [A]. Further inspection of the fracture surfaces reveals thin ratchet markings [B] within the matte (dull) region of the fracture surfaces, radial to the circumferences of the test specimens.

The matte regions [C], indicate crack growth regions which extend outwards in a convex manner from the point of crack initiation. These crack growth regions are thumbnail in shape and are found on corresponding fracture surfaces for all the test specimens. The matte (i.e. dull) nature of the regions can be associated with both cyclic loading and ductile overload during fracture.

After the crack initiation and propagation regions, a large region of increased surface roughness [D] is found on the annealed fracture surfaces. This roughness within these regions increases in the direction of crack propagation.

The rough internal fracture surfaces of the fractured test specimens are surrounded by a relatively smooth radial zone [E] (i.e. a smooth zone extends around the circumference of the test specimen fracture surfaces from the crack initiation site). This smooth radial zone surrounding a rough internal region is typical of a tensile "cup-and-cone" failure. Shear lips [F]were also observed along the entire circumference of the test specimens, and are indicative of the ductility present within the test specimens. The stress applied by the bending fixture visibly bent the specimens into a "U" shape about their middle during the cyclic fatiguing process. This resulted in the test specimen failing in a tensile manner where each test specimens was "pulled" apart about its middle. Failure resulted in a "cup-and-cone" like fracture surface.

Opposite the crack initiation sites on the fracture surfaces, post failure surface damage [G], caused by the final fracturing of the annealed test specimens, can be seen. As the tests specimens were highly ductile in the annealed state, they did not fracture into two separate halves on the bend test stand, due to the limits of the ESH machine being tripped. In order to reveal the fracture surfaces of the annealed test specimens, the test specimens had to be manually fractured, resulting in the post failure damage visible on the fractured surfaces.

SEM Fractography

The SEM fractograhs of various test specimens in the T6 condition from tests Groups 1 to 5 generally showed similar features (chapter 4, Section 1.5). The SEM fractographs of the specimens from Groups 1 to 4 show cracks [A] that initiated from multiple points along the circumference of the test specimens. This is indicative of the specimens experiencing a high stress level during fatigue loading.

The test specimen from Group 5 shows crack initiation at a distance of 0.23 mm away from the surface. This test specimen was polished prior to fatiguing and thus the majority of stress concentrations sites on the surface were removed. The applied bending stress combines with the peening induced residual stress, creating a resultant stress profile, where the highest stress on the profile is just below the surface hardened layer as shown in Figure 5.12. It is at this point where crack initiation occurs and is apparent in Figure 4.17 found in Chapter 4.

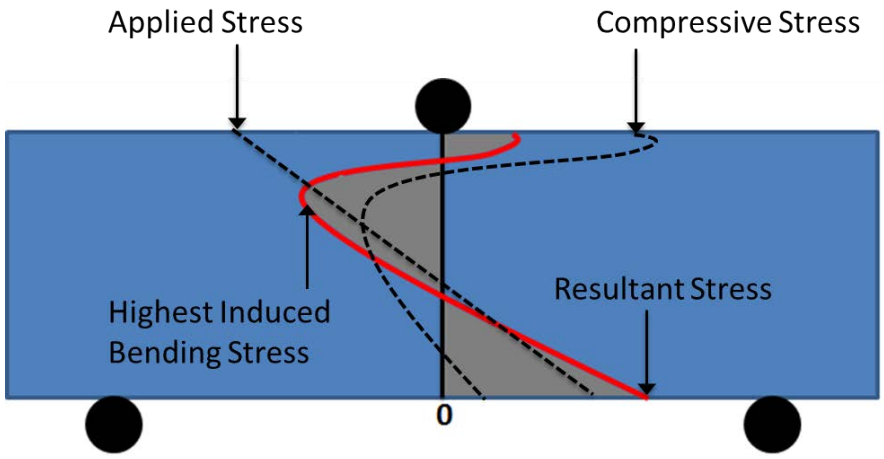

Figure 5.12: Resultant Stress Profile

5.5.2 Nomarski Lens Light Microscopy

Sections were taken from test specimens (in both the T6 and annealed material conditions) in test Groups 2, 3, 4 and 5. The sections were taken parallel to the extrusion direction of the aluminium in order to observe the microstructure of the AA7075 near the surfaces of the tests specimens and identify what influence the mechanical surface treatments had on the microstructure of the alloy.

i) Test Specimens in the T6 Material Condition

From the micrographs for the polished test specimen from test Group 2, elongated grains can be seen the extrusion direction, running parallel to the specimen surface. The surface of the polished test specimen is also relatively flat and smooth in the micrograph.

The micrographs of the shot peened specimen show the effect of shot peening on the surface of the specimens, creating a highly deformed and rough surface. This induced roughness is characteristic of the damage caused by the hard peening media used during the process. Elongated grains in the extrusion direction can also be seen in the micrograph. These grains are more compressed near the surface of the test specimen, characteristic of the deformation induced by the shot peening process.

The micrographs of the laser shock peened and fatigue life healed test specimens show some similarities. The laser shock peened specimen surface is slightly rougher as a result of the peening process, which uses a laser to vaporise a small section of the surface. This induced roughness is visibly less than the shot peened sample. The peening induced surface roughness in the fatigue life healed sample has been polished away (as part of the fatigue life recovery experimental procedure). Elongated grains in the extrusion direction can also be seen in both sets of micrographs, with the grains not appearing to be compressed near the surface of each test specimen. This is

consistent with the fact that laser shock peening strengthens AA7075-T6 through introducing compressive residual stresses into the surface layers of the test specimens rather that by increasing the hardness of the surface layers of the treated test specimens [115].

ii) Test Specimens in the Annealed Material Condition

The annealed micrographs revealed a similar bulk microstructure to one another. Variations between the annealed micrographs are seen at the specimens surface. The polished test specimen shows a flat and even surface. The shot peened test specimens has an extremely rough and damaged surface due to the increased ductility of the test specimens. The laser shock peened surface also shows peening induced damage, albeit to a lesser degree than that of the shot peened test specimen.

5.5.3 Microhardness Testing

The microhardness distributions of AA7075 (in both the T6 and fully annealed material conditions) were incrementally measured as a function of depth from the surfaces of the test specimens before and after the various surface treatment procedures utilised in this study.

A comparison of the shot peened AA7075-T6 and the unpeened AA7075-T6 microhardness profiles, show that shot peened samples have a distinct work hardened region. The shot peened sample also shows a rapid decrease in hardness within 340 microns into the sample. The maximum hardness induced by the shot peening process was nominally 192 HV and was observed just below the surface. This hardness value decreased over the next 340 microns to a value of nominally 168 HV. The repeated dimpling at the surface by the shot peening process, in order to achieve a uniform surface coverage, resulted in the highest cold worked layer/dislocation density at the surface and is consistent with the slight grain deformation seen in the micrograph of the T6/Shot peened specimen.

The shot peened AA7075 in the annealed test specimen showed that the shot peened samples had a distinct work hardened region which extend further below the surfaces of the shot peened specimens in the T6 material condition. The shot peened sample also shows a more gradual decrease in hardness within 420 microns into the sample. The maximum hardness induced by the shot peening process was 97 HV and was observed just below the surface. This hardness value decreased over the next 420 microns to a value of nominally 63 HV. This was an overall increase in the surface hardness from the average baseline material (64 HV) by 33.61 %. This large increase in the hardness of the material can be attributed to the increased ductility of the AA7075 in the annealed

condition. This increased ductility leads to an increase in the dislocation density at the surface of the test specimens.

The laser shock peened AA7075 in the T6 used in this study showed no appreciable increase in hardness within the laser affected zone when compared to un-peened test specimens of the same material condition. For the test specimens which underwent the laser shock peening process from test Group 4, a small change in hardness can be seen between the incremental depths of 0.58 mm and 0.64 mm, suggesting that the penetration depth of the laser shock peening process is within this region. The change in hardness is however small enough to be attributed to experimental errors relating to the reading of the harness values. Similar observations were found by Clauer *et al.* [115], who observed no increase in surface hardness for laser shock peened AA2024-T851 and AA7075-T73. It was hypothesised by Clauer *et al.* [115] that the precipitation hardening in the T6 condition is significantly large enough to mask any shock wave strain hardening. The longer pressure duration of the shot peening process results in greater plastic deformation which leads to higher dislocation generation and motion for the aluminium in the T6 condition.

The laser shock peened AA7075 in the annealed material condition used in this study showed a slight increase in hardness within the laser affected zone when compared to un-peened test specimens of the same material condition. The hardness value decreased from a value nominally 80 HV just below the surface of the specimen to a value of 63 HV of over 1140 microns. The change in hardness from the laser affected region to the unaffected region is more significant in the annealed material than the T6 aged material. This is because the two material conditions exhibit different strain hardening behaviours. The annealed material strain hardens more quickly than the T6 material as evidenced by their strain hardening coefficients (annealed - 0.37; T6 - 0.20), found during the tensile testing of the materials. If equivalent plastic strains are applied to both material conditions, the flow stress within the annealed material condition will be greater that the flow stress within the T6 material condition, thus resulting in an increase in plastic deformation.

The fatigue life healed AA7075 (effectively a double laser shock peening treatment) used in this study showed a distinct work hardened region. The fatigue life healed sample also showed a gradual decrease in hardness within 720 microns into the sample. The maximum hardness induced by the shot peening process was nominally 191 HV and was observed just below the surface (a small amount of the surface layer had to be polished away in order to facilitate the indentation process). This hardness value gradually decreased over the next 720 microns to a value of 168.0 HV. This was an overall increase in the in the surface hardness from the average baseline material (168.0 HV) by 12.23 %. The hardness of some metals does not respond to a single laser shot at

the peak pressures achievable by the laser. In this case, multiple shots can produce a progressive increase in hardness [116].

Chapter 6

Conclusions and Recommendations

6.1 Conclusions

The following conclusions are made based on the research presented.

1. Fatigue results of the AA7075-T6 test specimens show that the laser shock peened samples had the greatest overall improvement in fatigue life when compared to the baseline polished test specimens (x 2.4 life improvement). The shot peened samples also showed an increase in fatigue life when compared to the polished specimens (x 1.6 life improvement). It was found that main difference between the two mechanical surface treatment processes was their effect on surface roughening.

2. Peening induced surface roughness could be effectively polished away without compromising the induced residual compressive stresses. This polishing lead to a further increase in the fatigue life of the specimens when compared to the fatigued shot peened and laser shock peened specimens in the unpolished condition.

3. Test specimens that were polished after their respective shot peening procedures had an average increase in fatigue life of x 3.4. Test specimens in the T6 condition that were polished after the laser shock peening treatments had an average increase in fatigue life of x 5.4. This suggests that the magnitude of the residual stresses induced by the laser shock peening procedure are greater than those induced by the shot peening procedure.

4. The AA7075-O test specimens (annealed) showed no overall improvement in their fatigue life, regardless of the mechanical treatment received. The increased ductility of the specimens during the 3-point bending fatigue process led to a degree of stress relaxation, relieving of the peening induced compressive stresses within the surface layers of the specimens.

5. The cross-sectional microstructures of the peened samples in each material condition showed varied changes in the microstructure of the treated aluminium alloy. There was evidence of a large degree of plastic deformation near the surface of shot peened specimens in both material conditions. However, there was limited evidence of changes to the grains structure of the laser shock peened specimens in both material conditions.

6. The T6 material showed no appreciable increase in hardness as a result of the laser shock peening process. This suggests that the laser shock peen induced fatigue life strengthening of AA7075-T6 is as a result of induced residual compressive stresses and not the hardening of the surface layers of the AA7075. The annealed material showed a slight increase in hardness within the laser affected zone when compared to un-peened test specimens of the same material condition. This was attributed to the strain hardening rate of the material which allows for greater plastic deforming causing flow stress when compared to the T6 material.

7. Evidence of deformation of the surface layers of the shot peened samples (in both material conditions) was supported by hardness depth profiles for the shot peened treated samples. There was a distinct hardened region for the shot peened material when compared to the laser shock peened material. The longer pressure duration of the shot peening process appears to result in greater plastic deformation, leading to higher dislocation generation and motion which culminates in a hardened surface layer.

8. The laser shock peening of the small cracks initiated during the fatigue life extension process did little to effectively restore and extend fatigue life in the partially fatigued test specimens. A degree of life extension was present as cracks re-initiated after a few thousand cycles. This was attributed to crack tip closure. This closure led to a general reduction in the fatigue crack growth rate when compared to laser shock peened/polished test specimens fatigued at the same stress. The potential of "healing" fatigue cracks through laser shock peening is worth pursuing and needs to be undertaken at some point before the onset of crack initiation in order to ensure that any fatigue induced slip band dislocation damage can be effectively treated.

6.2 Recommendations for Future Work

In this Section recommendations are proposed for future work.

1. Residual stress relaxation in mechanically surface treated AA7075-T6 should be studied. Incremental residual stress measurements should be made in order to determine the effectiveness of peening procedures with increase cycle count.

2. The fatigue life healing process should be repeated, with partially fatigued test specimens laser shocked peened just before the onset of crack initiation. This would require that crack propagation curves (vs. number of cycles) be developed for the specimen material allowing for a region in which potential crack initiation occurs to be determined with a degree of confidence. By laser shock peening a component before this region of potential crack initiation, dislocation slip band damage within the components could potentially be eradicated, so extending the life of the component.

3. For 3-point bend test studies in general, it is recommended that longer test specimens with a diameter of between 10 and 12 mm be used. This will aid with specimen placement on the bending rig, specimen polishing and help reduce the time need for any required mechanical surface treatments. Stresses placed on the ESH fatiguing machine and bending stands are also significantly reduced. Furthermore, it is recommended that the calibration of the ESH load cell be checked.

4. An a.c. potential drop method should be developed to help detect crack initiation. This would further help investigations into the fatigue life recovery process and help narrow down the window where peening is re-introduced and effective life recovery can occur.

5. The effectiveness of combination peening should be studied. This entails that components be laser shock peened first and then shot peened. This could potentially create a high level of fatigue life improvement, especially if followed by polishing to a controlled surface roughness (i.e. 0.20 μm Ra).

6. Various peening parameters for AA7075 should also be looked at. It was shown in this study that laser shock peening an AA7075-T6 sample twice increase the depth of the induced plastically deformed region. This would suggest that laser shock peening a component multiple times would be more effective that simply laser shock peening it once.

References

[1] C.S. Montross et al. "Laser Shock Processing and its Effects on Microstructure and Properties of Metal Alloys". In: *International Journal of Fatigue* 24.10 (2002), pp. 1021–1036.

[2] T. Holmes. "Effect of Shot Peening and Residual Stress on the Fatigue Life of Sintered Titanium Alloy Ti-6Al-4V". Thesis. Cape Town: University of Cape Town, 2013.

[3] Lambda Technologies. *Laser Shock Peening*. Ed. by Unknown. 2012. URL: http://www.lambdatechs.com/laser-shock-peening.html.

[4] P. K. Sharp et al. "Fatigue Life Recovery in Aluminium Alloy Aircraft Structure". In: *Fatigue and Fracture of Engineering Materials and Structures* 25.2 (2002), pp. 99–110.

[5] S. Spanrad. "Fatigue Crack Growth in Laser Shock Peened Aerofoils Subjected to Foreign Object Damage". Thesis. Portsmouth: University of Portsmouth, 2011. URL: Accessedfrom: http://eprints.port.ac.uk/3365/.

[6] D. Broek. "Elementry Engineering Fracture Mechanics 4th Edition". In: Oxford: Martinus Nijhoff Publishers, 1986. Chap. 4, pp. 109–112.

[7] ASM International. "Elements of Metallurgy and Engineering Alloys". In: *ASM International*. Ed. by F. Campbell. ASM International, 2008, p. 243.

[8] W. Bradley. "Failure Investigation: Principles and Practice". In: *Fracture and Fracture Mechanics: Case Studies*. Ed. by R. Tait and G.Garrett. Oxford: Pergman Press, 1985, p. 3.

[9] W. Cui. "A State-of-the-art Review on Fatigue Life Prediction Method for Metal Structures". In: *Journal of Marine Science and technology* 7.1 (2002), p. 44.

[10] E. Hearn. "Mechanics of Materials 2". In: 3rd. Oxford: Betterworth Heinemann, 1997. Chap. 11, pp. 443–508.

[11] R. Tait. "Material Selection in the Mining Industry - Material Selection in the Mining Industry". In: *SAIMM Physical Metallurgy School*. Mintek, 1987.

[12] R.C. Juvinall and K.M Marshek. "Fundamentals of Machine Component Design". In: India: John Wiley and Sons, 2006. Chap. Fracture Mechanics - Basic Concepts, p. 231.

[13] Harshal Patel. *Introduction to Fracture Mechanics*. Ed. by Unknown. 2002. URL: https://www.slideshare.net/HarshalPatil7/introduction-to-fracture-mechanics.

[14] ASM International. "Elements of Metallurgy and Engineering Alloys". In: *ASM International*. Ed. by F. Campbell. ASM International, 2008, pp. 248–249.

[15] H. Tada, P.C. Paris, and G.R. Irwin. *The Stress Analysis of Cracks Handbook*. Hellertown, Pennsylvania: Del Research Corporation, 1973, pp. 2.1–2.36.

[16] ASM International. "Elements of Metallurgy and Engineering Alloys". In: *ASM International*. Ed. by F. Campbell. ASM International, 2008, pp. 252–254.

[17] ASM International. "ASTM E647-95a". In: *Standard Test Method for Measurement of Fatigue Crack Growth Rates*. 1995, pp. 557–593.

[18] W. Elber. "Damage Tolerance in Aircraft Structures". In: ASTM STP, 1971. Chap. The Significance of Fatigue Crack Closure, 230–242 and 486.

[19] N.A Alang, N.A. Razak, and A.K. Miskam. "Effect of Surface Roughness on Fatigue Life of Notched Carbon Steel". In: *International Journal of Engineering & Technology* 11.10 (2010), pp. 160–163.

[20] U. Krapp. "Fatigue Crack Propagation in Metals and Alloys". In: Germany: Wiley, 2007. Chap. 5, p. 102.

[21] A.D. Forest. "The Rate of Growth of Fatigue Cracks". In: *Journal of Applied Mechanics* 58 (1936), A23 A25.

[22] J. Schijve. "Fatigue of Structures and Materials". In: Netherlands: Kluwer Academic Publishers, 2001. Chap. 2, pp. 13–58.

[23] E. Hearn. "Mechanics of Materials 2". In: 3rd. Oxford: Betterworth Heinemann, 1997. Chap. 10, pp. 381–442.

[24] Niall Smith. "Effect on Fatigue Performance of Residual Stress induced via Laser Shock Peening in Mechanically Damaged 2024-T351 Aluminium Sheet". PhD thesis. Cranfield University, 2014.

[25] E. K. S. Maawad. "Residual Stress Analysis and Fatigue Behavior of Mechanically Surface Treated Titanium Alloys". MA thesis. Clausthal University of Technology, 2012.

[26] P. J. Withers and H. K. D. H. Bhadeshia. "Residual stress Part 1: Measurement techniques". In: *Materials Science and Technology* 17 (2000), p. 355.

[27] U.S. Geological Survey. *A Laboratory Manual for X-Ray Powder Diffraction*. Ed. by Unknown. 2002. URL: `http://pubs.usgs.gov/of/2001/of01-041/htmldocs/xrpd.htm`.

[28] M.E. Fitzpatrick et al. *Determination of Residual Stresses by X-ray Diffraction - Issue 2*. Ed. by None. National Physical Laboratory, 2005, 6–12 and 46.

[29] Nadeem Gamiet. "Numerical Analysis of Compressive Residual Stresses in Metallic Materials as a Result of Shot Peening". MA thesis. University of Cape Town, 2001.

[30] H & M Analytical Services Inc. *Analysis of Residual Stresses*. Ed. by Unknown. 2002. URL: http://h-and-m-analytical.com/wp/wp-content/uploads/2015/04/residual_stress.pdf.

[31] W. Cui. "A State-of-the-art Review on Fatigue Life Prediction Method for Metal Structures". In: *Journal of Marine Science and technology* 7.1 (2002), pp. 52–53.

[32] R. Ritchie. "Slow Crack Growth: Macroscopic and Microscopic Aspects". In: *Fracture and Fracture Mechanics: Case Studies*. Ed. by R. Tait and G.Garrett. Oxford: Pergman Press, 1985, pp. 115–116.

[33] J.D. Verhoeven. "Steel Metallurgy for the Non-Metallurgist". In: ASM International, 2007. Chap. 13, p. 189.

[34] ASM International. "Elements of Metallurgy and Engineering Alloys". In: *ASM International*. Ed. by F. Campbell. ASM International, 2008, pp. 385–396.

[35] J.D. Verhoeven. "Steel Metallurgy for the Non-Metallurgist". In: ASM International, 2007. Chap. 7, p. 63.

[36] T. Rajan, C.P. Sharma, and A. Sharma. "Heat Treatment: Principles and Techniques". In: New Delhi: PHI Private Learning Limited, 2011. Chap. 8, pp. 130–135.

[37] Key To Metals. *Nitriding*. Ed. by Unknown. 2003. URL: http://www.totalmateria.com/page.aspx?ID=CheckArticle&LN=EN&site=kts&NM=117.

[38] M. Yang. "Nitriding - Fundamentals, Modeling and Process Optimization". P.H.D. Worcester Polytechnic Institute, 2012, pp. 1–4.

[39] P. Juijerm and I. Altenberger. "Fatigue Performance Enhancement of Steels using Mechanical Surface Treatments". In: *Journal of Metals, Materials and Minerals* 17.1 (2007), pp. 59–65.

[40] Metal Improvement Company. *Shot Peening Applications Ninth Edition*. Ed. by Unknown. 2005, pp. 4–6.

[41] Indabrator. *Shot Peening for longer fatigue life*. Ed. by Unknown. n.d. URL: http://nesco.in/documents/SHOT%20Peening%20Equipments.pdf.

[42] J. Champagne. *Controlled Shot Peening*. Ed. by Unknown.] 1986. URL: http://www.shotpeener.com/library/pdf/1986002.pdf.

[43] R. Gillespie. *Shot Peening Media: Its Effect on Process Consistency and Resultant Improvement in Fatigue Characteristics*. Ed. by Unknown. n.d. URL: http://www.shotpeener.com/library/pdf/1993047.pdf.

[44] Metal Improvement Company. *Shot Peening Applications Ninth Edition*. Ed. by Unknown. 2005, pp. 40–42.

[45] R. Specht et al. *Process Control techniques for Laser Peening Metals*. Ed. by Unknown. n.d. URL: http://www.shotpeener.com/library/pdf/2002062.pdf.

[46] H.J. Grover. "Factors by Which Shot Peening Influences the Fatigue Strength of Parts". In: *The Shot Peener* 12.2 (1954), pp. 5–9.

[47] D. Kirk. *Residual Stresses in Shot Peened Components*. Ed. by Unknown. n.d. URL: http://www.shotpeener.com/library/pdf/2004003.pdf.

[48] K. Marsh. *Shot Peening: Techniques and Applications*. Ed. by Unknown. Glascow, 1993, pp. 278–281.

[49] J. Hoffman et al. "Thermal Relaxation of Shot Peened Residual Stress in the Differently Heat-treated Plain Carbon Steel CK45". In: *Shot Peening - Science, Technology, Application*. Ed. by H. Wohlfahrt, R. Kopp, and O. Vohringer. Oberursel, Germany: Informationsgesellschaft Verlag, Deutsche Gesellschaft fur Metallkunde, 1987, pp. 239–246.

[50] P. Peyre et al. "Laser Shock Processing of Aluminium Alloys: Application to High Cycle Fatigue". In: *Materials Science and Engineering* A210 (1996), pp. 102–113.

[51] D. Hammond and S.A. Meguid. "Crack Propagation in the Presence of Shot Peening Residual Stress". In: *Engineering Fracture Mechanics* 24.2 (1990), pp. 373–387.

[52] S. Bagheri and M. Guagliano. "Effects of Surfaces Nanocrystalllization Induced by Shot Peening on Material Properties: a Review". In: *Frattura ed Integrita Strutturale* 7.1 (2009), pp. 3–16.

[53] A.H. Clauer. "Laser Shock Peening for Fatigue Resistance". In: *Surface Performance of Titanium*. Ed. by J.K. Gregory, H.J. rack, and D. Eylon. Warrendale: TMS, 1996, pp. 271–230.

[54] J. Ramjith. "Experimental investigation into the comparison between Shot Peening and Laser Shock Peening on AA 6056-T4 Aluminium Alloy". Thesis. University of the Witwatersrand, 2014.

[55] Abdullahi K. Gujba and Mamoun Medraj. "Laser Peening Process and Its Impact on Materials Properties in Comparison with Shot Peening and Ultrasonic Impact Peening". In: *Materials* 7 (2014), pp. 7925–7974.

[56] J. Brjer. *Applications of Laser Shock Peening*. Ed. by Unknown. n.d. URL: http://stc.fs.cvut.cz/pdf14/4529.pdf.

[57] R. Marsh. "Experimental Analysis of Oil Based Cavitation Peening in Air". Thesis. Georgia: Georgia Institute of Technology, 2011. URL: http://eprints.port.ac.uk/3365/.

[58] K. Ding and L. Ye. "Laser Shock Peening". In: Cambridge: Woodhead Publishing, 2006. Chap. 2, pp. 17–34.

[59] J.E. Masse and G. Barreau. "Laser Generation of Stress Waves in Metal". In: *Surface Engineering* 33 (1995), pp. 1421–1429.

[60] J. Masse and G. Barreau. "Processing of Aluminium-coated 55C1 Steel in Water Confinement Regime, Characterization and Application to High Cycle Fatigue". In: *Surface and Coating Technology* 70 (1995), pp. 231–234.

[61] C. Correa et al. "Random-Type Scanning Patterns in Laser Shock Peening without Absorbing Coating in 2024-T351 Al Alloy: A solution to Reduce Residual Stress Anisotropy". In: *Optics and Laser Technology* 73 (2015), pp. 179–187.

[62] L. Berthe, R. FabR. Fabbro. Peyre, and E. Bartnicki. "Wavelength Dependant Laser Shockwave Generation in the Water-confinement Regime". In: *Applied Physics* 85 (1999), pp. 7552–7555.

[63] P. Peyre et al. "Laser Induced Shock Waves as a Surface Treatment for 7075-T7351 Aluminium Alloy". In: *Surface Engineering* 11 (1995), pp. 47–52.

[64] G. Singh. "Effective Simulation and Optimization of a Laser Peening Process". Thesis. Dayton: Wright State University, 2006. URL: `http://cecs.wright.edu/cepro/docs/thesis/Effective_Simulation_and_Optimization_of_a_Laser_Peening_Process_SINGH.pdf`.

[65] M. Shepard, P.R. Smith, and M.S. Amer. "Introduction of Compressive Residual Stresses in Ti-6Al-4V Simulated Airfoils via Laser Shock Processing". In: *Journal of Materials Engineering and Performance* 10.6 (2001), pp. 670–678.

[66] R. Caslaru. "Fabrication, Characterization and Tribological Performance of Micro Dent Arrays Produced by Laser Shock Peening on Ti-Al-4V Alloy". Thesis. Tuscaloosa: University of Alabama, 2010. URL: `http://acumen.lib.ua.edu/content/u0015/0000001/0000270/u0015_0000001_0000270.pdf`.

[67] A. Clauer, B.P. Fairand, and B.A. Wilcox. "Laser Shock Hardening of Weld Zones in Aluminium Alloys". In: *Mettalurgical Transactions* 8A (1976), pp. 1871–1876.

[68] Z. Hong and Y. Chengye. "Laser Shock processing of 2024-T62 Aluminium Alloy". In: *Materials Science and Engineering* A527 (1998), pp. 322–327.

[69] B.P. Fairand et al. "Laser Shock Induced Microstructural and Mechanical Property Changes in 7075 Aluminium". In: *Journal of Applied Physics* 43 (1972), pp. 3893–3895.

[70] C. Dane et al., eds. *High Laser Power for Peening of Metals Enabling Production Technology*. Advanced Aerospace materials and Processes Conference '98. Virginia, 1997.

[71] P. Ganesh et al. "Studies on Fatigue Life Enhancement of Pre-Fatigued Spring Steel Specimens using Laser Shock Peening". In: *Materials & Design* 54 (Feb. 2014), pp. 734–741.

[72] C.D. Jang, H.C. Song, and C.H. Lee. "Fatigue Life Extension of a Through-Thickness Cracks Using Local Heating". In: *International Journal of Offshore and Polar Engineering* 12.03 (2002).

[73] C. M. Branco, V. Infante, and R. Baptista. "Fatigue Behaviour of Welded Joints with Cracks, Repairedby Hammer Peening". In: *Fatigue & Fracture of Engineered Materials % Structures* 27.09 (2004), pp. 785–798.

[74] L. Boni et al. "Experimental and Analytical Assesment of Fatigue and Crack Propogation in Cold Worked Open Hole Specimens". In: *Fatigue and Fracture of Engineering Materiald and Structures* 36 (2013), pp. 930–941.

[75] Q. Liu et al. "The Effectiveness Of Repairing Fatigue Damaged 7050 Aluminium Alloy Using Shot Peening". In: *In Structural Integrity and Fracture International Conference*. 2004, pp. 241–247.

[76] E. Altus and E. Konstantino. "Optimum Laser Surface treatment of Fatigue Damaged Ti-6Al-4V Alloy". In: *Materials Science and Engineering* 302.01 (2001), pp. 100–105.

[77] R.K. Yee and K.S. Sidu. "Innovative Laser Heating Methodology Study for Crack Growth Retardation in Aircraft Structures". In: *International Journal of Fatigue* 27.3 (2005), pp. 245–253.

[78] The Aluminium Association. *International Alloy Designations and Chemical Composition Limits for Wrought Aluminum and Wrought Aluminum Alloys*. Tech. rep. The Aluminium Association, 2015.

[79] ASTM International. "Standard Test Method for Crack-Tip Opening Displacement (CTOD) Fracture Toughness Measurement". In: *ASTM Standard E1290-02* (2002).

[80] ASTM International. "Standard Test Method for Plane-Strain Fracture Toughness of Metallic Materials". In: *ASTM Standard E399-90* (1990).

[81] K-H. Grote and E. Antonsson. "Springer Handbook of Mechanical Engineering, Volume 10". In: Springer, 2009. Chap. 3, p. 113.

[82] ASTM International. "Standard Test Method for Metallic Materials". In: *ASTM Standard E8M* (2004).

[83] J.F. Li et al. "Mechanical Properties, Corrosion Behaviors and Microstructures of 7075 Aluminium Alloy with Various Aging Treatments". In: *Transactions of Nonferrous Metals Society of China* 4.18 (2008), pp. 245–253.

[84] P.M. Rammego. "Effect of Shot Peening and Shock Peening on Fatigue Life of High Strength Aluminium Alloy". Final Year Project. University of Cape town, 2014.

[85] Materials Evaluation and Engineering Inc. *Scanning Electron Microscopy (SEM)*. Online. [Accessed: 27 August 2015]. 2014. URL: http://www.mee-inc.com/hamm/scanning-electron-microscopy-sem/.

[86] V. Cain. "Influence of Grain Size and Niobium Content on the Creep Resistance of Ferritic Stainless Steels". Thesis. University of Cape Town, 2008.

[87] R. Clark et al. "On the Correlation of Mechanical and Physical Properties of 7075-T6 Al Alloy". In: *Engineering Failure Analysis* 12.4 (2005), pp. 520–526.

[88] G.E. Totten and D.S. MacKenzie. *Handbook of Aluminum Volume 1 Physical Metallurgy and Processes*. Marcel Dekker Inc., 2003, pp. 881–1063.

[89] J. Davies. "Aluminium and Aluminium Alloys". In: ASM International, 1993. Chap. 3, p. 295.

[90] ASTM International. "Heat Treatment of Wrought Aluminum Alloys". In: *ASTM Standard B918-01* (2001).

[91] T.P. Ntsoane. *Near-surface Diffraction Capabilities at NECSA*. Seminar. [Accessed: 05 May 2016]. NECSA, 2015. URL: http://lamp.tu-graz.ac.at/~nanoanal/de/sub_loesungen.php?cms_id=L11.

[92] B. He. *Stress and Texture by XRD*. Seminar. [Accessed: 05 May 2016]. Bruker ASX, 2011. URL: http://lamp.tu-graz.ac.at/~nanoanal/de/sub_loesungen.php?cms_id=L11.

[93] ASTM International. "Standard Test Method for Vickers Hardness of Metallic Materials". In: *ASTM Standard E92-82* (2003).

[94] P. Zhang, S.X. Li, and Z.F. Zhang. "General Relationship Between Strength and Hardness". In: *Materials Science and Engineering A* (2011). URL: http://www.synl.ac.cn/uppdf/010mse-2011-529-62.pdf.

[95] L. Konaur. *How do I calculate bending strength from yield strength?* Ed. by L. Konaur. 2001. URL: https://www.quora.com/How-do-I-calculate-bending-strength-from-yield-strength.

[96] K.L. Richards. *Design Engineer's Handbook*. CRC Press, 2012, p. 154.

[97] Roy Beardmore. *Roymech: Surface Texture (Finish)*. Online. [Acsessed: 10 July 2014]. 2013. URL: http://www.roymech.co.uk/Useful_Tables/Surface_Texture/Sur_Fin.html.

[98] British Standard. "Assesment of surface texture; methds and instrumentations". In: *British Standard: 1134* (1988).

[99] D.Kirk. *Almen Saturation Curve Solver Program*. Ed. by Unknown. 2005. URL: http://www.shotpeener.com/learning/solver.php.

[100] Y. Sano et al. "Retardation of Crack Initiation and Growth in Austenitic Stainless Steels by Laser Peening without Protective Coating". In: *Materials Science and Engineering* 416.A (2006), pp. 334–340.

[101] D. Glaser et al. "Laser Shock Peening on a 6056-T4 Aluminium Alloy for Airframe Applications". In: *Advanced Materials Research* 974–979 (2014), pp. 974–979.

[102] D.S. Pelso. *Basics of Signal Processing, Design of Specimens, System Acquisition*. Online. [Accessed: 07 July 2014]. n.d. URL: http://www.sasparm.ps/en/Uploads/file/02_actuationSystems.pdf.

[103] E. Hearn. "Mechanics of Materials 1". In: 3rd. Oxford: Betterworth Heinemann, 1997, p. 62.

[104] E. Hearn. "Metallic Materials and Elements for Aerospace Vehicle Structures". In: US Defence Force, 2003. Chap. 3, p. 406.

[105] S. Perkins. "Identification and Reconstruction of Bullets from Multiple X-Rays". MA thesis. University of Cape Town, 2004, pp. 1–7.

[106] Unknown. *Bruker MicroCT Microtomography*. Online. [Accessed: 14 April 2016]. n.d. URL: http://bruker-microct.com/company/methods.htm.

[107] Stellenbosch University. *CT Scanner Facility at Stellenbosch University: Introduction*. Online. [Accessed: 14 April 2016]. 2016. URL: http://blogs.sun.ac.za/ctscanner/introduction/.

[108] aluMATTER. *Physical and Elastic Properties*. Ed. by Unknown. 2001. URL: http://aluminium.matter.org.uk/aluselect/03_physical_browse.asp.

[109] ASTM International. "Standard Guide for Preparation of Metallographic Specimens". In: *ASTM Standard E3-01* (2001).

[110] E. Cerri and E. Evangelista. *Metallography of Aluminium Alloys*. Lecture. Universita di Ancona-Italy, 1991.

[111] ASTM International. "Standard Test Method for Microindentation Hardness of Materials". In: *ASTM Standard E384-99* (1999).

[112] aluMATTER. *Mechanical Properties*. Ed. by Unknown. 2001. URL: http://aluminium.matter.org.uk/aluselect/09_mech_browse.asp?.

[113] Elmira Tavasoli. *What is the relation between tensile strength and flexural strength in isotropic material?* Ed. by Unknown. 2015. URL: https://www.researchgate.net/post/What_is_the_relation_between_tensile_strength_and_flexural_strength_in_isotropic_material.

[114] J.B. Quinn et al. “Fractographic Analyses of Three Ceramic Whole Crown Restoration Failures”. In: *Dental Materials* 21 (2005), pp. 920–929.

[115] A. Clauer and B.P. Fairand. “Interaction of Laser-Induced Stress Waves with Metals”. In: *Applications of Laser in Material Processing* 8A (1970), pp. 1871–1876.

[116] A.H. Clauer, J.H. Holbrook, and B.P. Fairand. “Effects of Laser Induced Shock Waves on Metals”. In: Springer US, 1981. Chap. 38, pp. 675–702.

Appendix A

Material Data Sheet

Heat-Treatable Al-Zn-Mg-Cu Wrought Alloy 7075

Chemical Composition Limits (in %)

Cu	Mg	Si	Fe	Mn	Zn	Ti	Cr	Other elements Each	Other elements Total
1,2 2,0	2,1 2,9	0,4	0,5	0,3	5,1 6,1	0,2	0,18 0,28	0,05	0,15

Outstanding Characteristics:

Very high strength.

Standard Commodities:

Extrusions.

Typical Uses:

Aircraft structures. Armaments – forgings.

Typical Physical Properties

Density	2,80	g/cm³
Modulus of Elasticity	72	GPa
Melting Range	475–630	°C
Coefficient of linear expansion between 20–100 °C (293–373 K)	$23,5 \times 10^{-6}$	/K
Thermal Conductivity at 25 °C (298 K)	130	W/mK
Resistivity at 20 °C (293 K)	$0,052 \times 10^{-6}$	Ω m

Other Characteristics

Corrosion Resistance	: Poor
Weldability	: Not suitable
Formability	: Fair in O temper
Machinability	: Excellent
Anodizing	: Good
Brazeability	: Not brazeable

Mechanical Properties

Commodity and Temper	Gauge mm	0,2 % Proof Stress MPa	Ultimate Tensile Strength MPa	Elongation A_5 %	Brinell Hardness HB	Ultimate Shear Strength MPa
Extrusions						
T6	up to 75	480 (540)	540 (590)	5 (7)	150	
T8	up to 75	480 (540)	540 (590)	5 (7)	150	
T76*	up to 75	440 (480)	510 (540)	6 (7)		
Sheet and Plate						
O	3,0–100,0	80(–)145	180(–)275	16**		
T6	3,0–100,0	460(–)555	525(–)635	7**		

* Solution heat-treated and artificially aged to achieve optimum stress corrosion resistance but with 10 % lower tensile properties than T8.
** 50 mm gauge length

Heat Treatment

Solution Heat Treatment				Ageing	
Temper	Temperature °C	Time h	Quenching	Temperature °C	Time h
T6	465^{+3}_{-2}		In water	120 ± 3	24

Figure A.1: Material Data Sheet

Appendix B

Test Specimen and Bending Jig Drawings

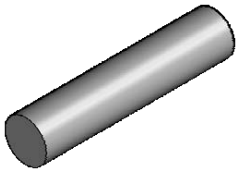

SCALE 1:2

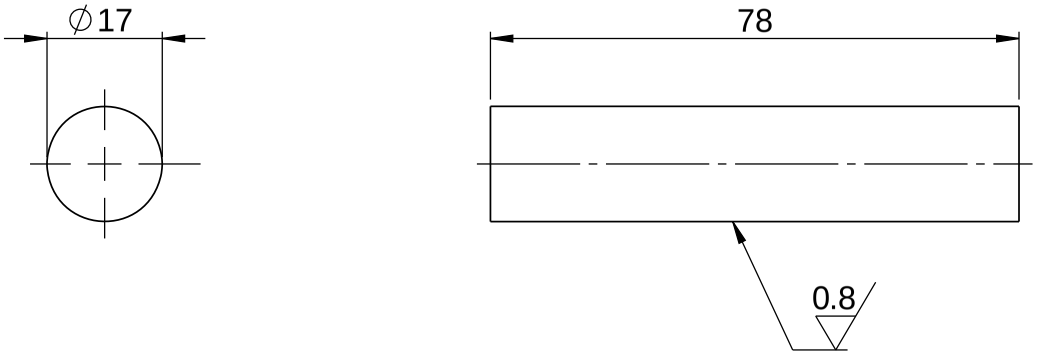

Note: There is no tolerencing as small variations in specimen length and diameter can be accounted for in bending stress calculations

A4 Landscape	University of Cape Town Department of Mechanical Engineering				
	Title: Cylindrical Test Specimen				
Quantity: 71	Part Finish Fine	Date: 2016/07/20	Scale: 1:1	Sheet 1	of 1
Material: AA 7075-T6	Drawn By: Alexander Becker			Drawing Number A	

Figure B.1: Test Specimen Drawing

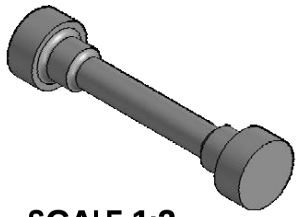

SCALE 1:2

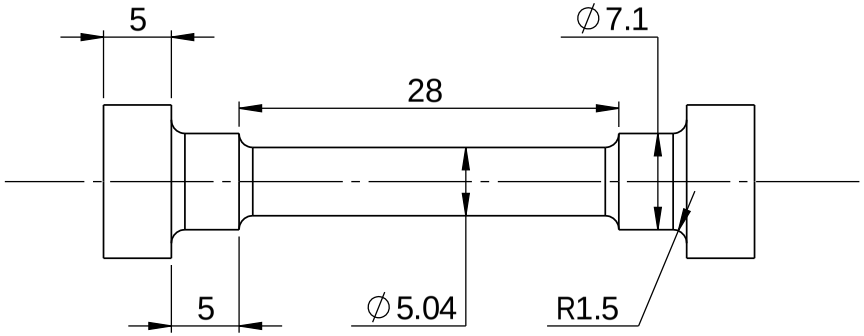

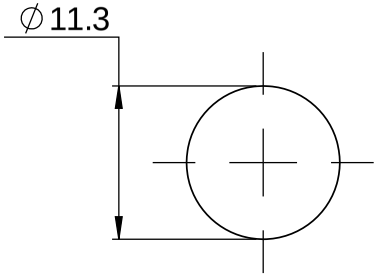

Note: All Rounds R1.5 mm

A4 Landscape	University of Cape Town Department of Mechanical Engineering				
	Title: Tensile Test Specimen				
Quantity: 6	Part Finish	Date: 2016/05/31	Scale: 2:1	Sheet 1	of 1
Material: AA 7075-T6	Drawn By: Alexander Becker			Drawing Number B	

Figure B.2: Tensile Test Specimen

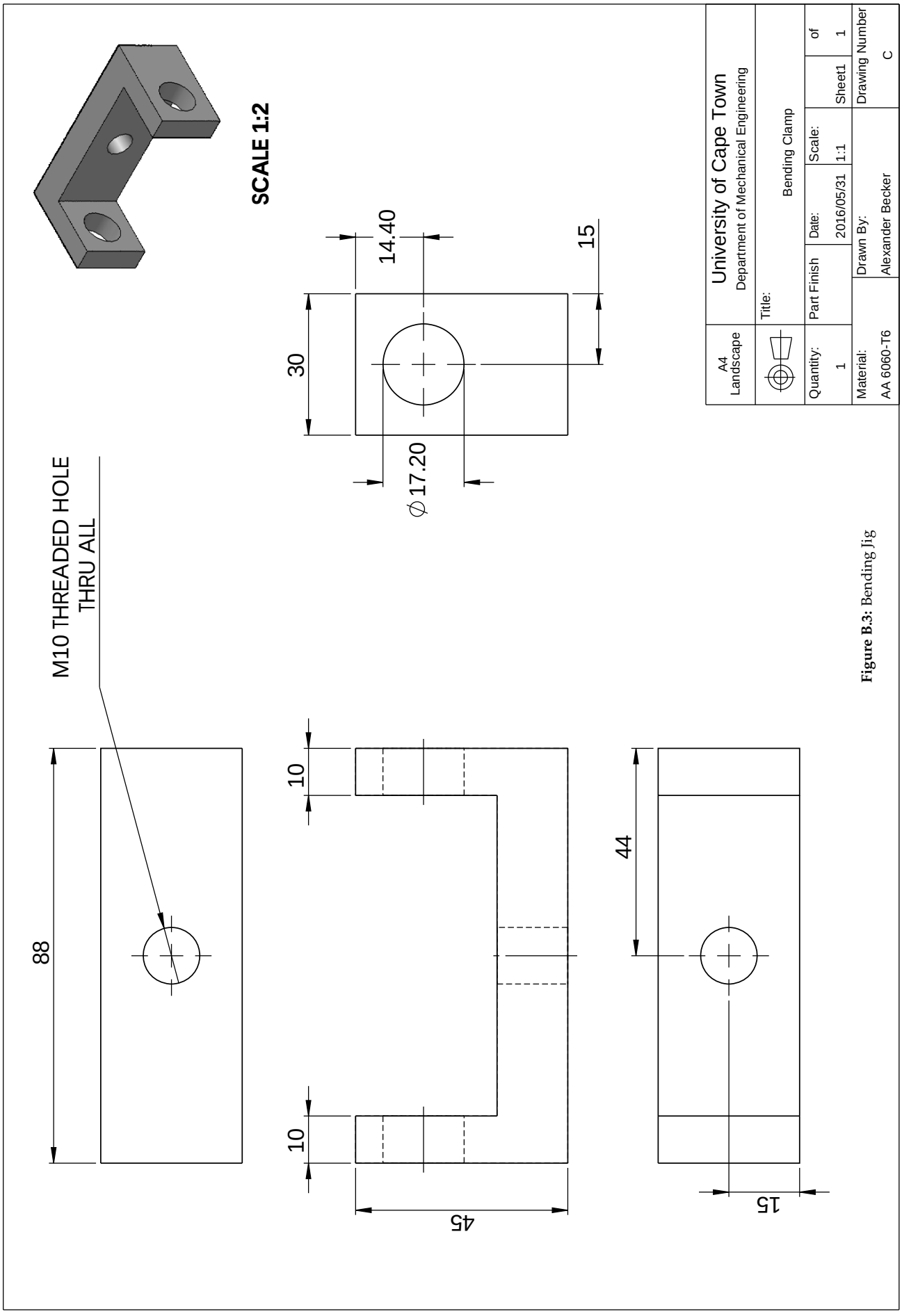

Figure B.3: Bending Jig

Appendix C

X-Ray Diffraction Data

2015/02/19 04:00:48 PM

Project: Stress_1D

Operator: Bruker Instrument Administrator

Site: NECSA

Measured : 02/09/15 10:39:19

Sample

Material	HKL	Wavelength	2theta	Poisson	Young	s1	1/2s2	Arx
Al	(4 2 2)	0.154055 (Cu_)Ka1	137.46	0.35	69300.00	-5.051E-6	1.948E-5	1.00

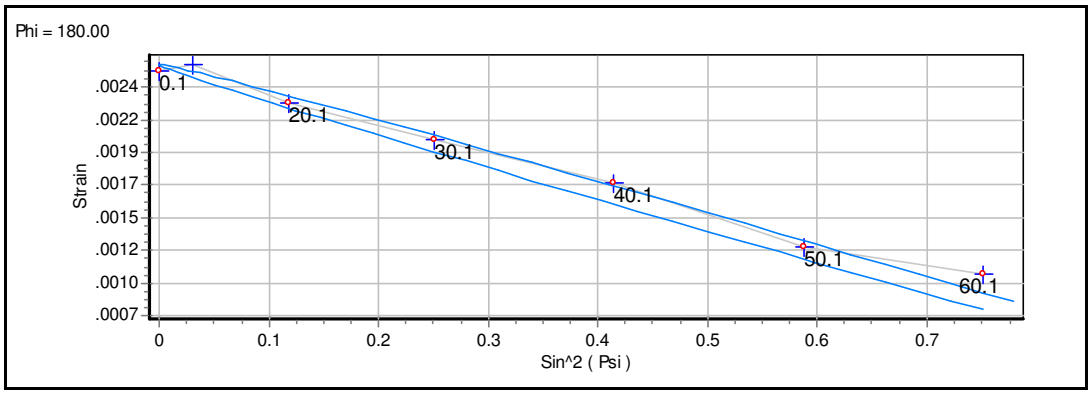

Corrections : Absorption , Background (5) , Polarisation , Smooth , K alpha 2 (0.50)

Psi values : 0.10, 10.10, 20.10, 30.10, 40.10, 50.10, 60.10

Peak Evaluation Method : Pearson VII

Stresss Model : Biaxial + Shear

Normal : -120.0 ± 13.6 **Shear :** 3.6 ± 5.3

Stress Tensor :

-120.0 ± 13.6	-11.7 ± 13.9	-3.6 ± 5.3
-11.7 ± 13.9	-193.5 ± 13.6	13.9 ± 5.3
-3.6 ± 5.3	13.9 ± 5.3	0.0 ± 0.0

Figure C.1: Specimen 1: Point 1

2015/02/19 04:35:33 PM

Project: Stress_1D

Operator: Bruker Instrument Administrator

Site: NECSA

Measured : 02/09/15 13:08:32

Sample

Material	HKL	Wavelength	2theta	Poisson	Young	s1	1/2s2	Arx
Al	(4 2 2)	0.154055 (Cu_)Ka1	137.46	0.35	69300.00	-5.051E-6	1.948E-5	1.00

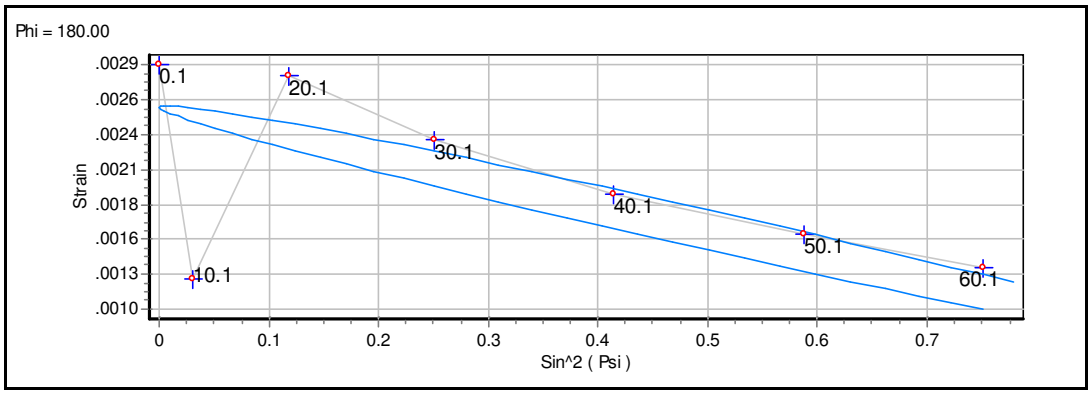

Corrections : Absorption , Background (5) , Polarisation , Smooth , K alpha 2 (0.50)

Psi values : 0.10, 10.10, 20.10, 30.10, 40.10, 50.10, 60.10

Peak Evaluation Method : Pearson VII

Stresss Model : Biaxial + Shear

Normal : -94.5 ± 15.2 **Shear :** 7.7 ± 5.9

Stress Tensor :

-94.5 ± 15.2	18.0 ± 15.5	-7.7 ± 5.9
18.0 ± 15.5	-97.1 ± 15.2	5.5 ± 5.9
-7.7 ± 5.9	5.5 ± 5.9	0.0 ± 0.0

Figure C.2: Specimen 1: Point 2

2015/02/19 05:08:20 PM

Project: Stress_1D

Operator: Bruker Instrument Administrator

Site: NECSA

Measured : 02/09/15 15:03:07

Sample

Material	HKL	Wavelength	2theta	Poisson	Young	s1	1/2s2	Arx
Al	(4 2 2)	0.154055 (Cu_)Ka1	137.46	0.35	69300.00	-5.051E-6	1.948E-5	1.00

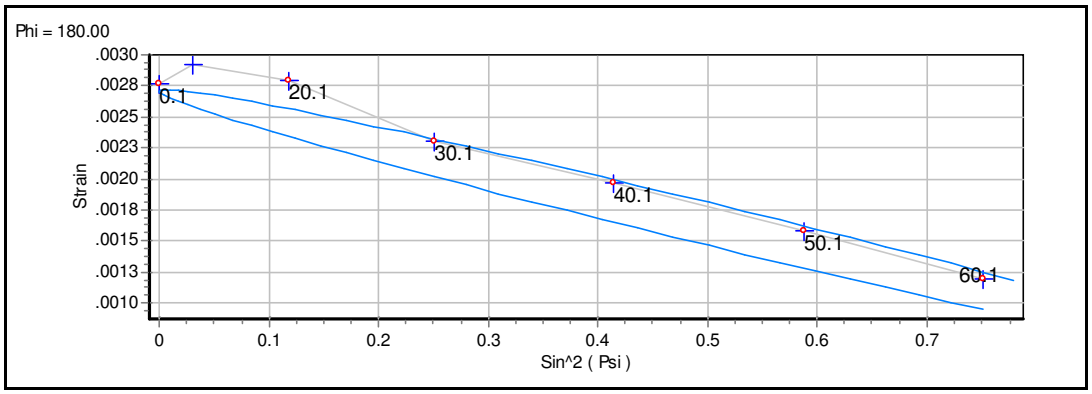

Corrections : Absorption , Background (5) , Polarisation , Smooth , K alpha 2 (0.50)

Psi values : 0.10, 10.10, 20.10, 30.10, 40.10, 50.10, 60.10

Peak Evaluation Method : Pearson VII

Stresss Model : Biaxial + Shear

Normal : -111.3 ± 18.9 **Shear :** 9.1 ± 7.4

Stress Tensor :

-111.3 ± 18.9	6.5 ± 19.3	-9.1 ± 7.4
6.5 ± 19.3	-128.0 ± 18.9	1.0 ± 7.4
-9.1 ± 7.4	1.0 ± 7.4	0.0 ± 0.0

Figure C.3: Specimen 1: Point 3

2015/03/03 03:15:20 PM

Project: Stress_1D

Operator: Bruker Instrument Administrator

Site: NECSA

Measured : 02/06/15 08:42:30

Sample

Material	HKL	Wavelength	2theta	Poisson	Young	s1	1/2s2	Arx
Al	(4 2 2)	0.154055 (Cu_)Ka1	137.46	0.35	69300.00	-5.051E-6	1.948E-5	1.00

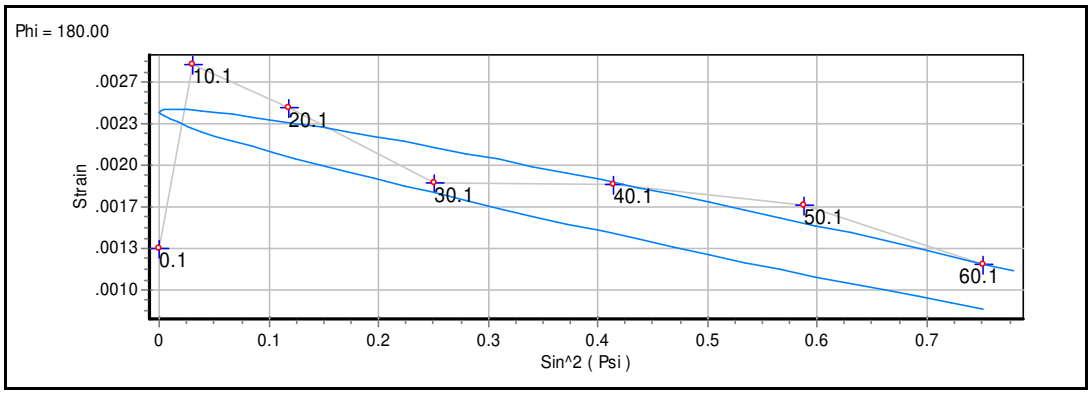

Corrections : Absorption , Background (5) , Polarisation , Smooth , K alpha 2 (0.50)

Psi values : 0.10, 10.10, 20.10, 30.10, 40.10, 50.10, 60.10

Peak Evaluation Method : Pearson VII

Stresss Model : Biaxial + Shear

Normal : -95.8 ± 22.0 **Shear :** 10.9 ± 8.6

Stress Tensor :

-95.8 ± 22.0	11.0 ± 22.4	-10.9 ± 8.6
11.0 ± 22.4	-133.8 ± 22.0	4.5 ± 8.6
-10.9 ± 8.6	4.5 ± 8.6	0.0 ± 0.0

Figure C.4: Specimen 2: Point 1

2015/03/03 03:25:25 PM

Project: Stress_1D

Operator: Bruker Instrument Administrator

Site: NECSA

Measured : 02/06/15 12:31:00

Sample

Material	HKL	Wavelength	2theta	Poisson	Young	s1	1/2s2	Arx
Al	(4 2 2)	0.154055 (Cu_)Ka1	137.46	0.35	69300.00	-5.051E-6	1.948E-5	1.00

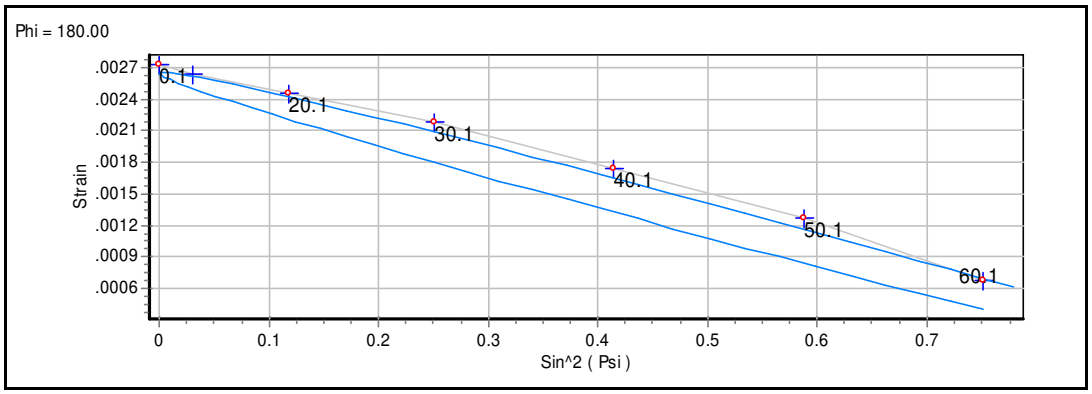

Corrections : Absorption , Background (5) , Polarisation , Smooth , K alpha 2 (0.50)

Psi values : 0.10, 10.10, 20.10, 30.10, 40.10, 50.10, 60.10

Peak Evaluation Method : Pearson VII

Stresss Model : Biaxial + Shear

Normal : -142.1 ± 9.9 **Shear :** 8.5 ± 3.8

Stress Tensor :

-142.1 ± 9.9	-18.8 ± 10.1	-8.5 ± 3.8
-18.8 ± 10.1	-121.5 ± 9.9	-2.1 ± 3.8
-8.5 ± 3.8	-2.1 ± 3.8	0.0 ± 0.0

Figure C.5: Specimen 2: Point 2

2015/01/28 02:58:45 PM

Project: Stress_1D

Operator: Bruker Instrument Administrator

Site: NECSA

Measured : 01/26/15 14:02:27

Sample

Material	HKL	Wavelength	2theta	Poisson	Young	s1	1/2s2	Arx
Al	(4 2 2)	0.154055 (Cu_)Ka1	137.46	0.35	69300.00	-5.051E-6	1.948E-5	1.00

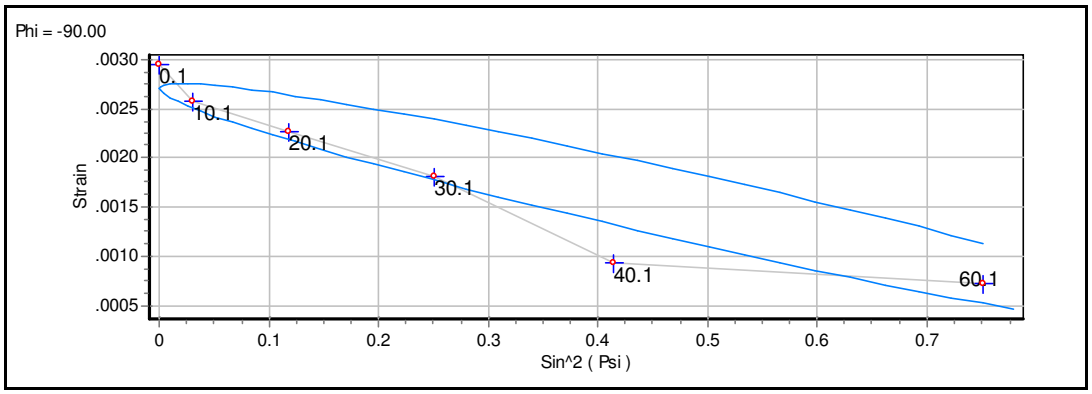

Corrections : Absorption , Background (5) , Polarisation , Smooth , K alpha 2 (0.50)

Psi values : 0.10, 10.10, 20.10, 30.10, 40.10, 60.10

Peak Evaluation Method : Pearson VII

Stresss Model : Biaxial + Shear

Normal : -128.4 ± 15.3 **Shear :** -18.3 ± 6.0

Stress Tensor :

-138.1 ± 15.3	-20.7 ± 16.2	5.7 ± 6.0
-20.7 ± 16.2	-128.4 ± 15.3	18.3 ± 6.0
5.7 ± 6.0	18.3 ± 6.0	0.0 ± 0.0

Figure C.6: Specimen 2: Point 3

2015/01/29 03:58:00 PM

Project: Stress_1D

Operator: Bruker Instrument Administrator

Site: NECSA

Measured : 01/28/15 16:03:57

Sample

Material	HKL	Wavelength	2theta	Poisson	Young	s1	1/2s2	Arx
Al	(4 2 2)	0.154055 (Cu_)Ka1	137.46	0.35	69300.00	-5.051E-6	1.948E-5	1.00

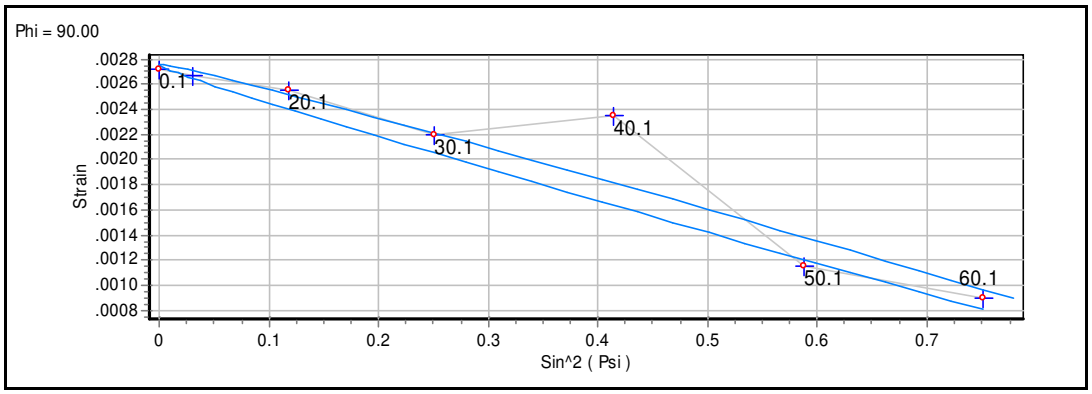

Corrections : Absorption , Background (5) , Polarisation , Smooth , K alpha 2 (0.50)

Psi values : 0.10, 10.10, 20.10, 30.10, 40.10, 50.10, 60.10

Peak Evaluation Method : Pearson VII

Stresss Model : Biaxial + Shear

Normal : -127.4 ± 8.0 **Shear :** 4.7 ± 3.1

Stress Tensor :

-135.3 ± 8.0	-32.3 ± 8.1	-6.2 ± 3.1
-32.3 ± 8.1	-127.4 ± 8.0	4.7 ± 3.1
-6.2 ± 3.1	4.7 ± 3.1	0.0 ± 0.0

Figure C.7: Specimen 3: Point 1

2015/03/03 03:59:56 PM

Project: Stress_1D

Operator: Bruker Instrument Administrator

Site: NECSA

Measured : 01/29/15 15:24:24

Sample

Material	HKL	Wavelength	2theta	Poisson	Young	s1	1/2s2	Arx
Al	(4 2 2)	0.154055 (Cu_)Ka1	137.46	0.35	69300.00	-5.051E-6	1.948E-5	1.00

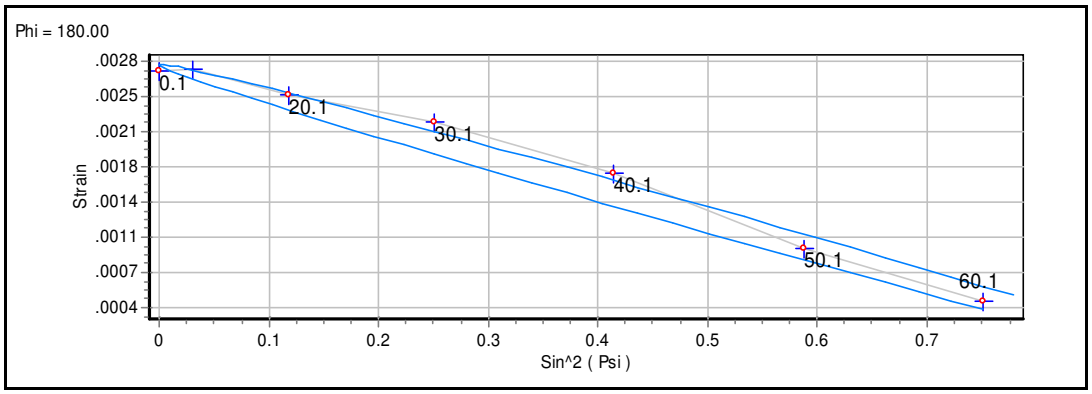

Corrections : Absorption , Background (5) , Polarisation , Smooth , K alpha 2 (0.50)

Psi values : 0.10, 10.10, 20.10, 30.10, 40.10, 50.10, 60.10

Peak Evaluation Method : Pearson VII

Stresss Model : Biaxial + Shear

Normal : -158.6 ± 22.1 **Shear :** 6.8 ± 8.6

Stress Tensor :

-158.6 ± 22.1	21.0 ± 22.5	-6.8 ± 8.6
21.0 ± 22.5	-163.4 ± 22.1	19.2 ± 8.6
-6.8 ± 8.6	19.2 ± 8.6	0.0 ± 0.0

Figure C.8: Specimen 3: Point 2

2015/03/03 04:11:48 PM

Project: Stress_1D

Operator: Bruker Instrument Administrator

Site: NECSA

Measured : 01/30/15 09:28:26

Sample

Material	HKL	Wavelength	2theta	Poisson	Young	s1	1/2s2	Arx
Al	(4 2 2)	0.154055 (Cu_)Ka1	137.46	0.35	69300.00	-5.051E-6	1.948E-5	1.00

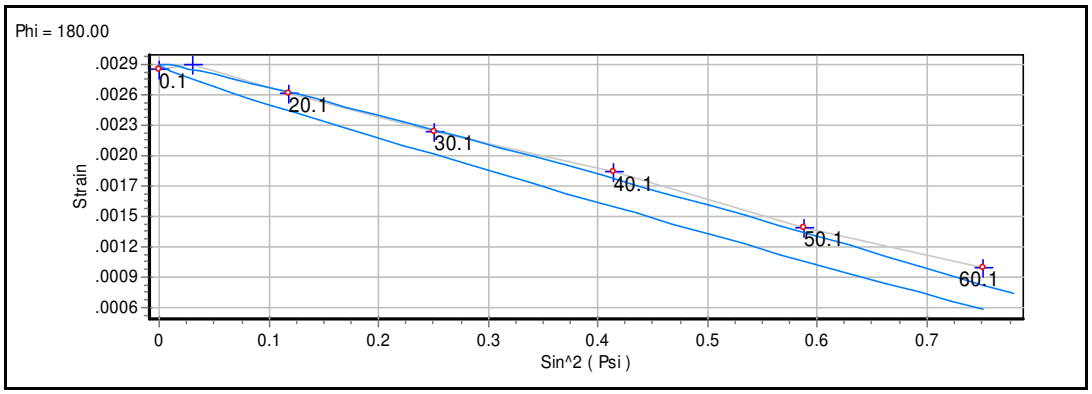

Corrections : Absorption , Background (5) , Polarisation , Smooth , K alpha 2 (0.50)

Psi values : 0.10, 10.10, 20.10, 30.10, 40.10, 50.10, 60.10

Peak Evaluation Method : Pearson VII

Stresss Model : Biaxial + Shear

Normal : -150.7 ± 19.5 **Shear :** 7.0 ± 7.6

Stress Tensor :

-150.7 ± 19.5	24.4 ± 19.9	-7.0 ± 7.6
24.4 ± 19.9	-172.3 ± 19.5	-8.1 ± 7.6
-7.0 ± 7.6	-8.1 ± 7.6	0.0 ± 0.0

Figure C.9: Specimen 3: Point 3

2015/02/19 03:06:49 PM

Project: Stress_1D

Operator: Bruker Instrument Administrator

Site: NECSA

Measured : 01/30/15 13:40:20

Sample

Material	HKL	Wavelength	2theta	Poisson	Young	s1	1/2s2	Arx
Al	(4 2 2)	0.154055 (Cu_)Ka1	137.46	0.35	69300.00	-5.051E-6	1.948E-5	1.00

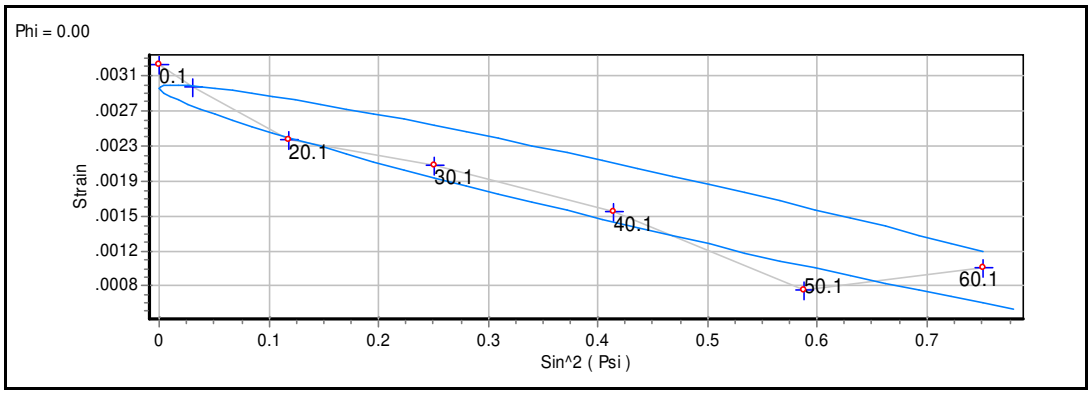

Corrections : Absorption , Background (5) , Polarisation , Smooth , K alpha 2 (0.50)

Psi values : 0.10, 10.10, 20.10, 30.10, 40.10, 50.10, 60.10

Peak Evaluation Method : Pearson VII

Stresss Model : Biaxial + Shear

Normal : -142.9 ± 14.0 **Shear :** -17.0 ± 5.5

Stress Tensor :

-142.9 ± 14.0	-20.7 ± 14.3	-17.0 ± 5.5
-20.7 ± 14.3	-185.5 ± 14.0	-5.7 ± 5.5
-17.0 ± 5.5	-5.7 ± 5.5	0.0 ± 0.0

Figure C.10: Specimen 4: Point 1

2015/02/19 03:19:20 PM

Project: Stress_1D

Operator: Bruker Instrument Administrator

Site: NECSA

Measured : 01/30/15 16:31:57

Sample

Material	HKL	Wavelength	2theta	Poisson	Young	s1	1/2s2	Arx
Al	(4 2 2)	0.154055 (Cu_)Ka1	137.46	0.35	69300.00	-5.051E-6	1.948E-5	1.00

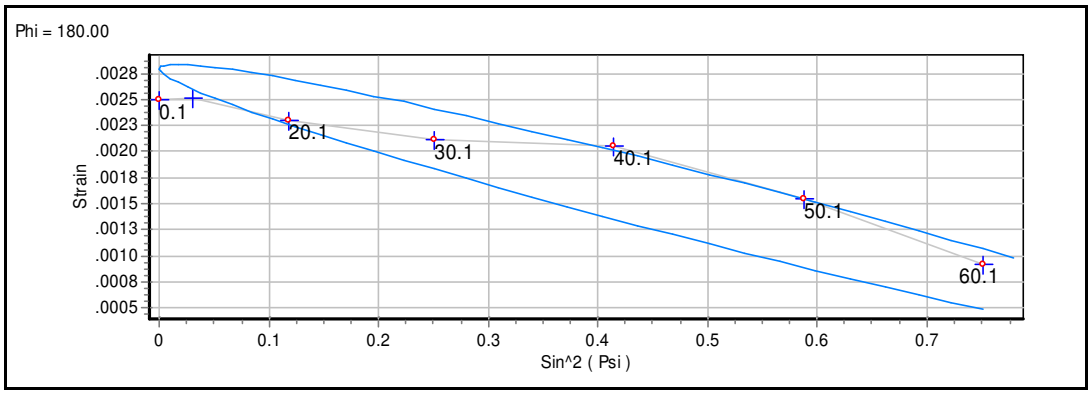

Corrections : Absorption , Background (5) , Polarisation , Smooth , K alpha 2 (0.50)

Psi values : 0.10, 10.10, 20.10, 30.10, 40.10, 50.10, 60.10

Peak Evaluation Method : Pearson VII

Stresss Model : Biaxial + Shear

Normal : -138.3 ± 17.0 **Shear :** 17.2 ± 6.6

Stress Tensor :

-138.3 ± 17.0	-19.1 ± 17.3	-17.2 ± 6.6
-19.1 ± 17.3	-172.3 ± 17.0	-13.4 ± 6.6
-17.2 ± 6.6	-13.4 ± 6.6	0.0 ± 0.0

Figure C.11: Specimen 4: Point 2

2015/02/19 03:39:41 PM

Project: Stress_1D

Operator: Bruker Instrument Administrator

Site: NECSA

Measured : 02/04/15 09:26:38

Sample

Material	HKL	Wavelength	2theta	Poisson	Young	s1	1/2s2	Arx
Al	(4 2 2)	0.154055 (Cu_)Ka1	137.46	0.35	69300.00	-5.051E-6	1.948E-5	1.00

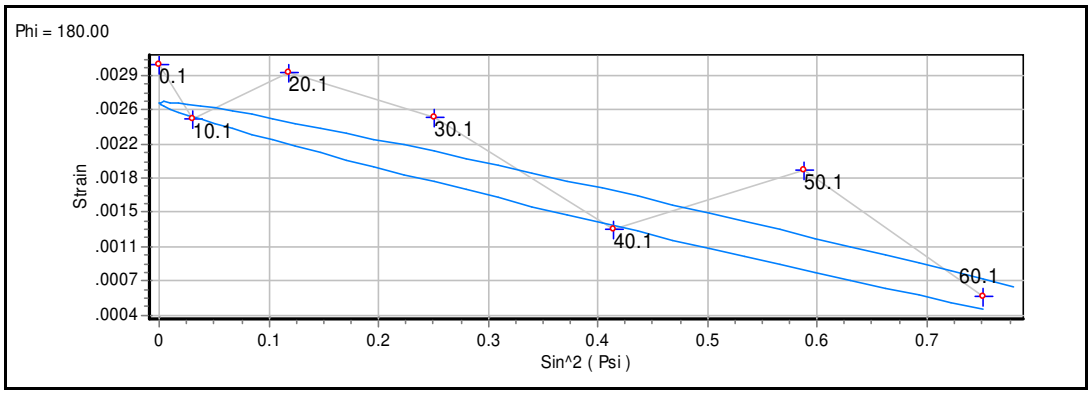

Corrections : Absorption , Background (5) , Polarisation , Smooth , K alpha 2 (0.50)

Psi values : 0.10, 10.10, 20.10, 30.10, 40.10, 50.10, 60.10

Peak Evaluation Method : Pearson VII

Stresss Model : Biaxial + Shear

Normal : -139.3 ± 31.9 **Shear :** 9.6 ± 12.4

Stress Tensor :

-139.3 ± 31.9	32.5 ± 32.5	-9.6 ± 12.4
32.5 ± 32.5	-163.6 ± 31.9	-24.1 ± 12.4
-9.6 ± 12.4	-24.1 ± 12.4	0.0 ± 0.0

Figure C.12: Specimen 4: Point 3

2015/02/19 02:25:08 PM

Project: Stress_1D

Operator: Bruker Instrument Administrator

Site: NECSA

Measured : 02/04/15 11:34:38

Sample

Material	HKL	Wavelength	2theta	Poisson	Young	s1	1/2s2	Arx
Al	(4 2 2)	0.154055 (Cu_)Ka1	137.46	0.35	69300.00	-5.051E-6	1.948E-5	1.00

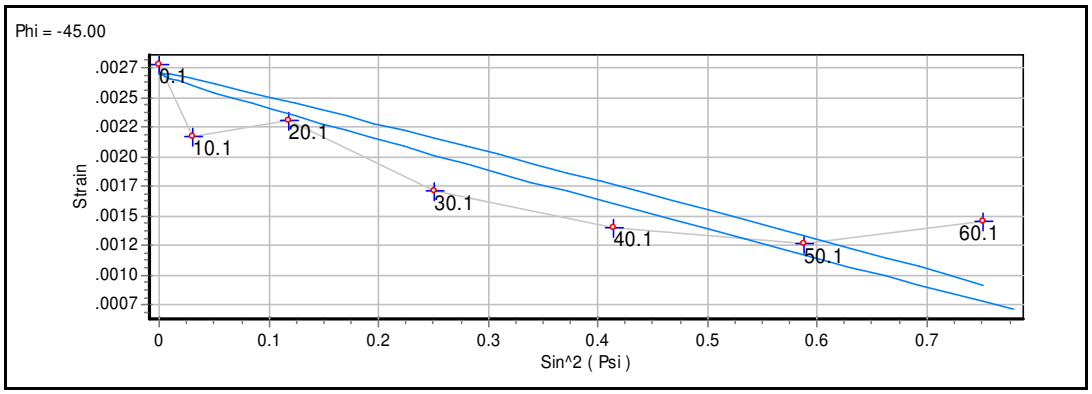

Corrections : Absorption , Background (5) , Polarisation , Smooth , K alpha 2 (0.50)

Psi values : 0.10, 10.10, 20.10, 30.10, 40.10, 50.10, 60.10

Peak Evaluation Method : Pearson VII

Stresss Model : Biaxial + Shear

Normal : -124.7 ± 9.3 **Shear :** -4.2 ± 3.0

Stress Tensor :

-112.0 ± 9.3	5.6 ± 9.5	-6.7 ± 3.6
5.6 ± 9.5	-126.1 ± 9.3	-0.8 ± 3.6
-6.7 ± 3.6	-0.8 ± 3.6	0.0 ± 0.0

Figure C.13: Specimen 5: Point 1

2015/02/19 02:51:05 PM

Project: Stress_1D

Operator: Bruker Instrument Administrator

Site: NECSA

Measured : 02/04/15 13:31:35

Sample

Material	HKL	Wavelength	2theta	Poisson	Young	s1	1/2s2	Arx
Al	(4 2 2)	0.154055 (Cu_)Ka1	137.46	0.35	69300.00	-5.051E-6	1.948E-5	1.00

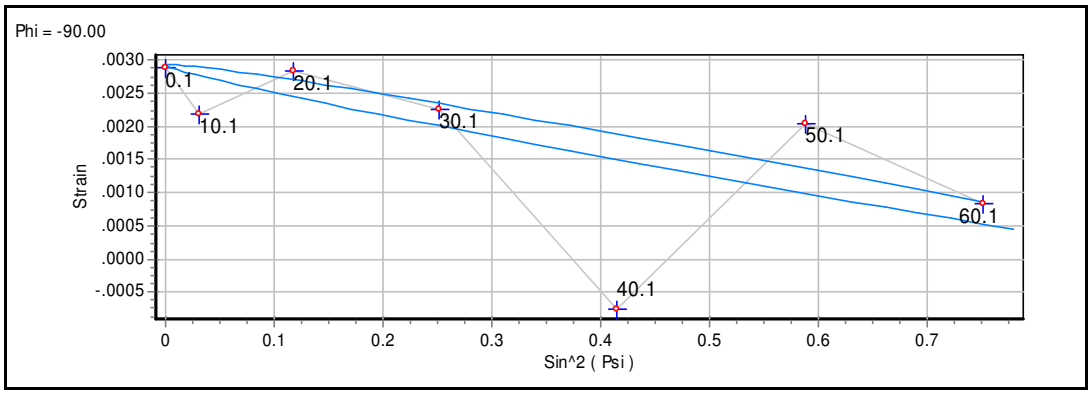

Corrections : Absorption , Background (5) , Polarisation , Smooth , K alpha 2 (0.50)

Psi values : 0.10, 10.10, 20.10, 30.10, 40.10, 50.10, 60.10

Peak Evaluation Method : Pearson VII

Stresss Model : Biaxial + Shear

Normal : -152.0 ± 20.1 **Shear :** -10.1 ± 7.8

Stress Tensor :

-135.4 ± 20.1	10.2 ± 20.5	-5.4 ± 7.8
10.2 ± 20.5	-152.0 ± 20.1	10.1 ± 7.8
-5.4 ± 7.8	10.1 ± 7.8	0.0 ± 0.0

Figure C.14: Specimen 5: Point 2

2015/02/19 02:44:06 PM

Project: Stress_1D

Operator: Bruker Instrument Administrator

Site: NECSA

Measured : 02/04/15 16:16:10

Sample

Material	HKL	Wavelength	2theta	Poisson	Young	s1	1/2s2	Arx
Al	(4 2 2)	0.154055 (Cu_)Ka1	137.46	0.35	69300.00	-5.051E-6	1.948E-5	1.00

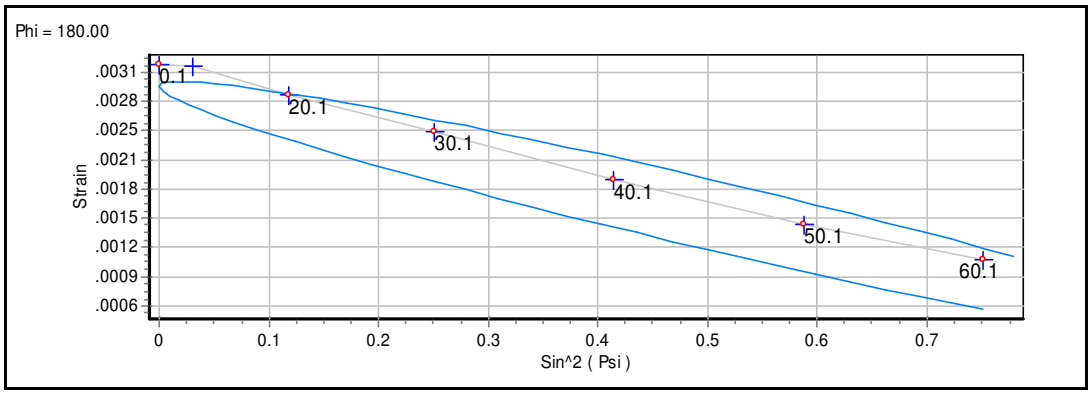

Corrections : Absorption , Background (5) , Polarisation , Smooth , K alpha 2 (0.50)

Psi values : 0.10, 10.10, 20.10, 30.10, 40.10, 50.10, 60.10

Peak Evaluation Method : Pearson VII

Stresss Model : Biaxial + Shear

Normal : -137.5 ± 21.3 **Shear :** 19.1 ± 8.3

Stress Tensor :

-137.5 ± 21.3	-17.4 ± 21.7	-19.1 ± 8.3
-17.4 ± 21.7	-195.4 ± 21.3	-26.6 ± 8.3
-19.1 ± 8.3	-26.6 ± 8.3	0.0 ± 0.0

Figure C.15: Specimen 5: Point 3

2015/01/30 01:40:29 PM

Project: Stress_1D

Operator: Bruker Instrument Administrator

Site: NECSA

Measured : 01/28/15 09:10:18

Sample

Material	HKL	Wavelength	2theta	Poisson	Young	s1	1/2s2	Arx
Al	(4 2 2)	0.154055 (Cu_)Ka1	137.46	0.35	69300.00	-5.051E-6	1.948E-5	1.00

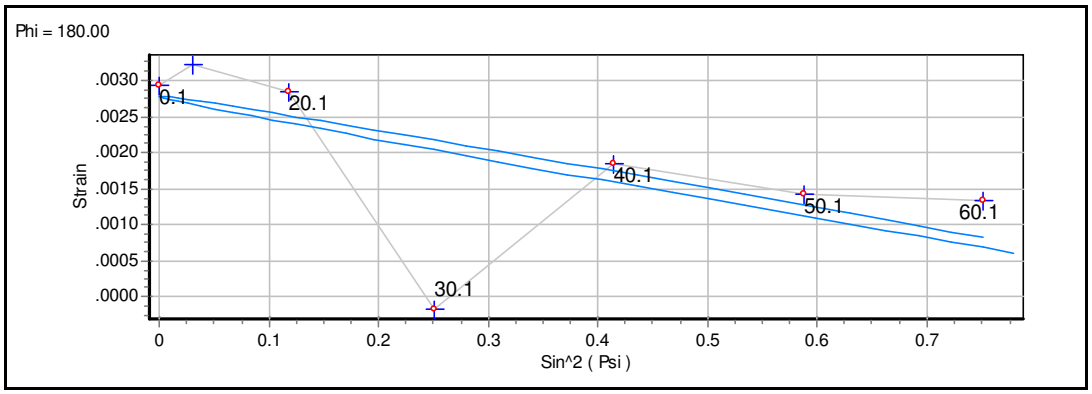

Corrections : Absorption , Background (5) , Polarisation , Smooth , K alpha 2 (0.50)

Psi values : 0.10, 10.10, 20.10, 30.10, 40.10, 50.10, 60.10

Peak Evaluation Method : Pearson VII

Stresss Model : Biaxial + Shear

Normal : -139.2 ± 25.0 **Shear :** -4.1 ± 9.7

Stress Tensor :

-139.2 ± 25.0	37.3 ± 25.5	4.1 ± 9.7
37.3 ± 25.5	-119.8 ± 25.0	-3.2 ± 9.7
4.1 ± 9.7	-3.2 ± 9.7	0.0 ± 0.0

Figure C.16: Specimen 6: Point 1

2015/01/30 01:57:56 PM

Project: Stress_1D

Operator: Bruker Instrument Administrator

Site: NECSA

Measured : 01/28/15 11:13:50

Sample

Material	HKL	Wavelength	2theta	Poisson	Young	s1	1/2s2	Arx
Al	(4 2 2)	0.154055 (Cu_)Ka1	137.46	0.35	69300.00	-5.051E-6	1.948E-5	1.00

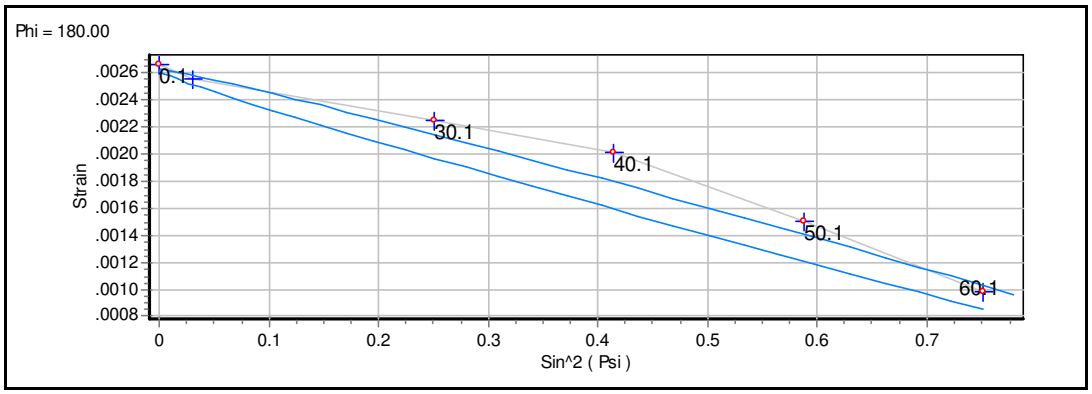

Corrections : Absorption , Background (5) , Polarisation , Smooth , K alpha 2 (0.50)

Psi values : 0.10, 10.10, 30.10, 40.10, 50.10, 60.10

Peak Evaluation Method : Pearson VII

Stresss Model : Biaxial + Shear

Normal : -114.7 ± 12.7 **Shear :** 5.2 ± 5.1

Stress Tensor :

-114.7 ± 12.7	2.0 ± 12.7	-5.2 ± 5.1
2.0 ± 12.7	-116.1 ± 12.7	2.4 ± 5.1
-5.2 ± 5.1	2.4 ± 5.1	0.0 ± 0.0

Figure C.17: Specimen 6: Point 2

2015/01/30 02:17:45 PM

Project: Stress_1D

Operator: Bruker Instrument Administrator

Site: NECSA

Measured : 01/28/15 13:33:47

Sample

Material	HKL	Wavelength	2theta	Poisson	Young	s1	1/2s2	Arx
Al	(4 2 2)	0.154055 (Cu_)Ka1	137.46	0.35	69300.00	-5.051E-6	1.948E-5	1.00

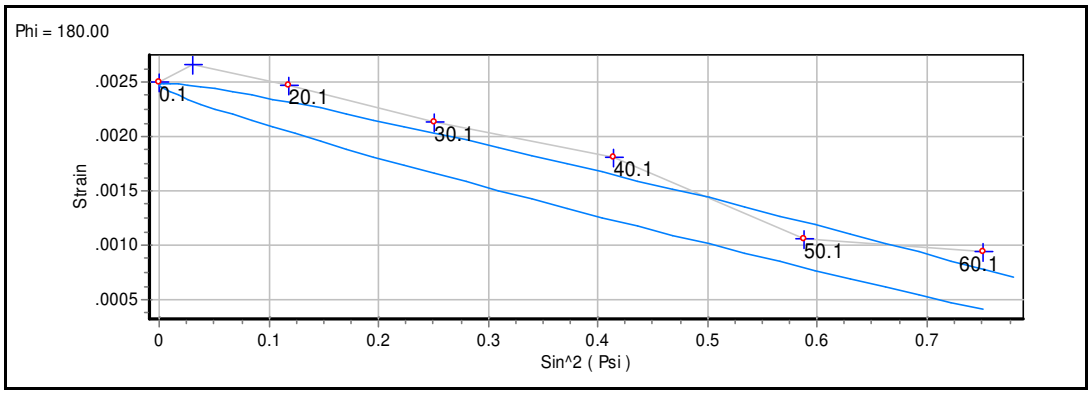

Corrections : Absorption , Background (5) , Polarisation , Smooth , K alpha 2 (0.50)

Psi values : 0.10, 10.10, 20.10, 30.10, 40.10, 50.10, 60.10

Peak Evaluation Method : Pearson VII

Stresss Model : Biaxial + Shear

Normal : -128.1 ± 26.1 **Shear :** 10.9 ± 10.2

Stress Tensor :

-128.1 ± 26.1	-28.9 ± 26.6	-10.9 ± 10.2
-28.9 ± 26.6	-85.5 ± 26.1	-11.3 ± 10.2
-10.9 ± 10.2	-11.3 ± 10.2	0.0 ± 0.0

Figure C.18: Specimen 6: Point 3

2015/01/29 04:08:15 PM

Project: Stress_1D

Operator: Bruker Instrument Administrator

Site: NECSA

Measured : 01/26/15 17:03:09

Sample

Material	HKL	Wavelength	2theta	Poisson	Young	s1	1/2s2	Arx
Al	(4 2 2)	0.154055 (Cu_)Ka1	137.46	0.35	69300.00	-5.051E-6	1.948E-5	1.00

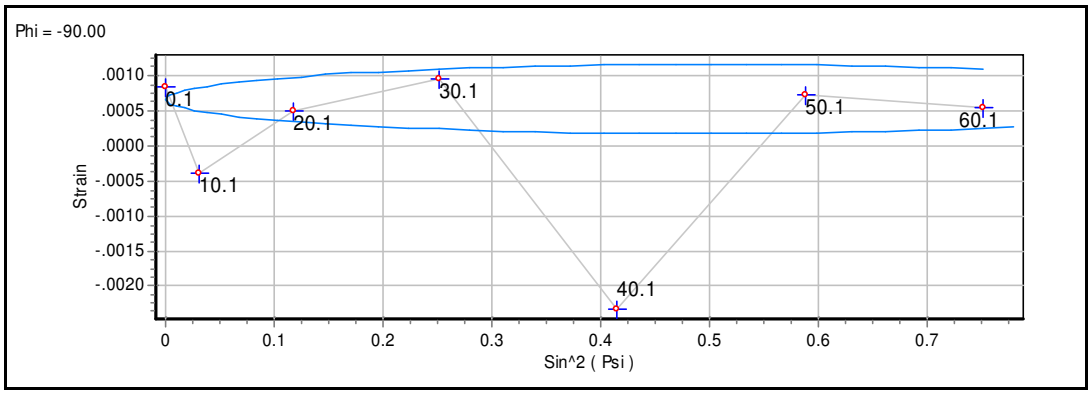

Corrections : Absorption , Background (5) , Polarisation , Smooth , K alpha 2 (0.50)

Psi values : 0.10, 10.10, 20.10, 30.10, 40.10, 50.10, 60.10

Peak Evaluation Method : Pearson VII

Stresss Model : Biaxial + Shear

Normal : 0.6 ± 25.6 **Shear :** -25.4 ± 10.0

Stress Tensor :

7.4 ± 25.6	-9.5 ± 26.1	1.8 ± 10.0
-9.5 ± 26.1	0.6 ± 25.6	25.4 ± 10.0
1.8 ± 10.0	25.4 ± 10.0	0.0 ± 0.0

Figure C.19: Specimen 7: Point 1

2015/01/29 04:20:18 PM

Project: Stress_1D

Operator: Bruker Instrument Administrator

Site: NECSA

Measured : 01/27/15 13:59:09

Sample

Material	HKL	Wavelength	2theta	Poisson	Young	s1	1/2s2	Arx
Al	(4 2 2)	0.154055 (Cu_)Ka1	137.46	0.35	69300.00	-5.051E-6	1.948E-5	1.00

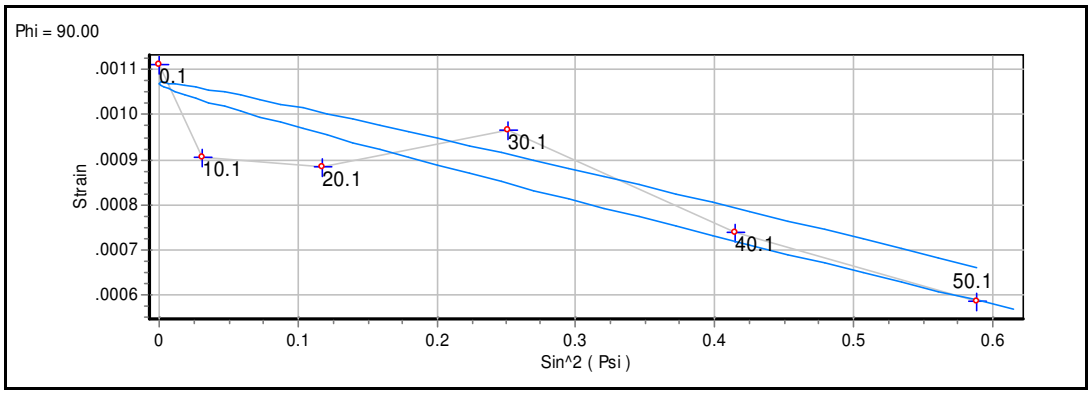

Corrections : Absorption , Background (5) , Polarisation , Smooth , K alpha 2 (0.50)

Psi values : 0.10, 10.10, 20.10, 30.10, 40.10, 50.10

Peak Evaluation Method : Pearson VII

Stresss Model : Biaxial + Shear

Normal : -38.6 ± 7.2 **Shear :** -1.9 ± 2.3

Stress Tensor :

-17.1 ± 7.2	-29.0 ± 7.4	-1.0 ± 2.3
-29.0 ± 7.4	-38.6 ± 7.2	-1.9 ± 2.3
-1.0 ± 2.3	-1.9 ± 2.3	0.0 ± 0.0

Figure C.20: Specimen 7: Point 2

2015/01/29 04:28:16 PM

Project: Stress_1D

Operator: Bruker Instrument Administrator

Site: NECSA

Measured : 01/27/15 16:21:23

Sample

Material	HKL	Wavelength	2theta	Poisson	Young	s1	1/2s2	Arx
Al	(4 2 2)	0.154055 (Cu_)Ka1	137.46	0.35	69300.00	-5.051E-6	1.948E-5	1.00

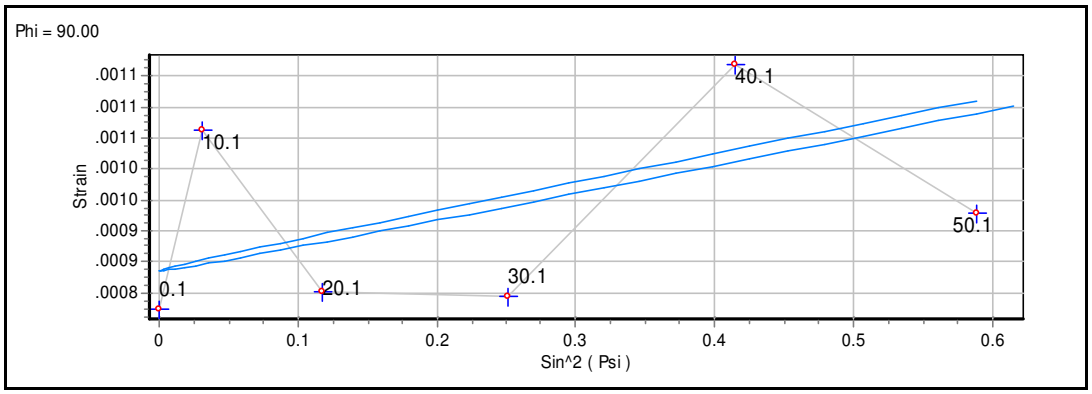

Corrections : Absorption , Background (5) , Polarisation , Smooth , K alpha 2 (0.50)

Psi values : 0.10, 10.10, 20.10, 30.10, 40.10, 50.10

Peak Evaluation Method : Pearson VII

Stresss Model : Biaxial + Shear

Normal : 23.1 ± 9.5 **Shear :** -0.5 ± 3.0

Stress Tensor :

0.5 ± 9.5	5.0 ± 9.8	-1.2 ± 3.0
5.0 ± 9.8	23.1 ± 9.5	-0.5 ± 3.0
-1.2 ± 3.0	-0.5 ± 3.0	0.0 ± 0.0

Figure C.21: Specimen 7: Point 3

2015/02/09 04:15:29 PM

Project: Stress_1D

Operator: Bruker Instrument Administrator

Site: NECSA

Measured : 02/05/15 08:05:35

Sample

Material	HKL	Wavelength	2theta	Poisson	Young	s1	1/2s2	Arx
Al	(4 2 2)	0.154055 (Cu_)Ka1	137.46	0.35	69300.00	-5.051E-6	1.948E-5	1.00

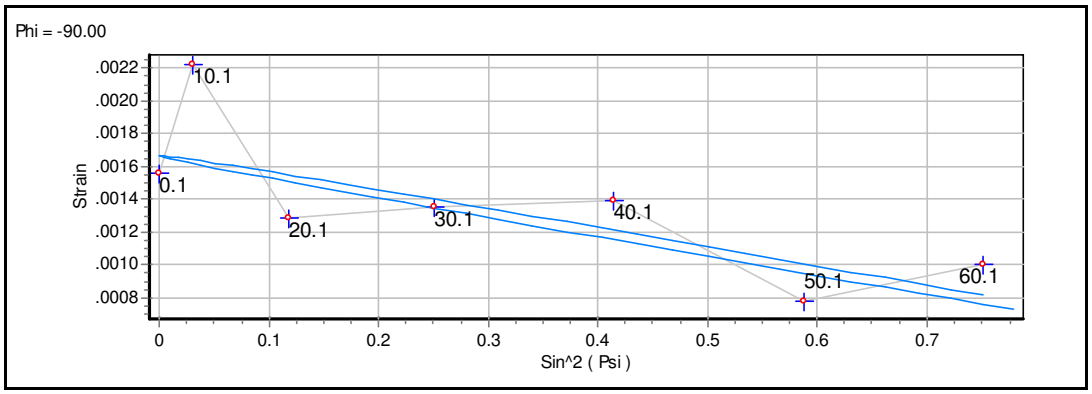

Corrections : Absorption , Background (5) , Polarisation , Smooth , K alpha 2 (0.50)

Psi values : 0.10, 10.10, 20.10, 30.10, 40.10, 50.10, 60.10

Peak Evaluation Method : Pearson VII

Stresss Model : Biaxial + Shear

Normal : -59.9 ± 11.5 **Shear :** -1.6 ± 4.5

Stress Tensor :

-52.0 ± 11.5	-23.3 ± 11.7	1.4 ± 4.5
-23.3 ± 11.7	-59.9 ± 11.5	1.6 ± 4.5
1.4 ± 4.5	1.6 ± 4.5	0.0 ± 0.0

Figure C.22: Specimen 8: Point 1

2015/02/10 01:39:59 PM

Project: Stress_1D

Operator: Bruker Instrument Administrator

Site: NECSA

Measured : 02/05/15 09:57:56

Sample

Material	HKL	Wavelength	2theta	Poisson	Young	s1	1/2s2	Arx
Al	(4 2 2)	0.154055 (Cu_)Ka1	137.46	0.35	69300.00	-5.051E-6	1.948E-5	1.00

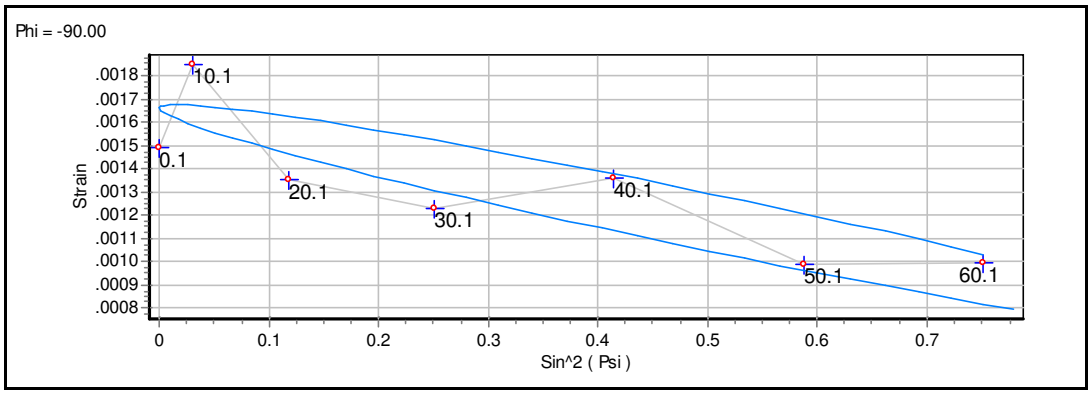

Corrections : Absorption , Background (5) , Polarisation , Smooth , K alpha 2 (0.50)

Psi values : 0.10, 10.10, 20.10, 30.10, 40.10, 50.10, 60.10

Peak Evaluation Method : Pearson VII

Stresss Model : Biaxial + Shear

Normal : -50.3 ± 11.7 **Shear :** -6.4 ± 4.6

Stress Tensor :

-45.2 ± 11.7	-16.9 ± 11.9	-8.1 ± 4.6
-16.9 ± 11.9	-50.3 ± 11.7	6.4 ± 4.6
-8.1 ± 4.6	6.4 ± 4.6	0.0 ± 0.0

Figure C.23: Specimen 8: Point 2

2015/02/10 01:47:44 PM

Project: Stress_1D

Operator: Bruker Instrument Administrator

Site: NECSA

Measured : 02/05/15 13:35:51

Sample

Material	HKL	Wavelength	2theta	Poisson	Young	s1	1/2s2	Arx
Al	(4 2 2)	0.154055 (Cu_)Ka1	137.46	0.35	69300.00	-5.051E-6	1.948E-5	1.00

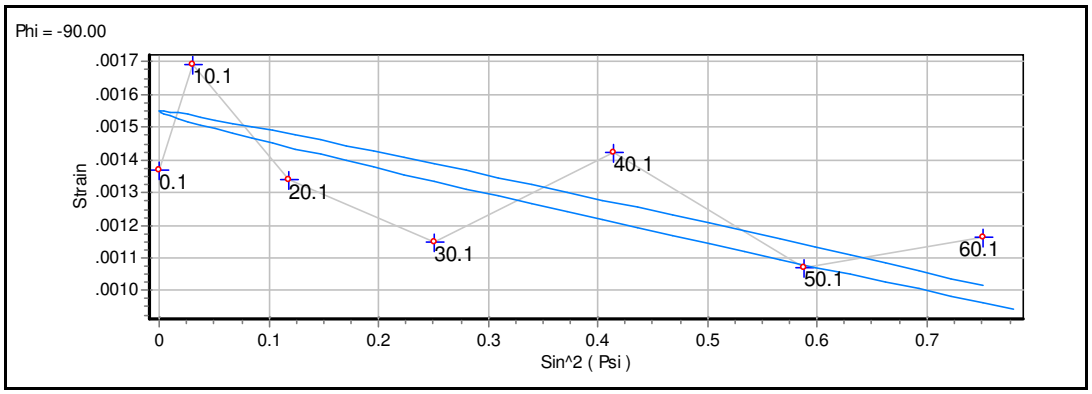

Corrections : Absorption , Background (5) , Polarisation , Smooth , K alpha 2 (0.50)

Psi values : 0.10, 10.10, 20.10, 30.10, 40.10, 50.10, 60.10

Peak Evaluation Method : Pearson VII

Stresss Model : Biaxial + Shear

Normal : -38.1 ± 7.8 **Shear :** -1.6 ± 3.0

Stress Tensor :

-37.6 ± 7.8	-16.1 ± 8.0	-3.2 ± 3.0
-16.1 ± 8.0	-38.1 ± 7.8	1.6 ± 3.0
-3.2 ± 3.0	1.6 ± 3.0	0.0 ± 0.0

Figure C.24: Specimen 8: Point 3

Appendix D

Tensile Test Results

D.0.1 T6 Material Condition Tensile Test Graphs

T6 Test Specimen 1

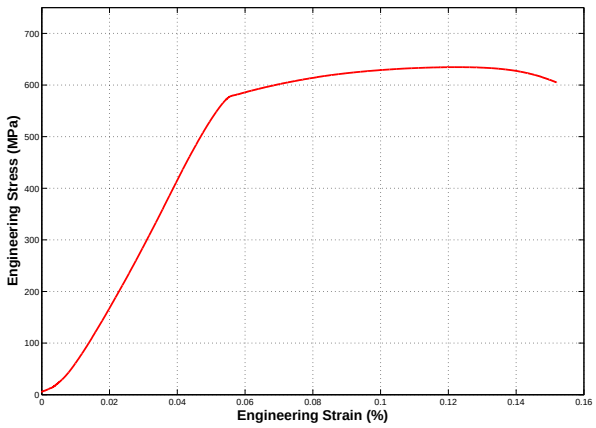

(a) Stress vs. Strain for T6 Test Specimen 1

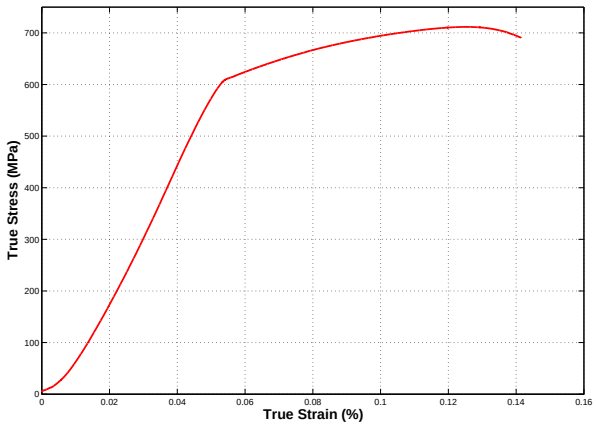

(b) True Stress vs. True Strain for T6 Test Specimen 1

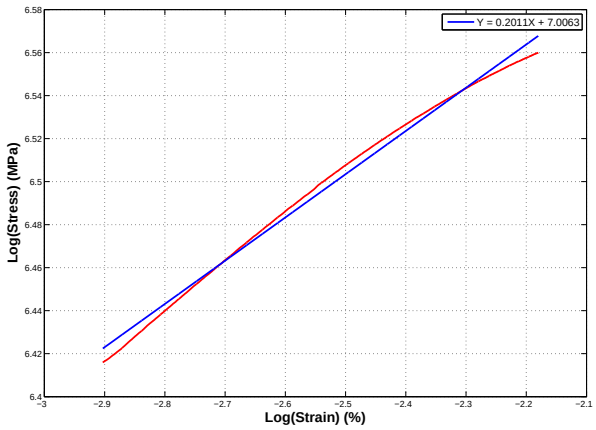

(c) Log(True Stress) vs. Log(True Strain) of Plastic Region for T6 Test Specimen 1

Figure D.0: Tensile Test Data for T6 Test Specimen 1

T6 Test Specimen 2

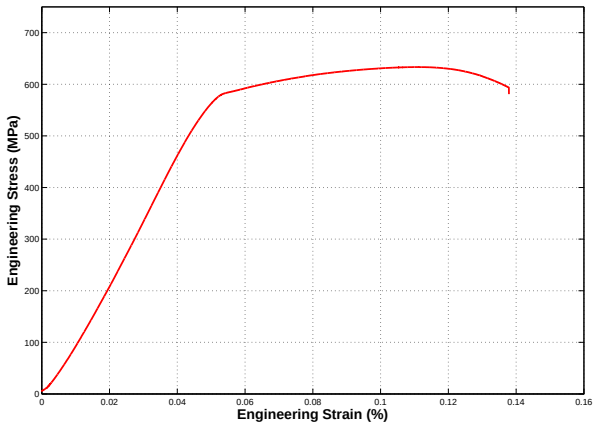

(d) Stress vs. Strain for T6 Test Specimen 2

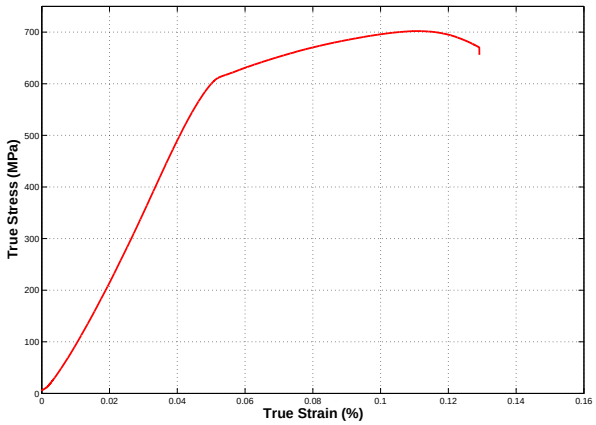

(e) True Stress vs. True Strain for T6 Test Specimen 2

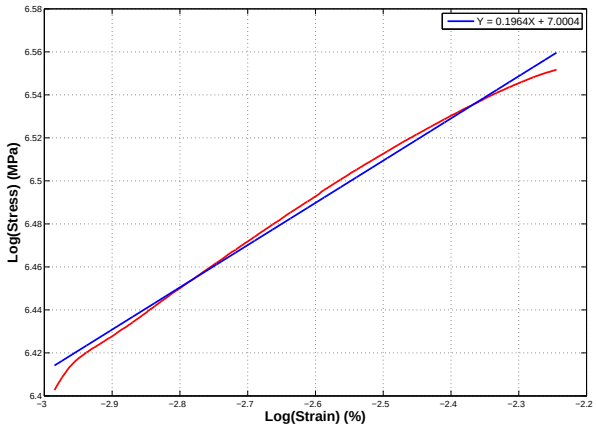

(f) Log(True Stress) vs. Log(True Strain) of Plastic Region for T6 Test Specimen 2

Figure D.0: Tensile Test Data for T6 Test Specimen 2

T6 Test Specimen 3

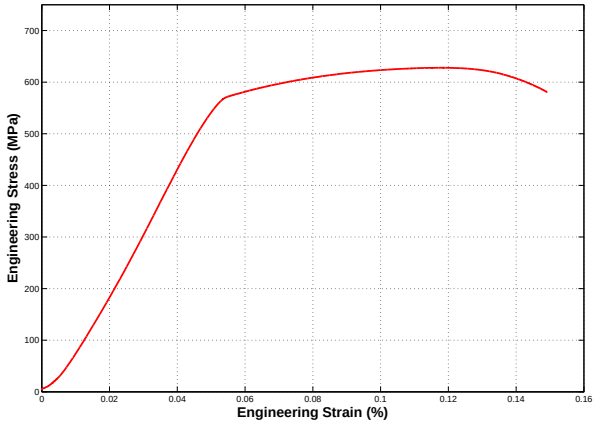

(g) Stress vs. Strain for T6 Test Specimen 3

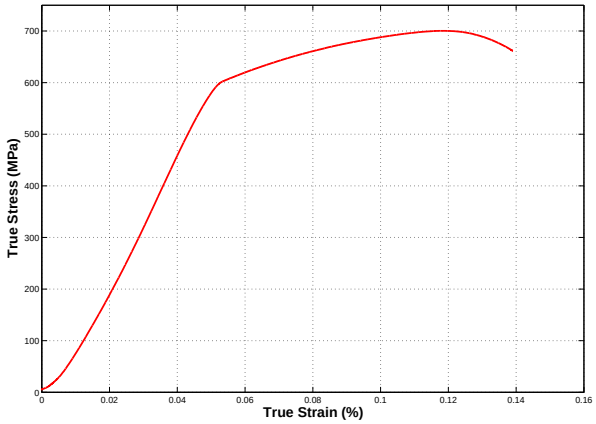

(h) True Stress vs. True Strain for T6 Test Specimen 3

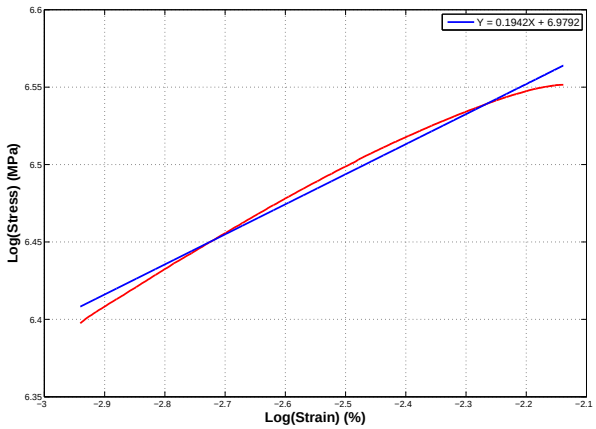

(i) Log(True Stress) vs. Log(True Strain) of Plastic Region for T6 Test Specimen 3

Figure D.0: Tensile Test Data for T6Test Specimen 3

D.0.2 Annealed Material Condition Tensile Test Graphs

Annealed Test Specimen 1

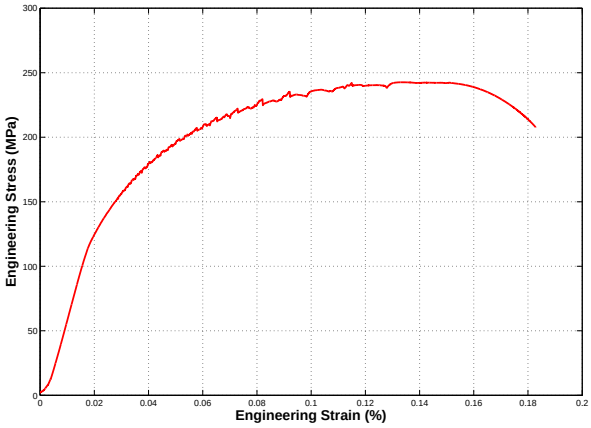

(j) Stress vs. Strain for Annealed Test Specimen 1

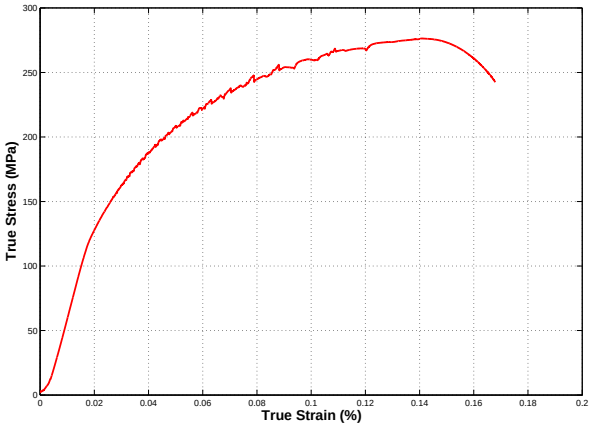

(k) True Stress vs. True Strain for Annealed Test Specimen 1

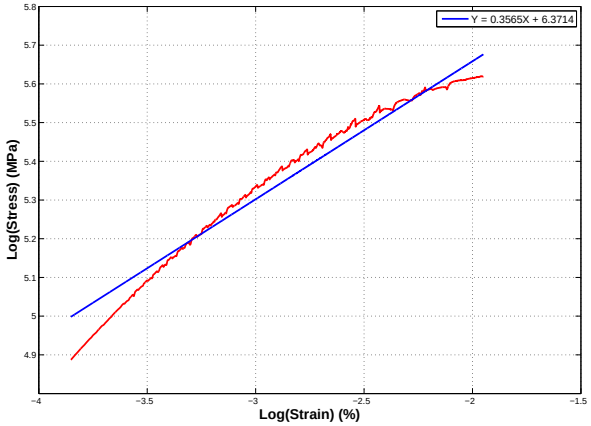

(l) Log(True Stress) vs. Log(True Strain) of Plastic Region for Annealed Test Specimen 1

Figure D.0: Tensile Test Data for Annealed Test Specimen 1

Annealed Test Specimen 2

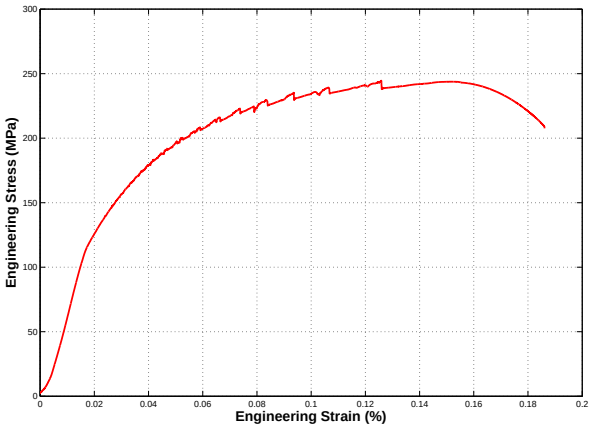

(m) Stress vs. Strain for Annealed Test Specimen 2

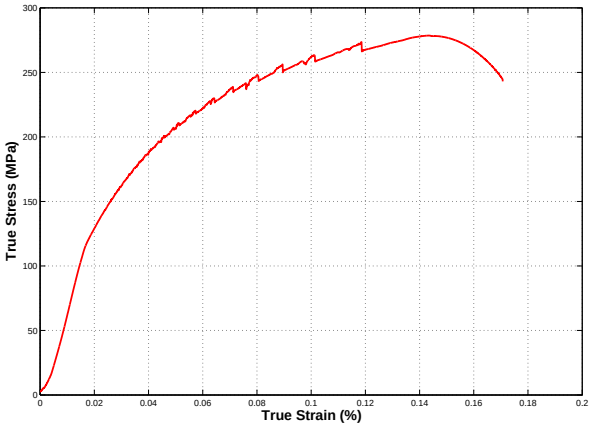

(n) True Stress vs. True Strain for Annealed Test Specimen 2

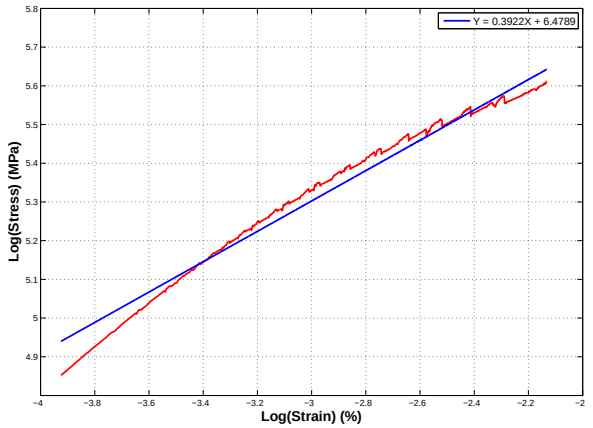

(o) Log(True Stress) vs. Log(True Strain) of Plastic Region for Annealed Test Specimen 2

Figure D.0: Tensile Test Data for Annealed Test Specimen 2

Annealed Test Specimen 3

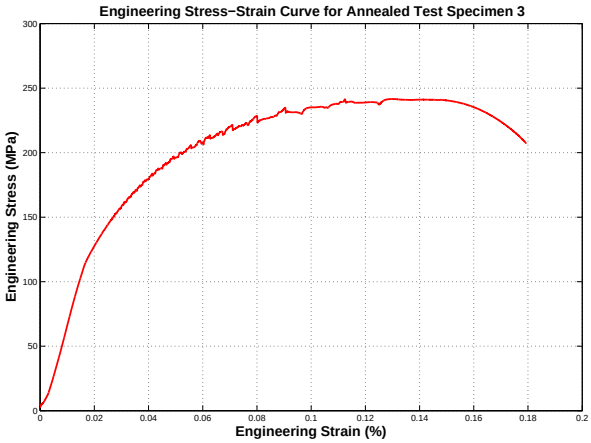

(p) Stress vs. Strain for Annealed Test Specimen 3

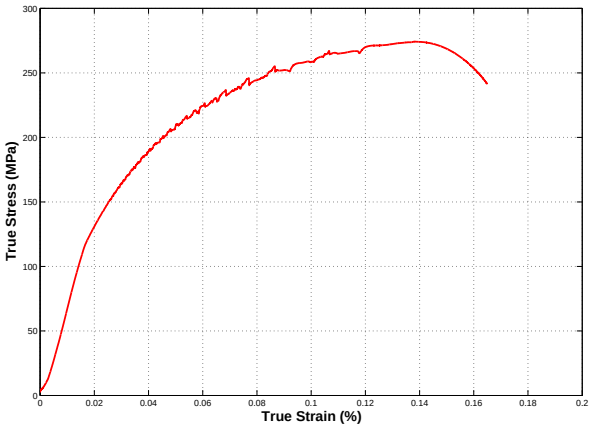

(q) True Stress vs. True Strain for Annealed Test Specimen 3

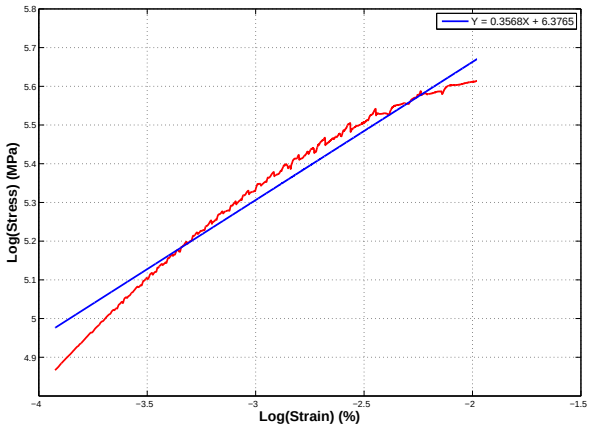

(r) Log(True Stress) vs. Log(True Strain) of Plastic Region for Annealed Test Specimen 3

Figure D.0: Tensile Test Data for Annealed Test Specimen 3

Appendix E

Surface Roughness Measurements

Group 1

- Material Condition: "As Machined"/T6

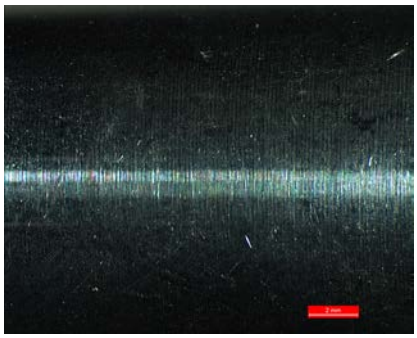

Figure E.1: "As Machined"/T6 Specimen Surface

Table E.1: Group 1: "As Machined" Surface Roughness Measurements (R_a)

Specimen Number	Diameter (mm)	Ra_1 (μm)	Ra_2 (μm)	Ra_3 (μm)	Ra_4 (μm)	Ra_5 (μm)	Std. Deviation	$Ra_{average}$ (μm)
1	16.98	0.68	0.75	0.68	0.66	0.65	0.03	0.68
2	16.93	0.82	0.80	0.82	0.82	0.80	0.01	0.81
3	16.92	0.75	0.73	0.72	0.72	0.76	0.02	0.74
4	16.94	0.77	0.72	0.73	0.70	0.70	0.03	0.72
				Average			**0.02**	**0.74**

- Material Condition: "As Machined"/Annealed

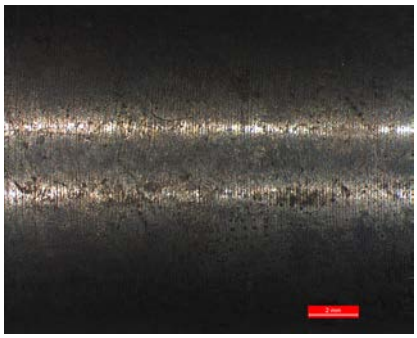

Figure E.2: "As Machined"/Annealed Specimen Surface

Table E.2: Group 1: Annealed Surface Roughness Measurements (R_a)

Specimen Number	Diameter (mm)	Ra_1 (μm)	Ra_2 (μm)	Ra_3 (μm)	Ra_4 (μm)	Ra_5 (μm)	Std. Deviation	$Ra_{average}$ (μm)
1	16.95	0.81	0.80	0.75	0.75	0.76	0.03	0.77
2	16.96	0.67	0.64	0.70	0.67	0.67	0.02	0.67
3	16.94	0.69	0.69	0.71	0.68	0.71	0.01	0.70
4	16.94	0.73	0.85	0.72	0.74	0.74	0.05	0.76
				Average			**0.03**	**0.72**

Group 2

- Material Condition: T6/Polished

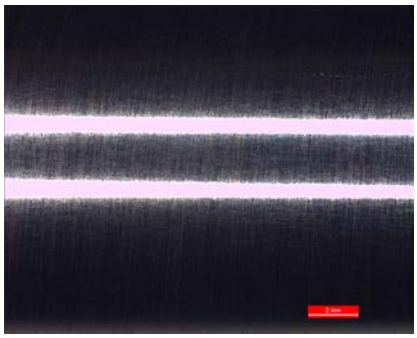

Figure E.3: T6/Polished Specimen Surface

Table E.3: Group 2: T6/Polished Surface Roughness Measurements (R_a)

Specimen Number	Diameter Before Polish (mm)	Diameter After Polish (mm)	Ra_1 (μm)	Ra_2 (μm)	Ra_3 (μm)	Ra_4 (μm)	Ra_5 (μm)	Std. Deviation	$Ra_{average}$ (μm)
1	16.95	16.90	0.19	0.22	0.20	0.23	0.22	0.01	0.21
2	17.00	16.94	0.22	0.25	0.22	0.24	0.22	0.02	0.23
3	16.98	16.93	0.23	0.23	0.21	0.22	0.21	0.01	0.22
4	16.99	16.93	0.22	0.22	0.23	0.23	0.23	0.00	0.23
					Average			**0.01**	**0.22**

- Material Condition: Annealed/Polished

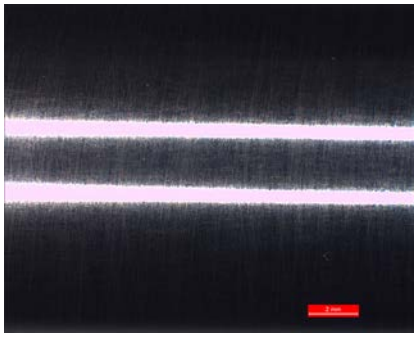

Figure E.4: Annealed/Polished Specimen Surface

Table E.4: Group 2: Annealed/Polished Surface Roughness Measurements (R_a)

Specimen Number	Diameter Before Polish (mm)	Diameter After Polish (mm)	Ra_1 (μm)	Ra_2 (μm)	Ra_3 (μm)	Ra_4 (μm)	Ra_5 (μm)	Std. Deviation	$Ra_{average}$ (μm)
1	17.00	16.94	0.19	0.22	0.20	0.23	0.22	0.01	0.21
2	17.00	16.96	0.22	0.25	0.22	0.24	0.22	0.02	0.23
3	16.98	16.90	0.23	0.23	0.21	0.22	0.21	0.01	0.22
4	16.90	16.86	0.22	0.22	0.23	0.23	0.23	0.00	0.23
					Average			**0.01**	**0.22**

Group 3

- Material Condition: T6/Polished/Shot Peened

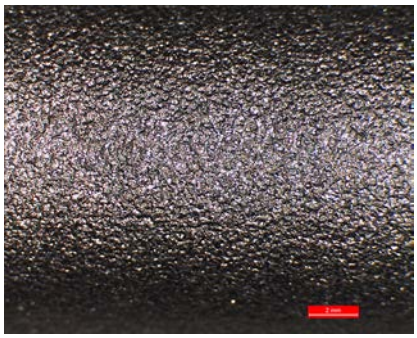

Figure E.5: T6/Polished/Shot Peened Specimen Surface

Table E.5: Group 3: T6/Polished/Shot Peened Surface Roughness Measurements (R_a)

Specimen Number	Diameter Before SP (mm)	Diameter After SP (mm)	Ra_1 (μm)	Ra_2 (μm)	Ra_3 (μm)	Ra_4 (μm)	Ra_5 (μm)	Std. Deviation	$Ra_{average}$ (μm)
1	17.10	17.08	8.23	7.98	9.81	8.96	8.30	0.66	8.66
2	17.07	17.04	8.00	8.99	8.33	8.46	8.82	0.35	8.52
3	17.06	17.04	8.04	8.52	8.28	8.40	8.90	0.28	8.43
				Average				**0.43**	**8.53**

- Material Condition: Annealed/Polished/Shot Peened

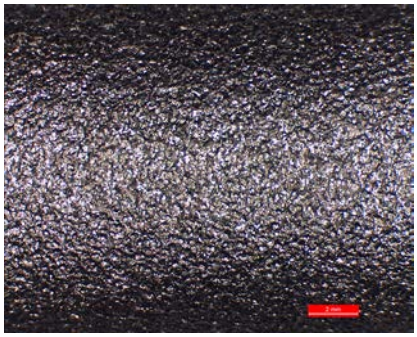

Figure E.6: Annealed/Polished/Shot Peened Specimen Surface

Table E.6: Group 3: Annealed/Polished/Shot Peened Surface Roughness Measurements (R_a)

Specimen Number	Diameter Before SP (mm)	Diameter After SP (mm)	Ra_1 (μm)	Ra_2 (μm)	Ra_3 (μm)	Ra_4 (μm)	Ra_5 (μm)	Std. Deviation	$Ra_{average}$ (μm)
1	17.08	17.05	11.55	12.03	12.68	11.30	11.93	0.47	11.90
2	17.09	17.06	10.13	11.30	10.53	12.60	12.75	1.06	11.46
3	17.10	17.07	11.28	10.18	11.87	11.10	11.11	0.54	11.11
				Average				**0.69**	**11.49**

Group 3

- Material Condition: T6/Polished/Shot Peened/Polished

Table E.7: Group 3: T6/Polished/Shot Peened/Polished Surface Roughness Measurements (R_a)

Specimen Number	Diameter (mm)	Ra_1 (μm)	Ra_2 (μm)	Ra_3 (μm)	Ra_4 (μm)	Ra_5 (μm)	Std. Deviation	$Ra_{average}$ (μm)
1 - Before Polish	17.03	6.33	7.10	7.52	8.01	8.46	0.74	7.48
1 - After Polish	16.94	0.24	0.24	0.27	0.24	0.24	0.01	0.25
2 - Before Polish	17.01	7.29	7.43	7.38	7.42	7.62	0.11	7.43
2 - After Polish	16.91	0.22	0.30	0.26	0.27	0.27	0.03	0.26
3 - Before Polish	17.04	8.07	7.72	8.76	9.17	8.05	0.53	8.35
3 - After Polish	16.96	0.20	0.22	0.23	0.20	0.20	0.01	0.21
Average - Before Polish							**0.46**	**7.76**
Average - After Polish							**0.02**	**0.24**

- Material Condition: Annealed/Polished/Shot Peened/Polished

Table E.8: Group 3: Annealed/Polished/Shot Peened/Polished Surface Roughness Measurements (R_a)

Specimen Number	Diameter (mm)	Ra_1 (μm)	Ra_2 (μm)	Ra_3 (μm)	Ra_4 (μm)	Ra_5 (μm)	Std. Deviation	$Ra_{average}$ (μm)
1 - Before Polish	17.05	9.81	11.09	11.86	10.63	10.14	0.72	10.71
1 - After Polish	16.90	0.20	0.21	0.19	0.22	0.20	0.01	0.20
2 - Before Polish	17.05	12.45	10.49	9.50	11.03	10.04	1.01	10.70
2 - After Polish	16.89	0.22	0.22	0.19	0.20	0.21	0.01	0.21
3 - Before Polish	17.06	9.61	10.83	12.82	10.23	10.29	1.10	10.76
3 - After Polish	16.93	0.20	0.20	0.23	0.20	0.21	0.01	0.21
Average - Before Polish							**0.94**	**10.72**
Average - After Polish							**0.01**	**0.21**

Group 4

- Material Condition: T6/Polished/Laser Shock Peened

Figure E.7: T6/Polished/Laser Shock Peened Specimen Surface

Table E.9: Group 4: T6/Polished/Laser Shock Peened Surface Roughness Measurements (R_a)

Specimen Number	Diameter Before LSP (mm)	Diameter After LSP (mm)	Ra_1 (μm)	Ra_2 (μm)	Ra_3 (μm)	Ra_4 (μm)	Ra_5 (μm)	Std. Deviation	$Ra_{average}$ (μm)
1	16.97	16.96	2.28	2.20	2.23	2.23	2.24	0.03	2.24
2	17.06	17.05	2.29	2.30	2.30	2.30	2.31	0.01	2.30
3	16.99	16.97	2.30	2.31	2.29	2.32	2.30	0.01	2.30
					Average			**0.02**	**2.28**

- Material Condition: Annealed/Polished/Laser Shock Peened

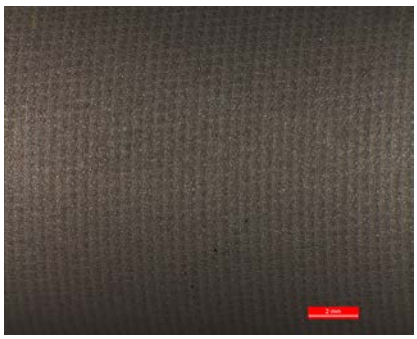

Figure E.8: Annealed/Polished/Laser Shock Peened Specimen Surface

Table E.10: Group 4: Annealed/Polished/Laser Shock Peened Surface Roughness Measurements (R_a)

Specimen Number	Diameter Before LSP (mm)	Diameter After LSP (mm)	Ra_1 (μm)	Ra_2 (μm)	Ra_3 (μm)	Ra_4 (μm)	Ra_5 (μm)	Std. Deviation	$Ra_{average}$ (μm)
1	17.05	17.03	3.14	3.20	3.22	3.25	3.20	0.04	3.25
2	17.02	17.00	3.35	3.36	3.32	3.37	3.35	0.02	3.35
3	17.00	16.98	3.21	3.33	3.29	3.24	3.26	0.04	3.27
					Average			**0.04**	**3.27**

Group 4

- Material Condition: T6/Polished/Laser Shock Peened/Polished

Table E.11: Group 4: T6/Polished/Laser Shock Peened/Polished Surface Roughness Measurements (R_a)

Specimen Number	Diameter (mm)	Ra_1 (μm)	Ra_2 (μm)	Ra_3 (μm)	Ra_4 (μm)	Ra_5 (μm)	Std. Deviation	$Ra_{average}$ (μm)
1 - Before Polish	17.17	2.22	2.23	2.25	2.25	2.26	0.01	2.24
1 - After Polish	17.12	0.20	0.19	0.20	0.21	0.21	0.01	0.20
2 - Before Polish	17.07	2.34	2.34	2.34	2.30	2.32	0.02	2.32
2 - After Polish	17.02	0.22	0.22	0.20	0.19	0.19	0.01	0.20
3 - Before Polish	17.07	2.26	2.30	2.31	2.30	2.31	0.02	2.30
3 - After Polish	17.01	0.19	0.19	0.21	0.20	0.20	0.01	0.20
Average - Before Polish							**0.03**	**2.29**
Average - After Polish							**0.01**	**0.20**

- Material Condition: Annealed/Polished/Laser Shock Peened/Polished

Table E.12: Group 4: Annealed/Polished/Laser Shock Peened/Polished Surface Roughness Measurements (R_a)

Specimen Number	Diameter (mm)	Ra_1 (μm)	Ra_2 (μm)	Ra_3 (μm)	Ra_4 (μm)	Ra_5 (μm)	Std. Deviation	$Ra_{average}$ (μm)
1 - Before Polish	17.05	3.22	3.20	3.25	3.25	3.25	0.02	3.23
1 - After Polish	17.00	0.19	0.18	0.18	0.20	0.18	0.01	0.19
2 - Before Polish	17.10	3.30	3.20	3.25	3.25	3.25	0.01	3.31
2 - After Polish	17.06	0.22	0.21	0.24	0.21	0.21	0.01	0.22
3 - Before Polish	17.07	3.33	3.33	3.29	3.34	3.32	0.02	3.32
3 - After Polish	17.02	0.24	0.20	0.20	0.20	0.21	0.02	0.21
Average - Before Polish							**0.03**	**3.29**
Average - After Polish							**0.01**	**0.18**

Group 5

- Material Condition: T6/Polished/Laser Shock Peened/Polished

Table E.13: Fatigue Life Healed Surface Roughness Measurements (R_a)

Specimen Number	Diameter (mm)	Ra_1 (μm)	Ra_2 (μm)	Ra_3 (μm)	Ra_4 (μm)	Ra_5 (μm)	Std. Deviation	$Ra_{average}$ (μm)
1 - Before Polish	16.97	2.30	2.25	2.28	2.23	2.28	0.02	2.27
1 - After Polish	16.92	0.18	0.18	0.22	0.21	0.20	0.02	0.20
2 - Before Polish	17.06	2.28	2.20	2.23	2.23	2.24	0.03	2.24
2 - After Polish	17.01	0.18	0.17	0.19	0.17	0.19	0.01	0.18
3 - Before Polish	17.06	2.29	2.30	2.30	2.30	2.31	0.01	2.30
3 - After Polish	17.00	0.17	0.18	0.17	0.17	0.19	0.01	0.18
4 - Before Polish	17.06	2.30	2.31	2.29	2.23	2.30	0.01	2.30
4 - After Polish	17.01	0.18	0.18	0.18	0.19	0.19	0.00	0.18
5 - Before Polish	17.10	2.28	2.28	2.31	2.30	2.30	0.01	2.29
5 - After Polish	17.05	0.17	0.19	0.19	0.18	0.17	0.01	0.18

Appendix F

Surface Roughness Profiles

Surface Morphology Results - Group 1

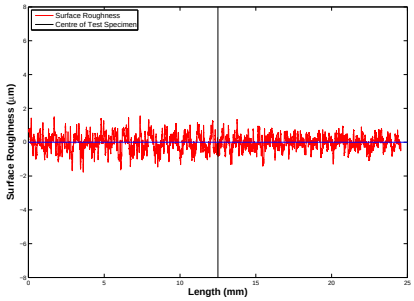

(a) Surface Roughness Profile of T6/"As Machined" Specimen 1

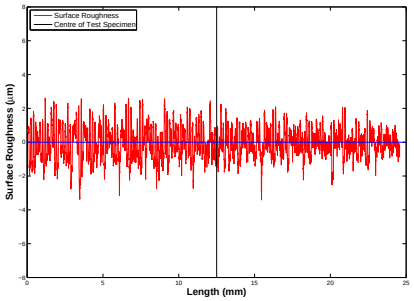

(b) Surface Roughness Profile of T6/"As Machined" Specimen 2

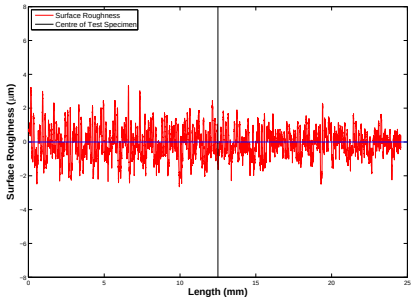

(c) Surface Roughness Profile of T6/"As Machined" Specimen 3

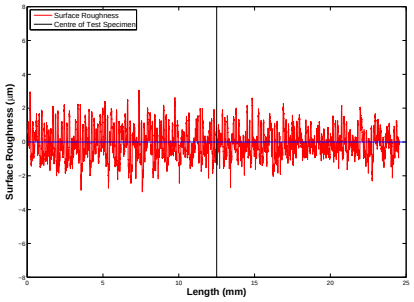

(d) Surface Roughness Profile of T6/"As Machined" Specimen 4

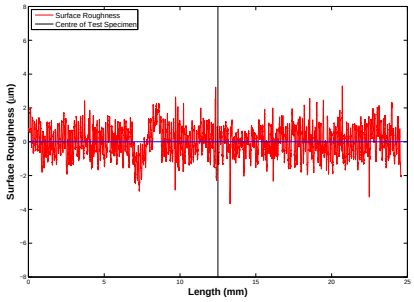

(e) Surface Roughness Profile of Annealed Specimen 1

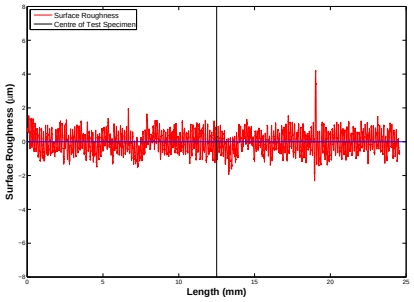

(f) Surface Roughness Profile of Annealed Specimen 2

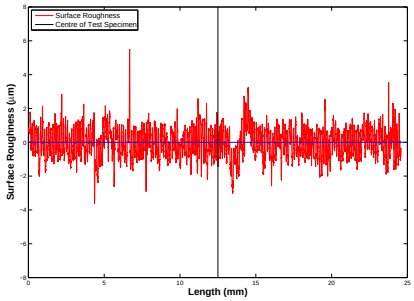

(g) Surface Roughness Profile of Annealed Specimen 3

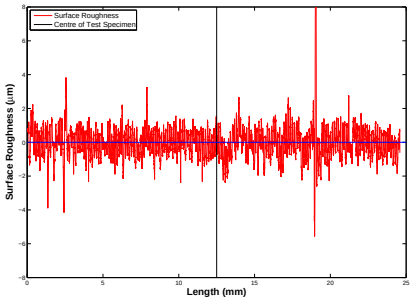

(h) Surface Roughness Profile of Annealed Specimen 4

Figure F.1: Group 1 Test Specimens Surface Roughness Profiles

Surface Morphology Results - Group 2

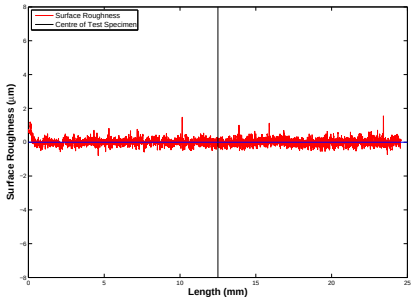

(a) Surface Roughness Profile of T6/Polished Specimen 1

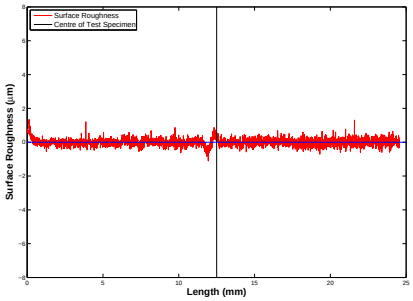

(b) Surface Roughness Profile of T6/Polished Specimen 2

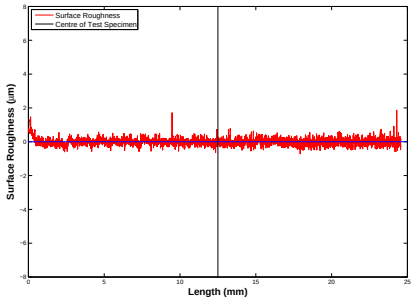

(c) Surface Roughness Profile of T6/Polished Specimen 3

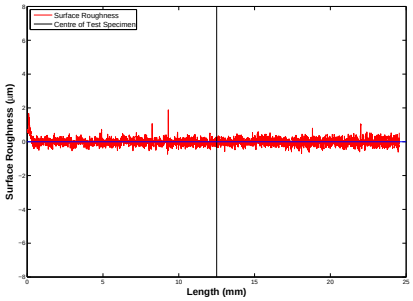

(d) Surface Roughness Profile of T6/Polished Specimen 4

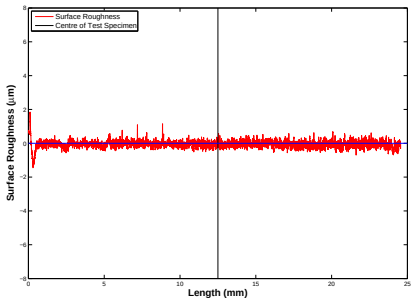

(e) Surface Roughness Profile of Annealed/Polished Specimen 1

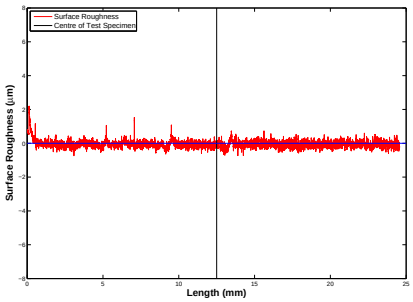

(f) Surface Roughness Profile of Annealed/Polished Specimen 2

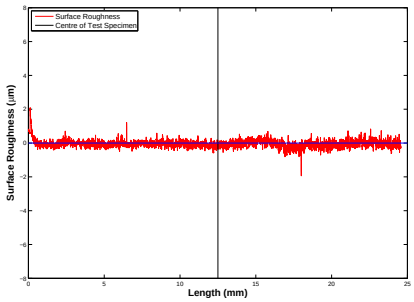

(g) Surface Roughness Profile of Annealed/Polished Specimen 3

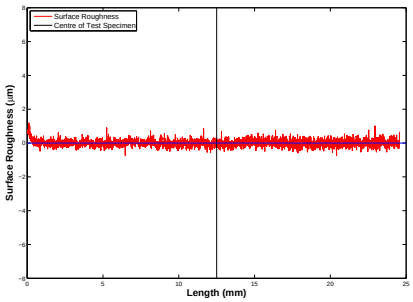

(h) Surface Roughness Profile of Annealed/Polished Specimen 4

Figure F.2: Group 2 Test Specimens Surface Roughness Profiles

Surface Morphology Results - Group 3 (Unpolished)

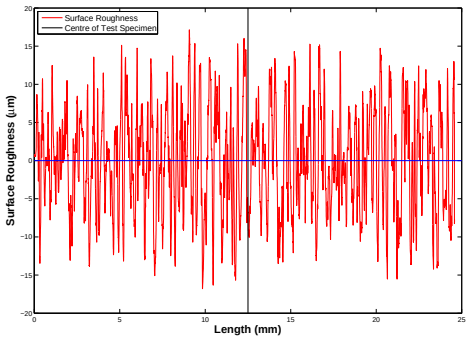

(a) Surface Roughness Profile of T6/Polished/Shot Peened Specimen 1

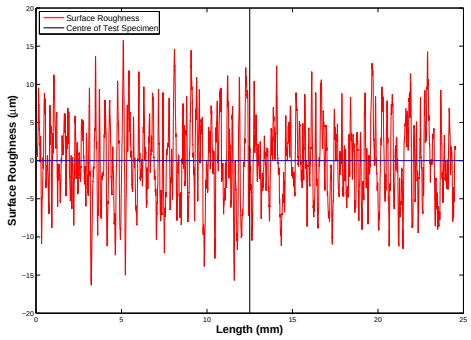

(b) Surface Roughness Profile of T6/Polished/Shot Peened Specimen 2

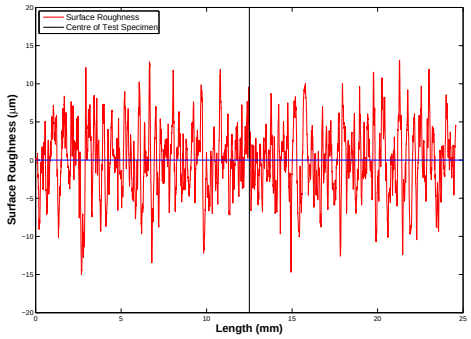

(c) Surface Roughness Profile of T6/Polished/Shot Peened Specimen 3

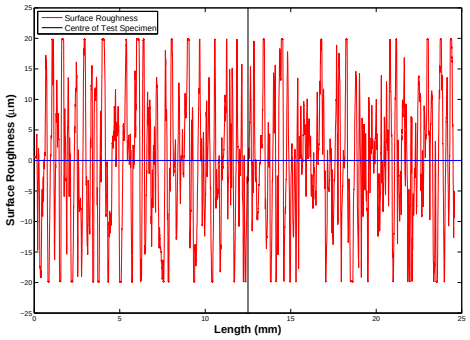

(d) Surface Roughness Profile of Annealed/Polished/Shot Peened Specimen 1

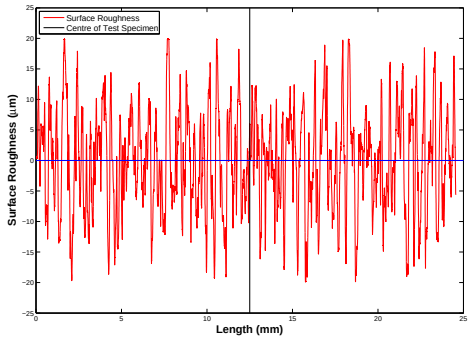

(e) Surface Roughness Profile of Annealed/Polished/Shot Peened Specimen 2

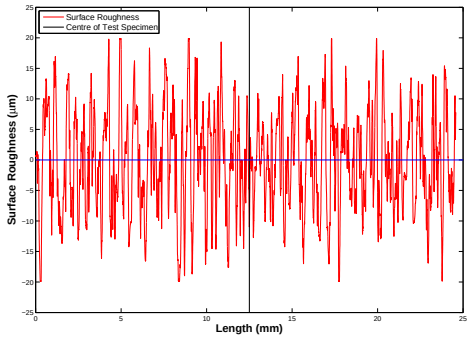

(f) Surface Roughness Profile of Annealed/Polished/Shot Peened Specimen 3

Figure F.3: Group 3 (Unpolished) Test Specimens Surface Roughness Profiles

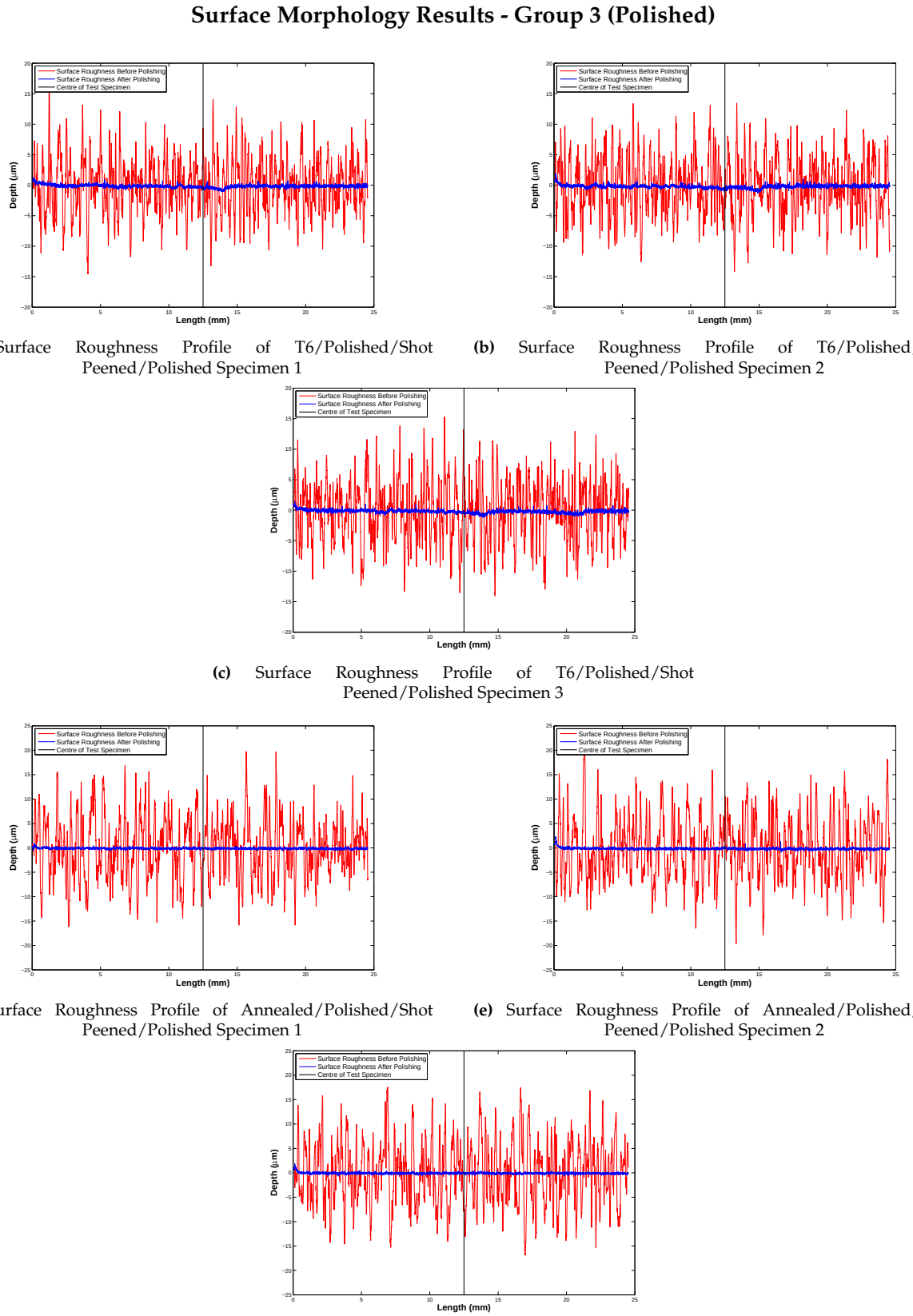

(a) Surface Roughness Profile of T6/Polished/Shot Peened/Polished Specimen 1

(b) Surface Roughness Profile of T6/Polished/Shot Peened/Polished Specimen 2

(c) Surface Roughness Profile of T6/Polished/Shot Peened/Polished Specimen 3

(d) Surface Roughness Profile of Annealed/Polished/Shot Peened/Polished Specimen 1

(e) Surface Roughness Profile of Annealed/Polished/Shot Peened/Polished Specimen 2

(f) Surface Roughness Profile of Annealed/Polished/Shot Peened/Polished Specimen 3

Figure F.4: Group 3 (Polished) Test Specimens Surface Roughness Profiles

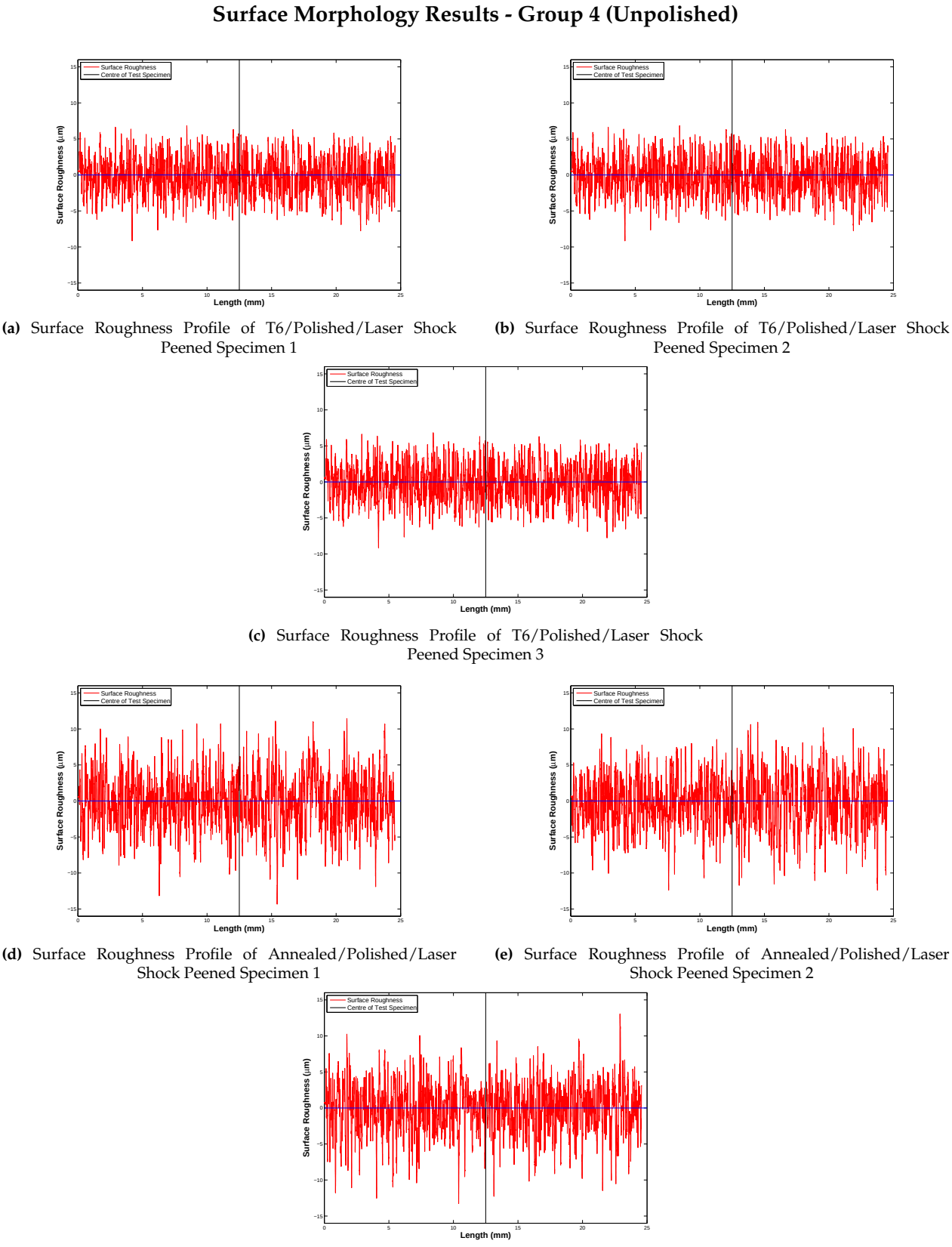

(a) Surface Roughness Profile of T6/Polished/Laser Shock Peened Specimen 1

(b) Surface Roughness Profile of T6/Polished/Laser Shock Peened Specimen 2

(c) Surface Roughness Profile of T6/Polished/Laser Shock Peened Specimen 3

(d) Surface Roughness Profile of Annealed/Polished/Laser Shock Peened Specimen 1

(e) Surface Roughness Profile of Annealed/Polished/Laser Shock Peened Specimen 2

(f) Surface Roughness Profile of Annealed/Polished/Laser Shock Peened Specimen 3

Figure F.5: Group 4 (Unpolished) Test Specimens Surface Roughness Profiles

Surface Morphology Results - Group 4 (Polished)

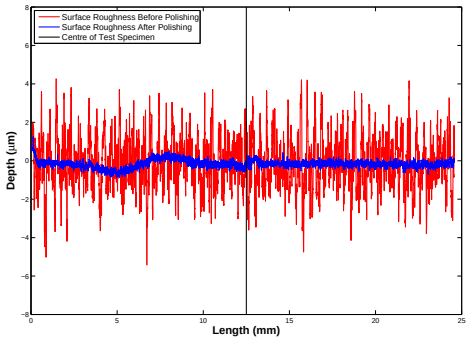

(a) Surface Roughness Profile of T6/Polished/Laser Shock Peened/Polished Specimen 1

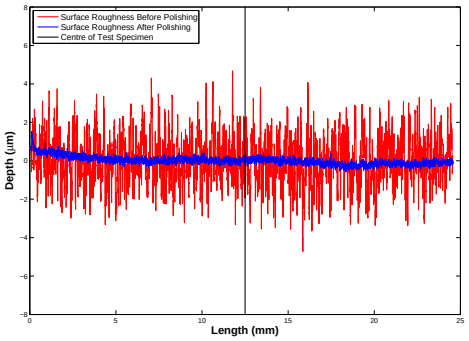

(b) Surface Roughness Profile of T6/Polished/Laser Shock Peened/Polished Specimen 2

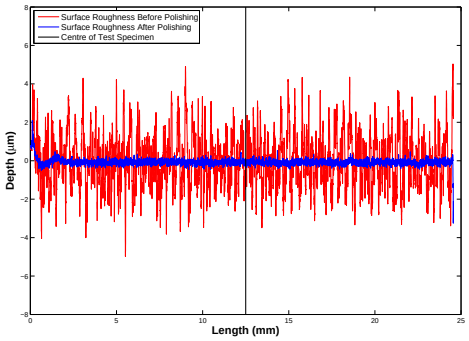

(c) Surface Roughness Profile of T6/Polished/Laser Shock Peened/Polished Specimen 3

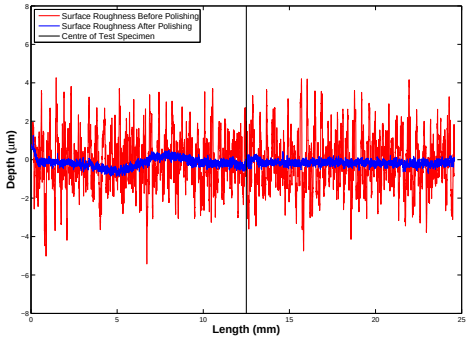

(d) Surface Roughness Profile of Annealed/Polished/Laser Shock Peened/Polished Specimen 1

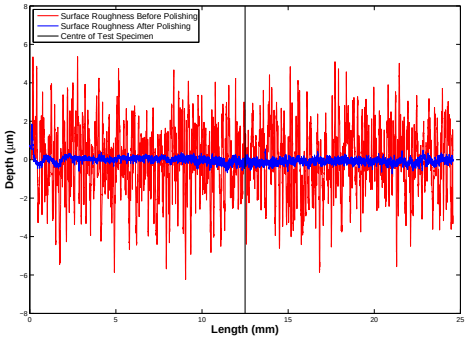

(e) Surface Roughness Profile of Annealed/Polished/Laser Shock Peened/Polished Specimen 2

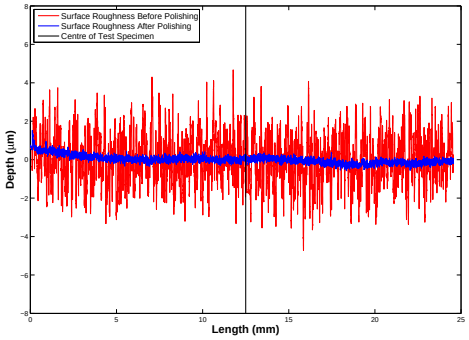

(f) Surface Roughness Profile of Annealed/Polished/Laser Shock Peened/Polished Specimen 3

Figure F.6: Group 4 (Polished) Test Specimens Surface Roughness Profiles

Surface Morphology Results: Group 5 - Before Partial Fatiguing Process

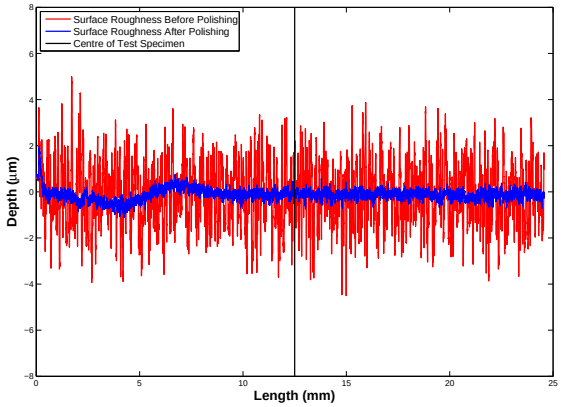

(a) Surface Roughness Profile of Fatigue Life Healed Specimen 1

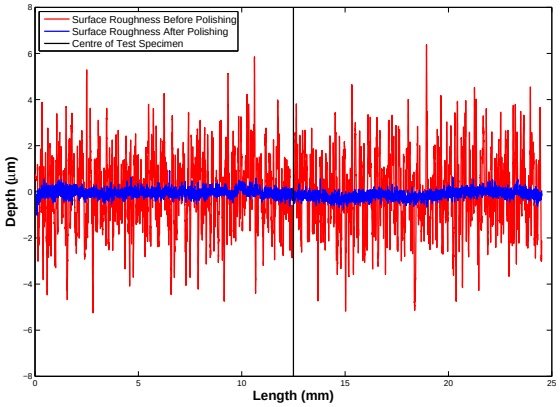

(b) Surface Roughness Profile of Fatigue Life Healed Specimen 2

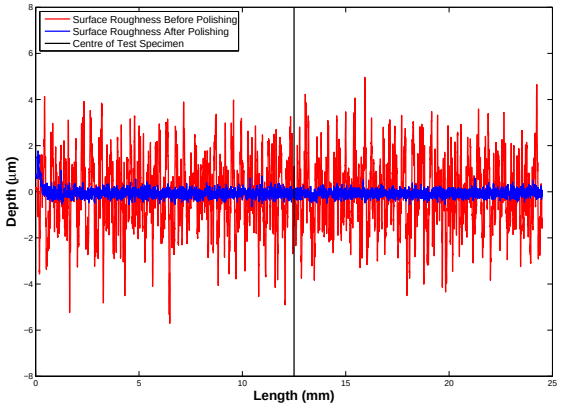

(c) Surface Roughness Profile of Fatigue Life Healed Specimen 3

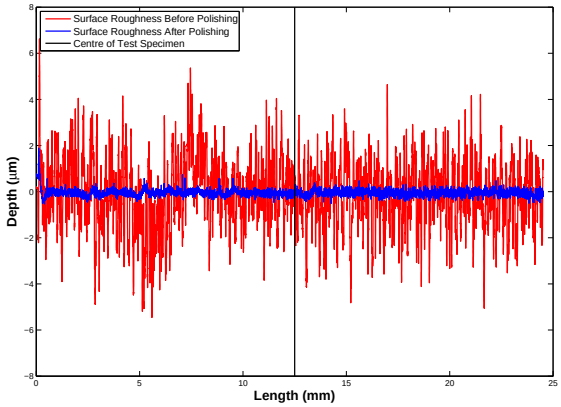

(d) Surface Roughness Profile of Fatigue Life Healed Specimen 4

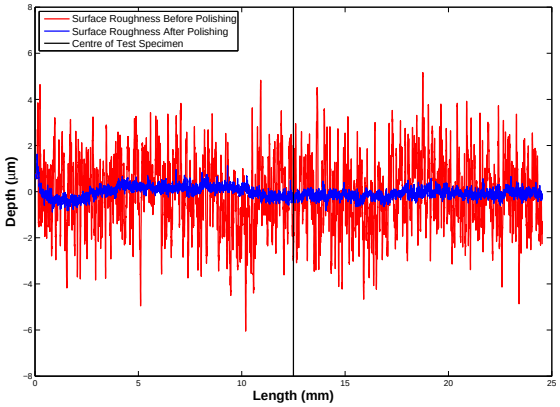

(e) Surface Roughness Profile of Fatigue Life Healed Specimen 5

Figure F.7: Surface Morphology Results: Group 5 - Before Partial Fatiguing Process

Surface Morphology Results: Group 5 - Before Final Fatiguing Process

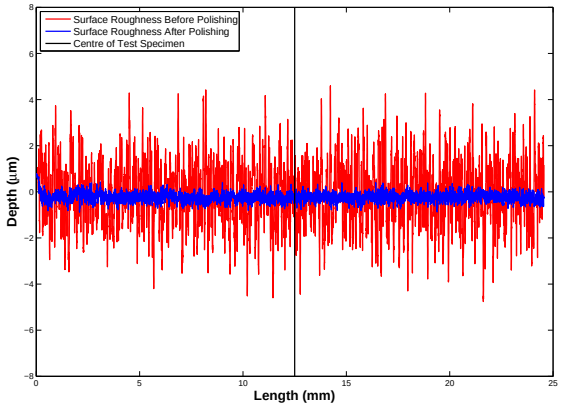

(a) Surface Roughness Profile of Fatigue Life Healed Specimen 1

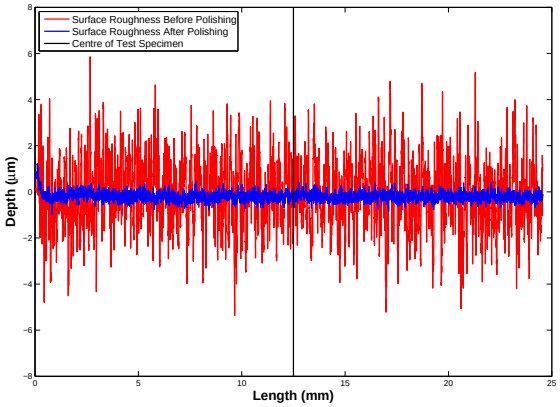

(b) Surface Roughness Profile of Fatigue Life Healed Specimen 2

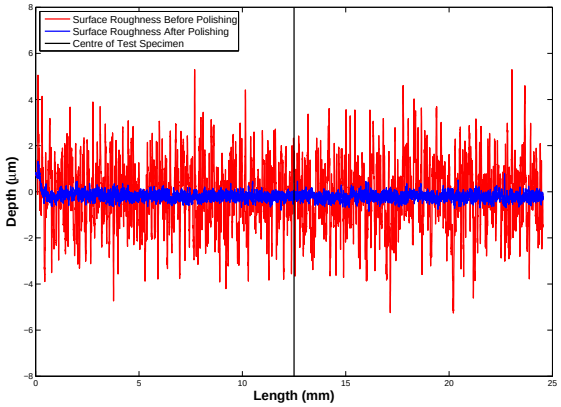

(c) Surface Roughness Profile of Fatigue Life Healed Specimen 3

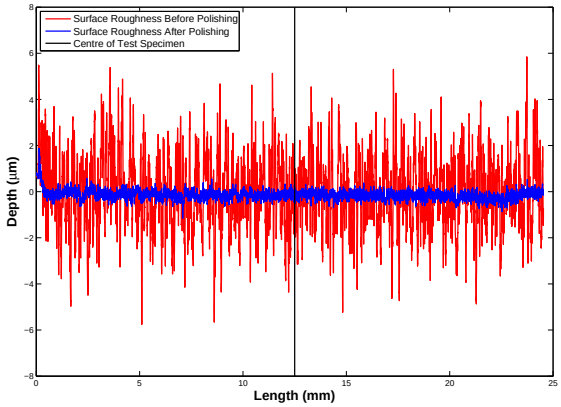

(d) Surface Roughness Profile of Fatigue Life Healed Specimen 4

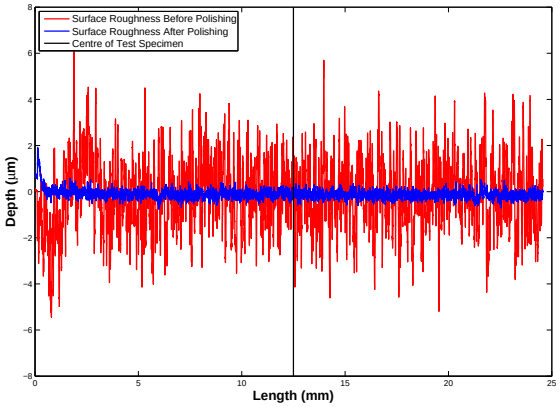

(e) Surface Roughness Profile of Fatigue Life Healed Specimen 5

Figure F.8: Surface Morphology Results: Group 5 - Before Final Fatiguing Process

Appendix G

Fatigue Life Test Results

All Test Groups

Table G.1: Experimental Process Fatigue Data Averages

Group	Material Condition	Average Diameter	Applied Stress	Average Observable Crack Length	Cycles to	Cycles to
	(mm)	(μm)	(kN)	(mm)	Crack Initiation	Failure
1	T6	16.94	585.00	2.95	28137	32167
	AN	16.95	450.00	2.48	26335	29190
2	T6	16.92	585.00	2.01	35722	39307
	AN	16.92	450.00	1.83	30102	33307
3	T6	17.05	585.00	3.70	59723	61971
SP	AN	17.06	450.00	3.47	14550	16276
3	T6	16.94	585.00	2.06	125693	131653
SP/Polished	AN	16.91	450.00	2.00	22236	25774
4	T6	16.99	585.00	3.37	91462	95806
LSP	AN	17.00	450.00	3.20	25471	27531
4	T6	16.99	585.00	1.60	207661	211271
LSP/Polished	AN	16.98	450.00	1.77	28317	32425

** Note: SP - Shot Peened; LSP - Laser Shock Peened; AN - Annealed*

Group 1

- Material Condition: "As Machined"/T6

Table G.2: Group 1 Fatigue Results: "As Machined"/T6 Test Specimens

Specimen Number	Diameter (mm)	Applied Stress (MPa)	Applied Force (kN)	P_{max} (kN)	P_{min} (kN)	P_{mean} (kN)	Amplitude (kN)	Crack Initiation Length (mm)	Cycles to Crack Initiation	Cycles to Failure
1	16.98	585.00	16.54	18.38	1.84	-10.11	8.27	3.00	24003	28434
2	16.93	585.00	16.39	18.22	1.82	-10.02	8.20	2.70	27046	30241
3	16.92	585.00	16.92	18.18	1.82	-10.00	8.18	2.80	28120	32980
4	16.94	585.00	16.42	18.25	1.82	-10.04	8.21	3.30	33378	37013
Average	**16.94**	**585.00**	**16.43**	**18.26**	**1.83**	**-10.04**	**8.22**	**2.95**	**28137**	**32167**

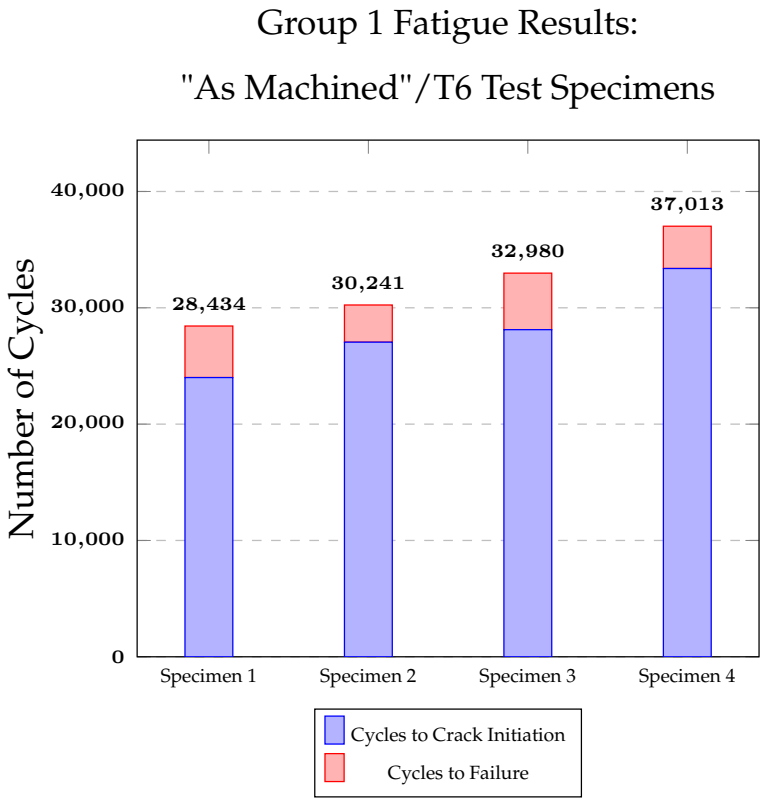

Figure G.1: Group 1 Fatigue Results: "As Machined"/T6 Test Specimens

- Material Condition: "As Machined"/Annealed

Table G.3: Group 1 Fatigue Results: "As Machined"/Annealed Test Specimens

Specimen Number	Diameter (mm)	Applied Stress (MPa)	Applied Force (kN)	P_{max} (kN)	P_{min} (kN)	P_{mean} (kN)	Amplitude (kN)	Crack Initiation Length (mm)	Cycles to Crack Initiation	Cycles to Failure
1	16.95	450.00	12.66	14.06	1.41	-7.73	6.33	2.20	30089	32198
2	16.96	450.00	12.68	14.09	1.41	-7.75	6.34	2.90	21236	24875
3	16.94	450.00	12.63	14.04	1.40	-7.72	6.32	2.00	24269	27017
4	16.94	450.00	12.63	14.04	1.40	-7.72	6.32	2.80	29747	32670
Average	**16.95**	**450.00**	**12.65**	**14.06**	**1.41**	**-7.73**	**6.32**	**2.48**	**26335**	**29190**

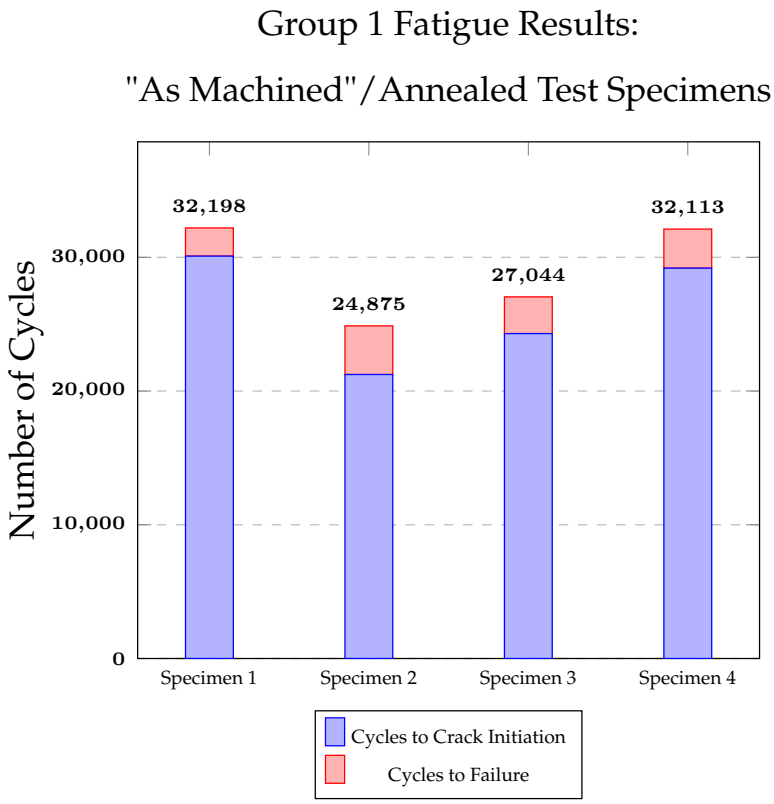

Figure G.2: Group 1 Fatigue Results: "As Machined"/Annealed Test Specimens

Group 2

- Material Condition: T6/Polished

Table G.4: Group 2 Fatigue Results: T6/Polished Test Specimens

Specimen Number	Diameter (mm)	Applied Stress (MPa)	Applied Force (kN)	P_{max} (kN)	P_{min} (kN)	P_{mean} (kN)	Amplitude (kN)	Crack Initiation Length (mm)	Cycles to Crack Initiation	Cycles to Failure
1	16.90	585.00	16.31	18.12	1.81	-9.97	8.15	2.80	37022	40037
2	16.94	585.00	16.42	18.25	1.82	-10.04	8.21	1.50	33812	37013
3	16.93	585.00	16.39	18.22	1.82	-10.02	8.20	1.90	36146	40058
4	16.93	585.00	16.39	18.22	1.82	-10.02	8.20	2.10	35906	40121
Average	**16.93**	**585.00**	**16.38**	**18.20**	**1.82**	**-10.01**	**8.19**	**2.01**	**35722**	**39307**

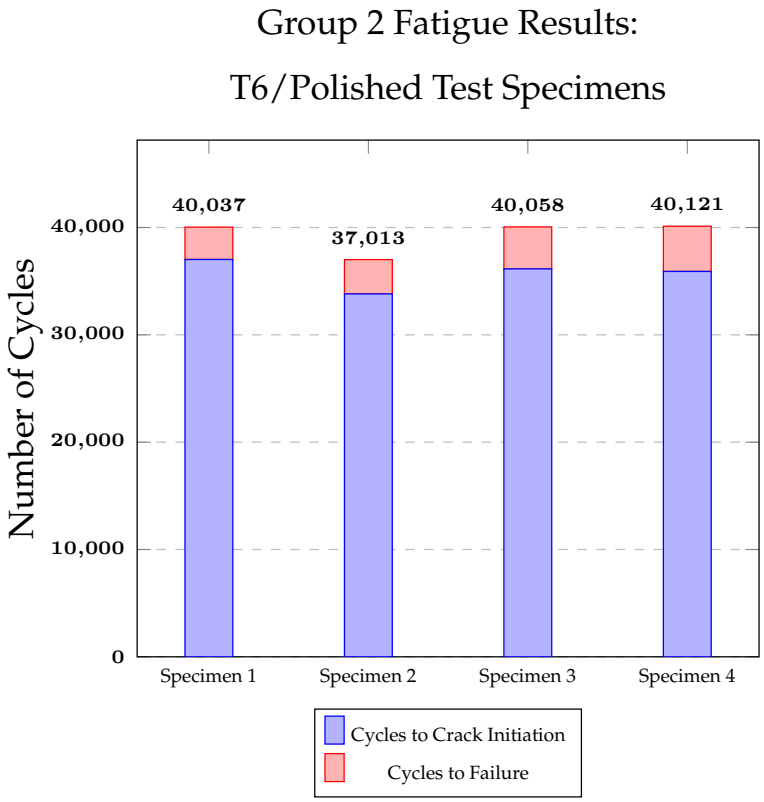

Figure G.3: Group 2 Fatigue Results: T6/Polished Test Specimens

- Material Condition: Annealed/Polished

Table G.5: Group 2 Fatigue Results: Annealed/Polished Test Specimens

Specimen Number	Diameter (mm)	Applied Stress (MPa)	Applied Force (kN)	P_{max} (kN)	P_{min} (kN)	P_{mean} (kN)	Amplitude (kN)	Crack Initiation Length (mm)	Cycles to Crack Initiation	Cycles to Failure
1	16.94	450.00	12.63	14.04	1.40	-7.72	6.32	2.20	31156	34243
2	16.96	450.00	12.68	14.09	1.41	-7.75	6.34	1.20	30776	34067
3	16.90	450.00	12.54	13.94	1.39	-7.67	6.27	1.90	28845	32166
4	16.86	450.00	12.45	13.84	1.38	-7.61	6.23	2.00	29632	32750
Average	**16.92**	**450.00**	**12.58**	**13.98**	**1.40**	**-7.67**	**6.23**	**1.83**	**30102**	**33307**

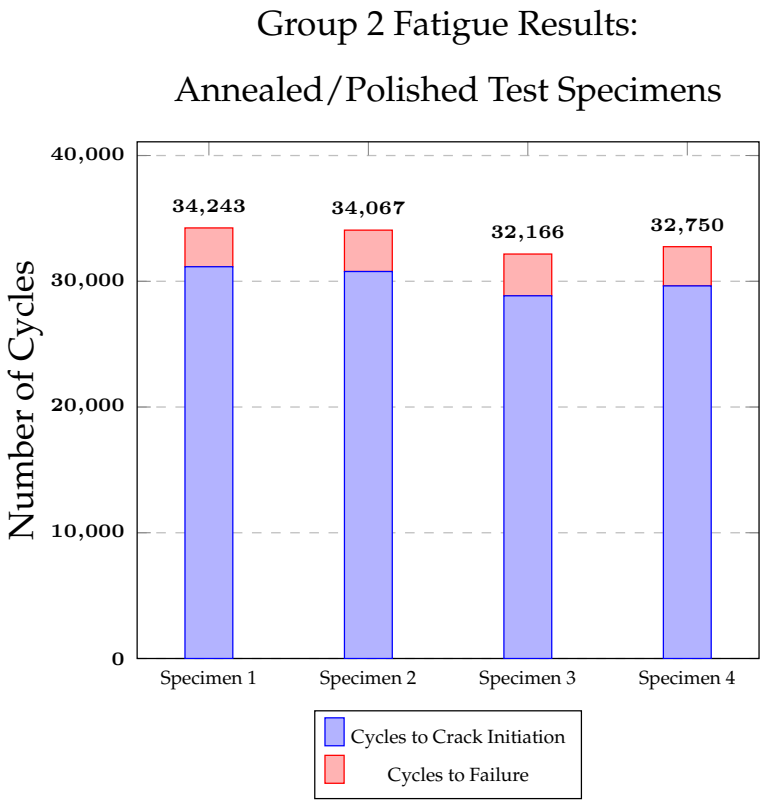

Figure G.4: Group 2 Fatigue Results: Annealed/Polished Test Specimens

Group 3

- Material Condition: T6/Polished/Shot Peened

Table G.6: Group 3 Fatigue Results: T6/Polished/Shot Peened Test Specimens

Specimen Number	Diameter (mm)	Applied Stress (MPa)	Applied Force (kN)	P_{max} (kN)	P_{min} (kN)	P_{mean} (kN)	Amplitude (kN)	Crack Initiation Length (mm)	Cycles to Crack Initiation	Cycles to Failure
1	17.08	585.00	16.83	18.70	1.87	-10.29	8.42	3.30	66848	69057
2	17.04	585.00	16.72	18.57	1.86	-10.21	8.36	4.00	53922	55870
3	17.04	585.00	16.72	18.57	1.86	-10.21	8.36	3.80	59723	61971
Average	**17.05**	**585.00**	**16.75**	**18.62**	**1.86**	**-10.24**	**8.38**	**3.70**	**59723**	**61971**

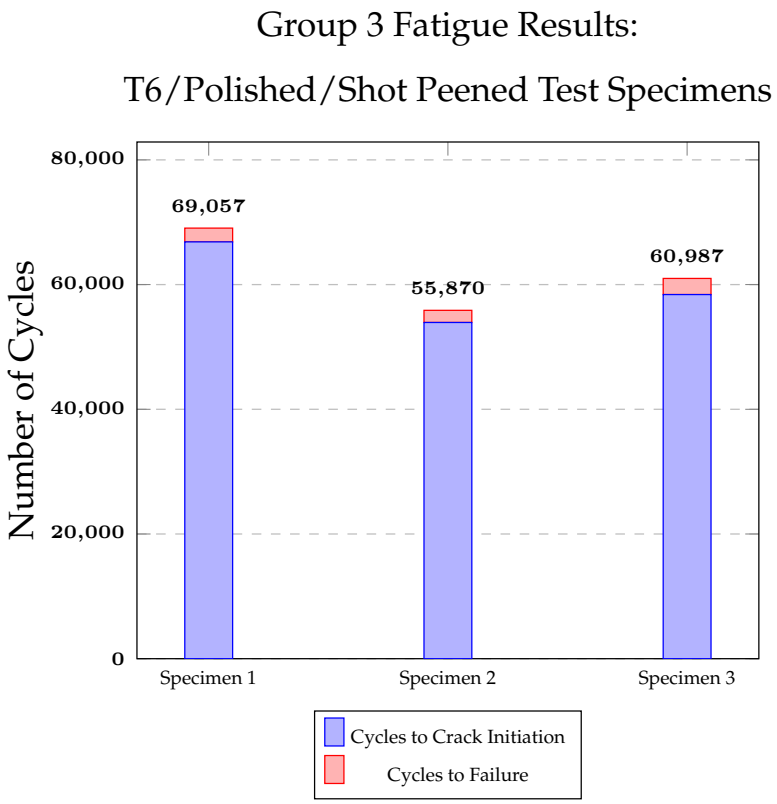

Figure G.5: Group 3 Fatigue Results: T6/Polished/Shot Peened Test Specimens

- Material Condition: Annealed/Polished/Shot Peened

Table G.7: Group 3 Fatigue Results: Annealed/Polished/Shot Peened Test Specimens

Specimen Number	Diameter (mm)	Applied Stress (MPa)	Applied Force (kN)	P_{max} (kN)	P_{min} (kN)	P_{mean} (kN)	Amplitude (kN)	Crack Initiation Length (mm)	Cycles to Crack Initiation	Cycles to Failure
1	17.05	450.00	12.88	14.31	1.43	-7.87	6.44	3.00	14432	16470
2	17.06	450.00	12.90	14.34	1.43	-7.89	6.45	3.40	12877	14361
3	17.07	450.00	12.93	14.36	1.44	-7.90	6.46	4.10	16341	17997
Average	**17.06**	**450.00**	**12.90**	**14.34**	**1.43**	**-7.89**	**6.45**	**3.50**	**14550**	**16276**

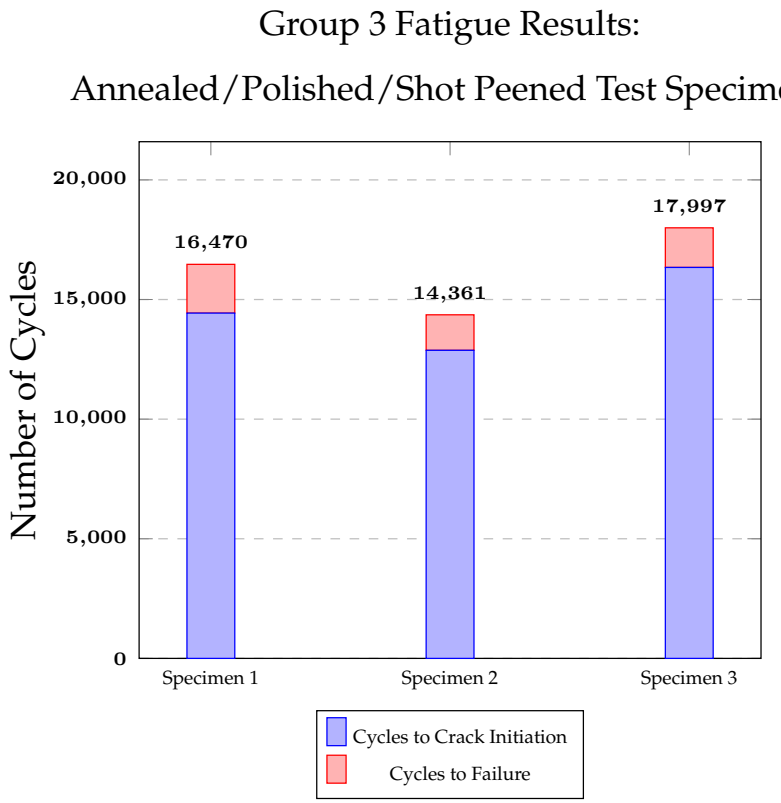

Figure G.6: Group 3 Fatigue Results: Annealed/Polished/Shot Peened Test Specimens

Group 3

- Material Condition: T6/Polished/Shot Peened/Polished

Table G.8: Group 3 Fatigue Results: T6/Polished/Shot Peened/Polished Test Specimens

Specimen Number	Diameter (mm)	Applied Stress (MPa)	Applied Force (kN)	P_{max} (kN)	P_{min} (kN)	P_{mean} (kN)	Amplitude (kN)	Crack Initiation Length (mm)	Cycles to Crack Initiation	Cycles to Failure
1	16.94	585.00	16.42	18.25	1.82	-10.04	8.21	2.10	145981	151867
2	16.91	585.00	16.34	18.15	1.82	-9.98	8.17	2.10	127520	133037
3	16.96	585.00	16.48	18.31	1.83	-10.07	8.24	2.00	103579	110056
Average	**16.94**	**585.00**	**16.41**	**18.24**	**1.82**	**-10.03**	**8.21**	**2.06**	**125693**	**131653**

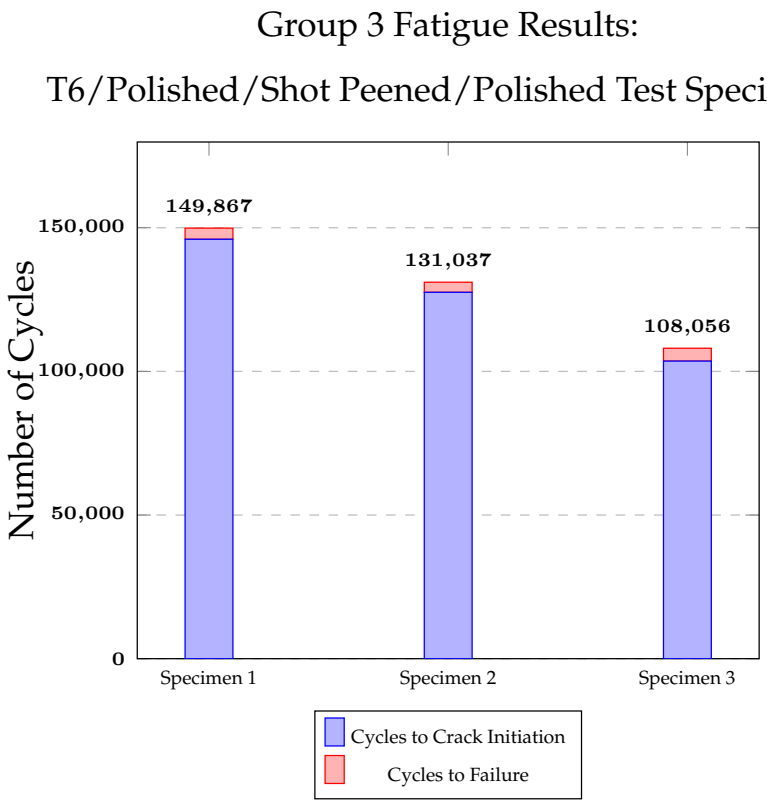

Figure G.7: Group 3 Fatigue Results: T6/Polished/Shot Peened/Polished Test Specimens

- Material Condition: Annealed/Polished/Shot Peened/Polished

Table G.9: Group 3 Fatigue Results: Annealed/Polished/Shot Peened/Polished Test Specimens

Specimen Number	Diameter (mm)	Applied Stress (MPa)	Applied Force (kN)	P_{max} (kN)	P_{min} (kN)	P_{mean} (kN)	Amplitude (kN)	Crack Initiation Length (mm)	Cycles to Crack Initiation	Cycles to Failure
1	16.90	450.00	12.54	13.94	1.39	-7.67	6.27	1.90	20860	23875
2	16.89	450.00	12.52	13.91	1.39	-7.65	6.26	2.10	21277	24630
3	16.93	450.00	12.61	14.01	1.40	-7.71	6.31	2.00	24570	28756
Average	**16.91**	**450.00**	**12.56**	**13.95**	**1.40**	**-7.67**	**6.28**	**2.00**	**22236**	**25754**

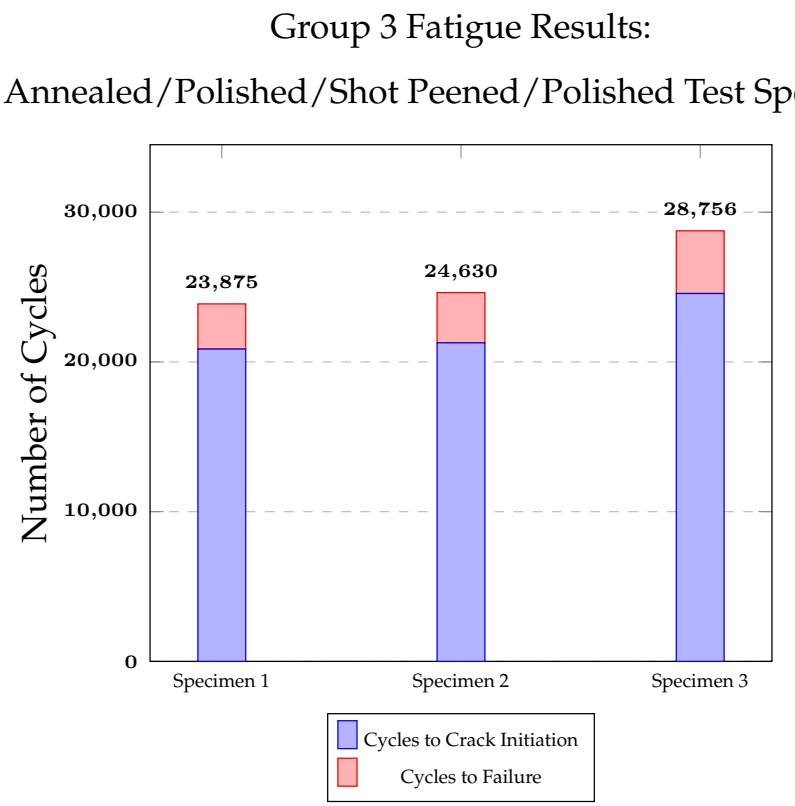

Figure G.8: Group 3 Fatigue Results: Annealed/Polished/Shot Peened/Polished Test Specimens

Group 4

- Material Condition: T6/Polished/Laser Shock Peened

Table G.10: Group 4 Fatigue Results: T6/Polished/Laser Shock Peened Test Specimens

Specimen Number	Diameter (mm)	Applied Stress (MPa)	Applied Force (kN)	P_{max} (kN)	P_{min} (kN)	P_{mean} (kN)	Amplitude (kN)	Crack Initiation Length (mm)	Cycles to Crack Initiation	Cycles to Failure
1	16.96	585.00	16.48	18.31	1.83	-10.07	8.24	3.20	98589	102786
2	17.05	585.00	16.72	18.61	1.86	-10.23	8.37	3.40	89500	92797
3	16.97	585.00	16.51	18.34	1.83	-10.09	8.26	3.50	86298	91834
Average	**16.99**	**585.00**	**16.58**	**18.42**	**1.84**	**-10.13**	**8.29**	**3.37**	**91462**	**95806**

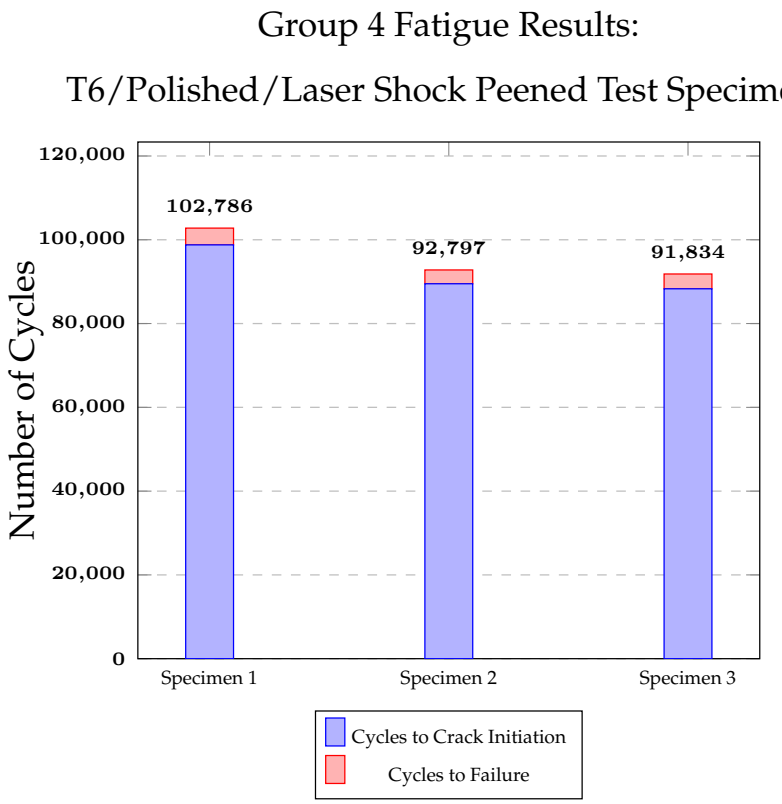

Figure G.9: Group 4 Fatigue Results: T6/Polished/Laser Shock Peened Test Specimens

- Material Condition: Annealed/Polished/Laser Shock Peened

Table G.11: Group 4 Fatigue Results: Annealed/Polished/Laser Shock Peened Test Specimens

Specimen Number	Diameter (mm)	Applied Stress (MPa)	Applied Force (kN)	P_{max} (kN)	P_{min} (kN)	P_{mean} (kN)	Amplitude (kN)	Crack Initiation Length (mm)	Cycles to Crack Initiation	Cycles to Failure
1	17.03	450.00	12.84	14.26	1.43	-7.84	6.42	3.50	26277	28423
2	17.00	450.00	12.77	14.19	1.42	-7.80	6.32	3.20	25000	26984
3	16.98	450.00	12.72	14.14	1.41	-7.77	6.36	2.90	25135	27187
Average	**17.00**	**450.00**	**12.78**	**14.19**	**1.42**	**-7.81**	**6.39**	**3.20**	**25471**	**27531**

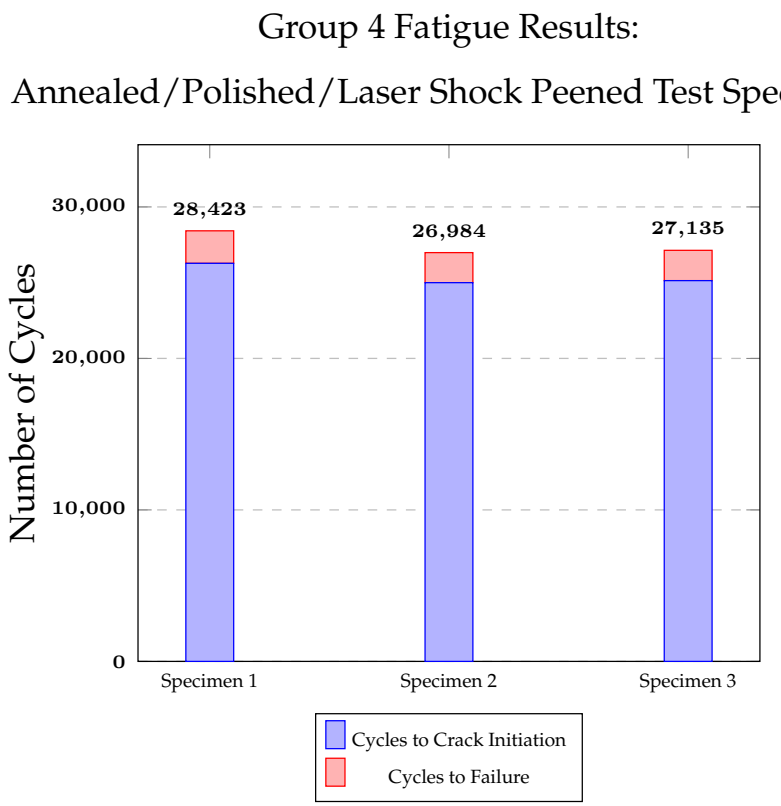

Figure G.10: Group 4 Fatigue Results: Annealed/Polished/Laser Shock Peened Test Specimens

Group 4

- Material Condition: T6/Polished/Laser Shock Peened/Polished

Table G.12: Group 4 Fatigue Results: T6/Polished/Laser Shock Peened/Polished Test Specimens

Specimen Number	Diameter (mm)	Applied Stress (MPa)	Applied Force (kN)	P_{max} (kN)	P_{min} (kN)	P_{mean} (kN)	Amplitude (kN)	Crack Initiation Length (mm)	Cycles to Crack Initiation	Cycles to Failure
1	16.96	585.00	16.48	18.31	1.83	-10.07	8.24	1.20	196660	200567
2	17.05	585.00	16.74	18.61	1.86	-10.23	8.37	1.50	251962	255338
3	16.97	585.00	16.51	18.34	1.83	-10.09	8.26	2.10	174360	177907
Average	**16.99**	**585.00**	**16.58**	**18.42**	**1.84**	**-10.13**	**8.29**	**1.60**	**207661**	**211271**

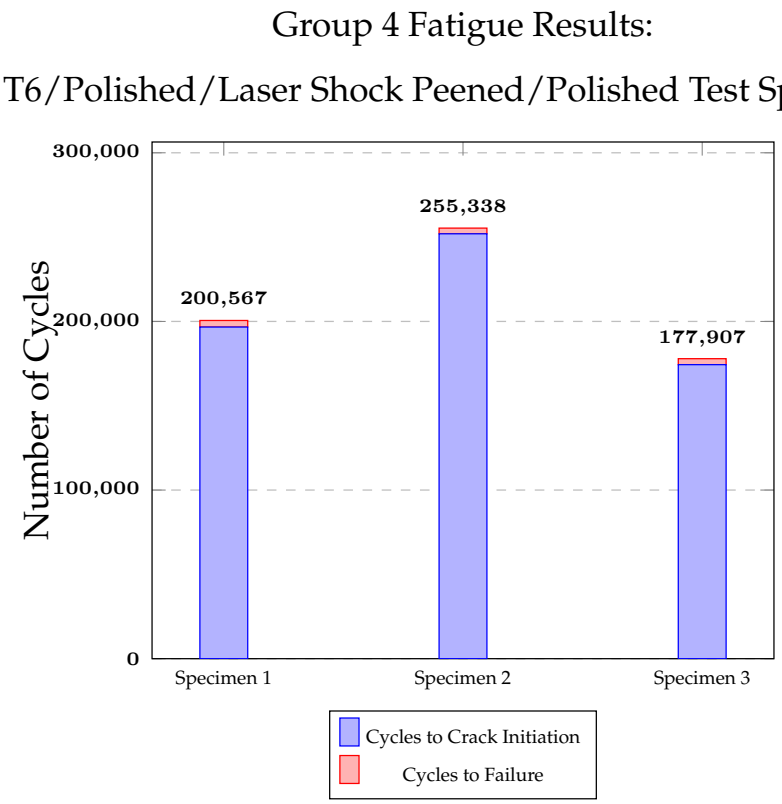

Figure G.11: Group 4 Fatigue Results: T6/Polished/Laser Shock Peened/Polished Test Specimens

- Material Condition: Annealed/Polished/Laser Shock Peened/Polished

Table G.13: Group 4 Fatigue Results: Annealed/Polished/Laser Shock Peened/Polished Test Specimens

Specimen Number	Diameter (mm)	Applied Stress (MPa)	Applied Force (kN)	P_{max} (kN)	P_{min} (kN)	P_{mean} (kN)	Amplitude (kN)	Crack Initiation Length (mm)	Cycles to Crack Initiation	Cycles to Failure
1	16.97	450.00	12.70	14.11	1.41	-7.76	6.35	1.20	27537	32104
2	16.99	450.00	12.75	14.16	1.42	-7.79	6.37	2.00	30852	34074
3	16.97	450.00	12.70	14.11	1.41	-7.76	6.35	2.10	26561	31098
Average	**16.98**	**450.00**	**12.72**	**14.13**	**1.41**	**-7.77**	**6.36**	**1.77**	**28317**	**32425**

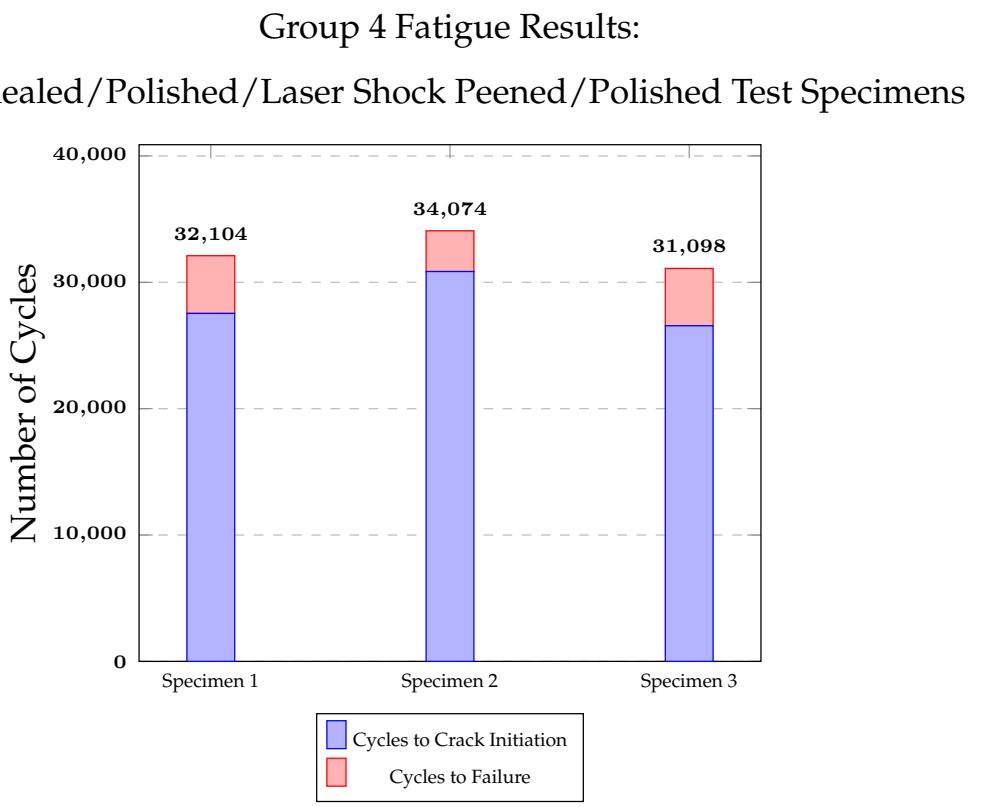

Figure G.12: Group 4 Fatigue Results: Annealed/Polished/Laser Shock Peened/Polished Test Specimens

Appendix H

CT Scan Images

CT Scanning: Pre-Fatiguing

Test Specimen 1

- Material Condition: T6/Polished/Laser Shock Peened/Polished

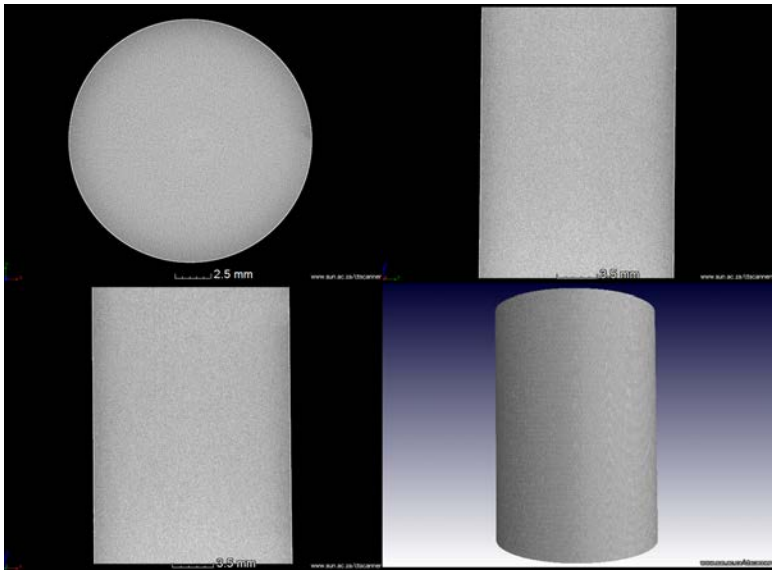

Figure H.1: CT Scan of Test Specimen 1

Test Specimen 2

- Material Condition: T6/Polished/Laser Shock Peened/Polished

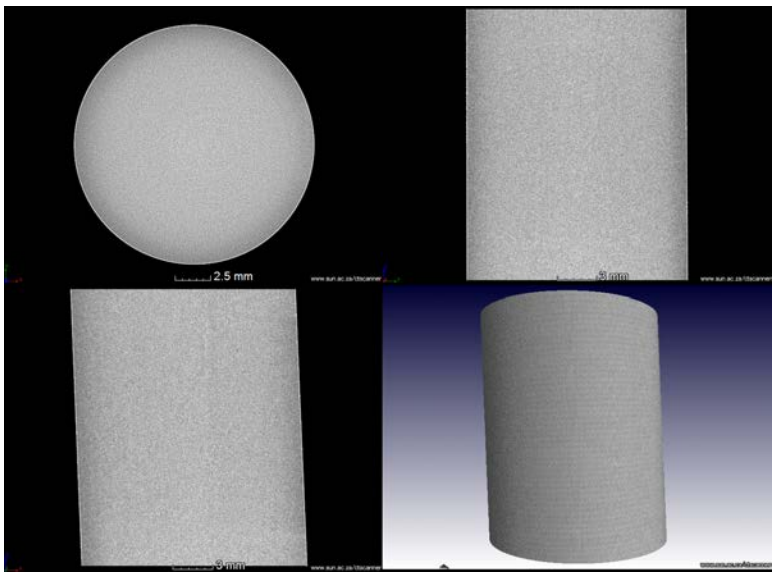

Figure H.2: CT Scan of Test Specimen 2

Test Specimen 3

- Material Condition: T6/Polished/Laser Shock Peened/Polished

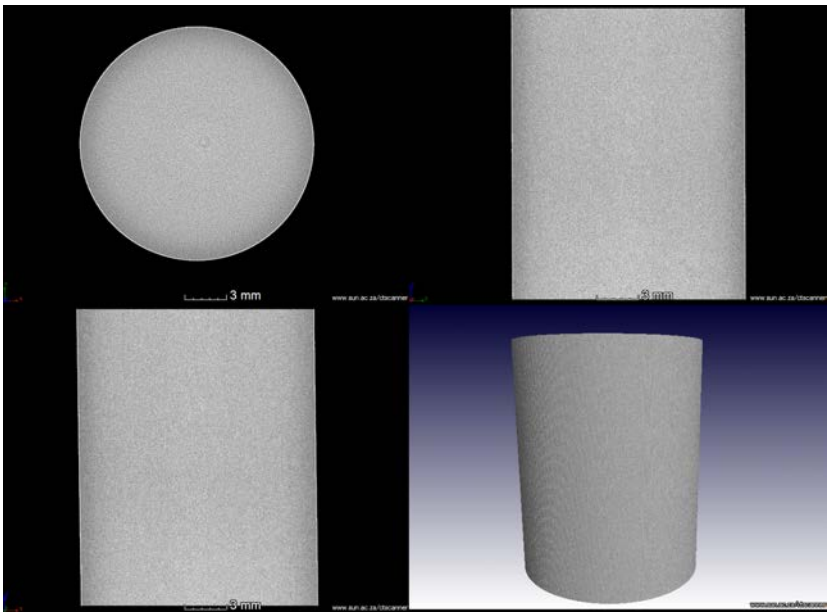

Figure H.3: CT Scan of Test Specimen 3

Test Specimen 4

- Material Condition: T6/Polished/Laser Shock Peened/Polished

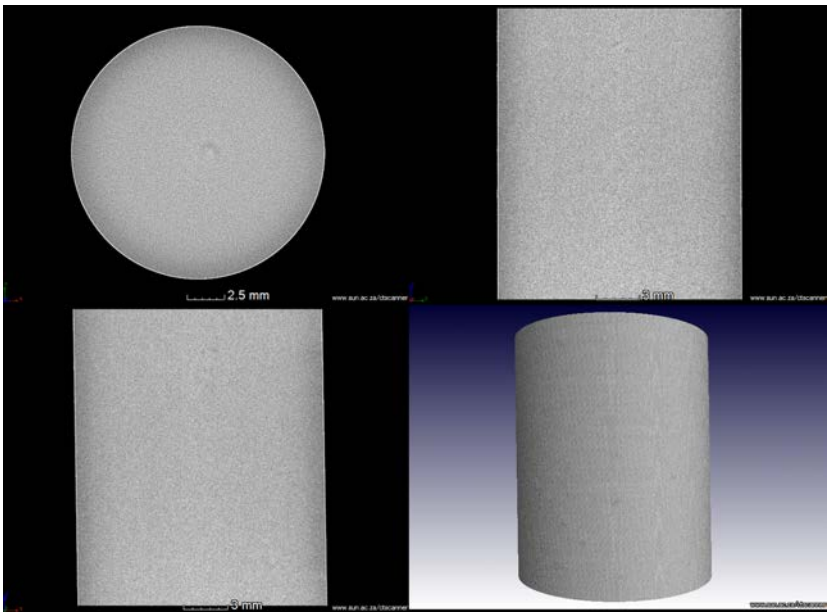

Figure H.4: CT Scan of Test Specimen 4

Test Specimen 5

- Material Condition: T6/Polished/Laser Shock Peened/Polished

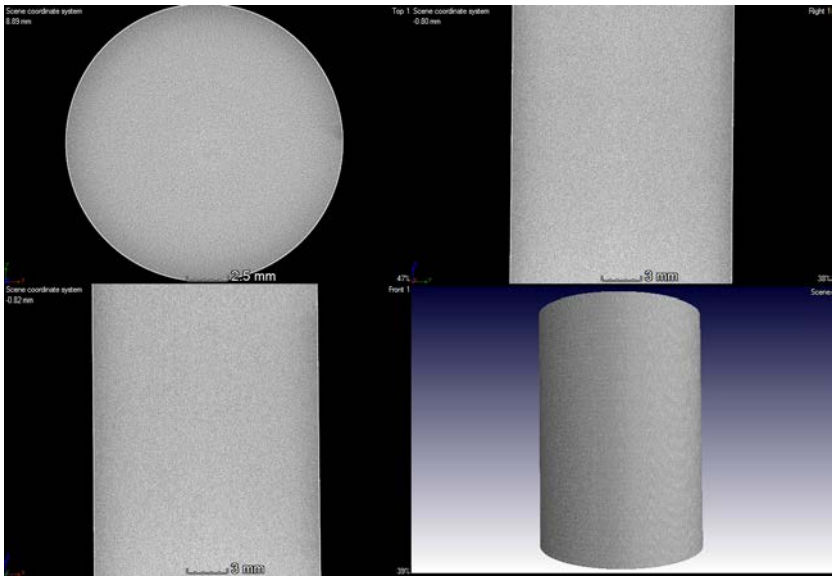

Figure H.5: CT Scan of Test Specimen 5

CT Scanning: Post Partial Fatiguing

Test Specimen 1

- Material Condition: T6/Polished/Laser Shock Peened/Polished/Partially Fatigued

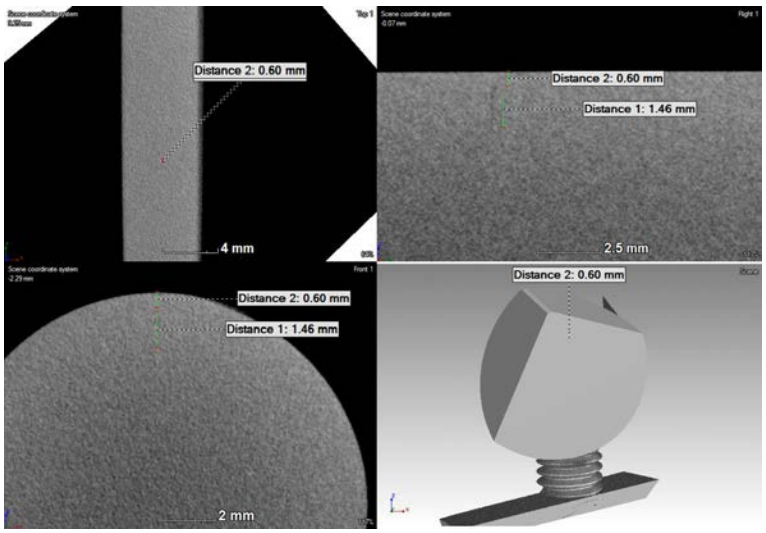

Figure H.6: CT Scan of Partially Fatigued Test Specimen 1

Test Specimen 2

- Material Condition: T6/Polished/Laser Shock Peened/Polished/Partially Fatigued

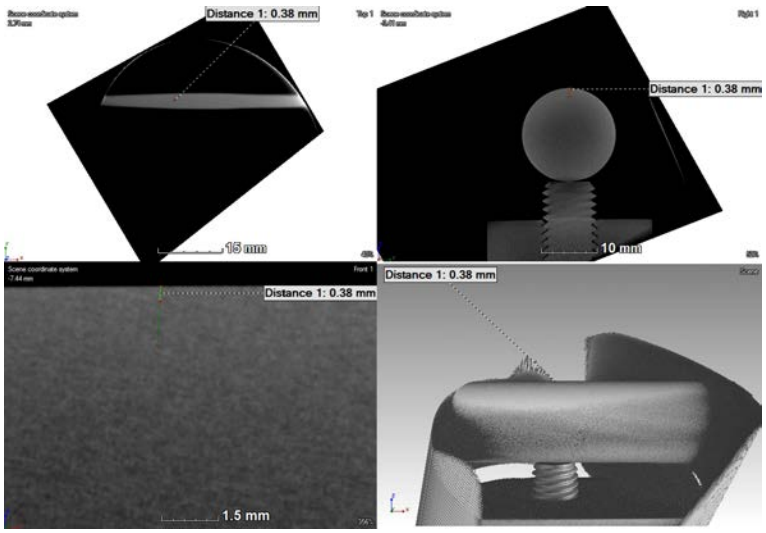

Figure H.7: CT Scan of Partially Fatigued Test Specimen 2

Test Specimen 3

- Material Condition: T6/Polished/Laser Shock Peened/Polished/Partially Fatigued

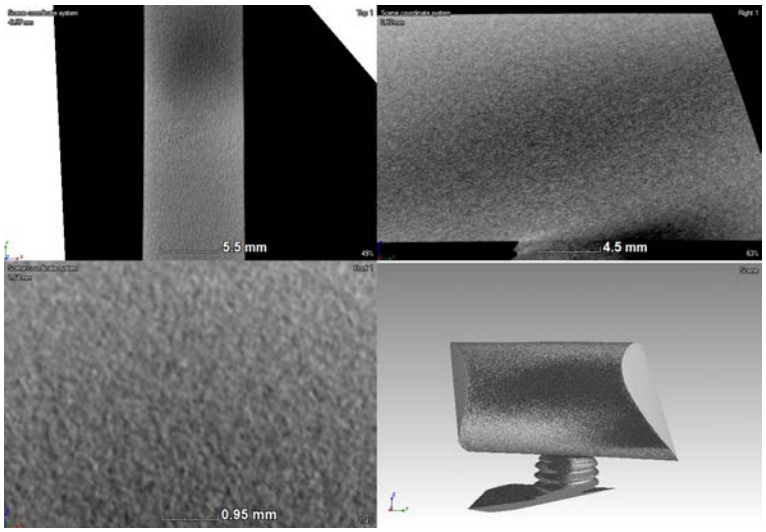

Figure H.8: CT Scan of Partially Fatigued Test Specimen 3

Test Specimen 4

- Material Condition: T6/Polished/Laser Shock Peened/Polished/Partially Fatigued

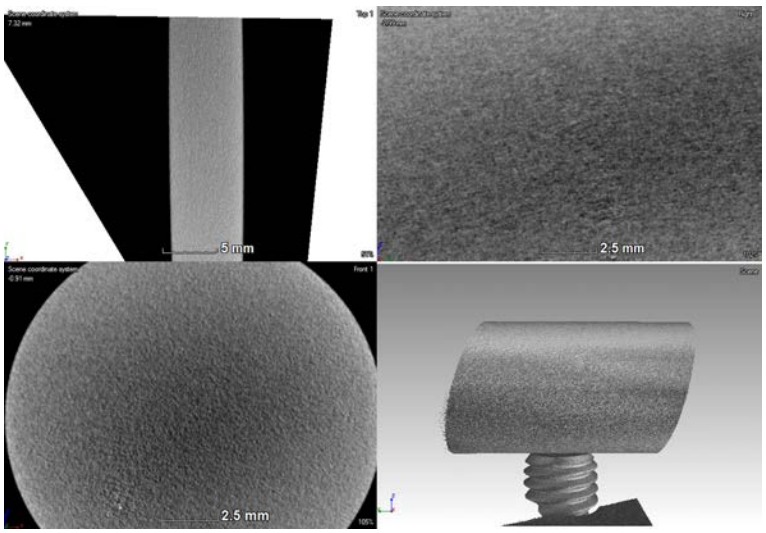

Figure H.9: CT Scan of Partially Fatigued Test Specimen 4

Test Specimen 5

- Material Condition: T6/Polished/Laser Shock Peened/Polished/Partially Fatigued

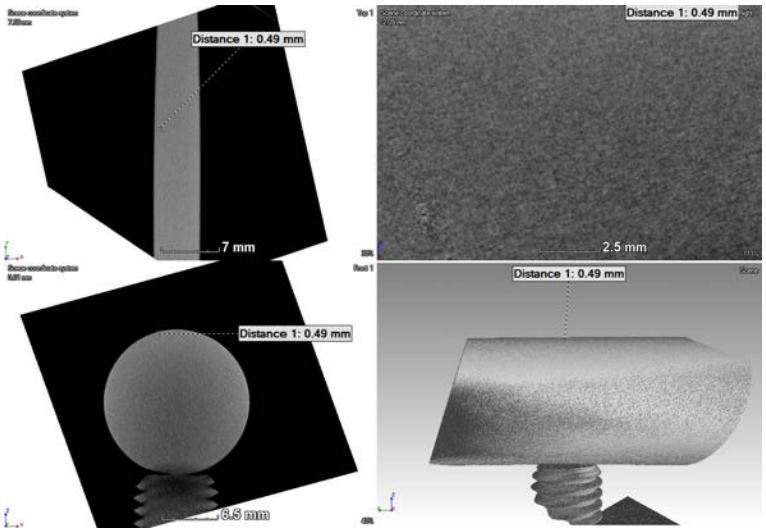

Figure H.10: CT Scan of Partially Fatigued of Test Specimen 5

CT Scanning: After Laser Shock Peening Treatment

Test Specimen 1

- Material Condition: T6/Polished/Laser Shock Peened/Polished/Partially Fatigued/Laser Shock Peened

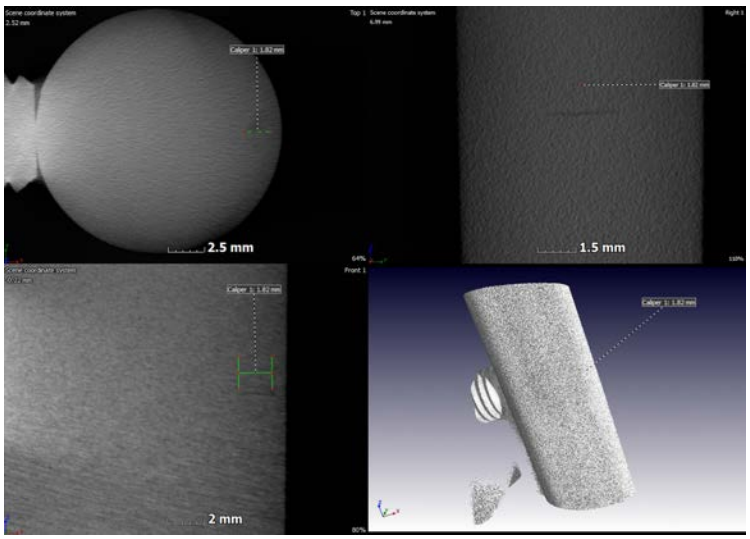

Figure H.11: CT Scan of Partially Fatigued Test Specimen 1

Test Specimen 2

- Material Condition: T6/Polished/Laser Shock Peened/Polished/Partially Fatigued/Laser Shock Peened

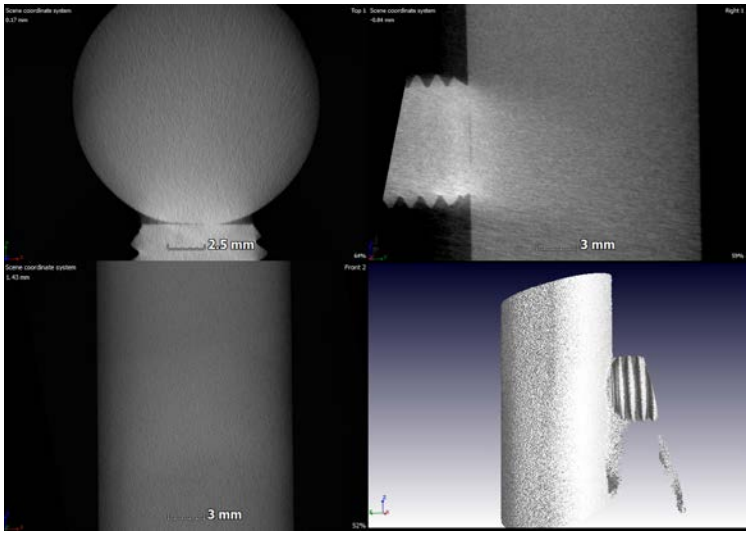

Figure H.12: CT Scan of Partially Fatigued Test Specimen 2

Test Specimen 5

- Material Condition: T6/Polished/Laser Shock Peened/Polished/Partially Fatigued/Laser Shock Peened

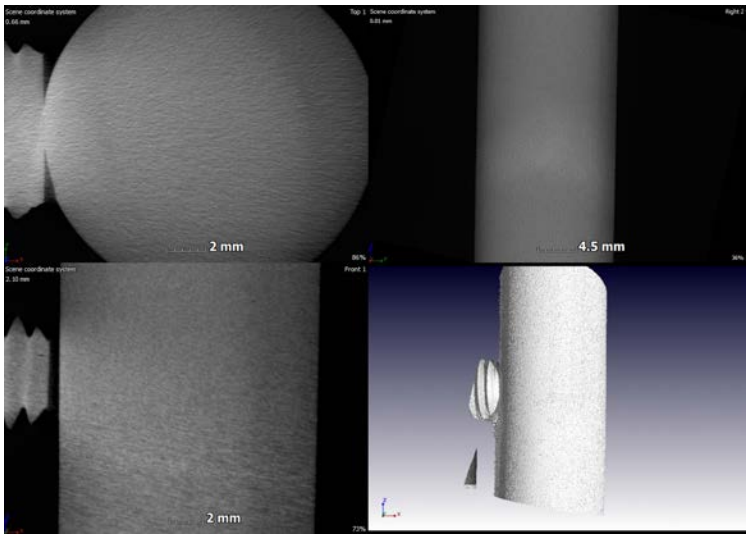

Figure H.13: CT Scan of Partially Fatigued Test Specimen 3

Appendix I

Optical Fractography Pictures

Table I.1:
T6 Fracture
Surface Labelling Key

Label	Surface Feature
A	Crack Initiation Site
B	Ratchet Marks
C	Crack Growth Region
D	Chevron Marks
E	Final Fracture Zone
F	Shear Lips
G	Compression/Cantilever Curl

Table I.2:
Annealed Fracture
Surface Labelling Key

Label	Surface Feature
A	Crack Initiation Site
B	Ratchet Marks
C	Crack Growth Region
D	Rough/Dimpled Surface
E	Smooth Radial Zone
F	Shear Lips
G	Post Fracture Damage

Group 1

- Material Condition: "As Machined"/T6

Test Specimen 1

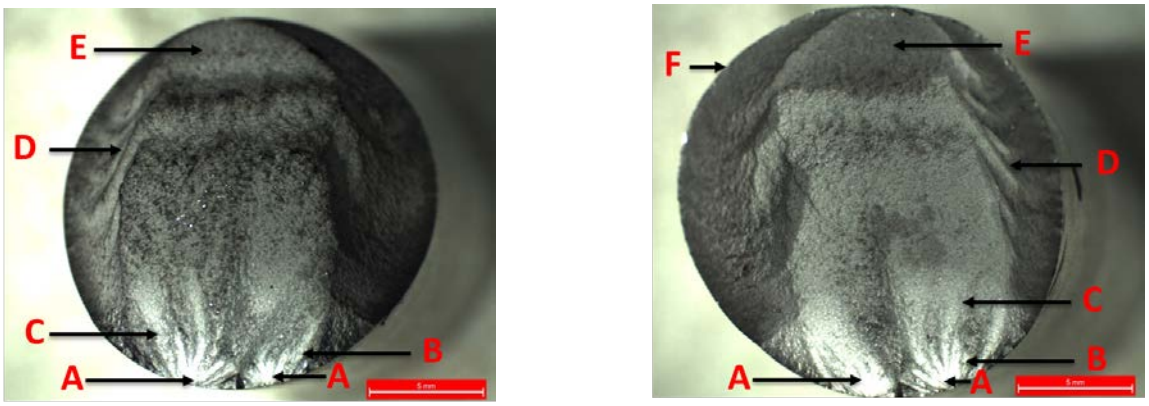

(a) **(b)**

Figure I.1: Fractograph of "As Machined"/T6 Test Specimen 1

Test Specimen 2

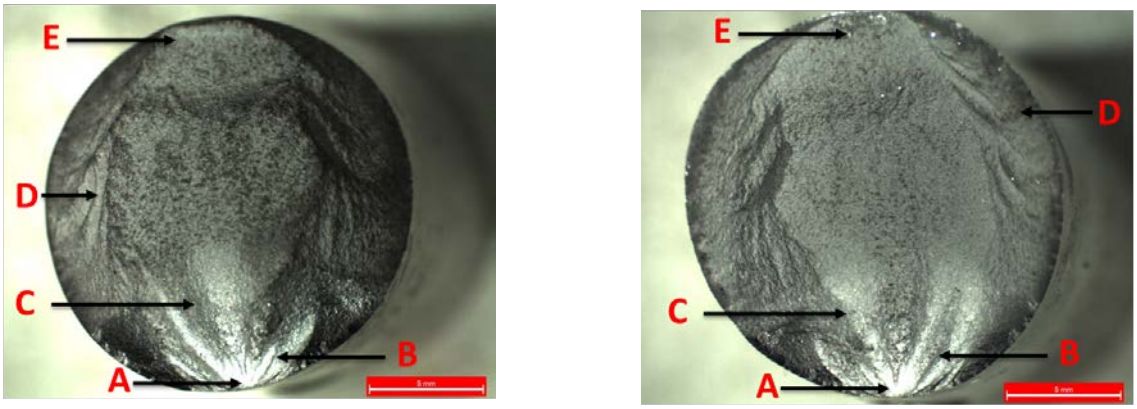

(a) **(b)**

Figure I.2: Fractograph of "As Machined"/T6 Test Specimen 2

Test Specimen 3

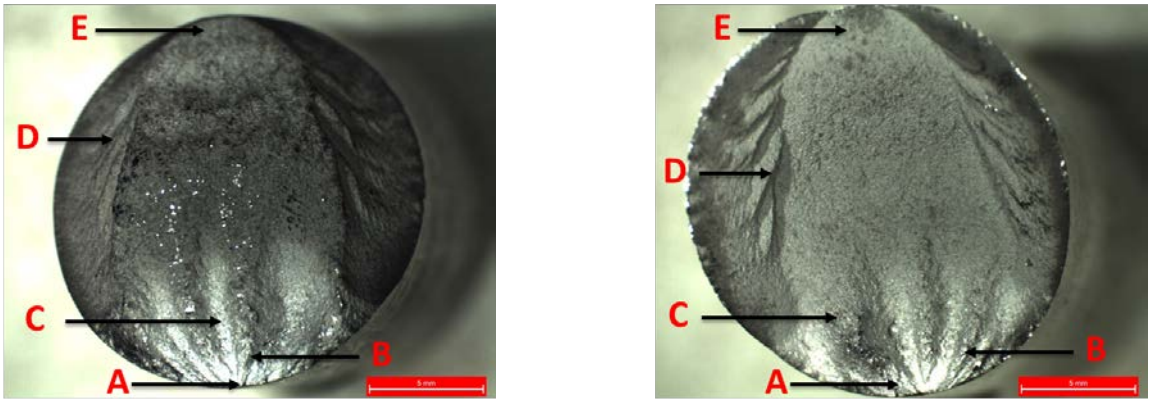

(a) **(b)**

Figure I.3: Fractograph of "As Machined"/T6 Test Specimen 3

Test Specimen 4

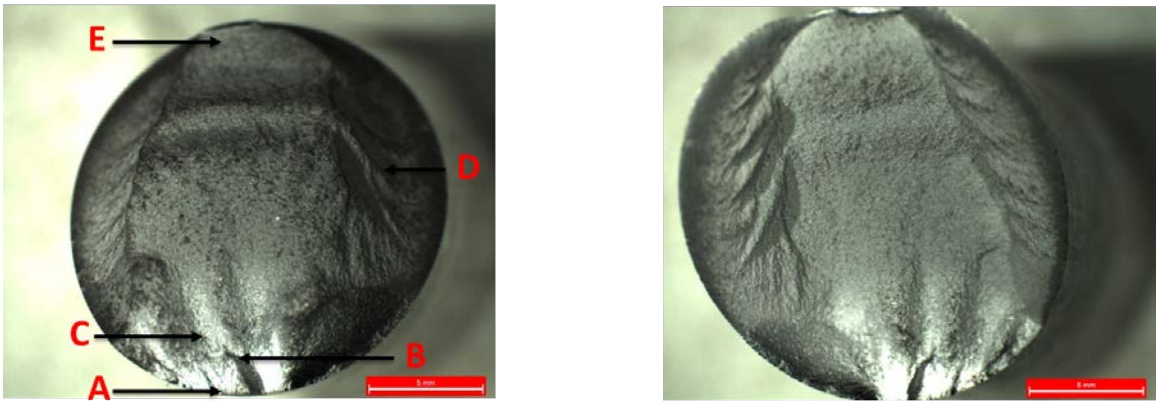

(a) **(b)**

Figure I.4: Fractograph of "As Machined"/T6 Test Specimen 4

- Material Condition: "As Machined"/Annealed

Test Specimen 1

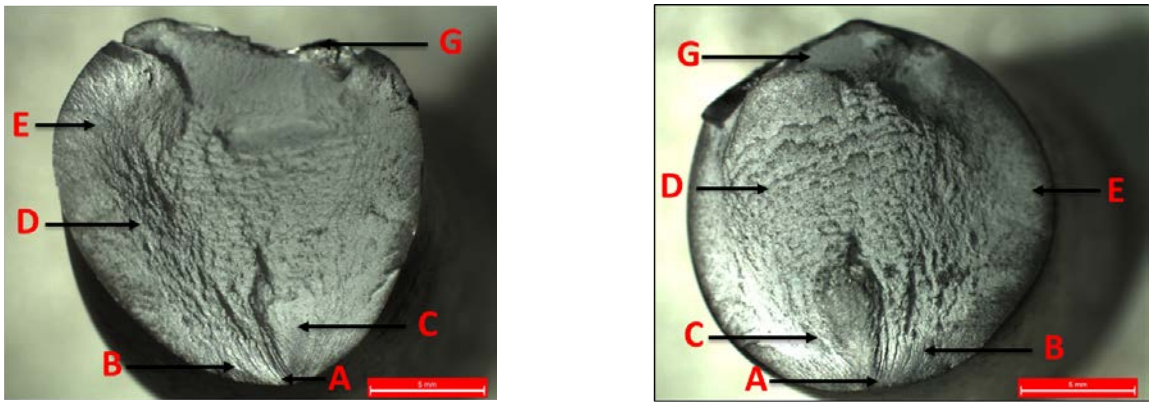

(a) **(b)**

Figure I.5: Fractograph of "As Machined"/Annealed Test Specimen 1

Test Specimen 2

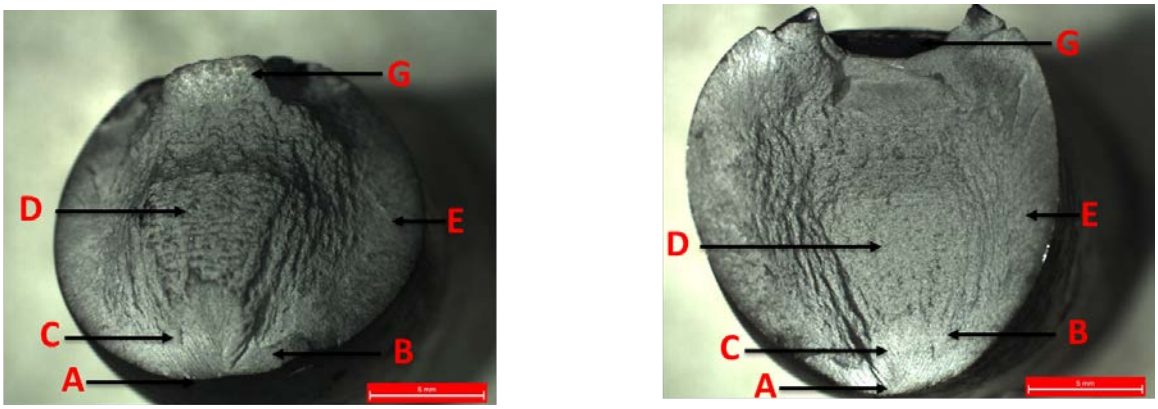

(a) **(b)**

Figure I.6: Fractograph of "As Machined"/Annealed Test Specimen 2

Test Specimen 3

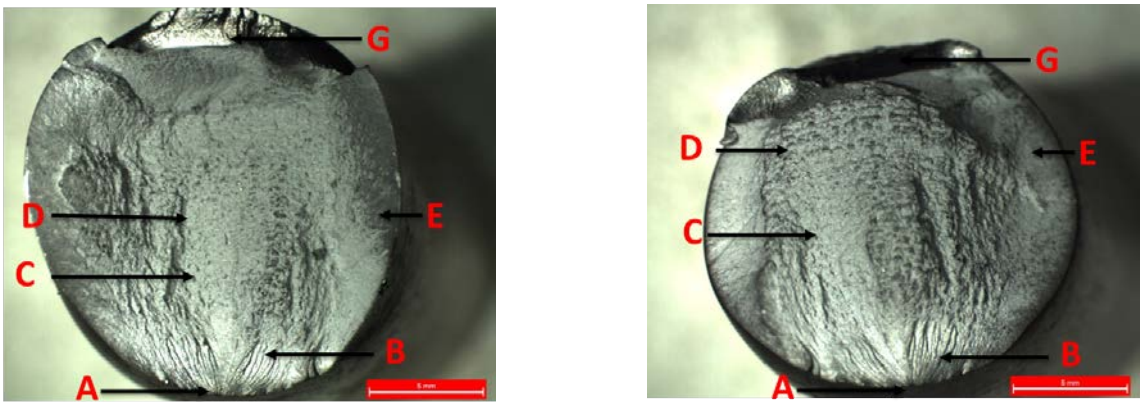

(a) **(b)**

Figure I.7: Fractograph of "As Machined"/Annealed Test Specimen 3

Test Specimen 4

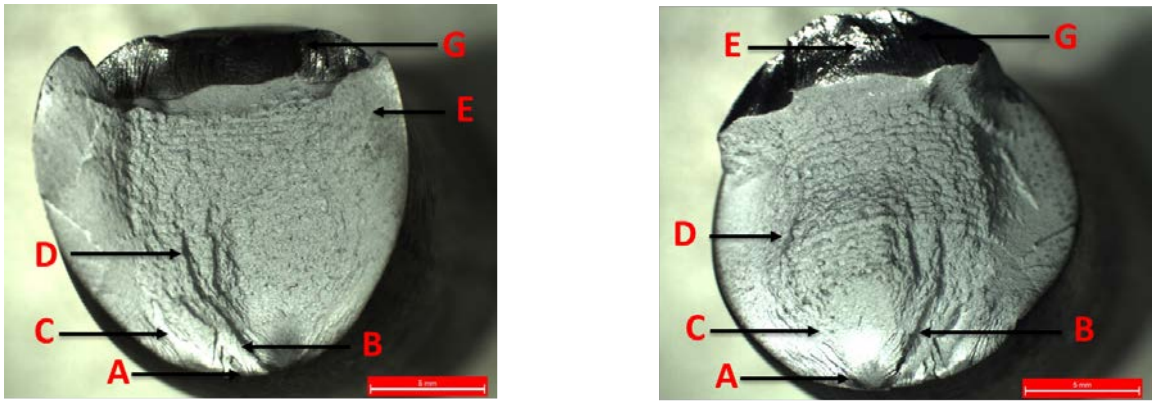

(a) **(b)**

Figure I.8: Fractograph of "As Machined"/Annealed Test Specimen 4

Group 2

- Material Condition: T6/Polished

Test Specimen 1

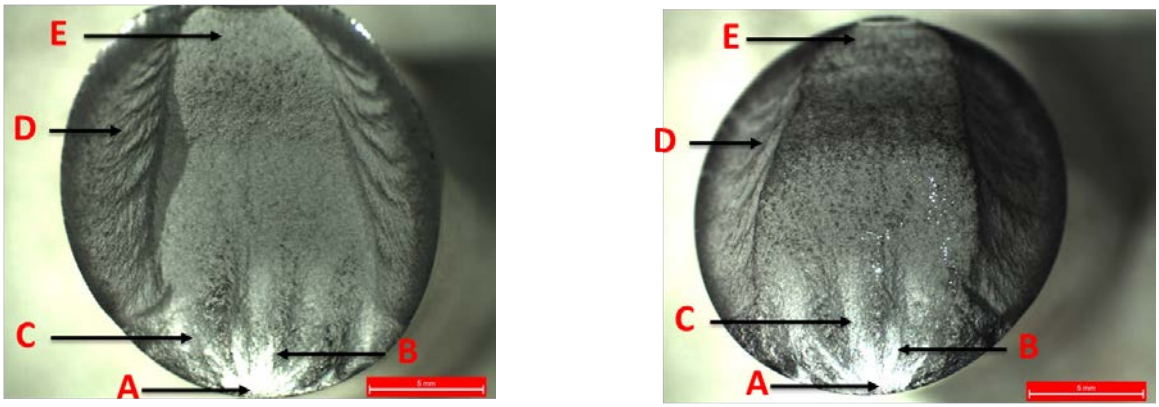

(a) **(b)**

Figure I.9: Fractograph of T6/Polished Test Specimen 1

Test Specimen 2

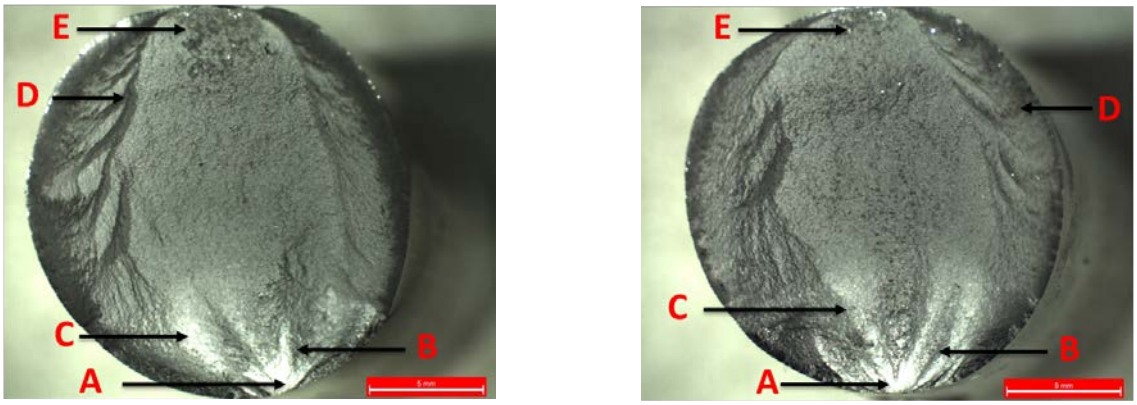

(a) **(b)**

Figure I.10: Fractograph of T6/Polished Test Specimen 2

Test Specimen 3

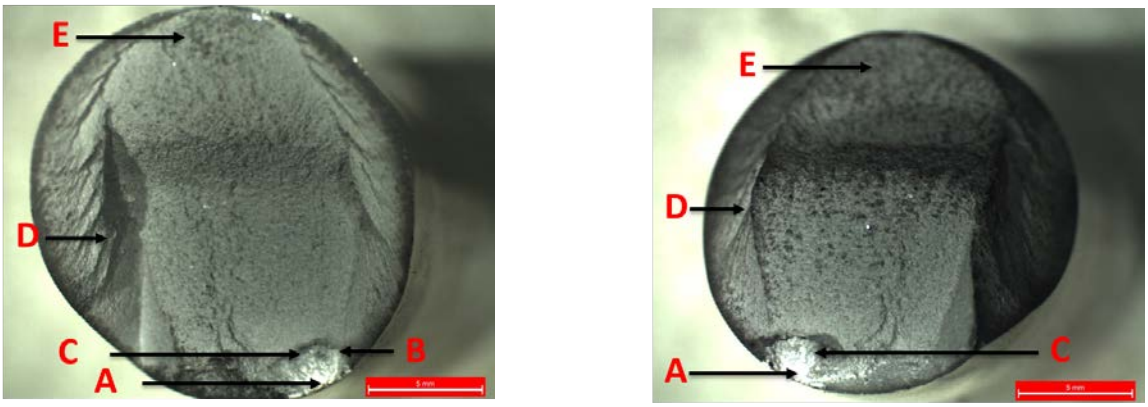

(a) **(b)**

Figure I.11: Fractograph of T6/Polished Test Specimen 3

Test Specimen 4

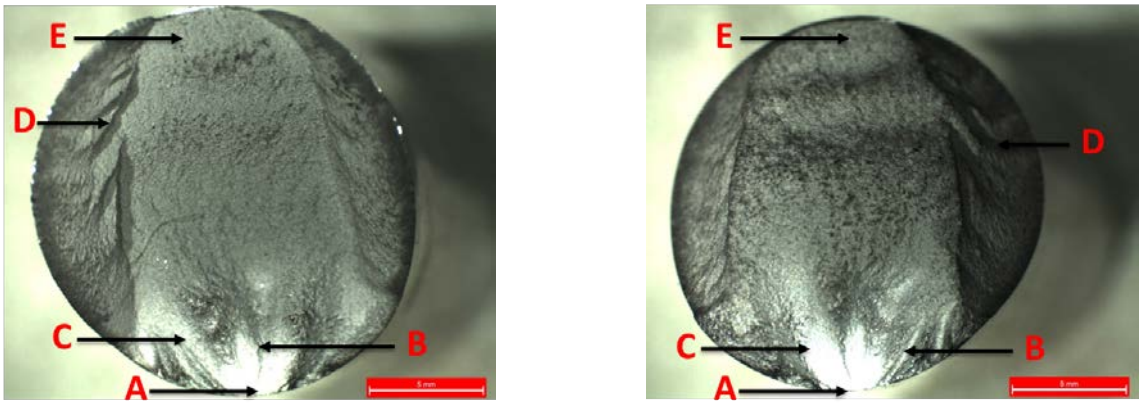

(a) **(b)**

Figure I.12: Fractograph of T6/Polished Test Specimen 4

- Material Condition: Annealed/Polished

Test Specimen 1

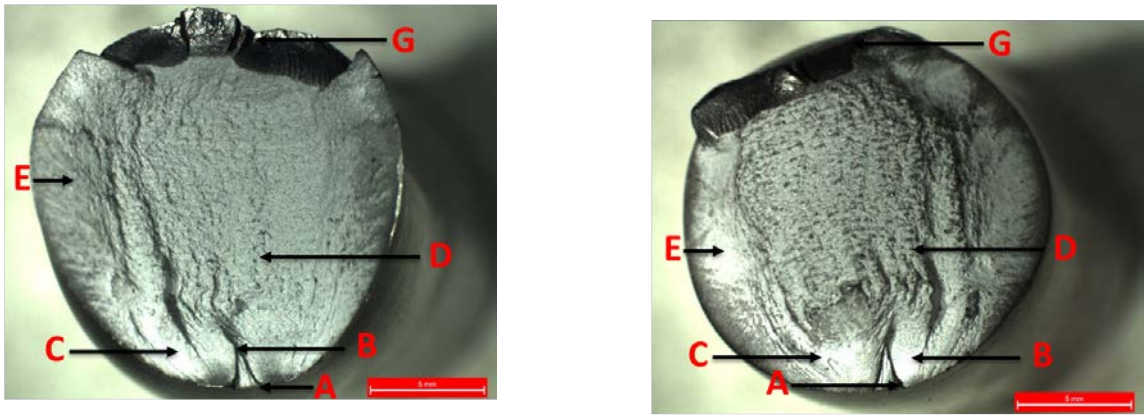

(a) **(b)**

Figure I.13: Fractograph of Annealed/Polished Test Specimen 1

Test Specimen 2

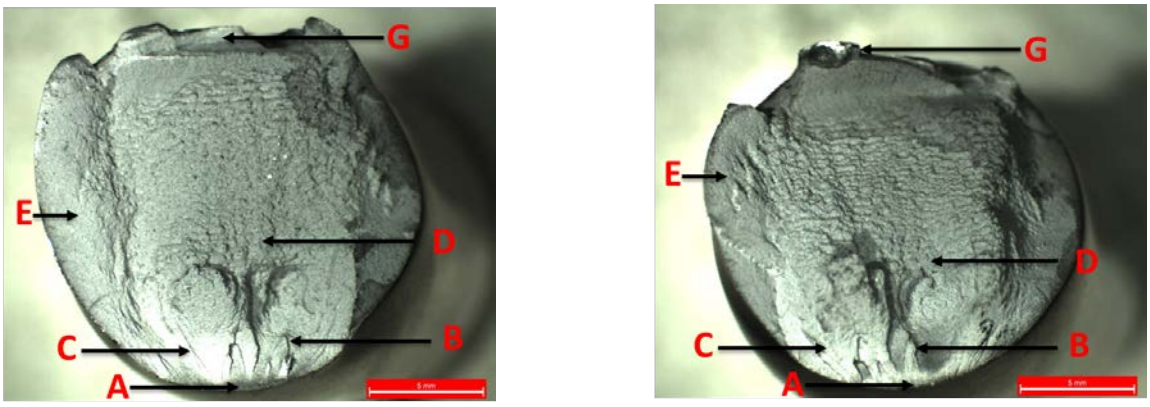

(a) **(b)**

Figure I.14: Fractograph of Annealed/Polished Test Specimen 2

Test Specimen 3

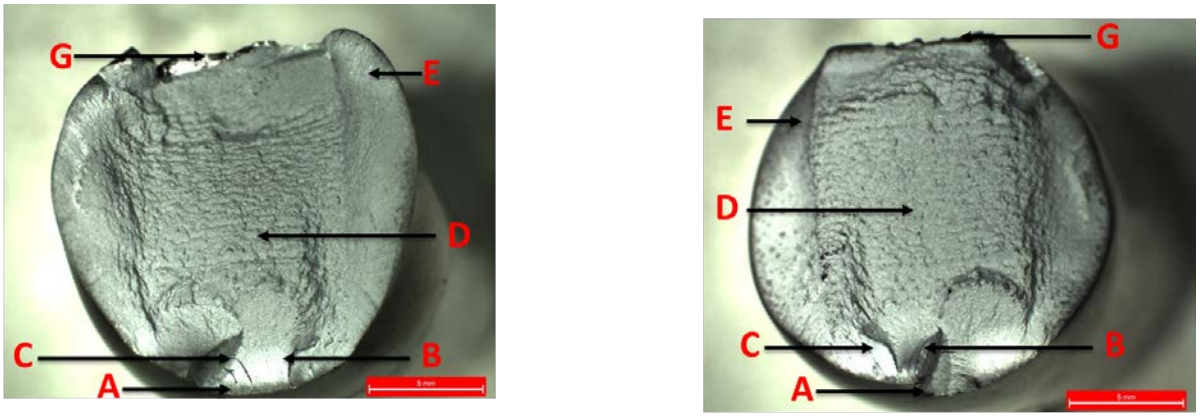

(a) **(b)**

Figure I.15: Fractograph of Annealed/Polished Test Specimen 3

Test Specimen 4

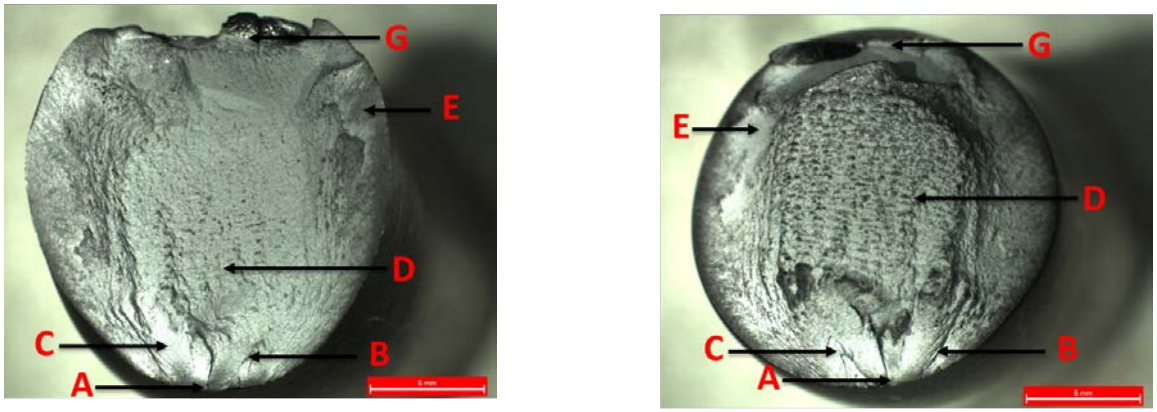

(a) **(b)**

Figure I.16: Fractograph of Annealed/Polished Test Specimen 4

Group 3

- Material Condition: T6/Polished/Shot Peened

Test Specimen 1

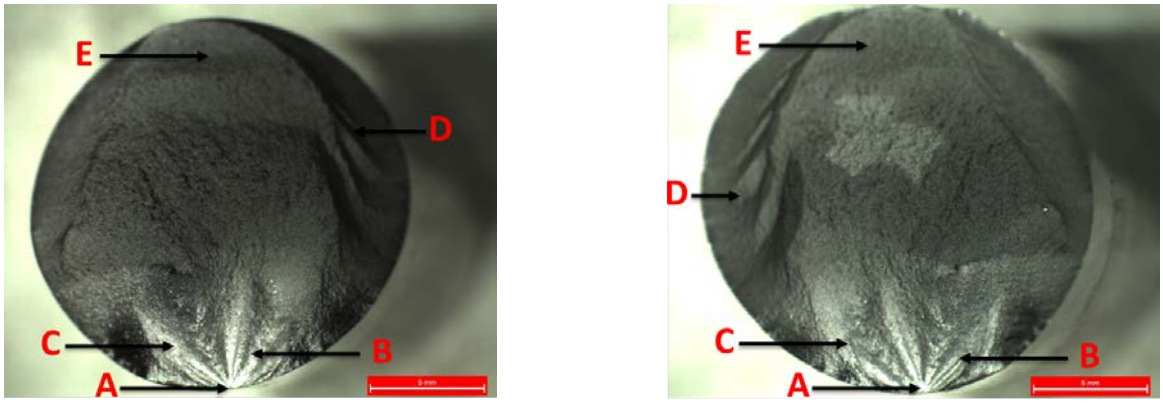

(a) **(b)**

Figure I.17: Fractograph of T6/Polished/Shot Peened Test Specimen 1

Test Specimen 2

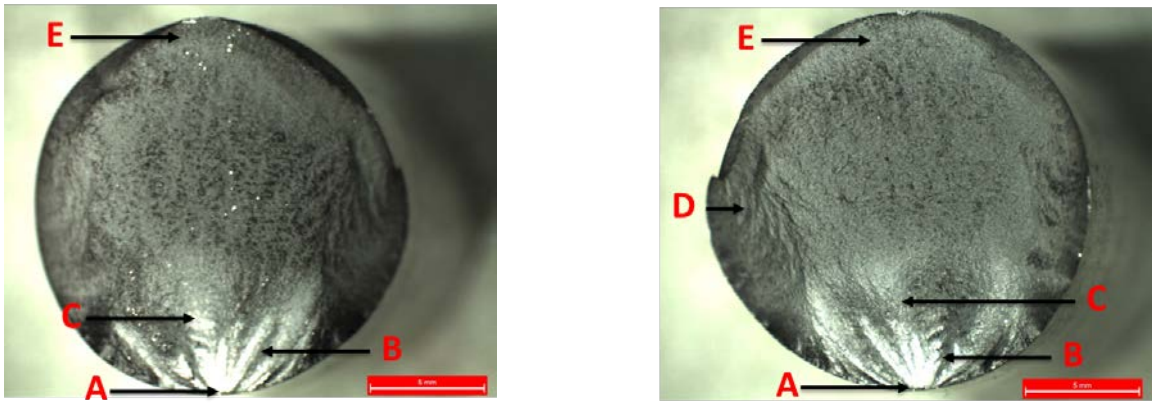

(a) **(b)**

Figure I.18: Fractograph of T6/Polished/Shot Peened Test Specimen 2

Test Specimen 3

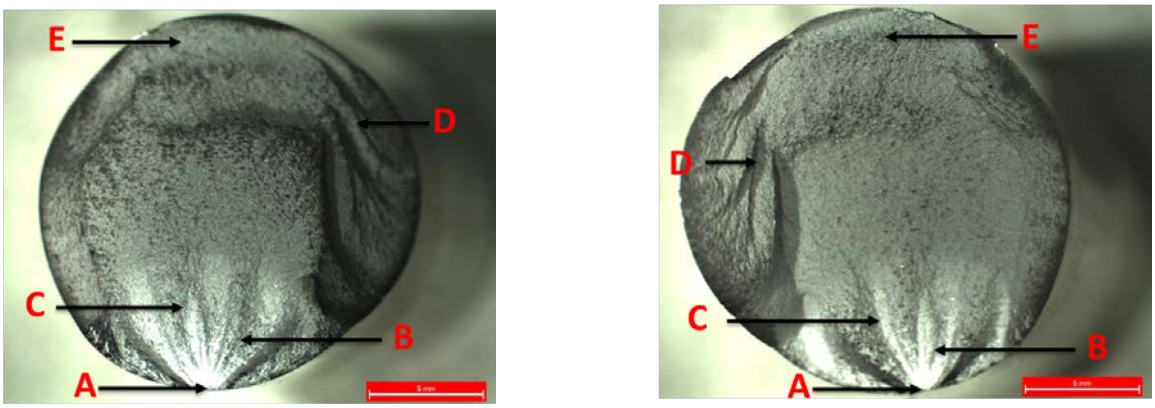

(a) **(b)**

Figure I.19: Fractograph of T6/Polished/Shot Peened Test Specimen 3

- Material Condition: Annealed/Polished/Shot Peened

Test Specimen 1

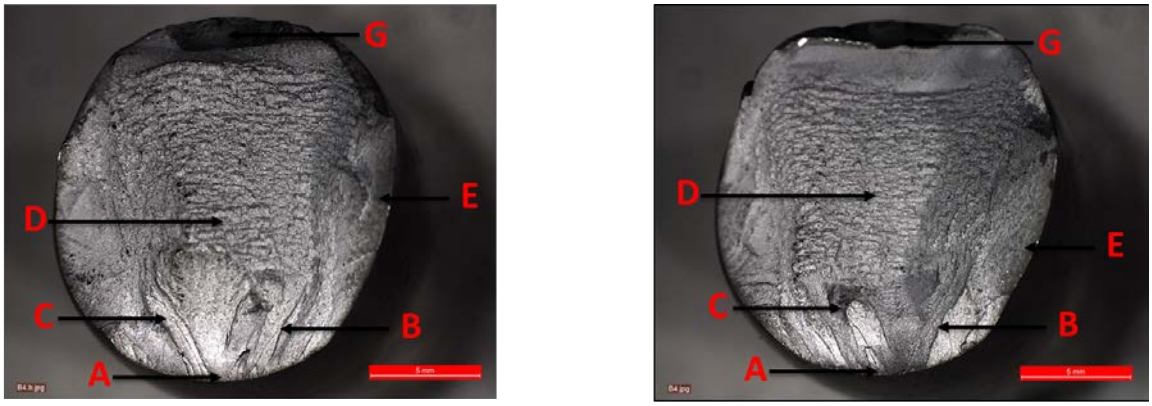

(a) **(b)**

Figure I.20: Fractograph of Annealed/Polished/Shot Peened Test Specimen 1

Test Specimen 2

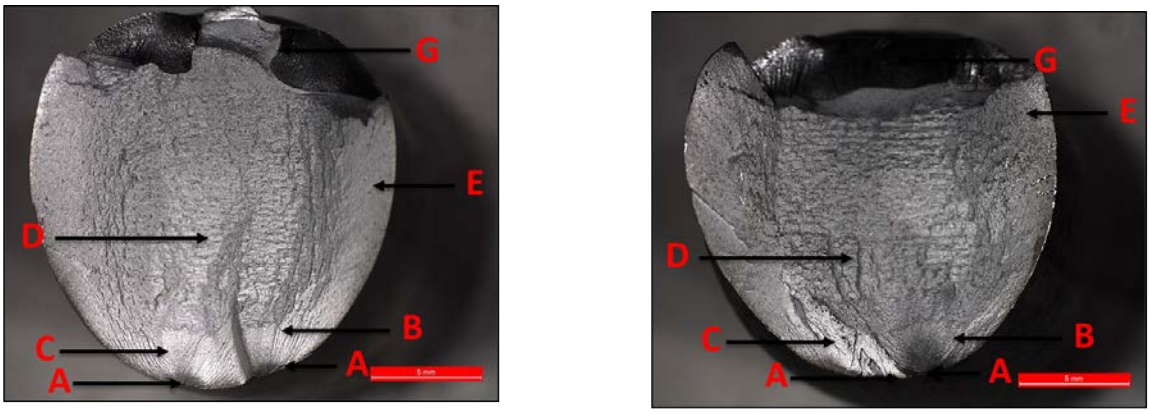

(a) **(b)**

Figure I.21: Fractograph of Annealed/Polished/Shot Peened Test Specimen 2

Test Specimen 3

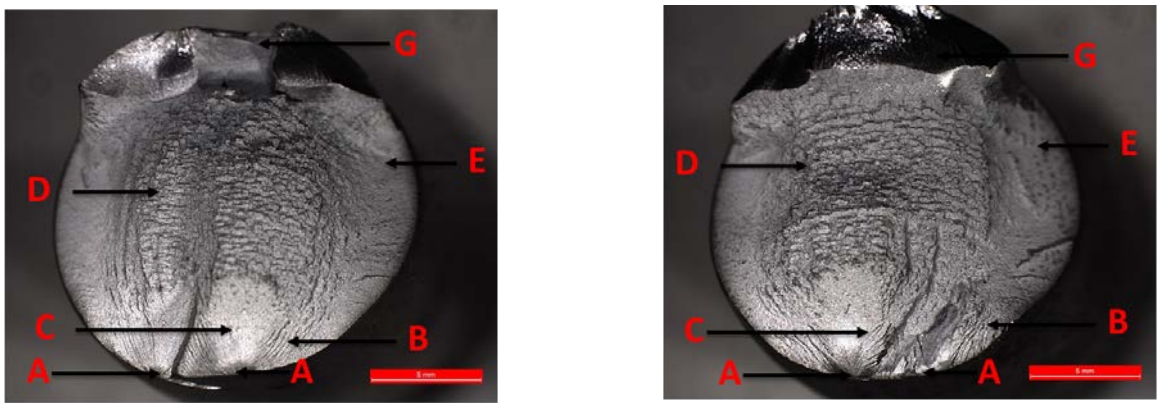

(a) **(b)**

Figure I.22: Fractograph of Annealed/Polished/Shot Peened Test Specimen 3

Group 3

- Material Condition: T6/Polished/Shot Peened/Polished

Test Specimen 1

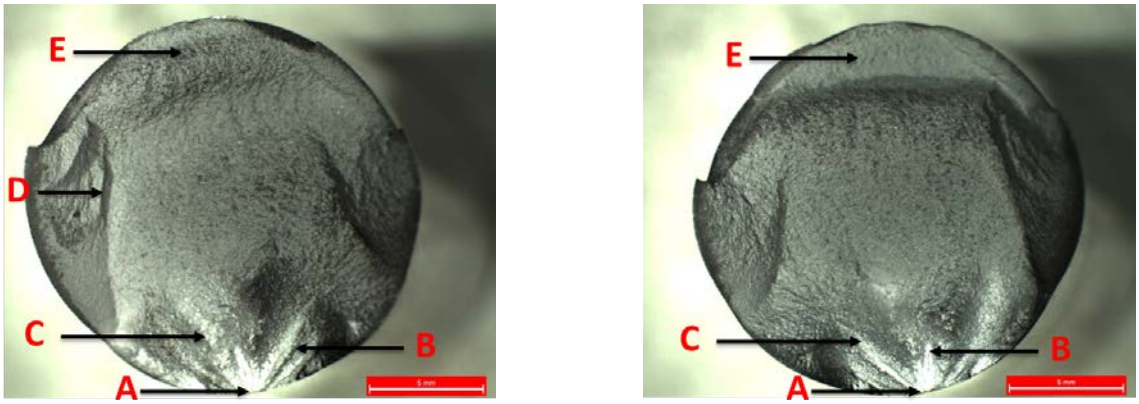

(a) **(b)**

Figure I.23: Fractograph of T6/Polished/Shot Peened/Polished Test Specimen 1

Test Specimen 2

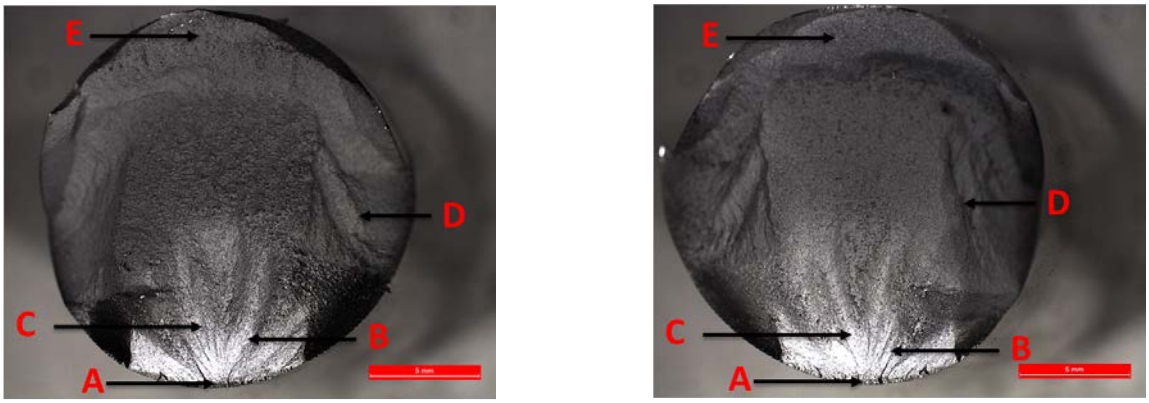

(a) **(b)**

Figure I.24: Fractograph of T6/Polished/Shot Peened/Polished Test Specimen 2

Test Specimen 3

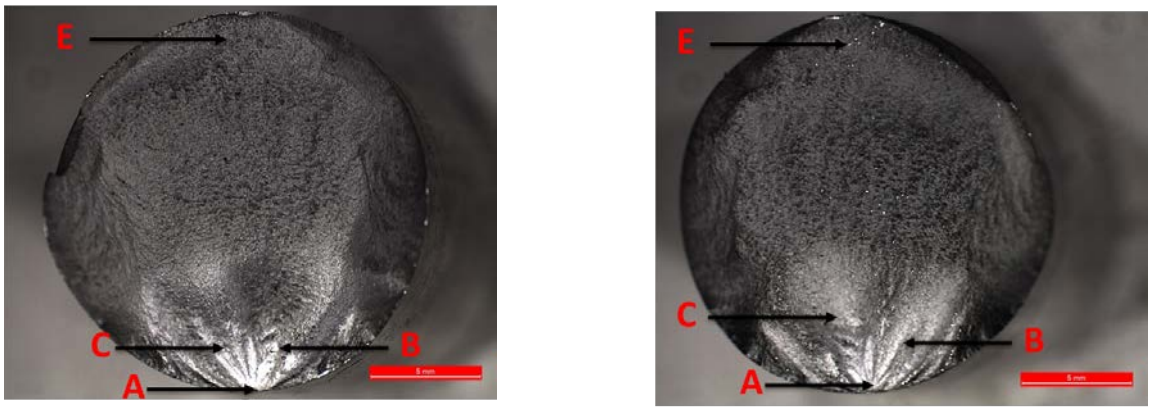

(a) **(b)**

Figure I.25: Fractograph of T6/Polished/Shot Peened/Polished Test Specimen 3

- Material Condition: Annealed/Polished/Shot Peened/Polished

Test Specimen 1

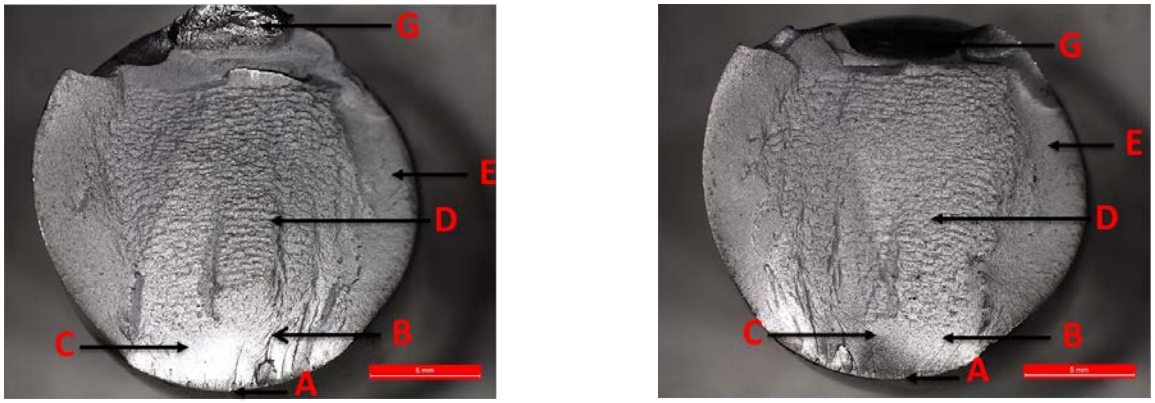

(a) **(b)**

Figure I.26: Fractograph of Annealed/Polished/Shot Peened/Polished Test Specimen 1

Test Specimen 2

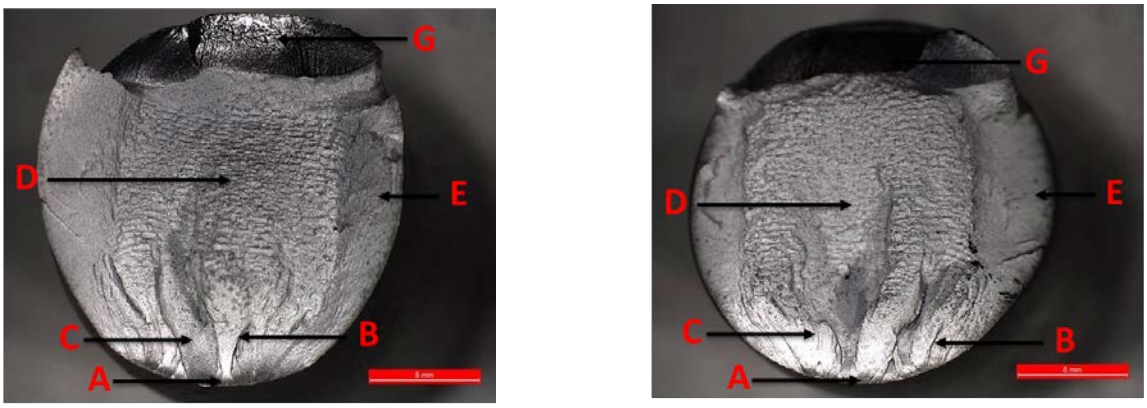

(a) **(b)**

Figure I.27: Fractograph of Annealed/Polished/Shot Peened/Polished Test Specimen 2

Test Specimen 3

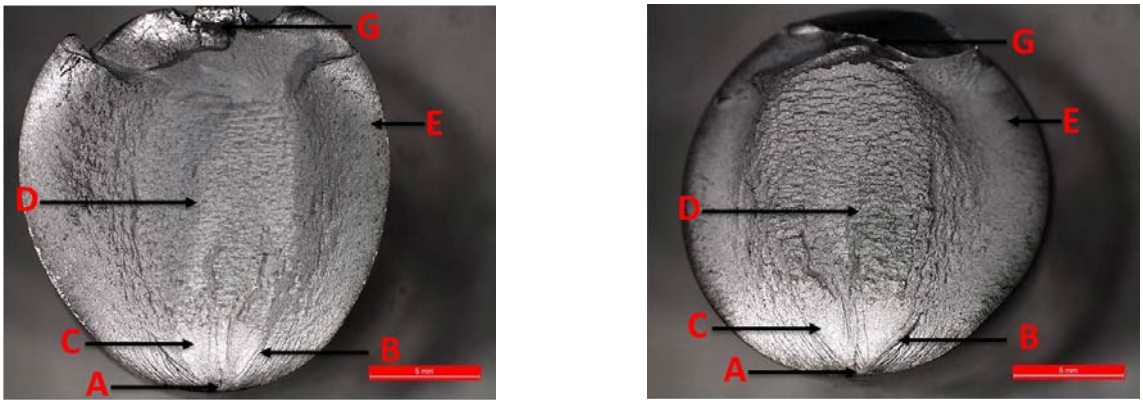

(a) **(b)**

Figure I.28: Fractograph of Annealed/Polished/Shot Peened/Polished Test Specimen 3

Group 4

- Material Condition: T6/Polished/Laser Shock Peened

Test Specimen 1

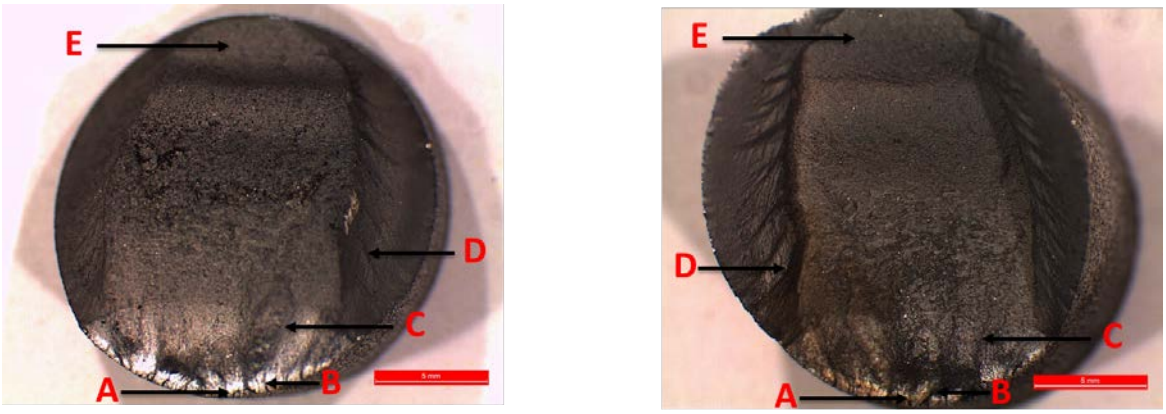

(a) **(b)**

Figure I.29: Fractograph of T6/Polished/Laser Shock Peened Test Specimen 1

Test Specimen 2

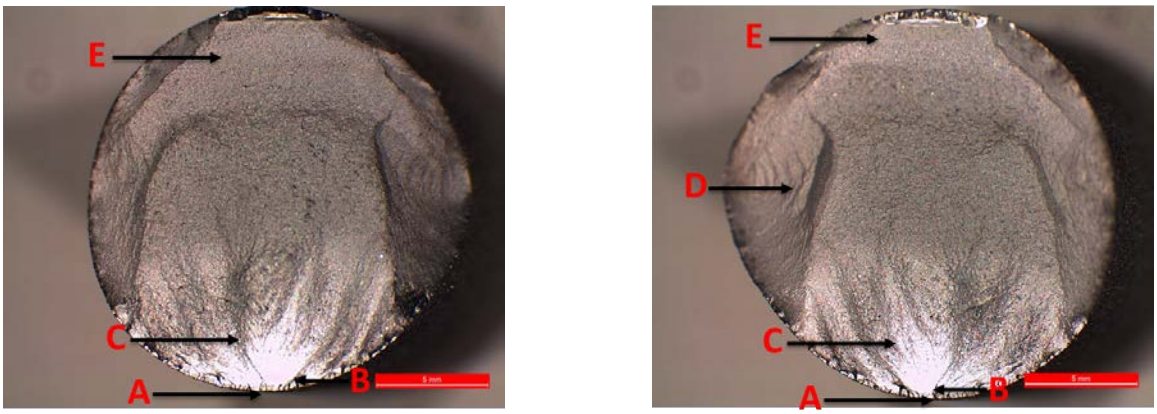

(a) **(b)**

Figure I.30: Fractograph of T6/Polished/Laser Shock Peened Test Specimen 2

Test Specimen 3

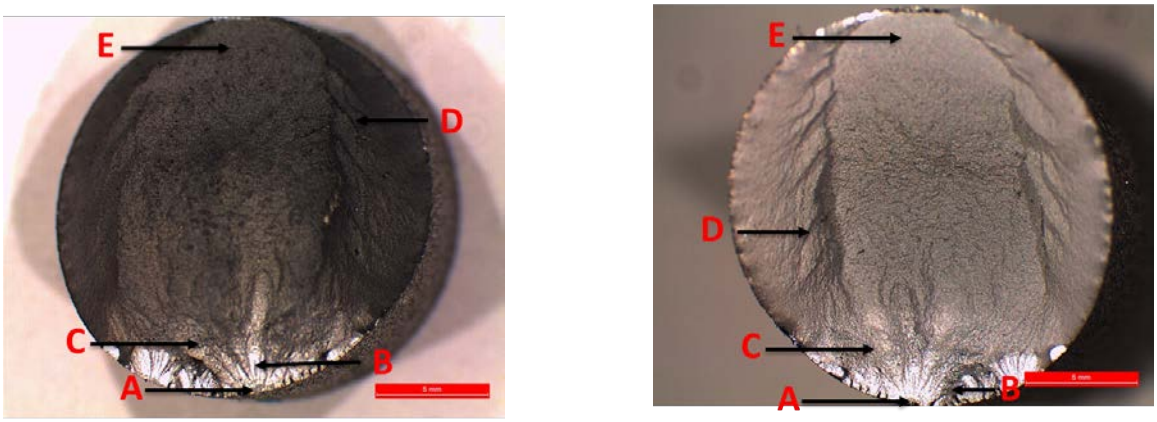

(a) **(b)**

Figure I.31: Fractograph of T6/Polished/Laser Shock Peened Test Specimen 3

- Material Condition: Annealed/Polished/Laser Shock Peened

Test Specimen 1

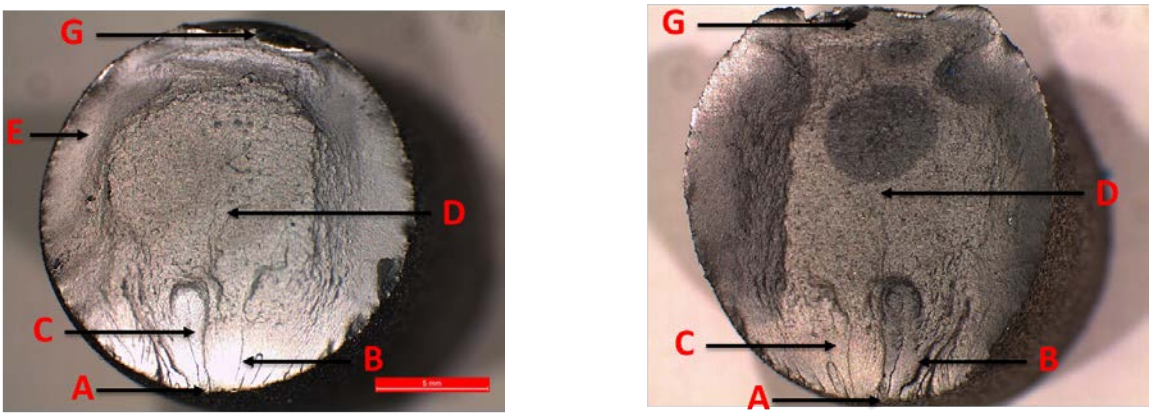

(a) **(b)**

Figure I.32: Fractograph of Annealed/Polished/Laser Shock Peened Test Specimen 1

Test Specimen 2

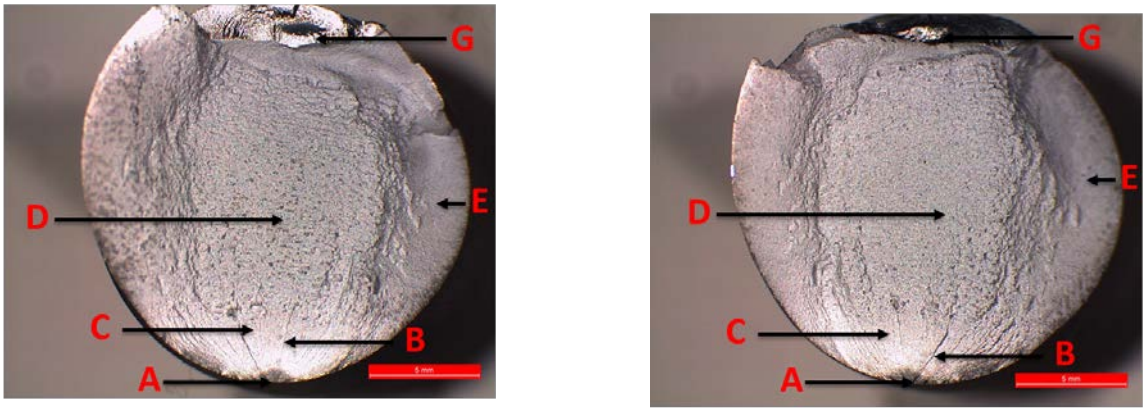

(a) **(b)**

Figure I.33: Fractograph of Annealed/Polished/Laser Shock Peened Test Specimen 2

Test Specimen 3

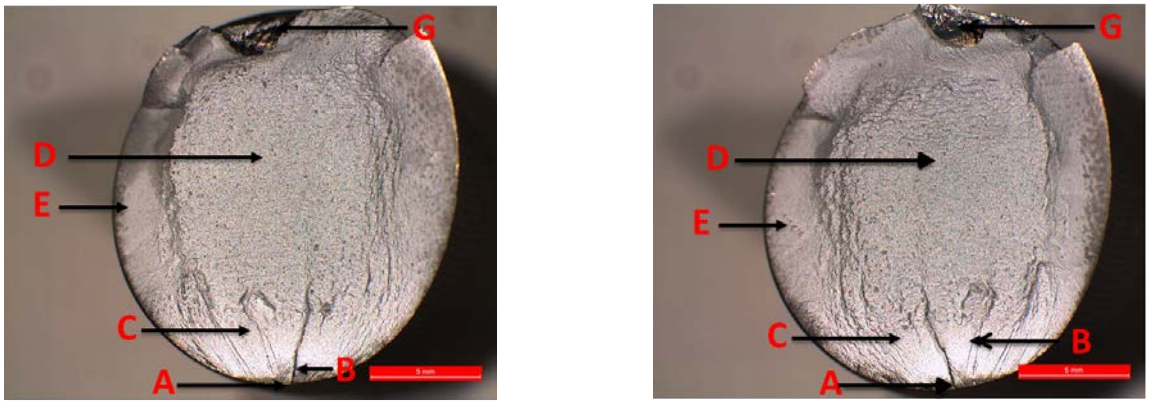

(a) **(b)**

Figure I.34: Fractograph of Annealed/Polished/Laser Shock Peened Test Specimen 3

Group 4

- Material Condition: T6/Polished/Laser Shock Peened/Polished

Test Specimen 1

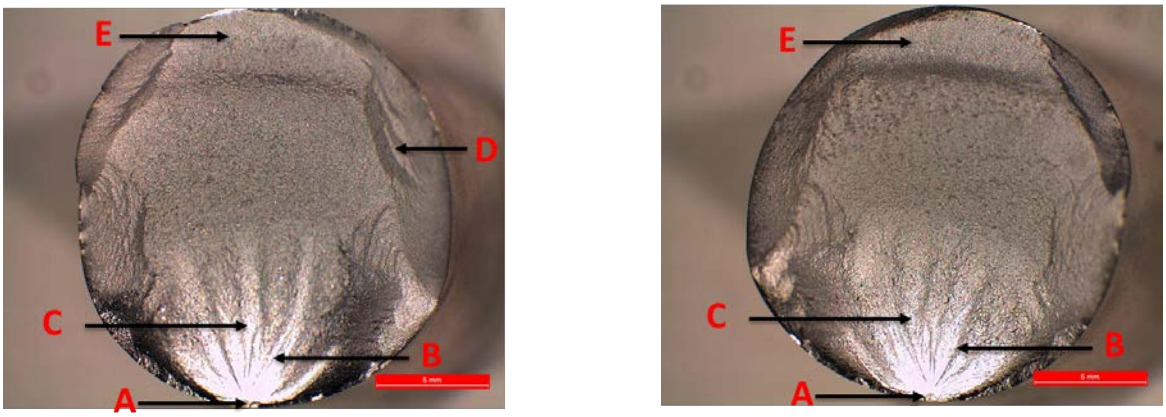

(a) **(b)**

Figure I.35: Fractograph of T6/Polished/Laser Shock Test Specimen 1

Test Specimen 2

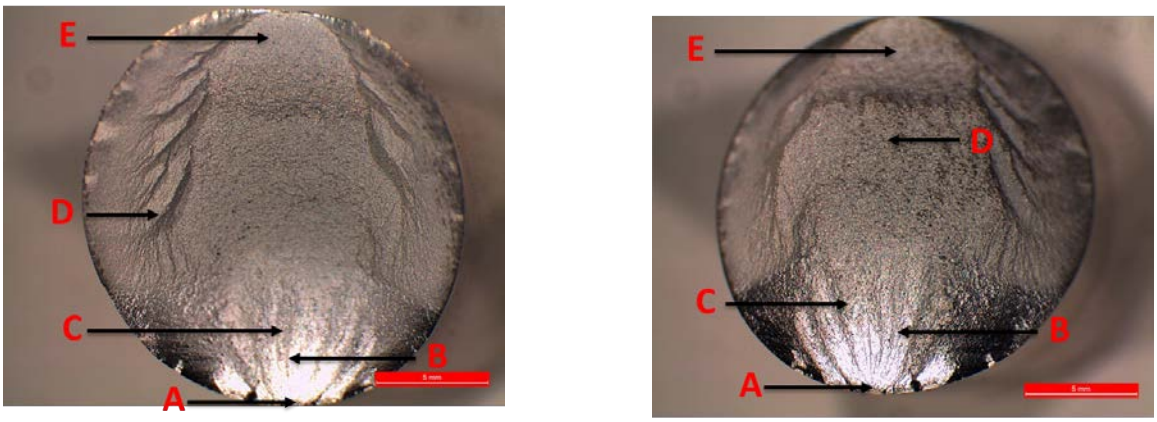

(a) **(b)**

Figure I.36: Fractograph of T6/Polished/Laser Shock Test Specimen 2

Test Specimen 3

(a) **(b)**

Figure I.37: Fractograph of T6/Polished/Laser Shock Test Specimen 3

- Material Condition: Annealed/Polished/Laser Shock Peened/Polished

Test Specimen 1

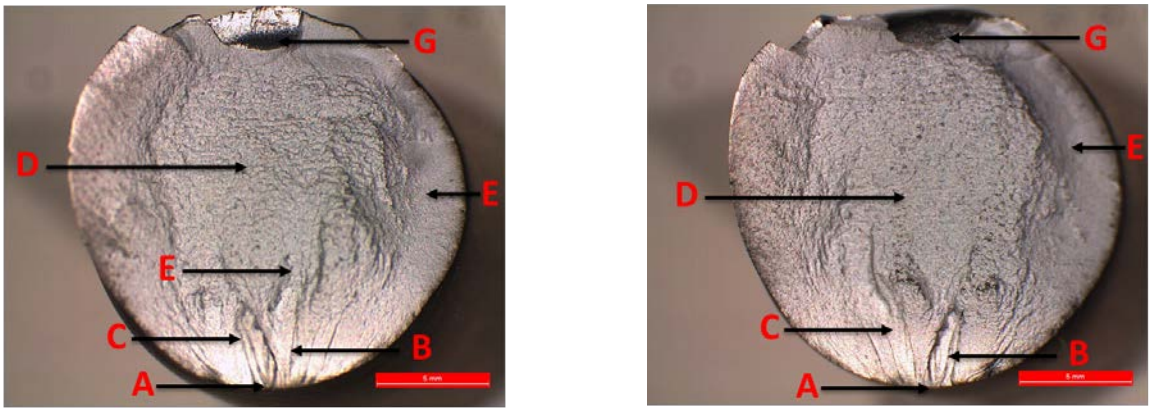

(a) **(b)**

Figure I.38: Fractograph of Annealed/Polished/Laser Shock Peened/Polished Test Specimen 1

Test Specimen 2

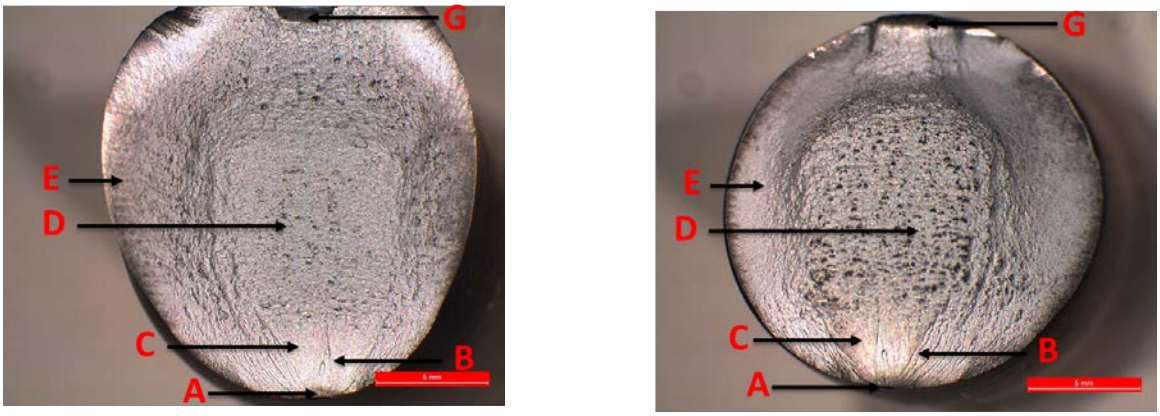

(a) **(b)**

Figure I.39: Fractograph of Annealed/Polished/Laser Shock Peened/Polished Test Specimen 2

Test Specimen 3

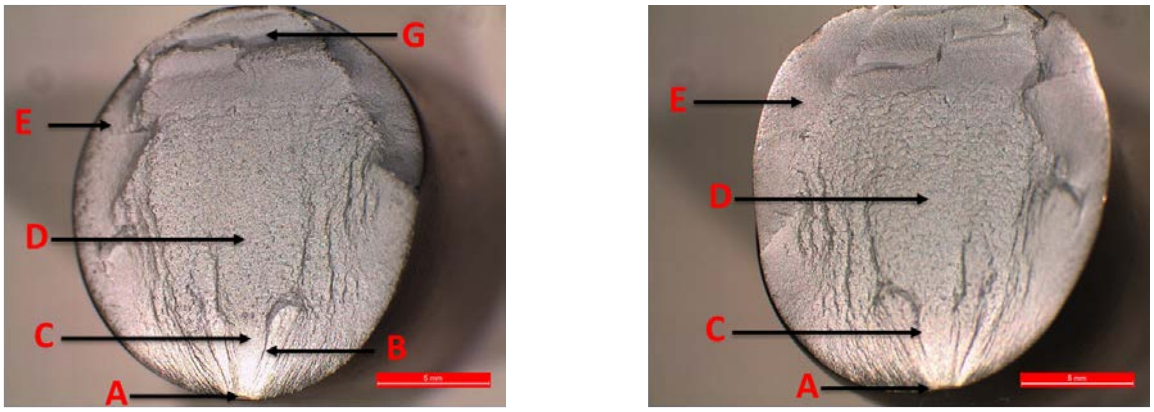

(a) **(b)**

Figure I.40: Fractograph of Annealed/Polished/Laser Shock Peened/Polished Test Specimen 3

Group 5

- Material Condition: T6/Polished/Laser Shock Peened/Polished/Partially Fatigued/Laser Shock Peened/Polished/Fatigued

Table I.3: Group 5 Fracture Surface Labelling Key

Label	Surface Feature
A	Crack Initiation Site
B	Ratchet Marks
C	Crack Growth Region
D	Chevron Marks
E	Final Fracture Zone
F	Shear Lips
G	Compression Curl
H	Fretting Fatigue

Test Specimen 1

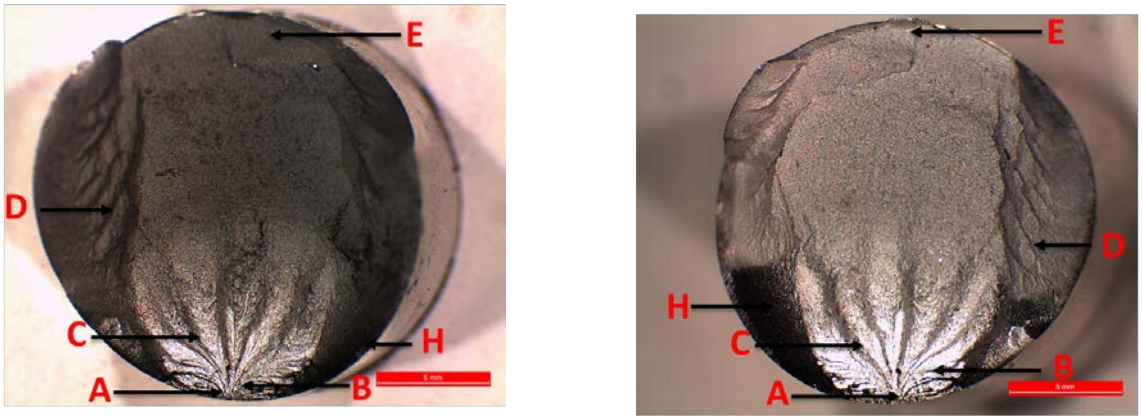

(a) **(b)**

Figure I.41: Fractograph of Fatigue Life Healed Test Specimen 1

Test Specimen 2

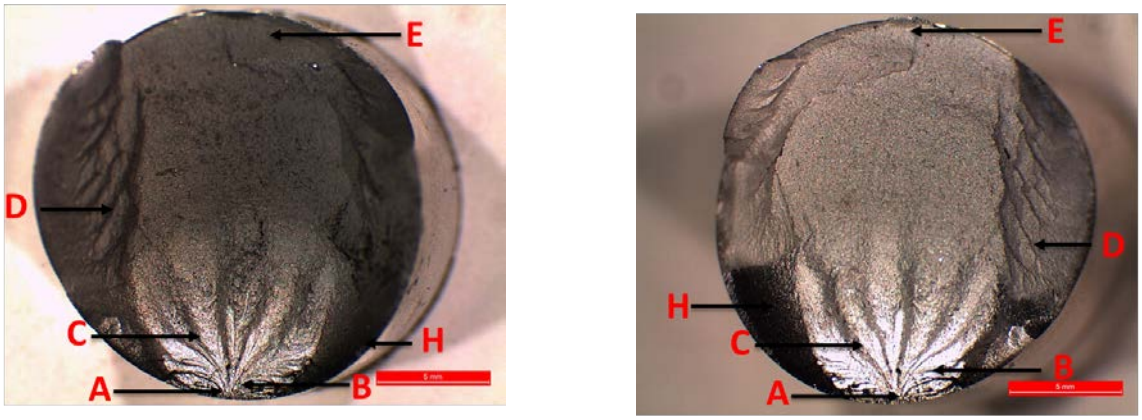

(a) **(b)**

Figure I.42: Fractograph of Fatigue Life Healed Test Specimen 2

Test Specimen 3

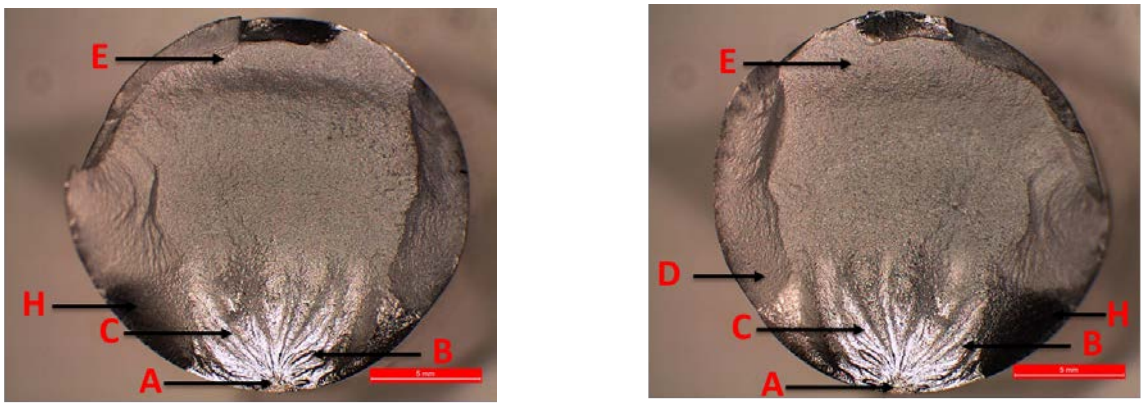

(a) **(b)**

Figure I.43: Fractograph of Fatigue Life Healed Test Specimen 3

Test Specimen 4

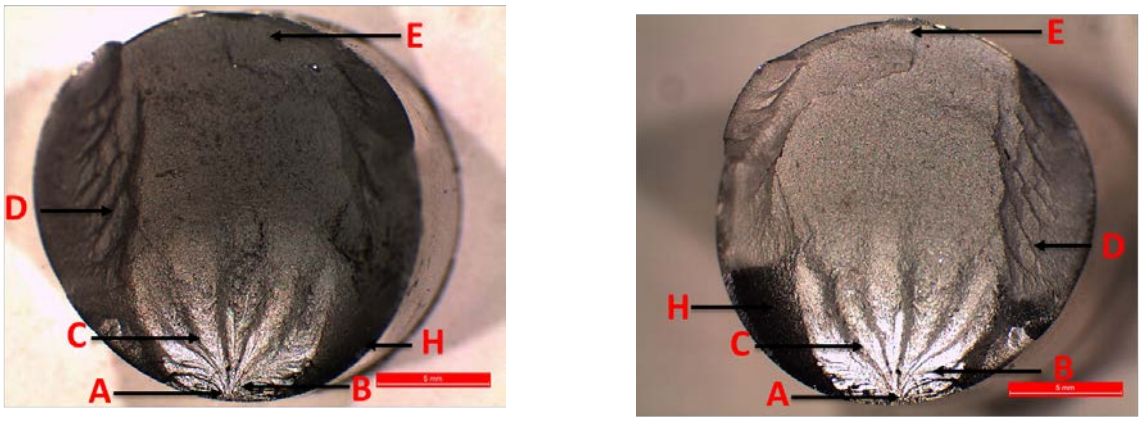

(a) **(b)**

Figure I.44: Fractograph of Fatigue Life Healed Test Specimen 4

Test Specimen 5

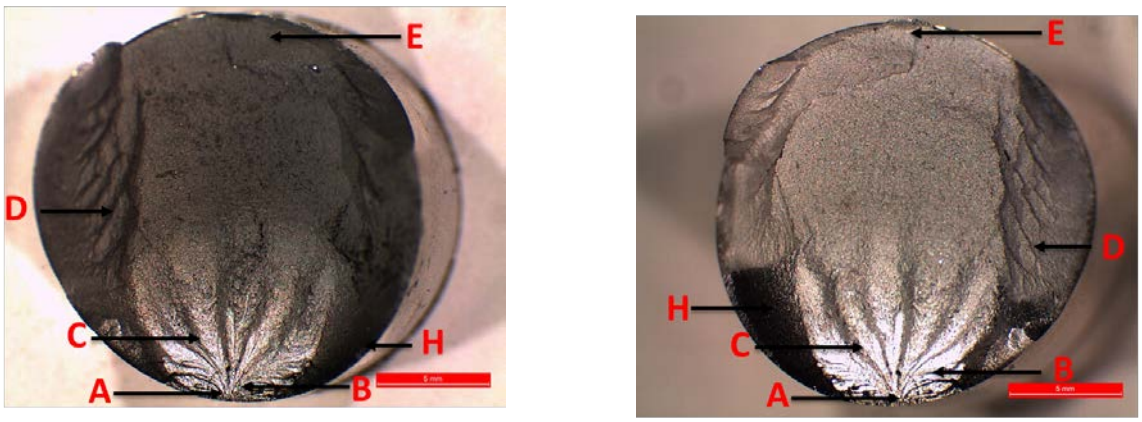

(a) **(b)**

Figure I.45: Fractograph of Fatigue Life Healed Test Specimen 5

Appendix J

Ethics Assessment

EBE Faculty: Assessment of Ethics in Research Projects

Any person planning to undertake research in the Faculty of Engineering and the Built Environment at the University of Cape Town is required to complete this form before collecting or analysing data. When completed it should be submitted to the supervisor (where applicable) and from there to the Head of Department. If any of the questions below have been answered YES, and the applicant is NOT a fourth year student, the Head should forward this form for approval by the Faculty EIR committee: submit to Ms Zakiya Chikte (Zakiya.chikte@uct.ac.za); New EBE Building, Ph 021 650 5739).

Please note – It is important to keep a signed copy of this form as students must include a copy of the completed form with the dissertation/thesis when it is submitted for examination.

Name of Principal Researcher/Student: ALEXANDER BECKER.

Department: MECHANICAL ENGINEERING.

If a Student: **Degree:** MSc

Supervisor:

If a Research Contract indicate source of funding/sponsorship:

Research Project Title: Effect of Laser Shock Peening and Shot Peening on the Fatigue Life of Aluminium Alloy.

Overview of ethics issues in your research project:

Question 1: Is there a possibility that your research could cause harm to a third party (i.e. a person not involved in your project)?	YES	~~NO~~ X
Question 2: Is your research making use of human subjects as sources of data? If your answer is YES, please complete Addendum 2.	YES	~~NO~~ X
Question 3: Does your research involve the participation of or provision of services to communities? If your answer is YES, please complete Addendum 3.	YES	~~NO~~ X
Question 4: If your research is sponsored, is there any potential for conflicts of interest? If your answer is YES, please complete Addendum 4.	YES	~~NO~~ X

If you have answered YES to any of the above questions, please append a copy of your research proposal, as well as any interview schedules or questionnaires (Addendum 1) and please complete further addenda as appropriate.

I hereby undertake to carry out my research in such a way that

- there is no apparent legal objection to the nature or the method of research; and
- the research will not compromise staff or students or the other responsibilities of the University;
- the stated objective will be achieved, and the findings will have a high degree of validity;
- limitations and alternative interpretations will be considered;
- the findings could be subject to peer review and publicly available; and
- I will comply with the conventions of copyright and avoid any practice that would constitute plagiarism.

Signed by:

	Full name and signature	Date
Principal Researcher/Student:	ALEXANDER BECKER. Signed by candidate Signature removed	01/01/2016
This application is approved by:		
Supervisor (if applicable):	Sarah George Signed by candidate Signature removed	[illegible]
Chair : Faculty EIR Committee For applicants other than undergraduate students who have answered YES to any of the above questions.		

Figure J.1: Assessment of Ethics in Research

ADDENDUM 1:
Please append a copy of the research proposal here, as well as any interview schedules or questionnaires:

ADDENDUM 2: To be completed if you answered YES to Question 2:

It is assumed that you have read the UCT Code for Research involving Human Subjects (available at http://web.uct.ac.za/depts/educate/download/uctcodeforresearchinvolvinghumansubjects.pdf) in order to be able to answer the questions in this addendum.

2.1 Does the research discriminate against participation by individuals, or differentiate between participants, on the grounds of gender, race or ethnic group, age range, religion, income, handicap, illness or any similar classification?	YES	NO
2.2 Does the research require the participation of socially or physically vulnerable people (children, aged, disabled, etc) or legally restricted groups?	YES	NO
2.3 Will you not be able to secure the informed consent of all participants in the research? (In the case of children, will you not be able to obtain the consent of their guardians or parents?)	YES	NO
2.4 Will any confidential data be collected or will identifiable records of individuals be kept?	YES	NO
2.5 In reporting on this research is there any possibility that you will not be able to keep the identities of the individuals involved anonymous?	YES	NO
2.6 Are there any foreseeable risks of physical, psychological or social harm to participants that might occur in the course of the research?	YES	NO
2.7 Does the research include making payments or giving gifts to any participants?	YES	NO

If you have answered YES to any of these questions, please describe how you plan to address these issues (append to form):

ADDENDUM 3: To be completed if you answered YES to Question 3:

3.1 Is the community expected to make decisions for, during or based on the research?	YES	NO
3.2 At the end of the research will any economic or social process be terminated or left unsupported, or equipment or facilities used in the research be recovered from the participants or community?	YES	NO
3.3 Will any service be provided at a level below the generally accepted standards?	YES	NO

If you have answered YES to any of these questions, please describe how you plan to address these issues (append to form)

ADDENDUM 4: To be completed if you answered YES to Question 4

4.1 Is there any existing or potential conflict of interest between a research sponsor, academic supervisor, other researchers or participants?	YES	NO
4.2 Will information that reveals the identity of participants be supplied to a research sponsor, other than with the permission of the individuals?	YES	NO
4.3 Does the proposed research potentially conflict with the research of any other individual or group within the University?	YES	NO

If you have answered YES to any of these questions, please describe how you plan to address these issues(append to form)

Figure J.2: Assessment of Ethics in Research